The Role of Cervical Reserve Cells in Epithelial Regeneration and Homeostasis in the Murine and Human Cervix

Lama A. Alzamil

Department of Pathology

Wolfson College, University of Cambridge

This thesis is submitted for the degree of

Doctor of Philosophy

July 2020

Declaration

This dissertation is the result of my own work and includes nothing which is the outcome of work done in collaboration except as declared in the Preface and specified in the text.
It is not substantially the same as any that I have submitted, or, is being concurrently submitted for a degree or diploma or other qualification at the University of Cambridge or any other University or similar institution except as declared in the Preface and specified in the text.
I further state that no substantial part of my dissertation has already been submitted, or, is being concurrently submitted for any such degree, diploma or other qualification at the University of Cambridge or any other University of similar institution except as declared in the Preface and specified in the text.
This thesis does not exceed the recommended word limit of 60,000 words set by the Degree Committee of Biology.

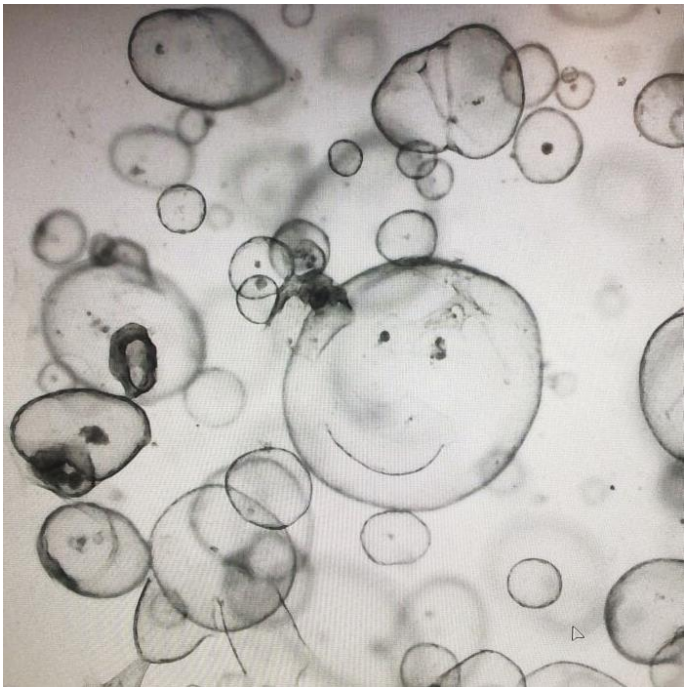

Endocervical organoid

Acknowledgments

First and foremost, I want to thank my supervisors Professor John Doorbar and Dr Margherita Turco. Professor John Doorbar gave me a chance to join his lab and undertake this study and for this and his constant support I am utterly grateful. Dr Margherita Turco for her mentorship, guidance and encouragement during this journey.

I would also like to acknowledge all past and current members of the Moffett, Turco and Doorbar labs. PhD can be daunting, but I was fortunate to have been around genuinely kind and supportive network of amazing scientists with a soft spot for cake. Special thanks to my office neighbour and fellow coffee-hunter Nina.

The breakfast club, JJ, Osh and Yass, you made my years in Cambridge unforgettable. Special thanks to Jyothi for all her warmth and home cooked meals..I felt like I had family in town. To all the ladies who gave me refuge throughout the years when I needed to feel home away from home, Layla, Ayda, Nahla, Abeer and Maysoon, I Cherish your friendship and support in this journey. Ala for being a constant inspiration.

I would also like thank my family, brothers, sisters and my niece and nephew, missing them grow up was the most difficult part of this. Specially my parents, my biggest fans who believed in me even when I did not believe in myself. Thanks to my girls back home, Aljoharah, Sarah M, Haifa, Sarah H and Nouf I love you. Special thanks to Haifa.. your phone calls and pep talks kept me sane.

Thanks to all the friends at Wolfson College, a place of education and community, special thanks to Hogai who always willing to lend an ear when I needed it.

There are not enough pages to mention all the helpful staff from various facilities at the University of Cambridge who were involved in this project in one way or another, the animal house staff, flow and histology facilities at the department of pathology thank you all. Thanks to Dr Miriam Baumgarten and the support staff at the human tissue bank at Addenbrooke's University Hospital who always made sure ''the cervix lady'' got her bits. Last but not least, thank you to all the women who have donated samples, your generosity is greatly appreciated.

None of the work I have done in this thesis would have been possible without the financial support from King Saud University, which provided me with a PhD studentship.

Abstract

How cervical epithelium maintains homeostasis and repair, and how the high-risk human papilloma viruses (HR-HPV) drive neoplasia at the cervical transformation zone (TZ) has been poorly researched. The cervical TZ is thought to be a stem cell niche as it harbours a unique cell population called reserve cells. Reserve cells (marked by KRT17) are believed to have a dual fate ability depending on local microenvironment, in a process of metaplasia (1). However, this belief was based on observational studies. Metaplasia is thought to be the way that the cervical epithelium recovers after an injury (2). Developing an *in vitro* model that is truly representative of normal cervical epithelium is crucial to address basic questions about homeostasis mechanism and the role of reserve cells in HR-HPV infections. In recent years, advances in modelling the human tissue in 3D manner using organoids have been made (3). In this thesis, a 3D murine cervical organoid model was established. Two distinct microenvironments for the growth of endocervix and ectocervix is defined. Generated cultures retain their proliferative capacity over several months and are representative of the epithelial population *in vivo.* Furthermore, steps were taken towards optimising human cervix organoids. The established *in vitro* system was exploited along with *in vivo* samples to further to uncover specific signalling pathways that regulate the different cervical lineages (endo and ectocervix) using Affymetrix microarray and immunofluorescence techniques. Wnt signalling was found to regulate the endocervical lineage, whilst Notch pathway was active in the ectocervix. Moreover, a novel P75 NGF receptor was found to be expressed in the basal squamous epithelium and in the reserve cells. Additionally, the established organoids were utilised together with lineage tracing techniques to investigate the dual-fate potential of KRT17 cells and their contribution in cervical TZ formation. Two transgenic mice strains were evaluated *Krt17tm1$^{(cre,Cerulean)Murr}$;ROSA26$^{(CAG-tdTomato)}$* and *Krt17Cre^{ERT2}; ROSA26 $^{(CAG-ZsGreen1).}$* The inducible regulation via tamoxifen in Krt17Cre^{ERT2} was found to have a confined KRT17 expression compared to the Cre/loxp only (Krt17tm1$^{(cre,Cerulean)Murr}$) strain.

(1) Martens JE, Arends J. Cytokeratin 17 and p63 are Markers of the HPV Target Cell, the Cervical Stem Cell. Anticancer Res. 2004;6.
(2) Giroux V, Rustgi AK. Metaplasia: tissue injury adaptation and a precursor to the dysplasia–cancer sequence. Nat Rev Cancer. 2017 Oct;17(10):594–604.
(3) Lancaster MA, Huch M. Disease modelling in human organoids. Dis Model Mech. 2019 Jul 1;12(7).

Contents

List of Figures

List of Tables

List of Appendices

1 General introduction

1.1 Development and anatomy of the cervix

1.1.1 Development of the cervix

Sex determination in placental mammals is genetic (1). The genetic sex of an embryo is established during gamete fusion at fertilization (2). In a human embryo, the *sex-determining region Y* gene (*SRY*) (3) upregulates *Sox9,* which induces sertoli cell differentiation driving testis formation (4) in males**.** Whilst in the absence of the *SRY* gene, the embryo becomes a female. Sexual differentiation of a female human embryo starts at week 7 gestational age (5). The absence of testosterone allows the Müllerian ducts (MD), also called paramesonephric ducts, to continue to develop, while the Wolffian ducts (WD) or mesonephric ducts, do not (6). MD are two simple tubes of pseudostratified columnar epithelium, that are believed to form the fallopian tubes, uterus, uterine cervix, and the upper vagina by fusion (6). In mice, sexual differentiation takes place after embryonic day 13.5 (E13.5). The absence of both androgen and anti- Müllerian hormone, WD regresses, while MD differentiates into the oviduct, uterine horns, cervix and upper vagina (7).

Homeobox genes (*HOX*) are a group of highly conserved genes that play a role in embryonic development. The differential expression of Homeobox genes (*HOX*) plays a key role in the development of the female reproductive tract in the MD (8). The *HOXA9* expression gives rise to the uterine tube, *HOXA10* the uterus, *HOXA11* is found in the lower uterus and the cervix, whilst *HOXA13* develops the ectocervix and vagina (8). This expression pattern is conserved between mice and humans.

1.1.2 Anatomy and physiology of the adult cervix

The cervix (which translates to *neck* in Latin) is located at the lowermost portion of the uterus, connecting it to the upper vagina. It is divided into three anatomically distinct regions: ectocervix; which joins the cervical canal to the vagina via the external os (EO), squamocolumnar junction (SCJ), and endocervix; which is separated from the uterine corpus by an internal os (IO) (9) (Figure 1.1).

The length and diameter of the cervix varies during a female's life, becoming mature during puberty, the period when glands are formed (10). The cervix measures between 2.5 to 3.0 cm in length in non-pregnant adults, and 3.0 to 4.0 cm during pregnancy with variations due to age, parity and stage of the menstrual cycle (11,12). In the mouse, although anatomical

differences between mice and humans in the uterine body exist, the SCJ is found. With two cervical canals, connecting two lateral uterine horns to the vagina, rather than one body of uterus in humans (13) (Figure 1.1).

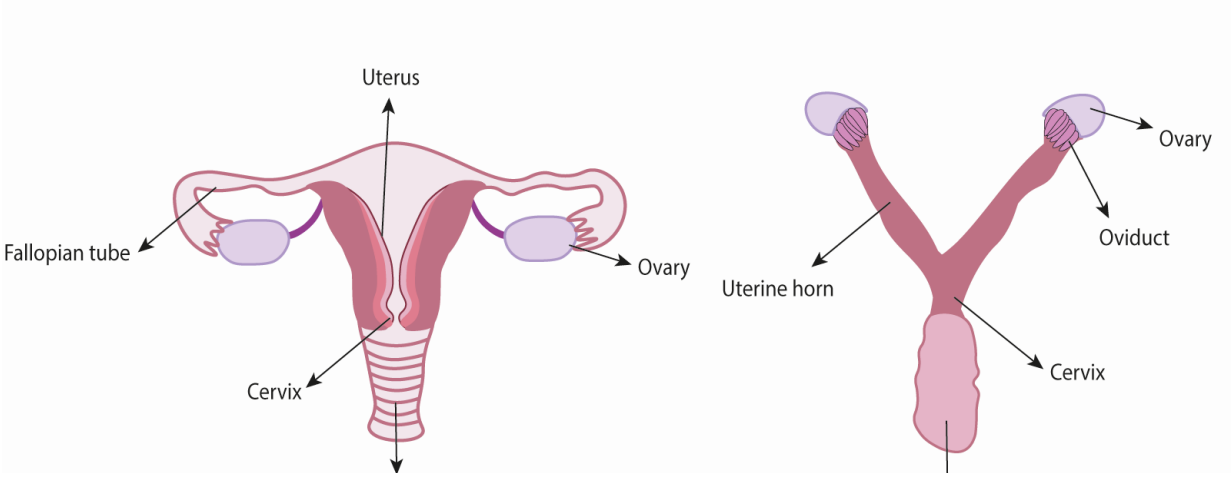

Figure 1.1: Overview of the anatomical arrangement of the female genital tract. In humans (left) and the female genital tract in mice (right), with two uterine horns that join leading to the vagina via two separate cervixes.

1.1.3 Histology and local organisation of the cervical epithelium

The endocervix is lined by a monolayer of tall columnar epithelial cells filled with mucin, which are sporadically ciliated (14). The cervix has no glands, instead the cells of the endocervix have infoldings that create gland-like structures called *plicae palmatae* (15). These are secretory and act as a storage of sperm post coitus (12). Occasionally, a population of sub-columnar cells (reserve cells) are observed (discussed in section 1.2.3). The stromal components of the endocervix are twice as much as the SCJ and ectocervix stroma and is composed of a thick layer of connective tissue and muscle fibres, with higher muscle fibres rate at the internal os (continuous with the myometrium) (16). Although estrogen does not stimulate proliferation of columnar cells, a profound increase in endocervical secretions is observed (17). Cytokeratin's (KRT) are the intermediate filament proteins that are found in the intracytoplasmic cytoskeleton in tissue-specific manner (18) and are used to mark different epithelia, including the cervix. KRT markers for endocervical tissue include KRTs 7,8,18 and 19 (19).

In contrast to the endocervix, the ectocervix is made of stratified non-keratinizing squamous epithelium similar to the vagina. This squamous epithelium is divided into basal, parabasal, intermediate and superficial, which is the most differentiated (20). These layers vary in the rate

of cell division, as Ki-67 in normal epithelium is mostly active in the parabasal layer (21). The different layers also respond differently to hormonal stimulation. When estrogen is present, it drives proliferation and maturation of all layers and stimulates glycogenation. While progesterone promotes the thickening of the intermediate layer only (21). In complete absence of both hormones, atrophy takes place, and glycogen is lost. Cytokeratin expression in ectocervical squamous epithelium is more complex than the endocervical epithelium, a differential pattern is observed through the stratified epithelium; superficial and intermediate layers express KRTs 4, 13 and occasionally 10 (22), while the parabasal layers expresses KRTs 13, 14 and a variable number of KRT10 (24). Lastly, the basal layer expresses KRT markers 5, 14, 18 and 19 (22,23).

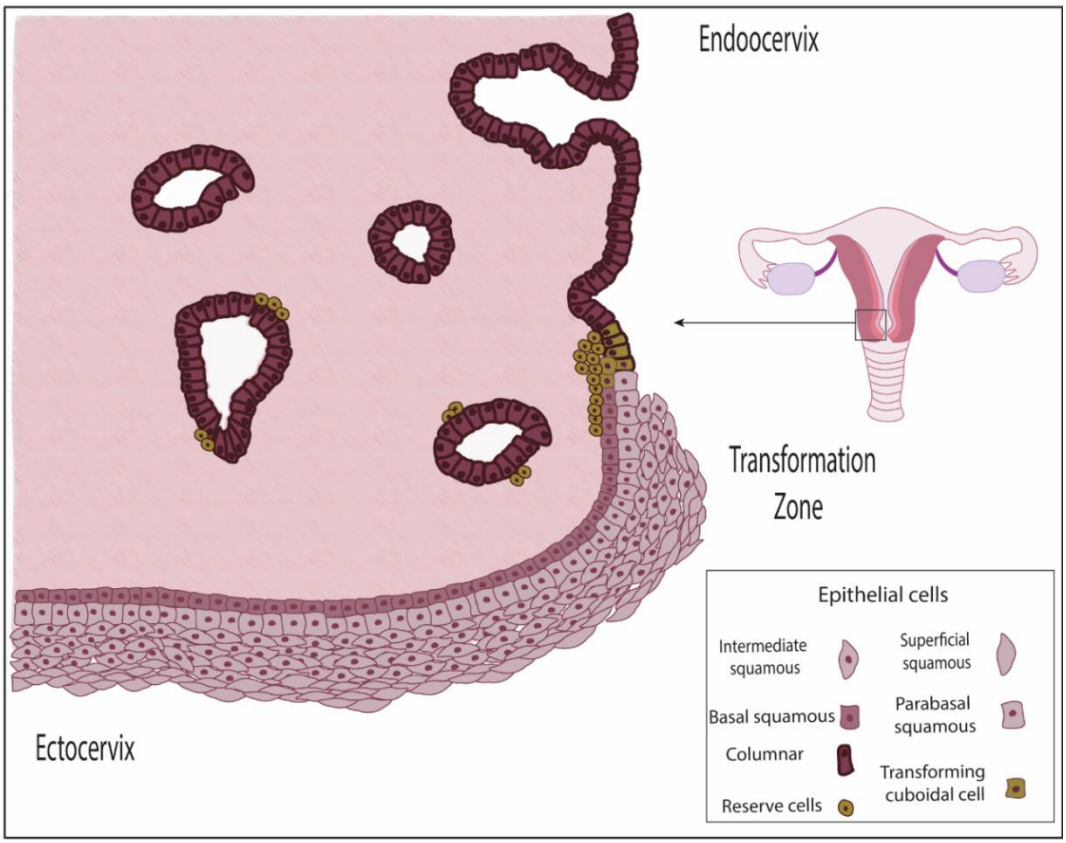

Figure 1.2: The cervix is comprised of two distinct epithelial types; columnar and stratified. The columnar epithelium of the endocervix, and the stratified epithelium of the ectocervix merge at the squamocolumnar junction (SCJ). The reserve cells (shown in green), lie under the columnar epithelium, and are believed to regulate the process of metaplasia, which results in the formation of a new stratified epithelium, producing the transformation zone (TZ).

The squamocolumnar junction (SCJ) is the area that links the simple columnar epithelium of the endocervix to the stratified squamous epithelium of the ectocervix (24). Neonatal or original SCJ is formed in late fetal stages in response to maternal hormones, when the uterine cavity covered by columnar epithelium of the müllerian duct extends towards the cervical canal, where contact with the vaginal squamous epithelium originating from the urogenital sinus takes place. Subsequently, the site of SCJ changes during puberty, pregnancy and menopause, by the process of squamous metaplasia (25) (discussed in section 1.2.2).

Similar to humans, mouse cervix is lined by single columnar epithelium at the endocervix and stratified squamous epithelium at the ectocervical end. In contrast to humans, squamous layers of the ectocervix are keratinized in mouse, with KRT8 marking the endocervix and KRTs 5, 13 and 14 marking the ectocervix with SCJ existing between the two (26,27). In contrast to what has been documented in humans (28–31), there has been no publications about physiological cervical metaplasia in mouse. However, there has been tissue recombination studies showing the ability of uterine and vaginal mesenchyme to specify epithelial differentiation in young mice (32). This suggests tissue plasticity and a possible dual columnar/squamous cell fate resembling the metaplastic model.

1.2 Regulation and function of the Cervix

1.2.1 Function and hormones

The cervix plays an important role as the gatekeeper of the reproductive tract, a delicate balance between the maintenance of immunological tolerance and biological defence. It also permits the entry and transportation of sperm. The muscular canal of the cervix is plugged with thick mucus secretions for most of the cycle and pregnancy. During the peak of ovulation, the increase in estrogen causes softening, opening, rising and production of cervical fluid allowing for smooth transit of sperm (33). These secretions also prevent pathogens ascending into the uterus. In addition, the cervix is important for retaining the conceptus in utero and short cervical length is associated with preterm delivery (34).

Estrogens, progestogens and prostaglandins regulate cervical function, cervical stroma has receptors for estrogen α and β and progesterone (35). Estrogen acts on the cervical stroma by changes in collagen and elastin promoting softening of the cervix, whilst progesterone acts on increasing the tissue stiffness of the stromal ECM (36). Additionally, estrogens and progesterone were found to influence the endocervical mucus composition during the menstrual cycle (37), during ovulation the ratio of proteins to mucous glycoprotein was low

(38). Whilst during the luteal phase, this ratio of proteins to mucous glycoprotein was increased (38). The secretion of mucous glycoprotein was its highest during ovulation (38).

1.2.2 Cervix homeostasis and metaplasia occurs at the cervical transformation zone

Metaplasia is the benign change of cells from one mature form to another. In the cervix, a migration of the SCJ occurs when the columnar epithelium of the endocervix is replaced by stratified squamous epithelium, producing a new SCJ. The area between the original SCJ and the current SCJ is called the transformation zone (TZ). The exact mechanism by which this change occurs is not clear, however, it has been presumed that age, hormones, chronic irritation and pH levels play a key role in the process (16,39) (Figure 1.2).

It is believed that the process of change starts with reserve cell hyperplasia, where sub-columnar cells in the endocervix actively divide (30,31). Subsequently, these cells differentiate into layers of immature stratified squamous epithelium, where components of both squamous and columnar nature can be detected, these progressively mature hence, blending with the original ectocervix. At the level of histology, mature squamous epithelium is largely indistinguishable from the original squamous epithelium of the ectocervix, with the presence of underlying endocervical crypts providing a convenient way of defining this region as the transformation zone (39).

It should be mentioned that other theories that do not involve reserve cells have been documented, in particular ‘’squamous epithelialization’’, in which the replacement eversion of endocervical epithelium onto squamous epithelium (*portio vaginalis*) occurs by an ingrowth of the basal squamous layer beneath the neighbouring columnar ones in response to a stimulus (40)**.**

1.2.3 Reserve cells

Reserve cells were described in 1910 by Meyers (41), but the use of the term ‘’reserve cells’’ was not widely used in the field until its reintroduction by Hellman in 1954 (42). In Meyers earliest studies, he described rows of small polyhedral basal cells located between the columnar epithelium and the basement membrane of the endocervix in a random manner (41,43). Since then, the nature of these cells has been debated but still poorly understood, mainly because of the lack of adequate experimental models. Earlier studies did however attempt to predict the nature of these cells. In a human uterine endocervix explant study, Schurch *et al.,* suggested that they originated from the secretory endocervical epithelium (44). In another study, microscopic analysis of early cervical metaplasia led to the hypothesis that these sub-columnar

progenitor cells may have migrated from the subepithelial stroma (45). A different view suggested that cervical reserve cells might be of embryonic remnants (30). Furthermore, some believe they may originate from a population of cuboidal cells found at the SCJ (29). And more recently, a publication suggests the possibility of reserve cells arising from the basal cells of the ectocervix (120).

Although the origin of reserve cells is still controversial, recent advances have allowed investigators to characterise these cells using immunohistochemical markers. Reserve cells demonstrate expression of cytokeratin 17, BCL-2 and TP63, a P53 homolog that has been described as a candidate marker of epithelial progenitor cells in multiple organs including the cervix (31,46,47). The importance of cervical reserve cells, is due to the hypothesis that they might be a possible progenitor of both squamous and columnar epithelia lineages (31,48), in addition to speculations involving the role of reserve cells in cervical cancer (49) (discussed in section 1.3.2).

1.3 Transformation zone and HPV

Human papillomavirus (HPV) infection drives cervical cancer (50). HPVs are a family of small double-stranded DNA viruses that infect the epithelia (51). They can be subdivided into high-risk (HR) and low-risk (LR) according to their association with neoplasia and cancer. LR types including HPV6 and HPV11 generally cause only benign warts, while the HR types, including HPV16 and HPV18 are potentially carcinogenic, and cause lesions that can progress to cancer. Although HR-HPV is found in 90–100% of cervical neoplasia, most infections in fact manifest as benign low-grade lesions that are cleared by the immune system (52). It is thought that in the rare occasion where the virus fails to produce a productive infection the viral gene expression becomes deregulated, and that over time, this deregulated viral gene expression predisposes to the development of cancer (52).

Although our knowledge of the mechanism by which HR- HPV viruses causes neoplasia has greatly increased in recent years, the target cell of the virus abortive infection remains unknown. Nevertheless, it has been observed that HPV associated cancers arise primarily in regions with epithelial transition zones such as: oropharyngeal-tonsils, gastro-oesophageal, uterine-cervix and ano-rectal (53). Little is known about why these sites are more susceptible to neoplasia. One reason may be that HPV infection starts with a micro-wound, which allows the virus to infect epithelial basal cells (52). At particular sites such as SCJ/TZ, basal cells, reserve cells and progenitor-like cells are more likely to be close to the epithelial surface and

may be more prone to infection. In contrast, other sites might have different wound repair machinery which might have facilitated the wound-healing process. In addition, recent data suggests that the unique gene expression of these complex sites harbours a possible stem cell niche. Claims have been based on the fact that stem cells have a unique cell cycle regulation to maintain self-renewal and differentiation into mature cells. Progenitor cells also persist for life, increasing the chances of accumulative mutations (49). Therefore, it may be presumed that the target cell for HR- HPV infection is the stem cell of the uterine cervical epithelium.

Several views have linked the HPV-target cell to the reserve cells, arguments supporting is the fact that high expression of cytokeratin 17 positive cells has been observed in high-grade cervical lesions and cervical cancer cases (54,55).

Importantly, this proposes that reserve cells might represent an abortive site for HR-HPV infections, in which deregulated viral gene expression is thought to drive HPV-mediated neoplasia. Another view suggested that a population of actively dividing SCJ cuboidal cells, with distinctive markers, one of which is Cytokeratin 7, are a possible site for HPV abortive infections. Supported by an observation of overlapping of their biomarkers with ones seen in high grade lesions (29).

1.3.1 Viral infection and immune response

HPV has evolved its life cycle to be linked to the epithelial differentiation program of the host, hence, there is no virus-induced cell death nor inflammatory-induced response (56). When stressed, keratinocytes can mediate immune responses by expressing toll-like receptors (TLRs) on its cell surface (TLR1, TLR2, TLR4, TLR5, and TLR6) and intracellularly where it is localised in the endosome (TLR3 and TLR9) (57). Activation of TLRs on keratinocytes leads to type I interferon production, and later Th1-type cytotoxic responses (58). During infection viral genome copy number is affected by type I interferons. The E6 and E7 viral oncoproteins expressed by the HR-HPV types of alpha genera interfere with type I Interferon response by inhibition of STAT. HR-E6 can also disrupt the Tyk2 downstream of the interferon signalling pathway (59). In addition, E7 hinders IRF-1, a transcription factor involved in the activation of interferon-stimulated genes (60). Also, E7 down-regulates the expression of components LMP2 and TAP1 of antigen presentation, thus avoiding Natural killer cell cytotoxicity (61). It is still debatable whether latency is a result of immune-mediated regression (62-64), but failure to control infection allows chronic deregulated gene expression, and the development of neoplasia and cancer.

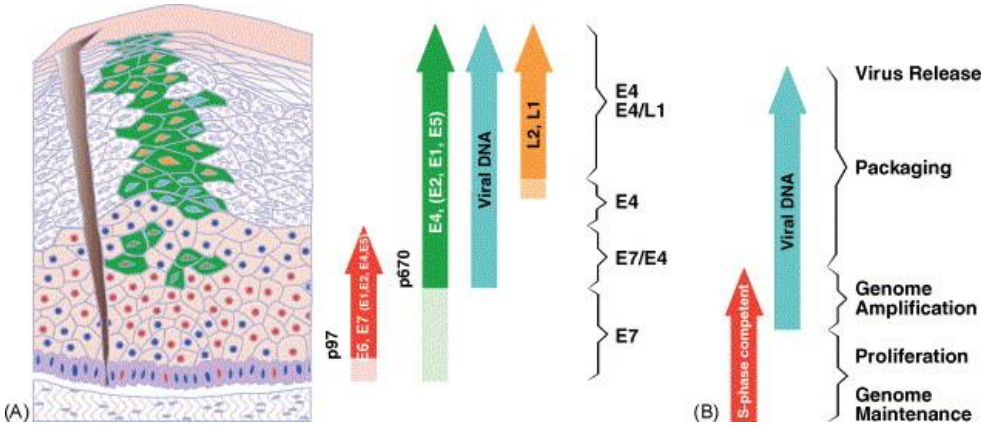

Figure 1.3: Life cycle of HPV types of alpha genera. (A) shows HPV16 gene expression pattern in an infected cell, during epithelial differentiation, expression of the E6 and E7 early genes is key for S-phase entry (red). In the higher epithelial layer's viral replication proteins (E1, E2, E4, E5) start to appear (green), and viral genome amplification is carried out (blue). E4 marking viral production is shown in the upper epithelial layers (yellow). (B) Cells in basal layers are S-phase state. Active proliferation and genome amplification appear in intermediate layers, whilst packaging and release of the virus occurs in the upper layers (adapted from Doorbar,2005).

1.3.2 Cervical neoplasia and its cellular origins

Most women infected with HR-HPV get viral clearance and resolution of infection via cell-mediated immunity within months or years and the chances of cervical neoplasia rising is relatively low (56). However, failure of the immune system to resolve the infection can lead to deregulation in gene expression resulting in the development of neoplasia and cancer (52). Whilst, early HPV proteins are associated with replication and maintenance of the viral genome, late ones are associated with the formation of the viral coat (65). In alpha HPV types, E6 and E7 genes regulate cell cycle entry (Figure 1.3), cell proliferation, and differentiation. Although HR-HPV types can infect various epithelial sites, including the penis, vagina, and vulva, cancer arising at these sites is rare (52).

Site-specific vulnerability for HPV associated neoplasia is not fully understood, however, speculations suggested that the lack of protective layers of differentiating cells at these sites and the presence of cells that cannot support the life cycle of the virus are to blame (66,67). It is proposed that the diversity of HPV infection consequences depends on the site of infection. With ectocervix, productive HPV infection and low grade squamous intraepithelial lesion (LSIL) is supported, whereas TZ and endocervix are associated with deregulated HPV gene expression leading to high grade squamous intraepithelial lesion (HSIL) (Figure 1.4). This was based on observation using biomarkers including HPV-encoded E4 protein and $p16^{INK4a}$ tumour suppressor protein. Where in high-grade lesions, E4 is absent and $p16^{INK4a}$ is extensive

indicating an abortive infection. Whilst in low-grade lesions, E4 showed high expression and $p16^{INK4a}$ was mostly negative indicating a productive virus infection (52,121). This was also investigated with organotypic raft culture derived from primary human keratinocytes showed that infection of the basal epithelial layer of stratified ectocervix results in a productive HPV infection (122). On the contrary, HPV infection of the columnar cells of the endocervix showed deregulation of viral gene expression and the development of neoplasia (67,123).

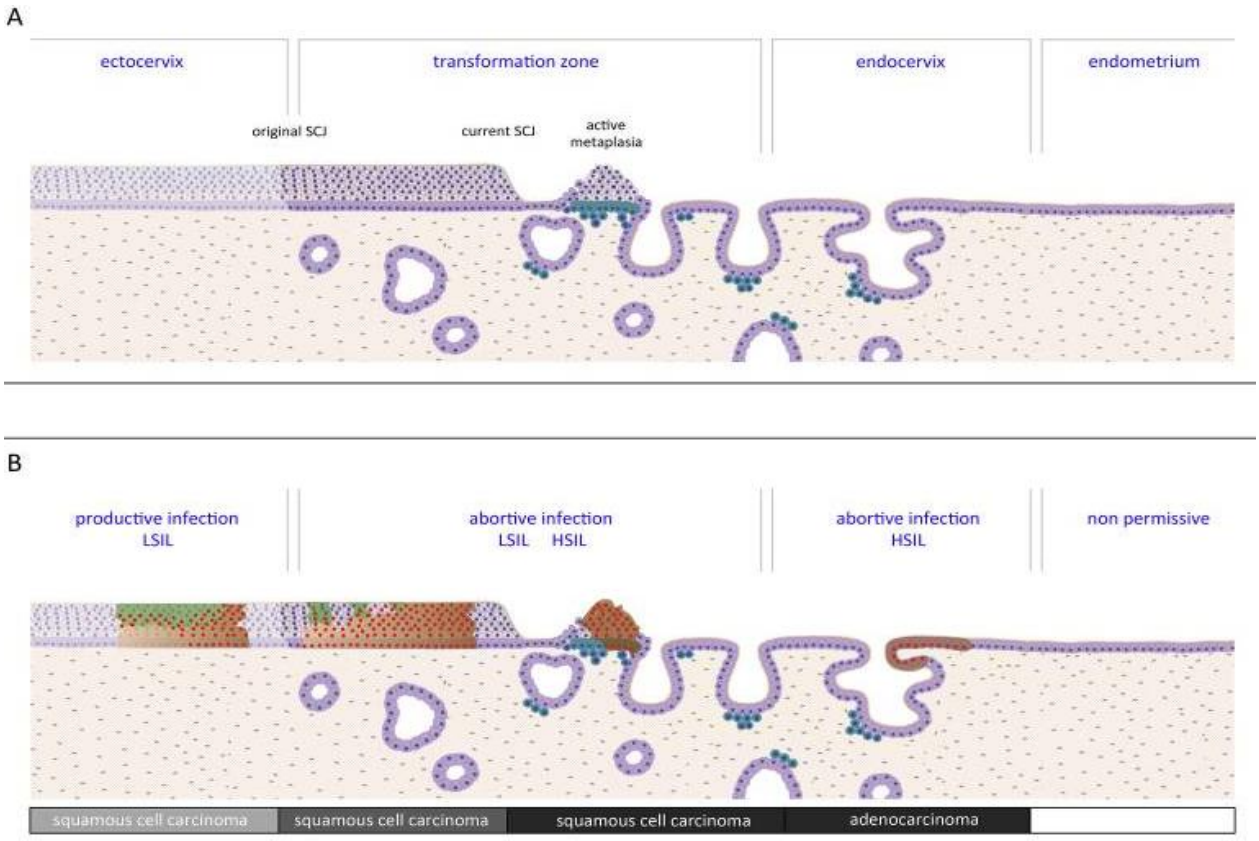

Figure 1.4: HPV Infection sites of the cervix and their possible associated consequence. (A) schematic representation of the epithelial types in the cervix, the ectocervix lined with stratified epithelium, the transformation zone, and the columnar epithelium of the endocervix. The reserve cells (turquoise) are under the columnar epithelium of the transformation zone, and are associated with the process of metaplasia which forms a new SCJ by building a new stratified epithelium when required. (B) The outcome of HPV infection differs depending on the site of infection. It is believed that the ectocervix is a site of productive HPV infection where LSIL is supported, whilst the TZ and endocervix are sites where deregulation of HPV gene expression occurs, leading to high grade lesions. E4 protein marking productive cycle (in green), p16 (brown) and MCM/Ki67 (red). (adapted from Doorbar, 2019).

1.4 Experimental models of the cervix

1.4.1 *In vitro* models: 2D and 3D

The tissue architecture of the cervix is complex and thus, has been challenging to study. In the past, the use of 2D carcinoma lines such as; HeLa (68), an aggressive cervical adenocarcinoma cell line, which is HPV18 positive (69), SiHa, a HPV16 positive grade II squamous cell carcinoma cell line (70), C33a, which is HPV negative and was derived from 3 poorly differentiated carcinomas of the cervix (71), and CaSki (72) derived from a metastasised squamous cell carcinoma of the human cervix, which is HPV16 positive. Although these 2D cancer cell lines have the ability to divide indefinitely, they carry a variety of mutations and chromosomal abnormalities, and do not represent the cervical cell-cell homeostasis.

Primary human foreskin keratinocytes (HFKs), are a keratinocyte cell line derived from newborn circumcisions (73), as these are primary cells, they have a limited lifespan with 15 population doublings, in addition to morphological changes which include flattening of cells (74). Hence was the use of spontaneously immortalised keratinocyte cell lines, these include: NM1 (75), HaCaT (76) and NIKS (77). NIKS are near diploid, that retain normal responses to contact inhibition and have been widely used as an infection model for HPV16, HPV18, HPV31, HPV45 and HPV58 (77). These cell lines offer an isogenic cell background that can eliminate batch effects that might be seen primary keratinocytes from different patients, however, as the cells are immortalised studying some viral functions can be more challenging. Immortalised keratinocyte cell lines have several undesirable mutations, for instance, NIKS carry a p53 mutation (78).

The development of immortalised keratinocytes allowed the development of organotypic raft cultures (79,80), the use of rafts allowed many aspects of the HPV productive life cycle to be studied and has provided a great insight about HPV proteins functions. Although a lot has been unleashed about the HPV biology, the knowledge about the specific site of the infection and the target cell is still limited and challenging to study, as the simplistic use of cells in culture, doesn't mimic the complex architecture of epithelial cells seen of the cervix.

1.4.2 *In vivo* models

Animal models for cervical dysplasia and cervical carcinoma are limited. Oncogenic HPV subtypes only cause cancer in humans, however mice can be genetically modified to facilitate the study of cervical carcinoma development. Targeted expression of E6 and E7 oncoproteins has been shown to cause neoplasia in transgenic mice (81). Moreover, E7 was found to increase

proliferation, whilst E6 contributed to p53 loss, and both E6 and E7 increased centrosome copy number (82), using mice that expressed the HPV-16 E6 protein (*Krt14*-E6), and E7 protein (Krt14-E7), or both (Krt14-E6:E7). Although these models allowed the study of the individual effect of each HPV oncogene in deriving cervical carcinogenesis, they are not without limitations. Since mouse cells require less mutations to become cancerous, mouse models exhibit less mutational diversity compared to human tumours, additionally, mouse cells metastasise less (83). Furthermore, the expression is regulated by *Krt14* promoter (not the endogenous PV promoter) which affects studying the role of hormones on viral transcription. Additionally, viral proteins have evolved in humans, and many of their effects is via protein-to-protein interactions, thus some differences can be expected when HPV protein function is examined in mouse cells. Moreover, using E6/E7 transgenic models, carcinomas were found to occur in other epithelial sites and only 40% were located at the TZ of the cervical epithelium. additionally, differences between mouse and human metabolism limits drug discovery experiments (84).

Xenograft models are when human cancer cell lines or biopsies are transplanted into animals, usually, immunocompromised mice (85). Limited number of xenograft models has been described for human cervical carcinomas. One model used primary tumour biopsies, both squamous cell carcinoma (SCC) and adenocarcinoma (86), the model demonstrated features of the tumour including growth and behaviour. Xenograft models can be useful for short-term virus infection experiments, and drug discovery testing, however, as the host is immunosuppressed, interactions between the tumour and the immune system was lacking.

1.4.3 Organoid models of human tissues

Three-dimensional cell culture that captures a near-physiological experimental environment has become the new frontier of tissue modelling. In contrast to cells in 2D, which are composed of undifferentiated cell types, organoids contain multiple differentiated cell types that are found in the target organ *in vivo* (87).

Two different approaches have been used to establish organoid cultures, either induced pluripotent stem cells (iPSC) derived organoids, or adult tissue epithelial (ATE) derived organoids. In our context, we will be focusing on ATE organoids unless stated otherwise. Organoids are a 3D culture system in which an extracellular matrix (ECM) hydrogel, Matrigel® is used to give the cells a basement membrane to anchor to. After tissue dissociation, progenitor cells within the mixture, if supplied with the right signalling, will self-assemble to

form symmetric cyst structures (spheres), which have the potential to give rise to more complex structures. The arrangement of these structures varies depending on the architecture of the tissue of origin. For example, intestinal epithelium tends to generate budding structures, while others have reported duct-like epithelial structures such as in liver organoids. The power of these cultures is that they hold the promise of recapitulating near-physiological conditions -*in vitro*- with no genetic alterations (87). Unlike *in vivo* models, organoids are fairly easy to manipulate, which allow investigators to explore the use of this technology as a model for viral infection, disease and in drug discovery.

Most of the published organoid cultures contain epithelial tissue only and lack the presence of any stromal components, or immune cells. The first gut organoid culture was published by Sato and Clevers in 2009 (88) and was derived from mouse small intestinal crypts. Since then, many adaptations have been reported by others for different epithelial tissues, including stomach (89), liver (90), colon (91), pancreas (92), Lung (93), prostate (94), and endometrium (95,96). In organoid cultures, signals that may regulate the differentiation and maturation of progenitor cells are supplied by adding extra-cellular factors, these factors should in theory mimic the micro-environmental niche of the target cell population to support growth, and the right organoid culture will express similar markers and functionality as the tissue of origin (97). Most of the reported organoid cultures used *EGF*, Noggin and R-spondin1 (ENR) medium (88) as a base, then tailor the added cytokines/factors according to the signalling to that of the desired tissue. ENR is enriched with EGF (promotes cell proliferation), R-Spondin (wnt pathway activator) and Noggin (BMP antagonist). Although investigations of these pathways in normal cervical epithelium is minimal in literature, there are reports about *EGF* and *Wnt/β-Catenin* signalling in cervical cancer and early stages of neoplasia (98,99).

ECM

Matrigel is derived from Engelbreth-Holm-Swarm (EHS) mouse sarcoma cells and is used to simulate the basement membrane matrix *in vitro*. Matrigel® is mainly composed of laminin, collagen and entactin, in addition to growth factors naturally occurring in the EHS tumour. These are kept to a minimum with the growth factor reduced matrigel® matrix. Having Extracellular membrane (ECM) is crucial for epithelial cell contact, which is required for integrin signalling preventing anoikis (100).

Wnt pathway

There are 19 wnt protein in humans and mice that bind to two receptor families: LDL receptor-related proteins 4, 5 and 6 (LRP4, LRP5 and LRP6) (101,102) and the Frizzled (Fz) seven-pass transmembrane receptors (103). In the current wnt model, the presence of wnt ligand bind to Fz/LRP receptor, which further prevents β-catenin degradation, allowing it to enter the nucleus and interacts with TCF/LEF proteins, thus activating wnt-regulated genes (102). In contrast, the absence of wnt ligand allows the destruction complex (CKIα, GSK3β, APC, Axin) to bind to β-catenin leading to its phosphorylation and release targeting its ubiquitination and degradation by proteasomes (87). R-spondin proteins are a group of secreted proteins that are known for their regulation of wnt/β -catenin signalling (104). Although R-spondin does not activate wnt, it is a potent wnt-signal enhancer (104). Upon binding to leucine-rich repeat-containing G-protein-coupled receptor 4/5 (LGR4/LGR5), R-spondin sustains the expression of wnt receptors by blocking RNF43/ZNRF3 mediated degradation, thus increasing cell surface availability (105).

TGF-β and BMP

The transforming growth factor β (TGFβ) superfamily are highly conserved cytokines that have been linked to a variety of cell regulatory functions, importantly, embryogenesis and later in life in growth regulation. Members of the family include; TGFβ isoforms, activins, nodal, inhibins and bone morphogenetic proteins (BMPs) (106). BMP4 and Activin A, have been attributed as key factors in determining epithelial cell fate in the müllerian ducts, by inducing the expression of ΔNp63 through SMAD4/RUNX1 (107).

The use of TGFβ inhibitor -A83-01- has been shown to be important to sustain stem cell-like population in several organoid cultures (106). Furthermore, Noggin, a BMP (bone morphogenetic protein) antagonist, has also shown to allow for stem cell expansion (91).

EGF

Almost all long-term organoid cultures have reported the need for epidermal growth factor (EGF) signal activation. EGF is a small protein -53 amino acids- which binds to epidermal growth factor receptor (EGFR) (108). This binding promotes cellular proliferation, differentiation, and survival (109).

FGF

There are 18 mammalian fibroblast growth factors (FGF) that bind to 4 main tyrosine kinase receptors (FGFRs). FGFs have an important role in organogenesis and tissue patterning and organogenesis. FGF7/10-FGFR2IIIb-MAPK have been found to be indispensable for MD cell fate in mice (110).

Notch

When Notch ligands bind to Notch receptors via γ-secretase/ADAM10-dependent regulation, Notch Intracellular Domain (NICD) is released. NICD will further interact with CBF1/Su(H)/Lag-1 complex (CSL), allowing the activation of Notch target genes (e.g. hes1) (111). Notch signaling has also been reported to regulate secretory lineage differentiation (112,113).

PGE2

Prostaglandin E2 (PGE2) has been reported to elevate β-catenin expression via cAMP/PKA, hence, enhancing wnt signaling. This PGE2/Wnt synergy has been found to control mouse stem cells in vitro (114), and zebrafish progenitor cells in vivo (115). In addition to maintaining LGR5+ colonic organoid culture viability (116). PGE2 has four receptors; EP1R to EP4R, the activation of EP2R and EP4R increases cyclic AMP production, while EP3R activation can have a diverse effect (117). PGF2α plays a key role in the regulation of the cervix by stimulating contractions of the myometrium (36).

1.4.4 Cervical organoids

Advances in female reproductive tract (FRT) modelling have been made in the past years. Organoids from the fallopian tubes (118), ovaries (119) and endometrium (95,96) have been reported. The majority of the established organoids are derived from single-lineage epithelial organs with simple or two-layered epithelia, thus cervical derivation is challenging to derive. In a recent study, Chumduri and colleagues (120) have generated organoids that recapitulate the site-specific epithelial architecture of the cervix, starting from adult cervical tissues. The term ‘cervical organoids’ describes both endo- and ecto-cervical organoids. The protocol generates organoids from anatomically normal tissues. Derivation of endocervical lineage required the presence of WNT signalling, while inhibition of Wnt was found critical for maintaining stratified squamous phenotype (79). Additionally, the paper reported that Notch signalling was key for squamous lineage differentiation in the junction (79). Although it is in

the early stages, cervical organoids if achieved right, can allow the study and understanding of the process of metaplasia, the technique could also assist identifying the origin of the progenitor cell in the cervix, in addition to settling the debate about HPV target cell.

1.5 Research objectives and thesis aims

The aim of this project is to understand the specific characteristics that renders the cervical epithelium to be vulnerable to the development of high-risk HPV-associated cancers. Like in other transition zones, the cervical transformation zone (TZ) is more liable to the development of HPV-associated cancers (49). The reason behind this is not clear, however, TZs are regions where the physiological change from columnar to squamous cell types takes place in a process of metaplasia (49). Additionally, it is thought to be a stem cell niche as it harbours a unique cell population called reserve cells (31). This has influenced hypotheses questioning the involvement of the TZ stem cell as a HPV target cell, however, the identity of this stem population is yet to be determined. Previous models of the cervix were mainly based on 2D cell lines, either carcinoma cells or primary immortalised, and can carry variety of mutations and chromosomal abnormalities. Such models do not represent the normal cervical cell-to-cell interaction, and since the main target of my project is to address basic questions about the role of reserve cells in maintaining the cervical TZ and in high-risk-HPV infections, the development an *in vitro* model that is truly representative of normal cervical epithelium is crucial. In recent years, advances using organoids to model the human tissue have been made (88). Organoids are 3D cell culture system that closely mimic the *in vivo* tissue of origin. At the time of starting this project, no established organoid model of the cervix has been reported. Therefore, I have followed the line of developing an *in vitro* organoid tissue culture model of the cervix. To do so, I planned my work in stages, with each stage contributing to my understanding of cervical biology and infection. The key steps in my research program are listed below:

- I start off by testing the validity of the current TZ progenitor theories (detailed in section 3.2.2) by examining a wide range of cervical tissue and using a panel of immunofluorescent antibodies.
- Second, I explored the utility of mouse models to study human cervical renewal dynamics, by following a time course of cervical development and used a set of immunofluorescent markers to identify epithelial lineages (section 3.2.3).

- Since having a physiologically relevant model is key for understanding the cellular to viral expression discrepancies, I start optimising the cervix organoids. Many organoid cultures start with mouse since it is more obtainable compared to human tissue (in chapter 4).
- The generation of murine cervix organoids provided a first insight as to how local factors may control the endocervix, the TZ, and the ectocervix. The goal was to utilise the model to study changes in cytokine expression, the patterns of signal transduction stimulation, and changes that are locally present at the site of metaplasia. This will provide insight into the mechanistic changes that regulates metaplasia and the role of reserve cells in this process.
- This was followed by optimisation of human cervical organoids (chapter 5). since the developed organoid model would also offer an indispensable HPV infection tool to study the different patterns of viral gene expression depending on the site of infection (ecto/endo/TZ).
- Last, I have also explored the use of lineage tracing transgenic mice (in 6.2.2), which will allow understanding the complex nature of the cervical transformation zone and the mechanisms that underlie HPV life cycle deregulation and progression to neoplasia.

Chapter 1 References

1 Swain A, Lovell-Badge R. Mammalian sex determination: a molecular drama. Genes Dev. 1999 Apr 1;13(7):755–67.

2 Goodfellow PN, Lovell-Badge R. SRY and Sex Determination in Mammals. Annu Rev Genet. 1993 Dec;27(1):71–92.

3 Sinclair AH, Berta P, Palmer MS, Hawkins JR, Griffiths BL, Smith MJ, et al. A gene from the human sex-determining region encodes a protein with homology to a conserved DNA-binding motif. Nature. 1990 Jul 19;346(6281):240–4.

4 Kashimada K, Koopman P. Sry: the master switch in mammalian sex determination. Development. 2010 Dec 1;137(23):3921–30.

5 Francavilla S, Cordeschi G, Properzi G, Concordia N, Cappa F, Pozzi V. Ultrastructure of fetal human gonad before sexual differentiation and during early testicular and ovarian development. J Submicrosc Cytol Pathol. 1990 Jul 1;22(3):389–400.

6 Sajjad Y. Development of the genital ducts and external genitalia in the early human embryo. J Obstet Gynaecol Res. 2010;36(5):929–37.

7 Yin Y, Ma L. Development of the mammalian female reproductive tract. J Biochem (Tokyo). 2005 Jun;137(6):677–83.

8 Du H, Taylor HS. The Role of Hox Genes in Female Reproductive Tract Development, Adult Function, and Fertility. Cold Spring Harb Perspect Med. 2016;6(1).

9 Colvin CW, Abdullatif H. Anatomy of female puberty: The clinical relevance of developmental changes in the reproductive system. Clin Anat N Y N. 2013 Jan;26(1):115–29.

10 El-Banna AA, Hafez ESE. The uterine cervix in mammals. Am J Obstet Gynecol. 1972 Jan 1;112(1):145–64.

11 Singer A, Jordan JA. The Functional Anatomy of the Cervix, the Cervical Epithelium and the Stroma. In: The Cervix. John Wiley & Sons, Ltd; 2009. p. 13–37.

12 Nott JP, Bonney EA, Pickering JD, Simpson NAB. The structure and function of the cervix during pregnancy. Transl Res Anat. 2016 Mar 1;2:1–7.

13 Manocha SL, Graham CE. Histochemistry of mouse cervical epithelium during chemical carcinogenesis. Histochem J. 1970 Sep 1;2(5):357–70.

14 Gould PR, Barter RA, Papadimitriou JM. An Ultrastructural, Cytochemical, and Autoradiographic Study of the Mucous Membrane of the Human Cervical Canal with Reference to Subcolumnar Basal Cells. p16.

15 Fluhmann CF. Cervix Uteri and Its Diseases. Elsevier Books, Oxford; 1961.

16 Jordan J, Singer A, Jones H, Shafi M. The Cervix. John Wiley & Sons; 2009. p681.

17 Dallenbach-Hellweg G, Doeberitz MV, Trunk-Gemacher M. Atlas of Histopathology of the Cervix Uteri. 2nd ed. Berlin Heidelberg: Springer-Verlag; 2006. p20.

18 Kim S, Coulombe PA. Intermediate filament scaffolds fulfill mechanical, organizational, and signaling functions in the cytoplasm. Genes Dev. 2007 Jul 1;21(13):1581–97.

19 Quinlan RA, Schiller DL, Hatzfeld M, Achtstätter T, Moll R, Jorcano JL, et al. Patterns of Expression and Organization of Cytokeratin Intermediate Filaments. Ann N Y Acad Sci. 1985;455(1):282–306.

20 Kurman RJ, editor. Blaustein's Pathology of the Female Genital Tract. 4th ed. New York: Springer-Verlag; 1994.

21 Kawaguchi K, Fujii S, Konishi I, Iwai T, Nanbu Y, Nonogaki H, et al. Immunohistochemical analysis of oestrogen receptors, progesterone receptors and Ki-67 in leiomyoma and myometrium during the menstrual cycle and pregnancy. Virchows Arch A. 1991 Jul 1;419(4):309–15.

22 Ivanyi D, Groeneveld E, Doornewaard GV, Mooi WJ, Hageman PC. Keratin Subtypes in Carcinomas of the Uterine Cervix: Implications for Histogenesis and Differential Diagnosis. :11.
23 Purkis PE, Steel JB, Mackenzie IC, Nathrath WB, Leigh IM, Lane EB. Antibody markers of basal cells in complex epithelia. J Cell Sci. 1990 Sep;97 (Pt1):39–50.
24 Fluhmann CF. The squamocolumnar transitional zone of the cervix uteri. Obstet Gynecol. 1959 Aug;14(2):133–48.
25 Anderson M. Pathology of the Uterine Cervix, Vagina, and Vulva. Vol 21. Major Problems in Pathology. J Clin Pathol. 1991 Jun;44(6):527.
26 Darwiche N, Celli G, Sly L, Lancillotti F, De Luca LM. Retinoid status controls the appearance of reserve cells and keratin expression in mouse cervical epithelium. Cancer Res. 1993 May 15;53(10 Suppl):2287–99.
27 Gimenez-Conti IB, Lynch M, Roop D, Bhowmik S, Majeski P, Conti CJ. Expression of keratins in mouse vaginal epithelium. Differentiation. 1994 May 1;56(3):143–51.
28 Hwang LY, Ma Y, Shiboski SC, Farhat S, Jonte J, Moscicki A-B. Active Squamous Metaplasia of the Cervical Epithelium Is Associated with Subsequent Acquisition of Human Papillomavirus 16 Infection Among Healthy Young Women. J Infect Dis. 2012 Aug 15;206(4):504–11.
29 Herfs M, Yamamoto Y, Laury A, Wang X, Nucci MR, McLaughlin-Drubin ME, et al. A discrete population of squamocolumnar junction cells implicated in the pathogenesis of cervical cancer. Proc Natl Acad Sci U S A. 2012 Jun 26;109(26):10516–21.
30 Martens JE, Smedts F, van Muyden RCPA, Schoots C, Helmerhorst TJM, Hopman A, et al. Reserve cells in human uterine cervical epithelium are derived from müllerian epithelium at midgestational age. Int J Gynecol Pathol Off J Int Soc Gynecol Pathol. 2007 Oct;26(4):463–8.
31 Martens JE, Arends J. Cytokeratin 17 and p63 are Markers of the HPV Target Cell, the Cervical Stem Cell. ANTICANCER Res. 2004;6.
32 Kurita T, Cooke PS, Cunha GR. Epithelial–Stromal Tissue Interaction in Paramesonephric (Müllerian) Epithelial Differentiation. Dev Biol. 2001 Dec;240(1):194–211.
33 Katz DF. Human cervical mucus: research update. Am J Obstet Gynecol. 1991 Dec;165(6 Pt 2):1984–6.
34 Medley N, Poljak B, Mammarella S, Alfirevic Z. Clinical guidelines for prevention and management of preterm birth: a systematic review. BJOG Int J Obstet Gynaecol. 2018 Oct;125(11):1361–9.
35 Cao Z-Y, Eppenberger U, Roos W, Torhorst J, Almendral A. Cytosol estrogen and progesterone receptor levels measured in normal and pathological tissue of endometrium, endocervical mucosa and cervical vaginal portion. Arch Gynecol. 1983 Apr 1;233(2):109–19.
36 Fernandes CB, Loux SC, Scoggin KE, Squires EL, Troedsson MH, Esteller-Vico A, et al. Sex-steroid receptors, prostaglandin E2 receptors, and cyclooxygenase in the equine cervix during estrus, diestrus and pregnancy: Gene expression and cellular localization. Anim Reprod Sci. 2017 Dec 1;187:141–51.
37 Gaton E, Zejdel L, Bernstein D, Glezerman M, Czernobilsky B, Insler V. The effect of estrogen and gestagen on the mucus production of human endocervical cells: a histochemical study. Fertil Steril. 1982 Nov 1;38(5):580–5.
38 Van Kooij RJ, Roelofs HJM, Kathmann GAM, Kramer MF. Human Cervical Mucus and its Mucous Glycoprotein during the Menstrual Cycle**Some preliminary results of this study have been published in Glycoconjugates: Proceedings of the Fifth International Symposium, Kiel, Federal Republic of Germany, Edited by R. Schauer, P. Boer, E. Buddecke, M. F. Kramer, J. F. G. Vliegenthart, and H. Wiegandt. Stuttgart, Georg Thieme Verlag, 1979, p546. Fertil Steril. 1980 Sep 1;34(3):226–33.

39 Vooijs GP. The problem of replacement and differentiation of the intestinal epithelium. Cancer Cytopathol. 1997;81(6):317–22.
40 Fluhmann CF. The histogenesis of squamous cell metaplasia of the cervix and endometrium. Surg Gynecol Obstet. 1953 Jul;97(1):45–58.
41 Meyer R. Die Epithelentwicklung der Cervix and Portio vaginalis uteri und die Pseudo-erosio congenital. Arch Gynǎk. 1910;91,579,658.
42 Hellman LM, Rosenthal AH, Kistner RW, Gordon R. Some factors influencing the proliferation of the reserve cells in the human cervix. Am J Obstet Gynecol. 1954 Apr 1;67(4):899–915.
43 Meyer R. über Epidermoidalisierung (Ersatz des Schleimepithels durch Plattenepithel) an der Portio vaginalis uteri nach Erosion, an Cervicalpolypen und in der Cervicalschlemhaut. Ein Beitrag zue Prage der Stückchendiagnose und des präcancerösen Stadiums. ZblGynǎk. 1923;(47):946.
44 Schürch W, McDowell EM, Trump BF. Long-Term Organ Culture of Human Uterine Endocervix. Cancer Res. 1978 Nov 1;38(11 Part 1):3723–33.
45 Lawrence WD, Shingleton HM. Early physiologic squamous metaplasia of the cervix: light and electron microscopic observations. Am J Obstet Gynecol. 1980 Jul 15;137(6):661–71.
46 Yang A, Kaghad M, Wang Y, Gillett E, Fleming MD, Dötsch V, et al. p63, a p53 homolog at 3q27-29, encodes multiple products with transactivating, death-inducing, and dominant-negative activities. Mol Cell. 1998 Sep;2(3):305–16.
47 Kurita T, Cunha GR, Robboy SJ, Mills AA, Medina RT. Differential expression of p63 isoforms in female reproductive organs. Mech Dev. 2005 Sep;122(9):1043–55.
48 Weikel W, Wagner R, Moll R. Characterization of subcolumnar reserve cells and other epithelia of human uterine cervix. Virchows Arch B. 1987 Dec 1;54(1):381–381.
49 Mcnairn AJ, Guasch G. Epithelial transition zones: merging microenvironments, niches, and cellular transformation. Eur J Dermatol EJD. 2011 May;21 Suppl 2:21–8.
50 zur Hausen H, Gissmann L, Steiner W, Dippold W, Dreger I. Human papilloma viruses and cancer. Bibl Haematol. 1975 Oct;(43):569–71.
51 zur Hausen H. Papillomaviruses and cancer: from basic studies to clinical application. Nat Rev Cancer. 2002 May;2(5):342–50.
52 Egawa N, Egawa K, Griffin H, Doorbar J. Human Papillomaviruses; Epithelial Tropisms, and the Development of Neoplasia. Viruses. 2015 Jul 16;7(7):3863–90.
53 Parkin DM, Bray F. Chapter 2: The burden of HPV-related cancers. Vaccine. 2006 Aug 31;24 Suppl 3:S3/11-25.
54 Regauer S, Reich O. CK17 and p16 expression patterns distinguish (atypical) immature squamous metaplasia from high-grade cervical intraepithelial neoplasia (CIN III). Histopathology. 2007;50(5):629–35.
55 Escobar-Hoyos LF, Yang J, Zhu J, Cavallo J-A, Zhai H, Burke S, et al. Keratin 17 in premalignant and malignant squamous lesions of the cervix: proteomic discovery and immunohistochemical validation as a diagnostic and prognostic biomarker. Mod Pathol Off J U S Can Acad Pathol Inc. 2014 Apr;27(4):621–30.
56 Stanley MA. Epithelial Cell Responses to Infection with Human Papillomavirus. Clin Microbiol Rev. 2012 Apr 1;25(2):215–22.
57 Nasu K, Narahara H. Pattern recognition via the toll-like receptor system in the human female genital tract. Mediators Inflamm. 2010;2010:976024.
58 Miller LS, Modlin RL. Human keratinocyte Toll-like receptors promote distinct immune responses. J Invest Dermatol. 2007 Feb;127(2):262–3.
59 Hibma MH. The Immune Response to Papillomavirus During Infection Persistence and Regression. Open Virol J. 2012 Dec 28;6:241–8.

60 Kanodia S, Fahey LM, Kast WM. Mechanisms used by human papillomaviruses to escape the host immune response. Curr Cancer Drug Targets. 2007 Feb;7(1):79–89.
61 Georgopoulos NT, Proffitt JL, Blair GE. Transcriptional regulation of the major histocompatibility complex (MHC) class I heavy chain, TAP1 and LMP2 genes by the human papillomavirus (HPV) type 6b, 16 and 18 E7 oncoproteins. Oncogene. 2000 Oct 5;19(42):4930–5.
62 Amella CA, Lofgren LA, Ronn AM, Nouri M, Shikowitz MJ, Steinberg BM. Latent infection induced with cottontail rabbit papillomavirus. A model for human papillomavirus latency. Am J Pathol. 1994 Jun;144(6):1167–71.
63 Maglennon GA, McIntosh P, Doorbar J. Persistence of viral DNA in the epithelial basal layer suggests a model for papillomavirus latency following immune regression. Virology. 2011 Jun 5;414(2):153–63.
64 Maglennon GA, McIntosh PB, Doorbar J. Immunosuppression Facilitates the Reactivation of Latent Papillomavirus Infections. J Virol. 2014 Jan;88(1):710–6.
65 Doorbar J, Quint W, Banks L, Bravo IG, Stoler M, Broker TR, et al. The Biology and Life-Cycle of Human Papillomaviruses. Vaccine. 2012 Nov 20;30:F55–70.
66 Doorbar J. Host control of human papillomavirus infection and disease. Best Pract Res Clin Obstet Gynaecol. 2018 Feb 1;47:27–41.
67 Doorbar J, Griffin H. Refining our understanding of cervical neoplasia and its cellular origins. Papillomavirus Res. 2019 Apr 8;7:176–9.
68 GEY GO. Tissue culture studies of the proliferative capacity of cervical carcinoma and normal epithelium. Cancer Res. 1952;12:264–5.
69 Lucey BP, Nelson-Rees WA, Hutchins GM. Henrietta Lacks, HeLa Cells, and Cell Culture Contamination. Arch Pathol Lab Med. 2009 Sep 1;133(9):1463–7.
70 Friedl F, Kimura I, Osato T, Ito Y. Studies on a new human cell line (SiHa) derived from carcinoma of uterus. I. Its establishment and morphology. Proc Soc Exp Biol Med Soc Exp Biol Med N Y N. 1970 Nov;135(2):543–5.
71 Auersperg N. Long-term cultivation of hypodiploid human tumor cells. J Natl Cancer Inst. 1964 Jan;32:135–63.
72 Pattillo RA, Hussa RO, Story MT, Ruckert AC, Shalaby MR, Mattingly RF. Tumor antigen and human chorionic gonadotropin in CaSki cells: a new epidermoid cervical cancer cell line. Science. 1977 Jun 24;196(4297):1456–8.
73 Schlegel R, Phelps WC, Zhang YL, Barbosa M. Quantitative keratinocyte assay detects two biological activities of human papillomavirus DNA and identifies viral types associated with cervical carcinoma. EMBO J. 1988 Oct 1;7(10):3181–7.
74 Choi M, Park M, Lee S, Lee JW, Cho MC, Noh M, et al. Establishment of Immortalized Primary Human Foreskin Keratinocytes and Their Application to Toxicity Assessment and Three-Dimensional Skin Culture Construction. Biomol Ther. 2017 May;25(3):296–307.
75 Baden HP, Kubilus J, Kvedar JC, Steinberg ML, Wolman SR. Isolation and characterization of a spontaneously arising long-lived line of human keratinocytes (NM 1). Vitro Cell Dev Biol J Tissue Cult Assoc. 1987 Mar;23(3):205–13.
76 Boukamp P, Petrussevska RT, Breitkreutz D, Hornung J, Markham A, Fusenig NE. Normal keratinization in a spontaneously immortalized aneuploid human keratinocyte cell line. J Cell Biol. 1988 Mar;106(3):761–71.
77 Allen-Hoffmann BL, Schlosser SJ, Ivarie CAR, Meisner LF, O'Connor SL, Sattler CA. Normal Growth and Differentiation in a Spontaneously Immortalized Near-Diploid Human Keratinocyte Cell Line, NIKS. J Invest Dermatol. 2000 Mar 1;114(3):444–55.
78 Lehman TA, Modali R, Boukamp P, Stanek J, Bennett WP, Welsh JA, et al. p53 mutations in human immortalized epithelial cell lines. Carcinogenesis. 1993 May;14(5):833–9.

79 Jacobs N, Moutschen MP, Franzen-Detrooz E, Boniver V, Boniver J, Delvenne P. Organotypic culture of HPV-transformed keratinocytes: a model for testing lymphocyte infiltration of (pre)neoplastic lesions of the uterine cervix. Virchows Arch Int J Pathol. 1998 Apr;432(4):323–30.
80 Michelini M, Rosellini A, Papini S, Revoltella RP, Michelini M, Rosellini A, et al. A three-dimensional organotypic culture of the human uterine exocervix for studying mucosal epithelial differentiation and migrating leukocytes. Differentiation. 2004 Apr 1;72(4):138–49.
81 Herber R, Liem A, Pitot H, Lambert PF. Squamous epithelial hyperplasia and carcinoma in mice transgenic for the human papillomavirus type 16 E7 oncogene. J Virol. 1996 Mar;70(3):1873–81.
82 Riley RR, Duensing S, Brake T, Münger K, Lambert PF, Arbeit JM. Dissection of human papillomavirus E6 and E7 function in transgenic mouse models of cervical carcinogenesis. Cancer Res. 2003 Aug 15;63(16):4862–71.
83 Cheon D-J, Orsulic S. Mouse models of cancer. Annu Rev Pathol. 2011;6:95–119.
84 Rangarajan A, Weinberg RA. Opinion: Comparative biology of mouse versus human cells: modelling human cancer in mice. Nat Rev Cancer. 2003;3(12):952–9.
85 Xu C, Li X, Liu P, Li M, Luo F. Patient-derived xenograft mouse models: A high fidelity tool for individualized medicine (Review). Oncol Lett. 2018 Dec 31;17(1):3–10.
86 Hoffmann C, Bachran C, Stanke J, Elezkurtaj S, Kaufmann AM, Fuchs H, et al. Creation and characterization of a xenograft model for human cervical cancer. Gynecol Oncol. 2010 Jul;118(1):76–80.
87 Lancaster MA, Huch M. Disease modelling in human organoids. Dis Model Mech. 2019 Jul 1;12(7).
88 Sato T, Vries RG, Snippert HJ, van de Wetering M, Barker N, Stange DE, et al. Single Lgr5 stem cells build crypt-villus structures in vitro without a mesenchymal niche. Nature. 2009 May 14;459(7244):262–5.
89 Barker N, Huch M, Kujala P, van de Wetering M, Snippert HJ, van Es JH, et al. Lgr5(+ve) stem cells drive self-renewal in the stomach and build long-lived gastric units in vitro. Cell Stem Cell. 2010 Jan 8;6(1):25–36.
90 Huch M, Dorrell C, Boj SF, van Es JH, Li VSW, van de Wetering M, et al. In vitro expansion of single Lgr5+ liver stem cells induced by Wnt-driven regeneration. Nature. 2013 Feb 14;494(7436):247–50.
91 Sato T, Stange DE, Ferrante M, Vries RGJ, Van Es JH, Van den Brink S, et al. Long-term expansion of epithelial organoids from human colon, adenoma, adenocarcinoma, and Barrett's epithelium. Gastroenterology. 2011 Nov;141(5):1762–72.
92 Huch M, Bonfanti P, Boj SF, Sato T, Loomans CJM, van de Wetering M, et al. Unlimited in vitro expansion of adult bi-potent pancreas progenitors through the Lgr5/R-spondin axis. EMBO J. 2013 Oct 16;32(20):2708–21.
93 Dye BR, Hill DR, Ferguson MA, Tsai Y-H, Nagy MS, Dyal R, et al. In vitro generation of human pluripotent stem cell derived lung organoids. eLife ;4.
94 Karthaus WR, Iaquinta PJ, Drost J, Gracanin A, van Boxtel R, Wongvipat J, et al. Identification of multipotent luminal progenitor cells in human prostate organoid cultures. Cell. 2014 Sep 25;159(1):163–75.
95 Turco MY, Gardner L, Hughes J, Cindrova-Davies T, Gomez MJ, Farrell L, et al. Long-term, hormone-responsive organoid cultures of human endometrium in a chemically defined medium. Nat Cell Biol. 2017 Apr 10;19:568.
96 Boretto M, Cox B, Noben M, Hendriks N, Fassbender A, Roose H, et al. Development of organoids from mouse and human endometrium showing endometrial epithelium physiology and long-term expandability. Dev Camb Engl. 2017 15;144(10):1775–86.

97 Clevers H. Modeling Development and Disease with Organoids. Cell. 2016 Jun 16;165(7):1586–97.
98 Soonthornthum T, Arias-Pulido H, Joste N, Lomo L, Muller C, Rutledge T, et al. Epidermal growth factor receptor as a biomarker for cervical cancer. Ann Oncol. 2011 Oct 1;22(10):2166–78.
99 Muñoz Bello JO, Olmedo Nieva L, Contreras Paredes A, Fuentes Gonzalez AM, Rocha Zavaleta L, Lizano M. Regulation of the Wnt/β-Catenin Signaling Pathway by Human Papillomavirus E6 and E7 Oncoproteins. Viruses. 2015 Aug 19;7(8):4734–55.
100 Date S, Sato T. Mini-gut organoids: reconstitution of the stem cell niche. Annu Rev Cell Dev Biol. 2015;31:269–89.
101 He X, Semenov M, Tamai K, Zeng X. LDL receptor-related proteins 5 and 6 in Wnt/beta-catenin signaling: arrows point the way. Dev Camb Engl. 2004 Apr;131(8):1663–77.
102 Clevers H, Nusse R. Wnt/β-Catenin Signaling and Disease. Cell. 2012 Jun 8;149(6):1192–205.
103 Logan CY, Nusse R. The Wnt signaling pathway in development and disease. Annu Rev Cell Dev Biol. 2004;20:781–810.
104 de Lau W, Peng WC, Gros P, Clevers H. The R-spondin/Lgr5/Rnf43 module: regulator of Wnt signal strength. Genes Dev. 2014 Feb 15;28(4):305–16.
105 Hao H-X, Xie Y, Zhang Y, Charlat O, Oster E, Avello M, et al. ZNRF3 promotes Wnt receptor turnover in an R-spondin-sensitive manner. Nature. 2012 Apr 29;485(7397):195–200.
106 Roberts AB, Heine UI, Flanders KC, Sporn MB. Transforming growth factor-beta. Major role in regulation of extracellular matrix. Ann N Y Acad Sci. 1990;580:225–32.
107 Laronda MM, Unno K, Ishi K, Serna VA, Butler LM, Mills AA, et al. Diethylstilbestrol induces vaginal adenosis by disrupting SMAD/RUNX1-mediated cell fate decision in the Müllerian duct epithelium. Dev Biol. 2013 Sep 1;381(1):5–16.
108 Carpenter G, Cohen S. Epidermal growth factor. J Biol Chem. 1990 May 15;265(14):7709–12.
109 Herbst RS. Review of epidermal growth factor receptor biology. Int J Radiat Oncol Biol Phys. 2004;59(2 Suppl):21–6.
110 Terakawa J, Rocchi A, Serna VA, Bottinger EP, Graff JM, Kurita T. FGFR2IIIb-MAPK Activity Is Required for Epithelial Cell Fate Decision in the Lower Müllerian Duct. Mol Endocrinol Baltim Md. 2016 Jul;30(7):783–95.
111 Tsai Y-H, VanDussen KL, Sawey ET, Wade AW, Kasper C, Rakshit S, et al. ADAM10 regulates Notch function in intestinal stem cells of mice. Gastroenterology. 2014 Oct;147(4):822-834.e13.
112 Jensen J, Pedersen EE, Galante P, Hald J, Heller RS, Ishibashi M, et al. Control of endodermal endocrine development by Hes-1. Nat Genet. 2000 Jan;24(1):36–44.
113 Es JH van, Gijn ME van, Riccio O, Born M van den, Vooijs M, Begthel H, et al. Notch/γ-secretase inhibition turns proliferative cells in intestinal crypts and adenomas into goblet cells. Nature. 2005 Jun;435(7044):959–63.
114 North TE, Goessling W, Walkley CR, Lengerke C, Kopani KR, Lord AM, et al. Prostaglandin E2 regulates vertebrate haematopoietic stem cell homeostasis. Nature. 2007 Jun 21;447(7147):1007–11.
115 Goessling W, North TE, Loewer S, Lord AM, Lee S, Stoick-Cooper CL, et al. Genetic interaction of PGE2 and Wnt signaling regulates developmental specification of stem cells and regeneration. Cell. 2009 Mar 20;136(6):1136–47.
116 Fan Y-Y, Davidson LA, Callaway ES, Goldsby JS, Chapkin RS. Differential effects of 2- and 3-series E-prostaglandins on in vitro expansion of Lgr5 + colonic stem cells. Carcinogenesis. 2014 Mar 1;35(3):606–12.
117 Negishi M, Sugimoto Y, Ichikawa A. Prostaglandin E receptors. J Lipid Mediat Cell Signal. 1995 Oct 1;12(2):379–91.

118 Kessler M, Hoffmann K, Brinkmann V, Thieck O, Jackisch S, Toelle B, et al. The Notch and Wnt pathways regulate stemness and differentiation in human fallopian tube organoids. Nat Commun. 2015 Dec 8;6(1):1–11.
119 Dumont S, Jan Z, Heremans R, Van Gorp T, Vergote I, Timmerman D. Organoids of epithelial ovarian cancer as an emerging preclinical in vitro tool: a review. J Ovarian Res. 2019 Nov 8;12(1):105.
120 Chumduri C, Gurumurthy RK, Berger H, Koster S, Brinkmann V, Klemm U, et al. Transition of Wnt signaling microenvironment delineates the squamo-columnar junction and emergence of squamous metaplasia of the cervix. bioRxiv. 2018 Oct 16;443770.
121 Griffin H, Soneji Y, Van Baars R, Arora R, Jenkins D, van de Sandt M, et al. Stratification of HPV-Induced Cervical Pathology using the Virally-Encoded Molecular Marker E4 in Combination with p16 or MCM. Mod Pathol Off J U S Can Acad Pathol Inc. 2015 Jul;28(7):977–93.
122 Kranjec C, Holleywood C, Libert D, Griffin H, Mahmood R, Isaacson E, et al. Modulation of basal cell fate during productive and transforming HPV-16 infection is mediated by progressive E6-driven depletion of Notch. J Pathol. 2017 Aug;242(4):448–62.
123 Kranjec C, Doorbar J. Human papillomavirus infection and induction of neoplasia: a matter of fitness. Curr Opin Virol. 2016;20:129–36.

2 Materials and methods

2.1 Tissue samples and cell culture

2.1.1 Human

Human samples used for immunohistochemistry, were provided from cervical biopsies of hysterectomy patients for benign, HPV unrelated conditions from Odense University Hospital, Demark. Local ethical approval for the study was obtained from the Institutional Review Board of Odense University Hospital. Tissue samples were transferred to the Department of Pathology, University of Cambridge under an agreement with the Region Syddanmark.
For human cervical organoid derivation and immunofluorescent images, samples were obtained via ethical approval to for fresh cervical benign hysterectomy tissue from the human tissue bank at Addenbrooke's University Hospital in Cambridge.

2.1.2 Mice

For mouse time course images and murine cervical organoid derivation, *C57BL/6J* (*JAX®*, 000664) adult mice between the age of 2 to 14 weeks were used.
For lineage tracing and transgenic mice immunofluorescent images *Krt17*$^{tm1(Cre,Cerulean)Murr}$ (*JAX®*, #018151) X B6.Cg-*Gt(ROSA)26Sor*$^{tm9(CAG\text{-}tdTomato)Hze}$/J (*JAX®*, #007909) And *Krt17*^{CreERT2} (1) X B6.Cg-*Gt(ROSA)26Sor*$^{tm6(CAG\text{-}ZsGreen1)Hze}$/J (*JAX®*, #007906) lines were used. Husbandry and experimental work were done conducted according to local ethical committee and UK Home Office regulations and were carried out under the licence of J.Doorbar.

2.1.2.1 Tamoxifen injections

Tamoxifen (Sigma-Aldrich) was dissolved in sunflower oil and was injected at final of 2 mg/ml intraperitoneally according to experimental protocol. Oil only was injected to controls.

2.1.3 Cell isolation

2.1.3.1 Human

Several approaches have been tested for isolating cells from human cervical tissue (optimisation described in chapter 5). The method that proved best at extracting human cervical cells was to first separate the dermis from the epidermis mechanically (with curved surgical scissors), followed by finely mincing the epidermis strip with surgical blade. The minced tissue

is then incubated for 30 min Trypsin (0.15%) at 37ºC with shaking (this process is repeated twice, with collecting the produced cells from the 1st round). The remaining epidermis mince is then incubated with 0.4mg/mL Collagenase V (Sigma, C-9263) diluted in DMEM at 37ºC with shaking. The suspension is collected with the suspension produced from trypsin.

2.1.3.2 Mice

Mice cervixes were minced and placed in basal media (Table 2.2) with dispase (0.5µg/ml Roche-applied-science, 04942078001) and amphotericin B (2.5µg/ml Sigma, A2942) overnight at 4ºC. The following day, the suspension was centrifuged (0.5 relative centrifugal force (rcf) for 5 minutes) then trypsinised in 10 mL of 0.15% trypsin for 10 minutes at 37ºC. The suspension was subsequently centrifuged, and the supernatant was collected, the process was repeated again before filtration through a 100um Cell Strainer (Falcon, catalogue no. 352360). Cells were further pelleted and washed with DMEM/F12, then plated in 20µl droplets of Matrigel® (Corning, 536231) using 48 well plates (costar, catalogue no. 3548) and incubated at 37.5ºC for 15 minutes to allow the Matrigel® to set (Figure 2.1) 250µl of corresponding medium was added to each well and placed at 37.5ºC in a 5% CO2 incubator. Culture medium was changed every 24-72 hours depending on the rate of cell growth and the change of pH indicated by phenol red.

2.1.4 Cell culture

EGF, Noggin and R-spondin1 (*ENR*) medium (4) was used as a basal medium (Table 2.1) Additional factors listed (Table 2.2) were added depending on the experiment. Cells were passaged approximately every 7-9 days, this was done when the cells were too dense, the Matrigel® became unstable, or the cells started to attach to the well. Passaging was performed by vigorous pipetting using an Eppendorf Xplorer® plus automated pipette at a volume of 150µl/maximum speed operated 300 times, washed with cold DMEM/F12 and repeated three times before plating again. The magnitude of splitting was estimated from the density of the plate and the size of the pellet before plating (estimated to 1:20 dilution). For ectocervical squamous organoids and additional dissociation step was carries out post manual pipetting with TrypLE® (Gibco, 12604021).

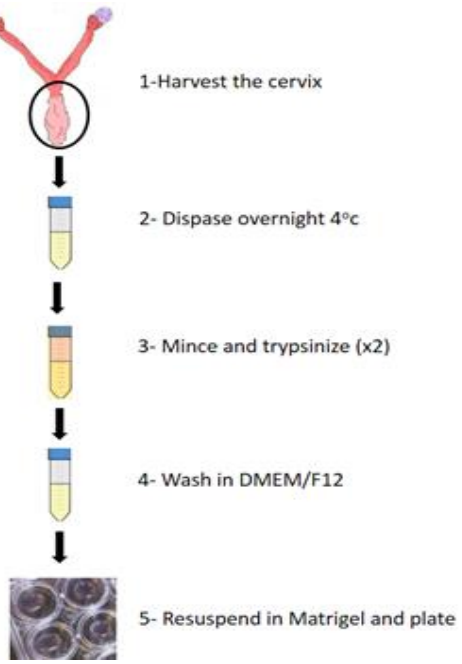

Figure 2.1: Summary of murine cervical epithelium isolation procedure for the generation of cervical organoids. Dispase incubation follows cervix harvest, then trypsin digestion the next day before medium wash and plating with Matrigel®.

Table 2.1: Components of ENR basal medium.

Reagent	Volume for 10mL	Stock	Final concentration	Manufacturer	Catalogue number
DMEM/F12	9.5 mL	X1	X1	Invitrogen	12634010
HEPES	95 µL	1 M	10 mM	Gibco	15630080
B27	200 µL	X50	X1	Invitrogen	12587010
L-Glutamine	100 µL	X100	2 mM	Gibco	25030081
N2	100 µL	X100	X1	Invitrogen	17502048
N-Acetyl-L-cysteine (NAC)	25 µL	X400	1.25 mM	Sigma	A9165-5G
Primocin	20 µL	X500	100 µg/mL	Invitrogen	Ant-pm-1
Noggin	10 µL	X1000	50 ng/mL	Peprotech	250-38
R-spondin	10 µL	X1000	500 ng/mL	Peprotech	120-39
EGF	5 µL	X2000	50 ng/mL	Peprotech	PMG8043

Table 2.2: Additional factors added to ENR.

Reagent	stock	Final concentration	Manufacturer	Catalogue number
A83-01 (TGFβi)	1 mM	500 nM	Tocris Bioscience	2939
FGF-10	100 µg/mL	100 ng/mL	PeproTech	100-26
Prostaglandin E2 (PGE2)	25 mM	25 nM	Tocris Bioscience	2296
MAPK p38 inhibitor (p38i)	10 mM	10 µM	Tocris Bioscience	1264
Nicotinamide	1 M	10 mM	Sigma-Aldrich	N0636
Activin A	X500	20 ng/mL	R&D systems	338-AC-010
HGF	50 µg/mL	50 ng/mL	Peprotech	100-39H
FGF-2	50 µg/mL	50 ng/mL	Peprotech	100-18B
CHIR99021 (GSK-3i)	1 mM	1 µM	Tocris Bioscience	4423
BMP7	100 µg/mL	100 ng/ml	Peprotech	120-03

Table 2.3: Different media tested for murine cervical organoid culture.

Factor	ENR	ENR-A	ENR-F	ENR-AF
A83-01 (TGFβi)	-	+	-	+
Fgf10	-	-	+	+

2.1.5 Freezing media

For freezing of organoid cultures, 70% of corresponding organoid medium was added to 20% FBS and 10% DMSO.

2.1.6 Organoid formation efficiency

For organoid formation efficiency quantification, organoid cultures were dissociated to single cells using TrypLE Express (Thermo fisher) for 5min at 37ºC before passed through a 0.2µm strainer. Cells were counted and a total of 1000 cells were seeded per well, with a total of 3 wells per condition. Medium was changed every three day and the organoid number was counted using optical microscopy 7-10 days post seeding.

2.2 Genotyping

2.2.1 DNA isolation from ear biopsies

Ear notches from mice were treated with 100 µl Chelex solution at 50°C for 45 minutes. Subsequently, samples were boiled at 95°C for 30 minutes to inactivate proteinase K enzyme. The resin was pelleted at 13,000 rpm and DNA was collected from the supernatant.

2.2.2 Genotyping by polymerase chain reaction (PCR)

For *Krt17*$^{tm1(Cre,Cerulean)Murr}$ touchdown PCR genotyping assay (2) with accordance to Jackson lab suggestion, the following primers were used in the PCR reaction (Table 2.4) forward: CTTCCATGCAGGGGACTGA, wild type reverse: TTCACTTCAGGTCAG CAAGC, mutant reverse: AATCGCGAACATCTTCAGGT, with expected band readout being, 460 bp for mutant , 310 bp and 460 bp for heterozygote and 310 bp for wild type. The initial annealing step of the reaction was done at 94ºC, followed by touchdown 10 cycles of (94ºC, 65ºC, 68ºC) where the annealing temperature is dropped by 0.5ºC per cycle, followed by 28 cycles of (94ºC, 60ºC, 72ºC) then a final extension at 72ºC.

Table 2.4: PCR reaction components and final concentrations used to carry out transgenic mice genotyping.

Reaction component	Final concentration
ddH2O	x
Kapa 2G HS buffer	1.30 X
MgCl2	2.60 mM
dNTPS-kapa	0.26 mM
Forward primer	0.50 uM
Reverse primer	0.50 uM
Glycerol	6.50 %
Dye	1.00 X
Kapa 2G HS taq polym	0.03 U/ul
DNA	x

Same touchdown PCR approach described above was done for tdTomato, using the reaction components in table 2.1 with accordance to Jackson lab suggestion, with the following primers used; wild type forward: AAGGGAGCTGCAGTG GAGTA, wild type reverse: CCGAAAATCTGTGGGAAGTC, mutant reverse (WPRE):

GGCATTAAAGCAGCGTATCC and mutant forward (tdTomato): CTGTTCCTGTACGGC ATGG.

For *Krt17CreERT2,* Cre detection was done using standard PCR using the following primers; cre forward: GCGGTCTGGCAGTAAAAACTATA and cre reverse: AGCGTTTTCGTTCTGCCAAT. And for *R26RZsGreen,* touchdown PCR approach described above was applied using the following primers; wild type forward: AAGGGAGCTGCAGTGGAGTA, wild type reverse: CCGAAAATCTGTGGGAAGTC, mutant forward (ZsGreen): AACCAGAAG TGGCACCTGAC and mutant reverse (WPRE): GGCATTAAAGCAGCGTATCC.

2.3 Laser capture

Laser Microdissection (LCM) method was optimised based on the protocol published by Erickson *et al.* (3). 3, 11-week-old mice were harvested and collected in Optimal cutting temperature compound (OCT compound) and subsequently frozen in -80ºC. Frozen mouse cervix sections were later cut to a thickness of 8µm using a cryostat and mounted on Polyethylene naphthalate (PEN) membrane frame slides (Life Technologies, Carlsbad, CA, USA), and stored in a 50ml falcon tube with silica beads to avoid moisture before stored in -80ºC. Before the laser cut, Cresyl Violet stain was used to visualise the structure of the epithelium (0.02mg of Cresyl Violet stain powder was mixed with 5ml of 100% ethanol, then strained by 0.2µm filter). LCM was performed using the ZEISS PALM MicroBeam (P.A.L.M. Microlaser Technologies, Bernried, Germany), infrared laser was used to melt the cap polymers to areas of interest and a UV laser was used to cut these selected cell populations, which were then collected on the cap. Collected cuts were incubated in the lysis buffer, and RNA extraction was carried out using the Arcturus PicoPure RNA Isolation Kit (Life Technologies, Carlsbad, CA, USA) according to the manufacturer's protocol. Approximately a total area of 50,000µm was aimed for within 30 minutes from the beginning to end of the procedure to ensure RNA integrity.

2.4 Cell sorting

To obtain single cell suspension from organoids, manual pipetting was carried out as described above in organoid formation protocol, followed by enzymatic digestion with TrypLE™ before passing the cells in 0.2µm strainer. Cells were blocked in 1% FBS in DPBS without Calcium

and Magnesium (ThermoFisher Scientific, 14190136). Cells were sorted using a DakoCytomation MoFlo cytometer and Summit 4.3 software.

2.5 Imaging and immunofluorescence

2.5.1 Human

For immunohistochemistry slides, the biopsies were fixed in 10% Neutral buffered formalin (NBF) and embedded in paraffin. Biopsy blocks were sequentially sectioned every 8μm and were stained for Krt17 (Cytokeratin 17) antibody followed by detection using horseradish peroxidase (HRP) and development with by 3,3′-Diaminobenzidine (DAB) at UCL Advanced Diagnostics using Leica automated system.

For Immunofluorescence, drying of paraffin embedded sections was carried out by overnight incubation in a 60ºC oven. Subsequently, sections were de-waxed in xylene for 10 minutes and then once again for 5 minutes. Gradual rehydration was then performed; twice in 100% ethanol, followed by 80%, 50% and 30% ethanol for two minutes for each step, then hydrated in dH2O for five minutes before being washed with PBS twice; 10 minutes then 5 minutes (rocking). Slides were then soaked in antigen retrieval solution (10mM citric acid, 0.05% Tween 20, pH6), and boiled in a pressure cooker at 110ºC for 15 minutes. After the antigen retrieval step, slides were washed twice in PBS (as described above), before marking around the tissue with a hydrophobic pen (ImmEdgeTM by Vector). Slides were then blocked in 2.5% horse serum/in PBS for 30 minutes in a humidity chamber. Antibody binding was detected using tyramide signal amplification (TSA) method using an ImmPRESS™ HRP Anti-Rabbit IgG (Peroxidase) Polymer Detection Kit (Vectorlabs, catalogue no. MP-7401) and ImmPRESS™ HRP Anti-Mouse IgG (Peroxidase) Polymer Detection Kit (Vectorlabs, catalogue no. MP-7402).

2.5.2 Mouse

2.5.2.1 Paraffin-embedded sections

Mouse cervixes were fixed in NBF and embedded in paraffin overnight. Organoids were incubated in Corning Cell Recovery Solution (Catalogue no.354253) for 1 hour on ice to dissolve the Matrigel®. Cells were then washed in ice cold PBS and centrifuged for 6 minutes at 0.6rcf, before being fixed in NBF for 20 minutes at room temperature. Organoids were subsequently suspended in liquid agar (2% agarose in PBS), poured into cloning rings (7mm diameter) and left to set. Once solidified, they were embedded in paraffin and the same protocol described in section 2.8.1 was applied.

2.5.2.2 Frozen sections

Mouse cervixes were fixed in cutting temperature compound (OCT) and allowed to freeze on pre-cooled acetone (-20°C) for 5-10 minutes, before transferred to -80°C until needed.

2.5.3 Cytospin Technique

Cell suspension of $5x10^5$/ml was prepared with 10% Fetal Calf Serum, and the slides were mounted with the paper pad and the cuvette in the metal holder, 200µl of cell suspension was loaded and cytocentrifuged at 800 rpm for 5 min. slides were left to dry at room temperature for 24 hours.

Table 2.5: Primary antibodies used to characterise murine cervical organoids and follow up experiments.

Antibody	Dilution	Host	Amplification	Manufacturer	Catalogue number
Pan-keratin	1:100	Mouse	-	SIGMA-ALDRICH	C2562
Cytokeratin 17	1:250	Rabbit	-	abcam	ab51056
Cytokeratin 15	1:50	Rabbit	-	abcam	ab52816
Cytokeratin 13	1:100	Mouse	-	abcam	ab16112
Cytokeratin 8	1:50	Mouse	-	Santa Cruz	ac-374275
Cytokeratin 7	1:100	Rabbit	-	abcam	ab181598
Cytokeratin 5	1:500	Rabbit	-	BioLegend	PRB-160P
Vimentin	1:100	Mouse	-	NeoMarkers	MA5-11880
Tp63	1:100	Mouse	Yes	abcam	ab735
P75	1:50	Rabbit	-	abcam	ab52987
MCM7	1:100	Rabbit	Yes	abcam	ab52489
Ki-67	1:200	Rabbit	-	abcam	ab16667
Mucin 1	1:50	Rabbit	-	abcam	ab109185
Mucin 5AC	1:500	Rabbit	Yes	Altlas	HPA040615

Table 2.6: List of the secondary antibodies used.

Antibody	Dilution	Host	Manufacturer	Catalogue number
Alexa Fluor® 488	1:150	Donkey anti-mouse IgG	Invitrogen	A21202
Alexa Fluor® 488	1:150	Goat anti-rabbit IgG	Invitrogen	A11034
Alexa Fluor® 594	1:150	Goat anti-rabbit IgG	Invitrogen	A11037
Alexa Fluor® 594	1:150	Goat anti-mouse IgG	Invitrogen	A11032

DAPI (4',6-diamidino-2-phenylindole) was added to all slides with the secondary antibodies at a 1:1000 dilution (600nM) in order to visualise cell nuclei.

2.5.4 Microscopy

Monitoring the growth of the cell cultures was achieved using bright field illumination with an EVOS XL Core microscope (Life Technologies, ZP-PKGA-0665). Fluorescent images were captured by either Zeiss Axiovert 100M microscope or Pannoramic MIDI scanner and 3DHISTECH software (3DHISTECH Ltd, Budapest, Hungary).

2.6 Molecular Biology

2.6.1 RNA Extraction

For organoids, pellets were snap-frozen in matrigel and subsequently homogenized using RLT buffer (guanidine thiocyanate buffer with Mercaptoethanol (β-ME) and 27-gauge syringe. RNA was then retrieved using a Qiagen RNeasy® Micro kit (catalogue no. 74004) according to the manufacturer's Protocol using on-column DNAse digest. RNA was eluted in 14µl of nuclease-free water and evaluated by NanoDrop spectrophotometer.

2.6.2 cDNA synthesis

100ng of total RNA was retro-transcribed using the Invitrogen™ SuperScript® III First-Strand Synthesis System (catalogue no. 18080051) following the manufacturer's protocol, using a DNA Engine Tetrad® 2 Thermal Cycler. A genomic DNA control was included which was prepared from a sample containing the same amount of RNA but without retrotranscriptase enzyme was (-RT control).

2.6.3 qPCR

qPCR was carried out using the Applied Biosystems® TaqMan® Fast Advanced Master Mix (catalogue number: 4444557) with TaqMan® probes (Table 2.7) on a 384 plate ViiA™ 7 Real-Time PCR System with the following reaction parameters: 50^{o}C for 2 minutes, 95^{o}C for 20 seconds and 40 cycles of (95ºC for 1 second, 60ºC for 20 seconds). For each sample, 5ng of cDNA was used per reaction, and each was performed in triplicate. Reaction components are shown in Table 2.8.

Tata binding protein (*TBP*) was used as a housekeeping gene, and fold-change was calculated using the delta-delta-CT method (5). For each primer (Table 2.7), both –RT and non-template controls (NTC) were included. Each reaction was run in triplicates.

Table 2.7: Taqman probes used for relative quantification.

Probe/primer	Product code
Cytokeratin 17	Mm00495207_m1
Cytokeratin 8	Mm00835759_m1
LGR5	Mm00438890_m1
EpCAM	Mm00493214_m1
Tbp	Mm00446973_m1

Table 2.8: qPCR reaction reagents and their final concentrations.

Reagent	Final concentration	Volume per well
TaqMan® Fast Advanced Master Mix	X1	5 µL
TaqMan probes	X1	0.5 µL
cDNA	5 ng/well	4.5 µL

2.7 Microarray

A total of 3 ectocervical samples, 3 endocervical pieces, 4 stromal samples derived from mouse cervix, 4 ectocervical organoids and 4 endocervical organoids. RNA was assessed for concentration and quality using a SpectroStar (BMG Labtech, Aylesbury, UK) and a Bioanalyser (Agilent Technologies, Cheadle, UK). Microarray experiments were performed according to manufacturer's instructions by the Cambridge Genomic Services at the University of Cambridge, using a Clariom S Mouse HT Array Plate (Affymetrix, Wooburn Green, UK) in combination with WT PLUS amplification kit (Affymetrix).

2.7.1 Bioinformatics

The data was processed by the Cambridge Genomic Services at the University of Cambridge, in R using the lumi package for normalisation and the limma package for comparisons. Heatmaps were generated using the heatmap.2 function of the R package 'gplots' the input is a correlation matrix based on samples' expression profile.

The cluster analysis was done using the R sva package, expression values from all genes were transformed by removing the baseline differences between samples due to host origin. Then, cluster analysis was done on a selected group of genes (those differentially expressed between the compared groups using the R stats package. The distance matrix was computed using 1-correlation as the distance measure, and hierarchical clustering was performed using the complete linkage method.

Chapter 2 References

1. Doucet YS, Woo S-H, Ruiz ME, Owens DM. The touch dome defines an epidermal niche specialized for mechanosensory signaling. Cell Rep. 2013 Jun 27;3(6):1759–65.
2. Touchdown PCR for increased specificity and sensitivity in PCR amplification | Nature Protocols.2008.133
3. Erickson HS, Albert PS, Gillespie JW, Rodriguez-Canales J, Linehan WM, Pinto PA, et al. Quantitative RT-PCR gene expression analysis of laser microdissected tissue samples. Nat Protoc. 2009;4(6):902–22.
4. Sato T, Vries RG, Snippert HJ, van de Wetering M, Barker N, Stange DE, et al. Single Lgr5 stem cells build crypt-villus structures in vitro without a mesenchymal niche. Nature. 2009 May 14;459(7244):262–5.
5. Livak KJ, Schmittgen TD. Analysis of relative gene expression data using real-time quantitative PCR and the 2(-Delta Delta C(T)) Method. Methods San Diego Calif. 2001 Dec;25(4):402–8.

3 Investigation of KRT17+ reserve cells and its role in the homeostasis of the cervical epithelium in mouse and humans

3.1 Introduction

The cervix contains three distinct epithelial regions: the endocervix, which is lined by a simple columnar secretory epithelium; the ectocervix, which is comprised of a stratified squamous epithelium that is non-keratinized in humans; and a transformation zone (TZ) at the endocervical-ectocervical junction. The TZ is a unique site where two different types of epithelia meet and is found in different tissues including the cornea-conjunctiva, the esophago-gastric, the ano-rectal and the endo-ectocervix junctions. Numerous human TZs have been reported to be susceptible to tumour development (1-4).

This increased cancer prevalence in the TZ led to the notion that these sites have an inherent susceptibility to dysregulation and disruption of homeostasis (5). The cervix is a particularly striking example with highest global rates of carcinoma with over 500,000 cases per year (6). All cervical carcinomas are due to HPV infections and arise in TZ (6). The cervical TZ is not abrupt but rather it is continuous and varies in length during a woman's life. This continuity requires the transformation from one epithelium into the other by means of a process called metaplasia. Several factors have been linked to drive metaplasia, including direct exposure of the low pH of the vagina and parity (7). Metaplasia is believed to be mediated by a type of stem cell that is located at the TZ that has also been proposed as the target cell for HPV infection (8). However, the identity of the TZ stem cell that maintains the homeostasis of this region and the molecular pathways that are involved in the regeneration of the cervical epithelium are poorly understood. Three main models have been hypothesized. The first proposes that a specialised type of stem cells called 'reserve cells' (marked by expression of KRT17) are present under the columnar epithelium of the TZ and drives the process of cervical metaplasia (8). A second theory suggests that cervical metaplasia is driven by a distinct group of cuboidal cells at the SCJ marked by KRT7 (9). The most recent hypothesis, which was reported towards the completion of my project, proposes that reserve cells are squamous basal cells that acquire a different behaviour under the influence of the stromal microenvironment (10).

In this chapter, I explore these with a focus in the KRT17 reserve cell theory as the published evidence that I examined seems to suggest this is the most likely (8,11). To do so, I used tissue sections from benign hysterectomies from women of reproductive or pre-menopausal age.

These hysterectomies were carried out for non-HPV-associated reasons, at the human tissue bank at Addenbrooke's University Hospital in Cambridge. In addition, I explore the utilisation of the mouse as a potential experimental model for cervical metaplasia. To identify similarities and differences between mouse and human cervix I designed an extensive panel of markers that would allow me to distinguish the different epithelial cell types proposed in the models, including: KRT17 to identify reserve cells; KRT7 to identify potential cuboidal cells; KRT8 as a columnar marker; and TP63 as a squamous cell marker. This approach will allow me to: i) identify the location of the different epithelial subtypes; ii) analyse the similarities and differences between the murine and human cervix.

3.2 Results

3.2.1 Characterisation of KRT17 expression in the normal human cervix

KRT17+ reserve cells are reported to be located in areas of cervical metaplasia based on studies by Martens and colleagues (8,11). I set out to examine the pattern of KRT17 expression and its validity as a marker in 49 biopsy sections from benign hysterectomies carried out for non-HPV-associated pathologies. Initially, I used Panoramic MIDI automatic digital slide scanner to identify and examine the TZ using H&E staining. Based on this I selected only those samples that had a clear area of TZ for further analysis. I subsequently performed immunohistochemistry (IHC) using an anti-KRT17 antibody peroxidase-conjugate and DAB (3,3'-Diaminobenzidine) chromogen system on these samples to analyse its pattern of expression.

For each sample, I identified areas of metaplasia morphologically, with the use of H&E, and KRT17 staining to mark the reserve cells (11). KRT17 in the normal cervical epithelium is mostly restricted to the sub-columnar cells in the TZ and in the endocervix (Figure 3.1). Furthermore, I observed KRT17 positivity in metaplastic stratified squamous epithelium at the squamocolumnar junction (Figure 3.1) which is associated with reserve cell hyperplasia. This is in agreement with the reports of Martens and colleagues (11,12). Therefore, using these large sample numbers of the normal cervix from women of (range) age, I confirmed the utility of KRT17 as a marker of cervical reserve cells.

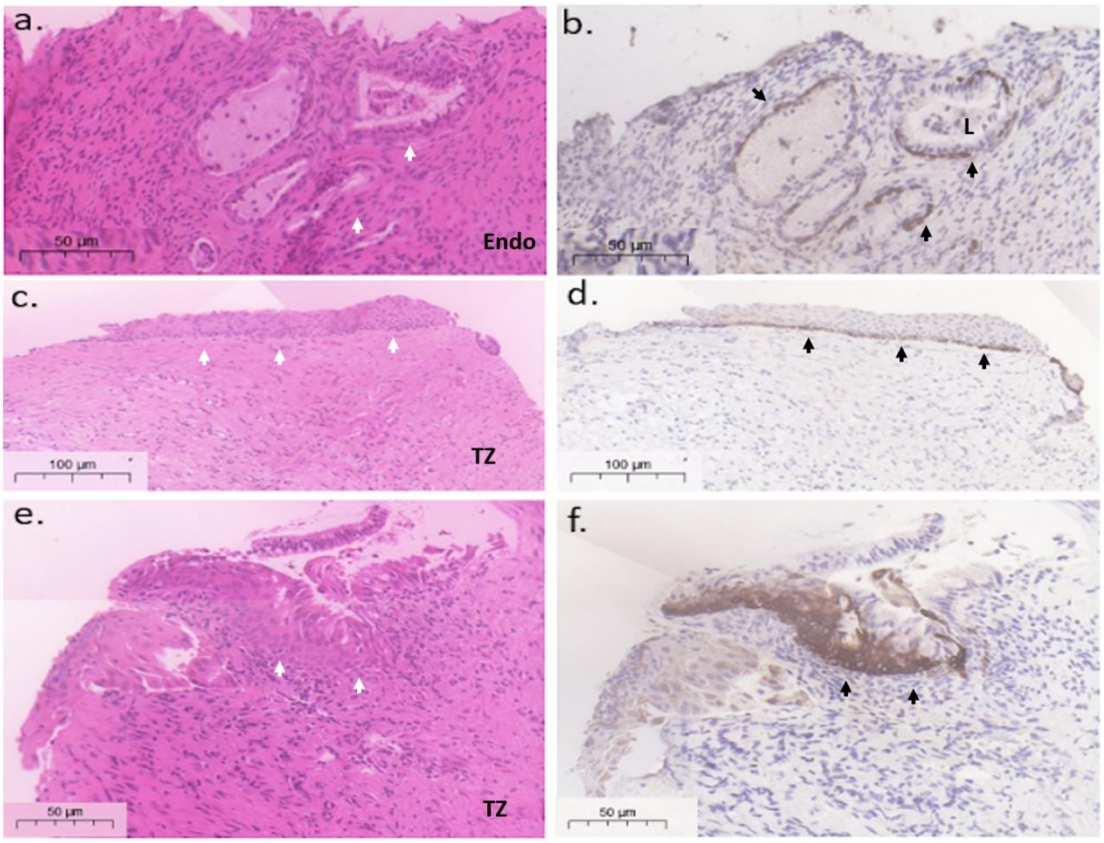

Figure 3.1: Cervical reserve cells marked by KRT17. Representative H&E and IHC images showing KRT17+ subcolumnar reserve cells in the endocervix (a,b), scale bar=50µm. Additionally reserve cells are seen in areas of immature metaplasia at the TZ (c,d), scale bar=100 µm. And in reserve cell hyperplasia in TZ (e,f), scale bar=50µm. Black arrows indicate KRT17+ cells (positive staining in brown by DAB) and the corresponding regions are shown by white arrows in the H&E staining. Abbreviations: Endo=endocervix, TZ=transformation zone and L= lumen.

3.2.2 Using KRT17 to identify stages of cervical metaplasia

Although metaplasia is a physiological process, it is generally regarded as a precursor to low-grade dysplasia (7). There have been theories on how cervical metaplasia can progress to dysplasia, but a clear staging of this process has never been done. Understanding the molecular events of metaplasia and how reserve cells might potentially build a new squamous epithelium will not only pave the way to understand how cervical TZ is regulated but also why is it vulnerable for HPV-derived neoplasia. Thus, to address this, I subsequently select samples that show well-defined areas of metaplasia (both mature and immature) and carried out immunofluorescence (IF) staining with a more extensive panel of molecular markers (explained in table 3.1).

To identify metaplasia, I examined samples for those with a distinct TZ in which both elements of squamous and columnar epithelia are found, using H&E staining. I then assessed the sections

carefully for small cuboidal cells either under the columnar crypts or at the SCJ, as the presence of reserve cells in these areas has been long noticed by pathologists and reported by many (8,13,14). Mature metaplasia is when the transformation process from columnar to squamous is complete and can only be distinguished as a new squamous epithelium by the presence of columnar crypts in the stroma. Whilst immature metaplasia is when the process of transformation is still in progress (15).

I found that in metaplastic squamous epithelium, the distribution of KRT17 expressing cells is dependent on the stage of the metaplastic process. In regions of immature metaplasia, I detected KRT17 cells in the basal and parabasal layers (Figure 3.2) but as the epithelium matures, its expression is only detected at low levels or is even absent (Figure 3.2). This supports the idea that reserve cells may give rise to TZ layers, creating the new squamocolumnar junction.

Table 3.1: IF markers used to characterise human immature metaplasia.

Marker	Expected pattern of expression	Rationale behind use
KRT17	Localizes in the cytoplasm of reserve cells	Reported marker for cervical reserve cells (11).
KRT8	Localizes in the cytoplasm of columnar epithelia	Marker for endocervical columnar epithelia (16).
KRT7	Localizes in the cytoplasm of columnar epithelia	Marker for endocervical columnar epithelia (17).
TP63	Localizes in the nuclei in the basal layers of stratified squamous epithelia and in reserve cells (5).	Tumour suppressor transcription factor, that is active in embryonic stages of development (18) and thought to be important in stem cell regulation (19).
MCM7	Localizes in the nucleus of marking cells in proliferation.	Cell cycle activity marker and a component of cellular replication complex (20).
Ki-67	Nuclear protein expressed in cells undergoing active phases of the cell cycle	Essential role in mitosis (21).

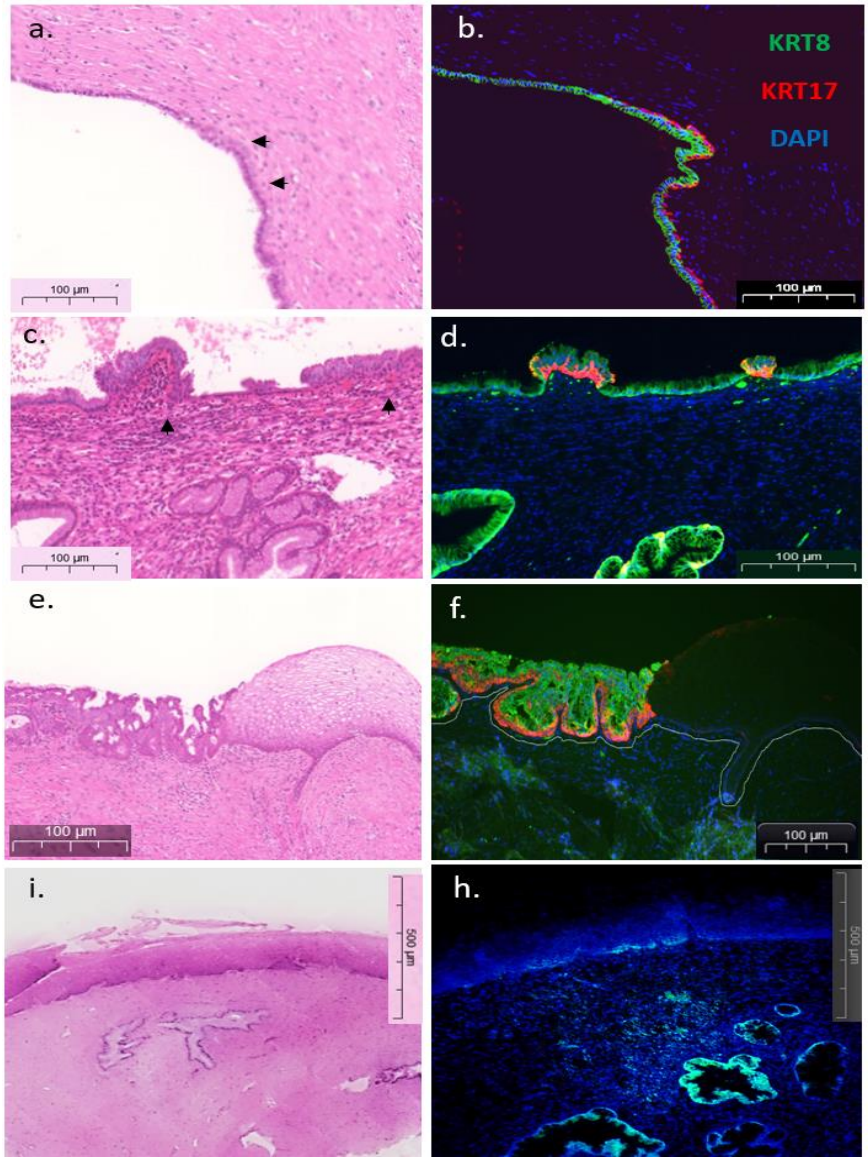

Figure 3.2: KRT17 cells pattern in metaplasia. Representative IF images showing stages of metaplastic cervical epithelia, rows of reserve cells (marker by KRT17 in red) align underneath the columnar epithelium (marker by KRT8 in green) of the endocervix (a,b), and the start of hyperproliferation of reserve cells in (c,d), which give rise to immature metaplasia in the TZ (e,f), which eventually matures (i,h). Blue colour indicates DAPI nuclear staining, scale bar=100 µm.

KRT8 is a marker of simple columnar epithelium and therefore is a marker of endocervix (16). I found that they are often present in the cell population above the KRT17 positive cell layers in the TZ as the process of metaplasia occurs (Figure 3.2). These results correspond with those from previous studies, which suggested a similar epithelial keratin pattern in immature squamous metaplasia (22).

TP63 is a transcription factor expressed in basal/parabasal layers of squamous epithelium and was reported to be expressed by reserve cells (11,14,23). To further characterise the KRT17+ cells I also investigated the pattern of TP63 expression in these samples. I often found TP63 expression in KRT17+ cells. These KRT17+TP63+ were found in the basal and parabasal cells of immature squamous metaplasia of the cervix (Figures 3.3, 3.5) and in the basal layers of the ectocervix. Additionally, TP63 staining was also apparent in the sub-columnar reserve cells in TZ and endocervix (Figures 3.3, 3.5).

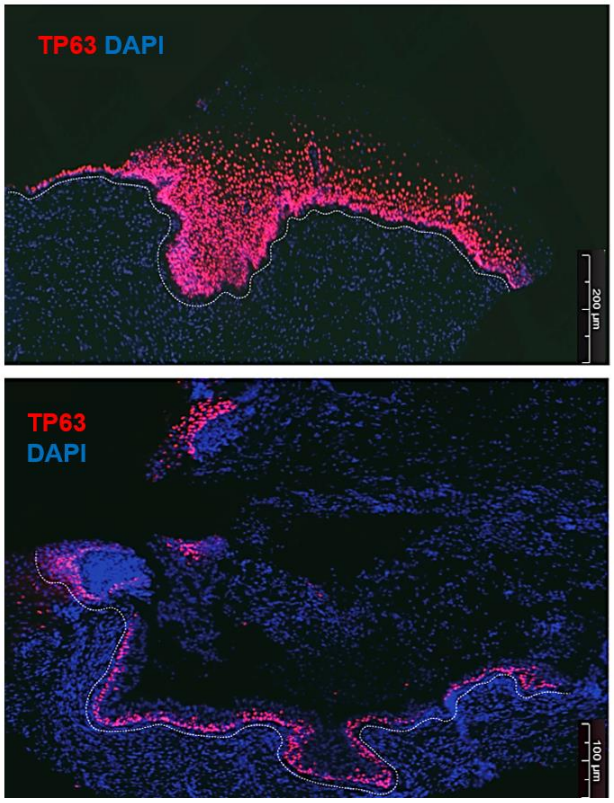

Figure 3.3: TP63 in the human cervix. Representative IF images showing TP63 pattern of TP63 is seen in parabasal layers of the ectocervix (top), scale bar=200 µm. And was found to have a similar pattern to KRT17+ cells (i.e. under KRT8+ cells) in an area of immature metaplasia (bottom) in human sample. White dotted lines indicated epidermis-dermis junctions, blue colour indicates DAPI nuclear staining and the scale bar=100 µm.

In order to examine the proliferative status of the KRT17+ cells, I performed IF staining for Mini-Chromosome Maintenance protein 7 (MCM7), is a marker of cells that are progressing through the cell cycle (20,24), and the a marker of cells that are actively cycling, Ki-67 (21,25). MCM7 staining was strongly positive in the parabasal layers of the stratified squamous epithelium of the ectocervix and sporadic in both the ectocervical glands and the TZ (Figures 3.4, 3.5). This agrees with others reporting restricted Ki-67 immunoreactivity in TZ with immature metaplasia (26), which we also confirmed by IF staining (Figure 3.4).

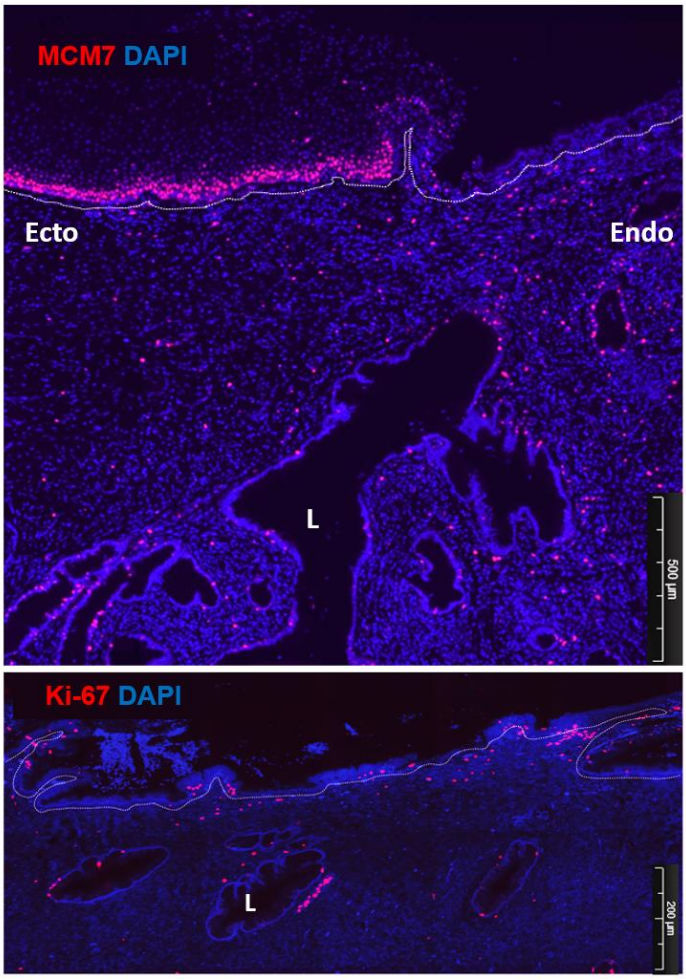

Figure 3.4: MCM7 staining in the human TZ. Representative IF images showing MCM7 staining (top) expression pattern in areas of immature metaplasia in a human cervical TZ, scale bar=500µm. Ki-67 (bottom) is shown in a different TZ section with sporadic positivity in areas of reserve cell hyperplasia and also in endocervical glands, scale bar=200µm. White dotted lines indicated epidermis-dermis junctions and the blue colour indicates DAPI nuclear staining.

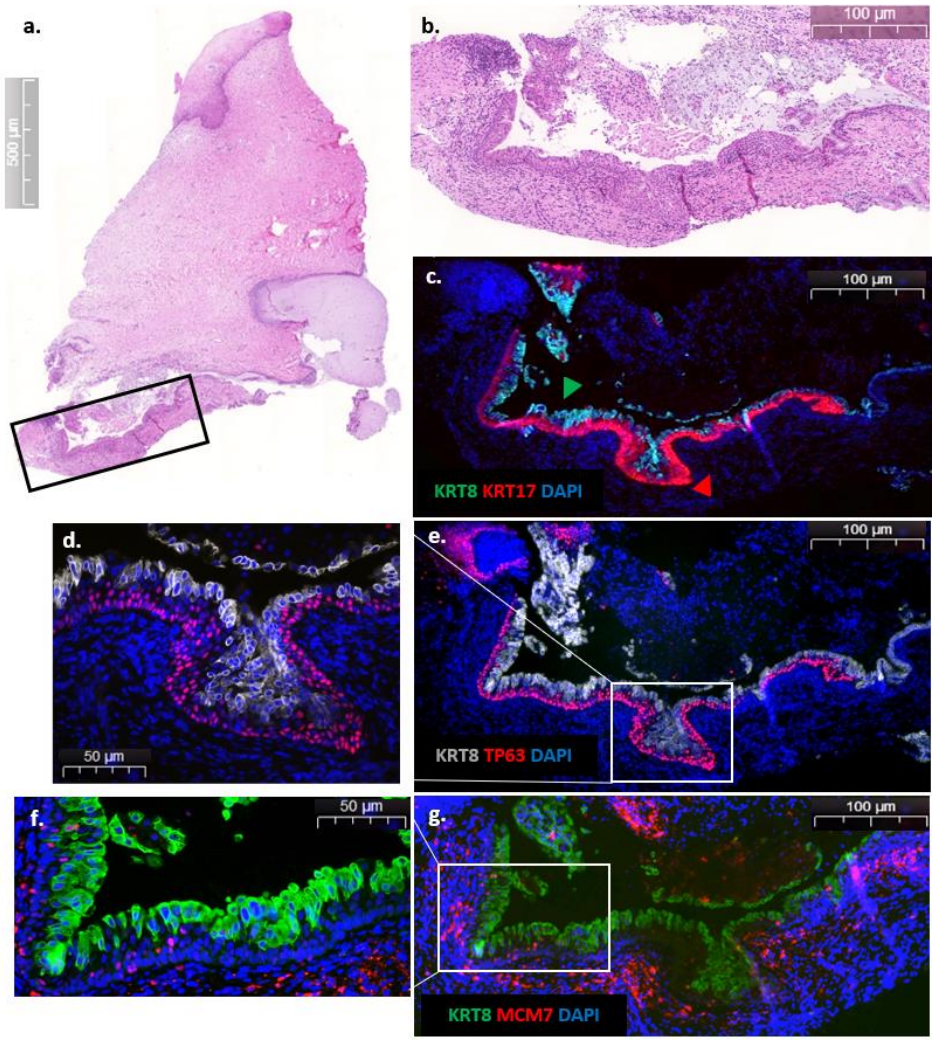

Figure 3.5: An area of human cervical immature metaplasia. (a) Representative H&E of cervical human biopsy, scale bar=500µm. (b) Magnified H&E of an area with immature metaplasia, scale bar=100µm. (c) IF staining with columnar marker KRT8 (green) and reserve cell marker KRT17 (red), scale bar=100 µm. (d,e) TP63 pattern (red) of expression is showing a similar pattern to KRT17+ with cells showing positivity under KRT8+ (grey) cells in an area of immature metaplasia in human sample, scale bar=50µm and 100µm respectively. (f,g) MCM7 staining (red) showing low expression in areas of immature metaplasia in a human sample, scale bar=50µm and 100µm respectively. White dotted lines indicated epidermis-dermis junctions and the blue colour indicates DAPI nuclear staining.

Herfs cuboidal cell theory suggests that there is a discrete KRT7+ cell population found near the SCJ which gives rise to reserve cells (9). To examine this hypothesis, I stained for KRT7 in sections with different stages of metaplasia. I found that KRT7 had the same pattern of expression as KRT8 and did not find a special junctional population as the Herfs theory suggested (Figure 3.6).

To summarise, during a metaplastic process, reserve cells residing at the cervical TZ are positive for KRT17 and TP63, however expression declines as the metaplastic progresses into mature metaplasia (fully formed squamous epithelium). MCM7/Ki-67 activity during metaplasia differs from the adjacent ectocervix, where the MCM7 activity is occasionally seen in confined areas of the basal layer, compared to an active MCM7 expression in the parabasal of the ectocervix and its expression is restricted in the basal layers (slow cycling). KRT8+ columnar cells are seen on top of an immature metaplasia in the normal human cervix. KRT7 co-localises with KRT8 and did not mark a different population.

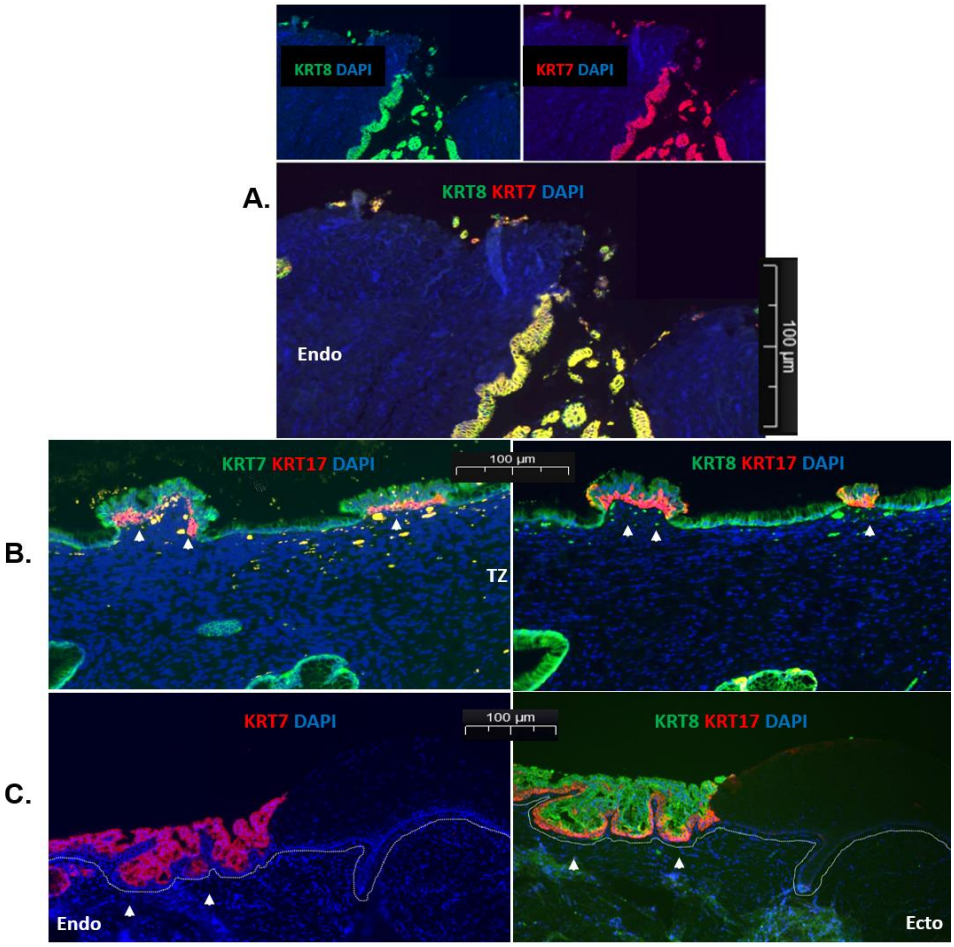

Figure 3.6: IF staining pattern of KRT7 in the different regions of the cervix. Representative KRT7 IF staining (red) in the endocervix near the SCJ (A), in reserve cell hyperplasia (green) (B) and in immature metaplasia (red) (C). White dotted lines indicated epidermis-dermis junctions, blue colour indicates DAPI nuclear staining and the scale bar=100µm.

3.2.3 Using the mouse model to study the process of metaplasia

Cervical metaplasia is a poorly understood process due to the lack of physiologically relevant experimental models. Although there are anatomical differences between the human and mouse cervix as described in the introduction (section 1.1), the mouse model may be a viable alternative to study cervical metaplasia due to the fact that mice have been used previously to provide insight of female genital chlamydial infections (27). Additionally, mice are easy to handle, breed and modify genetically.

Here, I explore the possibility to use the mouse model to study the dynamics of the human cervical epithelium by systematically defining their similarities and differences. I examined several timepoints during the development of the mouse cervixes from the ages of 2 weeks (pre-puberty) to 14 weeks (adult). I dissected the cervix and oriented it flat to obtain a cut that contains the all the regions of interest: the endocervix, SCJ and the ectocervix (Figure 3.7). I subsequently stained the sections with haematoxylin and eosin stain and with immunofluorescence using the same panel of markers described above (Table 3.1).

I found that in mouse cervix, two SCJs exist. Unlike humans, it has two uterine horns and thus at the lower end of each horn there is an SCJ. The SCJ link the uterine horns to the vaginal opening. At the earliest time point at two weeks, I saw a clear definition of the horns with a SCJ that is still developing as it shows the columnar lineage marker KRT8 extending to the ectocervix (Figure 3.8). Following the development of SCJ into week 4, I observed rows of KRT17+ cells under the developing endocervix resembling the resting reserve cell pattern I detected in the human endocervix (Figure 3.9). In post-natal week 6 samples, the endocervical-ectocervical junction is more defined, and by week 8 a complete SCJ is formed with two distinct epithelial lineages merging.

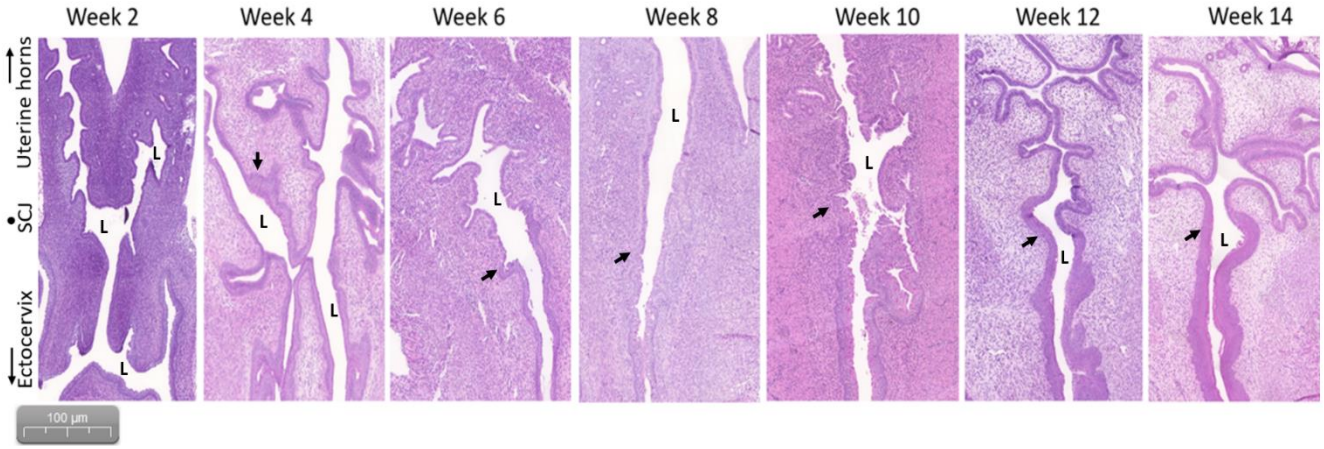

Figure 3.7: H&E of mouse cervix development time-course from 2 to 14 weeks post-birth. Defined SCJ is seen clearly post 8 weeks with haematoxylin and eosin, with full development of the squamous ectocervix, scale bar=100µm, L=lumen.

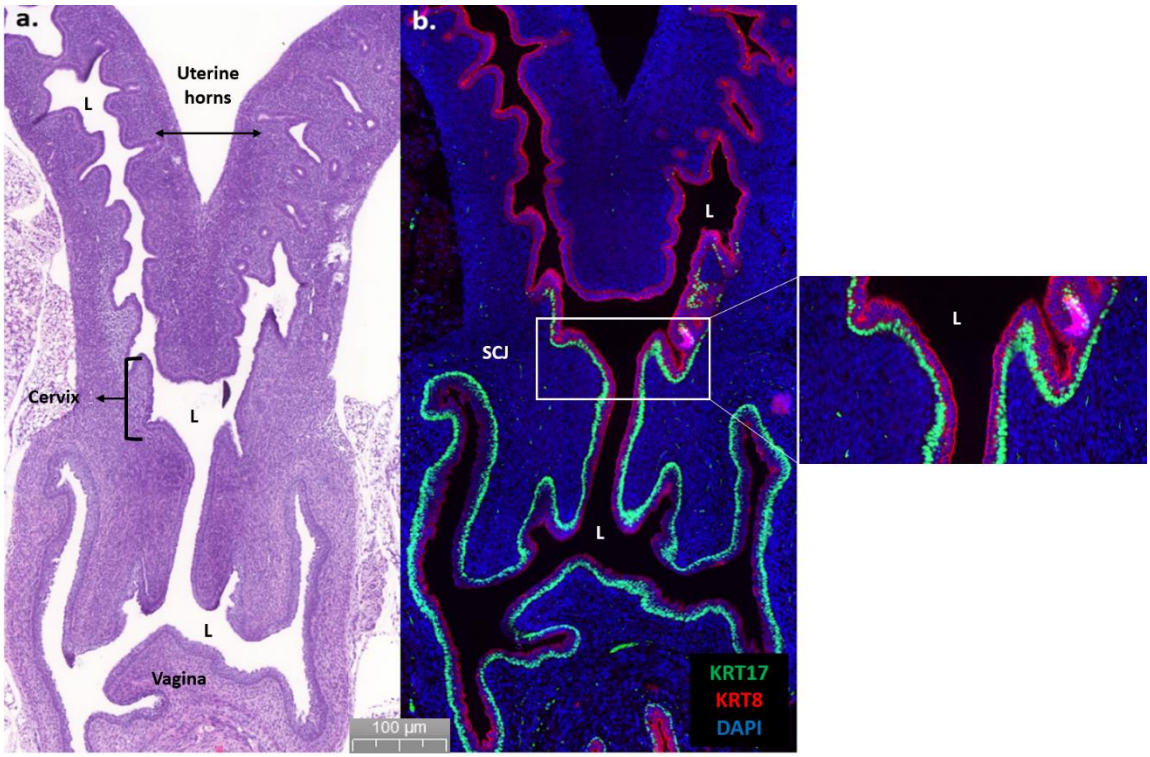

Figure 3.8: KRT17 cells in underdeveloped cervix. (a) Representative H&E images of an early mouse reproductive tract (week 2) showing underdeveloped SCJ region. (b) Representative IF staining showing both squamous and columnar markers (KRT17 (green) and KRT8 (red), respectively) in the lower area of the genital tract, scale bar=100µm, L=lumen and the blue colour indicates DAPI nuclear staining.

In the first few weeks after birth, the developing cervical epithelium shows high proliferative capacity throughout its length, with extensive positivity of MCM7 proliferative marker in the columnar epithelium at week 2 post-birth. At week 6, the SCJ is more defined and the pattern of MCM7 changes, with confined positivity appearing in the columnar cells of the endocervical crypts (Figure 3.10). The proliferative cells in mature stratified squamous tissues are located in the parabasal layer as seen in the ectocervix and other sites (28).

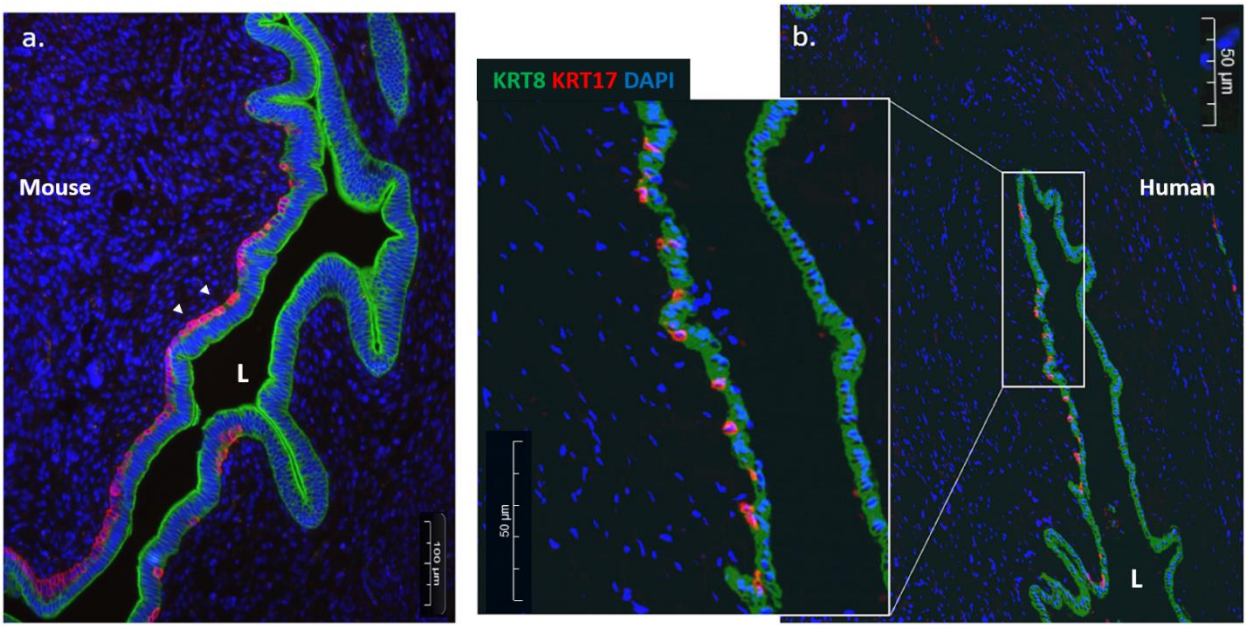

Figure 3.10: KRT17 cells in mouse resembles reserve cells seen in the human cervix. Representative IF images showing rows of KRT17+ cells (red) seen under the developing cervix in week 4 mouse (a), scale bar=100µm, which resembles what is observed in human endocervix (b), scale bar=50µm, L=lumen and the blue colour indicates DAPI nuclear staining.

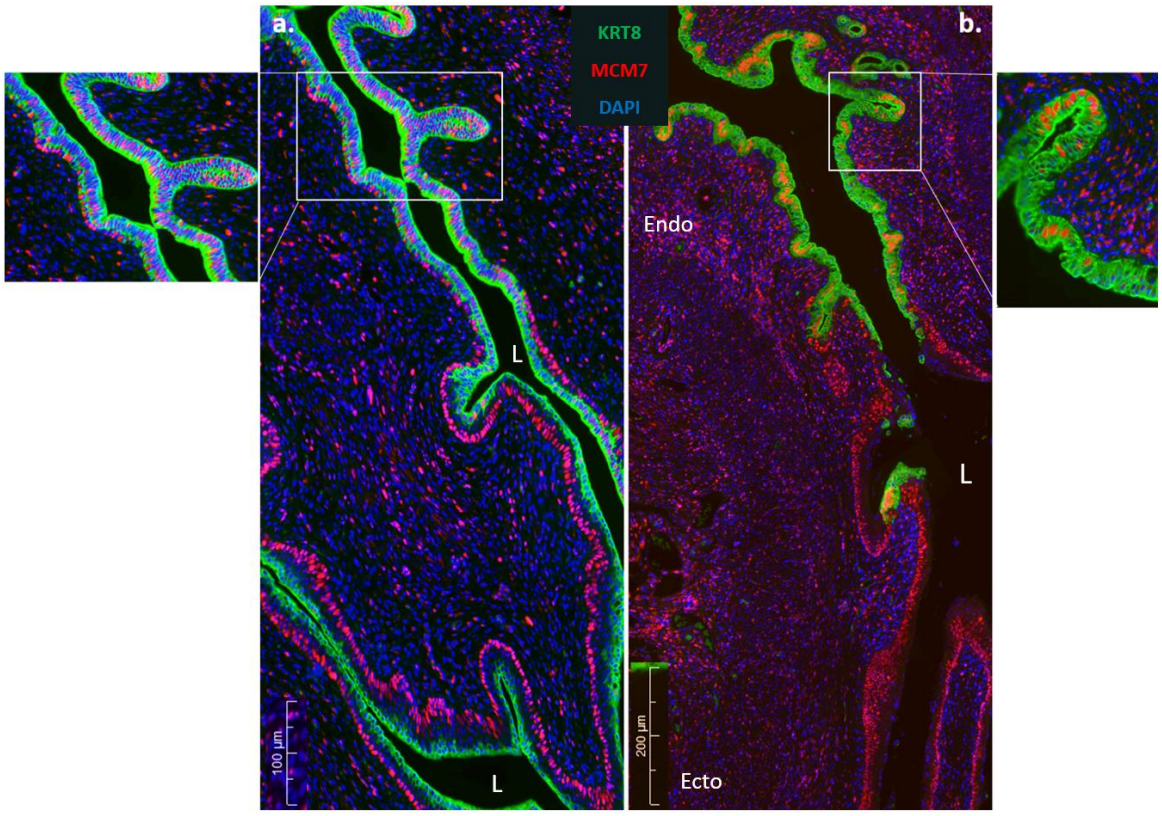

Figure 3.9: IF expression pattern of MCM7 and KRT8 in mouse cervix. Representative IF images of (a) Post-natal week 2 mouse uterine cervix with extensive positivity of MCM7 (red) proliferative marker in the columnar epithelium (marked by KRT8 in green), scale bar=100µm. (b) Post-natal week 6 mouse cervical SCJ, with confined positivity is observed in the columnar cells of the endocervical crypts, scale bar= 200 µm. Blue colour indicates DAPI nuclear staining, L=lumen.

In the cervix of an adult mouse (week 8 onwards), KRT17 is expressed in the basal and differentiated ectocervical squamous epithelium (Figure 3.11). This is in contrast to what I observed in the human cervix, where KRT17 is only seen in the basal layers of forming squamous epithelium. The endocervical columnar epithelium, was mostly negative for KRT17 except near the SCJ where an occasional KRT17+ cell was detected (Figure 3.11). In the SCJ, both keratin elements are present, with KRT8 sometimes appearing above the KRT17 cells, similar to what I found in human immature metaplasia (Figure 3.11).

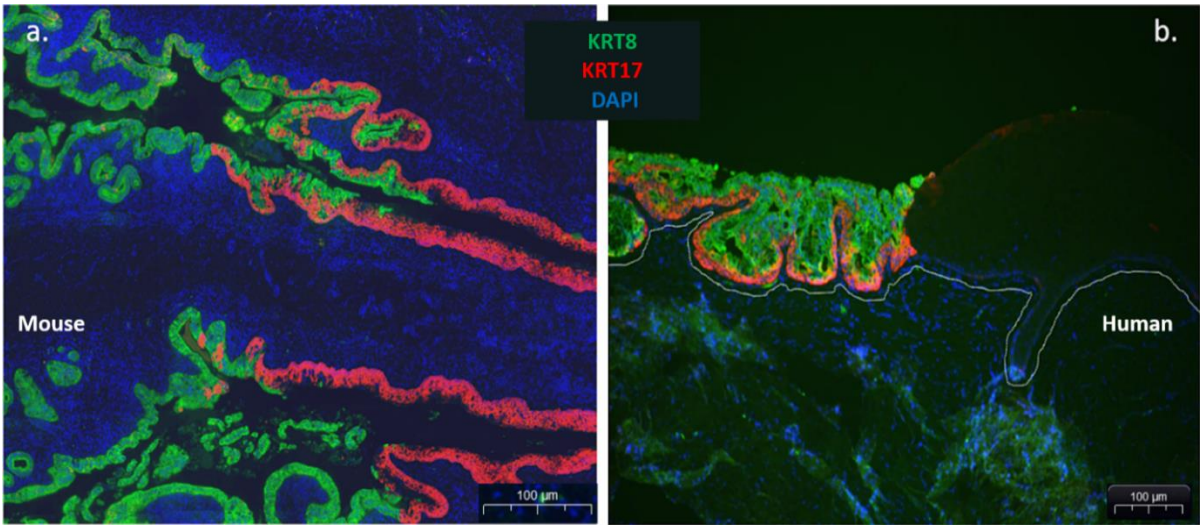

Figure 3.11: Expression of KRT17 and KRT8 in adult mouse cervix. Representative IF images of (a) SCJ of adult mouse (8 weeks), both keratin elements are present, with KRT8 (green) seen on top of the KRT17 cells (red), similar to what is seen in human immature metaplasia (b). White dotted lines indicated epidermis-dermis junctions, blue colour indicates DAPI nuclear staining and the scale bar=100µm.

As observed in human immature metaplasia, TP63 expression pattern co-localises with KRT17+ cells (Figure 3.12). Furthermore, their cell cycle activity determined by MCM7 expression, was remarkably low in the SCJ of adult mouse (week 8) when compared to the ectocervical epithelium (Figure 3.12). This is similar to in the patterns of expression human immature metaplastic epithelium (Figure 3.4).

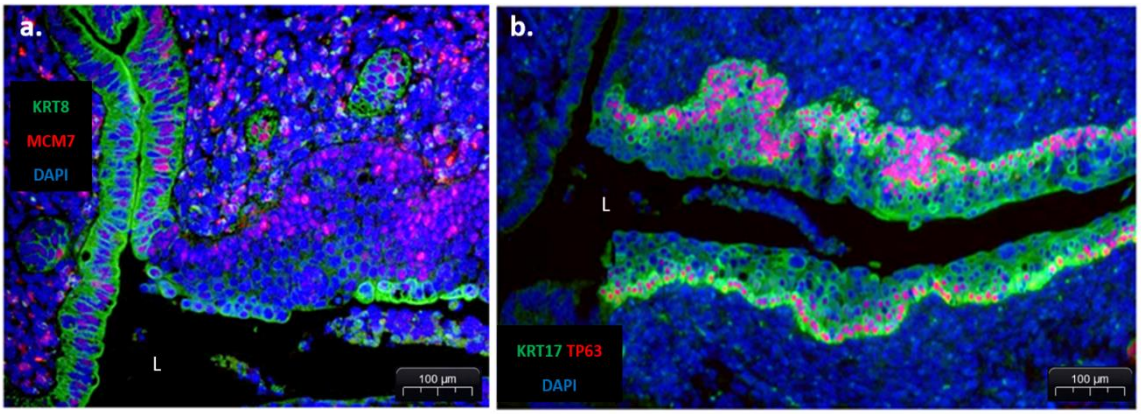

Figure 3.12: Expression of MCM7 and TP63 in mouse SCJ. Representative IF images of (a) MCM7 (red) KRT8 (green) expression in SCJ of adult (week 8) mouse, showing low MCM7 expression at the SCJ. (b) TP63 (red) KRT17 (green) expression in SCJ of adult murine SCJ, with TP63 expression pattern localises with KRT17 positive cells in the basal and parabasal layers of the squamous epithelium. Blue colour indicates DAPI nuclear staining, scale bar=100µm and L=lumen.

To summarise, when I observed the development of mouse cervix in the context of KRT17 expression, I found a row of KRT17 cells under the developing cervical epithelium (at week 4). This pattern bears a resemblance to the reserve cell pattern I found in the human TZ. The expression of KRT17 changes later in development of the cervix as the adult SCJ (week 8) forms, I see multi-layered KRT17 cells underneath the KRT8, similar to what I saw in human immature metaplasia. Additionally, TP63 colocalises with KRT17 cells closely recapitulating my observations in human cervix. Moreover, the developed SCJ has confined MCM7 activity like human metaplasia.

3.2.4 Examining KRT17 expression in mouse cervix post-injury

KRT17 has been reported as an early marker of keratinocyte activation after injury (24). To understand KRT17+ expression in context of cervical injury, I decided to investigate a physiological process injury, which is the cervix after birth. Therefore, I harvested and examined the postpartum murine cervix. As revealed by H&E staining of mouse postpartum cervix, the cervical epithelium was folded at 24 hours postpartum (Figure 3.13). When I stained postpartum mouse cervix with KRT17 I saw a row of reserve cell emerging underneath the columnar glands of the endocervix near the junction (Figure 3.14), and occasional KRT17 colocalised in columnar cells and not underneath them (as normally seen in adult mouse cervix) (Figure 3.14).

Figure 3.13: H&E of 24h postpartum mouse cervix. Representative H&E images showing epithelial folding, one of the implantation sites is seen and the lumen (L) of the endometrial and endocervical glands is filled with red blood cells (RBCs). Scale bar=1000µm.

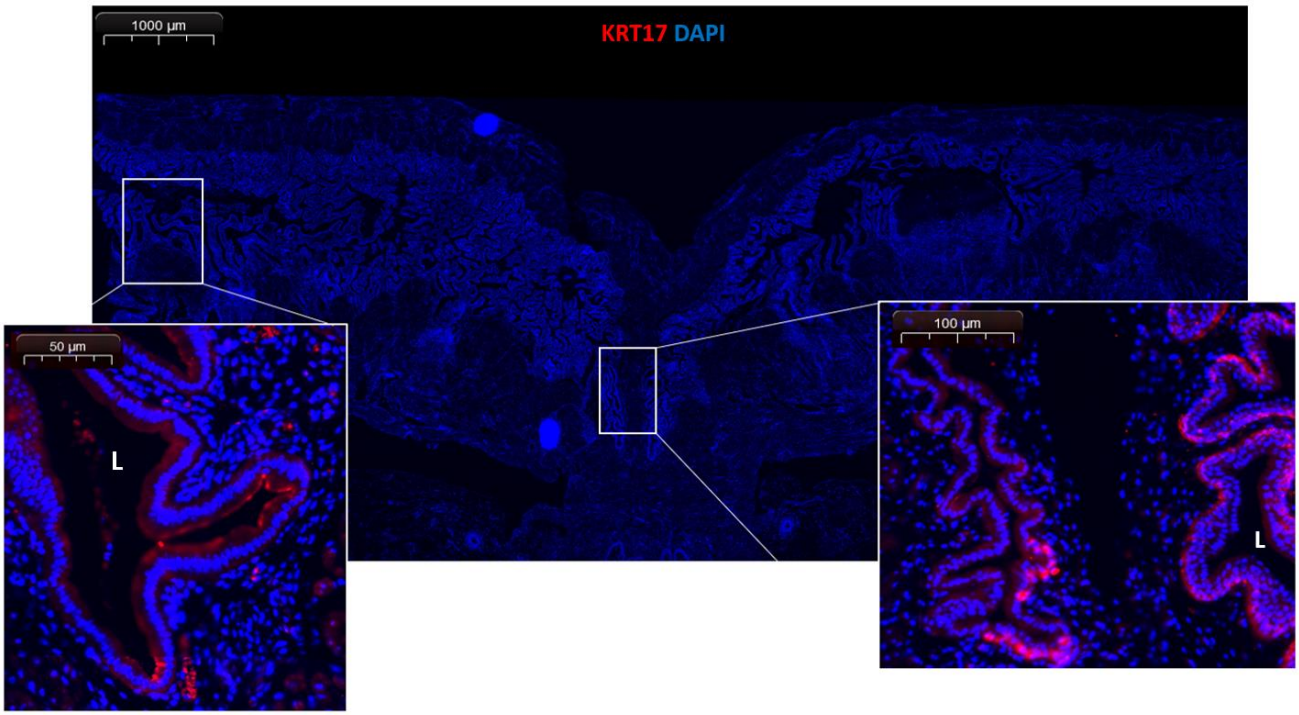

Figure 3.14: KRT17 IF staining of 24h postpartum mouse cervix. Representative IF images of KRT17+ cells (red) in postpartum mouse cervix, scale bar=1000µm. Two patterns of KRT17 are seen, underneath the columnar glands (right), scale bar=100µm, and also in columnar cells (left), scale bar=50µm. Blue colour indicates DAPI nuclear staining and L=lumen.

3.3 Discussion

This chapter is focused on the characterisation and staging of reserve cells along the uterine cervical canal in humans and mouse. Reserve cells have been described previously (13,29), and the possibility of reserve cells being a population of cervical stem cells have been proposed (11), but never proven. I screened cervical sections for KRT17 expression, and I confirmed the presence of a discrete population of KRT17 positive cells (KRT17+) in the cervical TZ. I found KRT17+ cells as individual small flat cells either under the columnar cells of the endocervical crypts or in groups near the TZ. After I selected slides with positive KRT17, I used a defined set of markers (Table 3.1) to understand the distribution pattern of reserve cells. The findings suggest that reserve cells contribute to the formation of a new squamous epithelium via the process of metaplasia, in order to build a new SCJ. It appears that reserve cells, marked by both KRT17 and TP63, reside in a quiescent state (based on proliferation markers MCM7/Ki-67) in the endocervix (marked by KRT8, close to SCJ) (Figures 3.2, 3.3, 3.4 and 3.5). Once they are stimulated to proliferate, these cells form rows that continue to build a squamous epithelium (immature metaplasia) (Figures 3.2 and 3.5). Reserve cell hyperplasia continues and over time a fully matured stratified squamous epithelium is formed (mature metaplasia) (Figure 3.2). These findings support the theory of reserve cells being the progenitor cell of columnar and squamous lineages in the cervical epithelium (11). In addition, I have examined the cell proliferative pattern using MCM7. MCM7 was highly positive in the parabasal layers of the squamous epithelium of the ectocervix, and occasionally in the endocervix and TZ.

To explore the alternative reserve cell theory, I have also investigated the junctional KRT7 cuboidal cells theory (9). Contrary to the report by Herfs et. al., my staining did not show a special population at the SCJ that is highly positive for KRT7. Although using the same antibody, I found that KRT7 was abundant and co-localised with columnar marker KRT8. Possible reason for this contradictory data is the sample size analysed by Herfs and colleagues. To be able to test the dual fate ability of the KRT17+ reserve cells in generating both columnar and squamous lineages, I explored the utility of the mouse model. Some anatomical differences are apparent, for example mice have two uterine horns, therefore two SCJs exists, unlike one in humans. However, when I compared the human and mouse cervical epithelium, a number of fundamental similarities were noticed. At two weeks post-birth, the cervix was developing and the SCJ was not well defined (Figure 3.7), at week 4 a row of KRT17 cells appear under the columnar epithelium of the developing uterine horns, similar to the reserve cell pattern I

observed in human cervix (Figure 3.9). At week 8, columnar and squamous lineages are histologically distinct, with KRT8+ columnar cells occupy the endocervical end, and KRT17+ TP63+ cover the ectocervical end, the two lineages meet in a junction where KRT17 cells underly columnar marker KRT8 cells, similar to what I saw in human immature metaplasia (Figure 3.10). Another important difference is the persistence of KRT17 expression along the squamous cells of the ectocervix in mice unlike humans. However, there are enough similarities that suggest that murine cervical epithelium may serve as a useful model to study some aspects cervical metaplasia, in particular the regulatory mechanisms that control the potential ability of the KRT17+ reserve cell to differentiate into either a single layered columnar epithelium, or the multi-layered epithelium of the squamous transformation zone.

I investigated the proliferation patterns in the mouse cervix during its development. MCM7 in adolescent mice (2-week-old mice) showed a high proliferative capacity throughout its length (Figure 3.11), with extensive positivity of MCM7 proliferative marker in the columnar epithelium. At week 6, the SCJ is more defined and the patter of MCM7 changes, with positivity only in the endocervical crypts and throughout the endocervical epithelium (Figure 3.11).

Postpartum repair is poorly studied, and since metaplasia is a form of physiological injury response, I decided to examine the cervical epithelium response postpartum. At 24 hours postpartum, the uterine horns were folded with blood cells infiltrations (Figure 3.13). When I stained with KRT17 I observed two types of expression patterns: small flat cells underneath the columnar crypts; and those localised in columnar cells (Figure 3.14). Based on my results, I hypothesize that two forms of KRT17 activation is found, one where small flat progenitor cell derive the metaplastic process and building a new squamous epithelium, and that is triggered by wound healing response and arise away from the SCJ (Figure 3.14). However further experiments must be carried out to confirm this as it was only performed twice. This is in agreement with what was observed in the human skin keratinocytes that express KRT6, KRT16 and KRT17 when wounded (30-32).

Graphical summary for chapter 3

1.

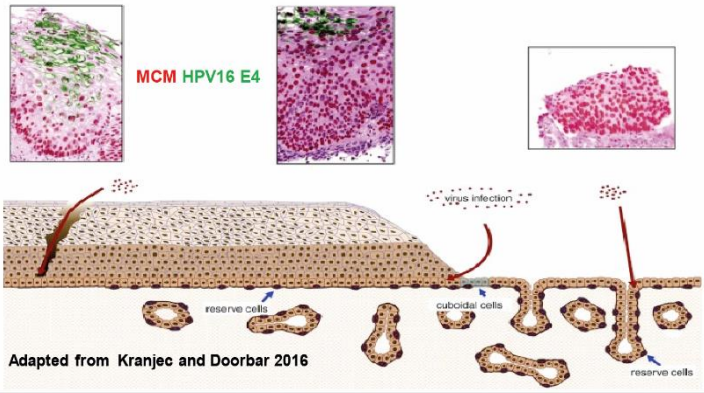

• The clinical outcome of HPV infections is highly dependent on the infected site. Productive HPV infection with low grade squamous intraepithelial lesion is seen when HPV infects the ectocervix, whereas in the TZ and endocervix deregulation of HPV genes leads to high grade squamous intraepithelial lesion.

2.

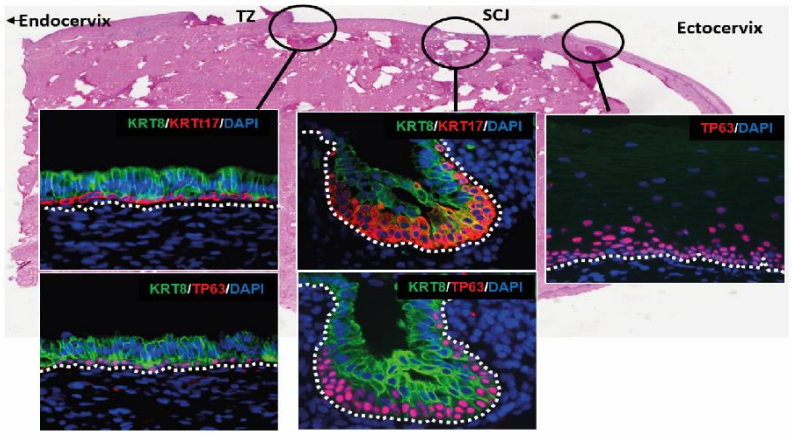

• The stem cell and target cell of cervical cancer is unkown. Several theoeies exist including KRT17+ reserve cells and KRT7+ cuboidal cells. Here my data agrees with the KRT17 theory with presence of KRT17+TP63+ in the metaplastic TZ. And no KRT7 specific pattern was found.

3.

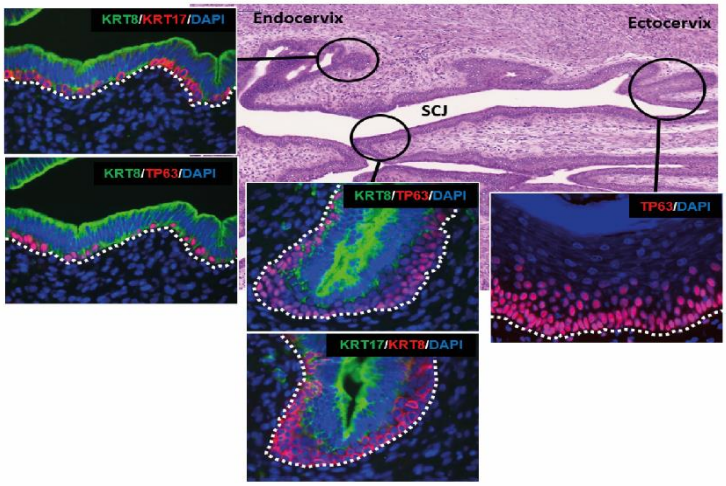

• Next, I wanted to find tools to test the KRT17 as a stem/target cell of HPV infection. Mouse is accessible and easy to genetically manipulate. Hence I examined the similarities of mouse and human cervix and found similar patterns with KRT17+TP63+ cells in SCJ but also in ectocervix. Additionally, developing mouse cervix 2-4 weeks showed a pattern similar to human metaplasia.

Chapter 3 References

1. Fluhmann CF. Carcinoma in situ and the transitional zone of the cervix uteri. Obstet Gynecol. 1960 Oct;16:424–37.
2. Grodsky L. TRANSITIONAL CELL CANCER OF THE ANUS AND RECTUM. Calif Med. 1961 Dec;95(6):386–90.
3. McKelvie PA, Daniell M, McNab A, Loughnan M, Santamaria JD. Squamous cell carcinoma of the conjunctiva: a series of 26 cases. Br J Ophthalmol. 2002 Feb;86(2):168–73.
4. Trudgill NJ, Suvarna SK, Royds JA, Riley SA. Cell cycle regulation in patients with intestinal metaplasia at the gastro-oesophageal junction. Mol Pathol MP. 2003 Dec;56(6):313–7.
5. Mcnairn AJ, Guasch G. Epithelial transition zones: merging microenvironments, niches, and cellular transformation. Eur J Dermatol EJD. 2011 May;21 Suppl 2:21–8.
6. de Martel C, Georges D, Bray F, Ferlay J, Clifford GM. Global burden of cancer attributable to infections in 2018: a worldwide incidence analysis. Lancet Glob Health. 2020 Feb;8(2):e180–90.
7. Giroux V, Rustgi AK. Metaplasia: tissue injury adaptation and a precursor to the dysplasia–cancer sequence. Nat Rev Cancer. 2017 Oct;17(10):594–604.
8. Martens JE, Smedts FMM, Ploeger D, Helmerhorst TJM, Ramaekers FCS, Arends JW, et al. Distribution Pattern and Marker Profile Show Two Subpopulations of Reserve Cells in the Endocervical Canal. Int J Gynecol Pathol. 2009 Jul;28(4):381.
9. Herfs M, Yamamoto Y, Laury A, Wang X, Nucci MR, McLaughlin-Drubin ME, et al. A discrete population of squamocolumnar junction cells implicated in the pathogenesis of cervical cancer. Proc Natl Acad Sci U S A. 2012 Jun 26;109(26):10516–21.
10. Chumduri C, Gurumurthy RK, Berger H, Koster S, Brinkmann V, Klemm U, et al. Transition of Wnt signaling microenvironment delineates the squamo-columnar junction and emergence of squamous metaplasia of the cervix. bioRxiv. 2018 Oct 16;443770.
11. Martens JE, Arends J. Cytokeratin 17 and p63 are Markers of the HPV Target Cell, the Cervical Stem Cell. ANTICANCER Res. 2004;6.
12. Ikeda K, Tate G, Suzuki T, Mitsuya T. Coordinate expression of cytokeratin 8 and cytokeratin 17 immunohistochemical staining in cervical intraepithelial neoplasia and cervical squamous cell carcinoma: an immunohistochemical analysis and review of the literature. Gynecol Oncol. 2008 Mar;108(3):598–602.
13. Weikel W, Wagner R, Moll R. Characterization of subcolumnar reserve cells and other epithelia of human uterine cervix. Virchows Arch B. 1987 Dec 1;54(1):98–110.
14. Witkiewicz AK, Hecht JL, Cviko A, McKeon FD, Ince TA, Crum CP. Microglandular hyperplasia: a model for the de novo emergence and evolution of endocervical reserve cells. Hum Pathol. 2005 Feb;36(2):154–61.
15. Moscicki A, Singer A. The cervical epithelium during puberty and adolescence. In: The cervix. 2nd ed. Massachusetts: Blackwell Publishing Professional; 2006. p. 81–101.
16. Moll R, Levy R, Czernobilsky B, Hohlweg-Majert P, Dallenbach-Hellweg G, Franke WW. Cytokeratins of normal epithelia and some neoplasms of the female genital tract. Lab Investig J Tech Methods Pathol. 1983 Nov;49(5):599–610.
17. van Dorst EB, van Muijen GN, Litvinov SV, Fleuren GJ. The limited difference between keratin patterns of squamous cell carcinomas and adenocarcinomas is explicable by both cell lineage and state of differentiation of tumour cells. J Clin Pathol. 1998 Sep;51(9):679–84.
18. Yang A, Kaghad M, Wang Y, Gillett E, Fleming MD, Dötsch V, et al. p63, a p53 homolog at 3q27-29, encodes multiple products with transactivating, death-inducing, and dominant-negative activities. Mol Cell. 1998 Sep;2(3):305–16.

19. Nekulova M, Holcakova J, Nenutil R, Stratmann R, Bouchalova P, Müller P, et al. Characterization of specific p63 and p63-N-terminal isoform antibodies and their application for immunohistochemistry. Virchows Arch. 2013; 463:415–425DOI 10.1007/s00428-013-1459-4.
20. Freeman A, Morris LS, Mills AD, Stoeber K, Laskey RA, Williams GH, et al. Minichromosome maintenance proteins as biological markers of dysplasia and malignancy. Clin Cancer Res Off J Am Assoc Cancer Res. 1999 Aug;5(8):2121–32.
21. Sun X, Kaufman PD. Ki-67: more than a proliferation marker. Chromosoma. 2018 Jun;127(2):175–86.
22. Smedts F, Ramaekers F, Robben H, Pruszczynski M, van Muijen G, Lane B, et al. Changing patterns of keratin expression during progression of cervical intraepithelial neoplasia. Am J Pathol. 1990 Mar;136(3):657–68.
23. Quade BJ, Yang A, Wang Y, Sun D, Park J, Sheets EE, et al. Expression of the p53 Homologue p63 in Early Cervical Neoplasia. Gynecol Oncol. 2001 Jan 1;80(1):24–9.
24. Stoeber K, Tlsty TD, Happerfield L, Thomas GA, Romanov S, Bobrow L, et al. DNA replication licensing and human cell proliferation. J Cell Sci. 2001 Jun 1;114(11):2027–41.
25. Scholzen T, Gerdes J. The Ki-67 protein: From the known and the unknown. J Cell Physiol. 2000;182(3):311–22.
26. Kalof AN, Cooper K. Our approach to squamous intraepithelial lesions of the uterine cervix. J Clin Pathol. 2007 May;60(5):449–55.
27. De Clercq E, Kalmar I, Vanrompay D. Animal Models for Studying Female Genital Tract Infection with Chlamydia trachomatis. Infect Immun. 2013 Sep;81(9):3060–7.
28. Dowdall JR, Sadow PM, Hartnick C, Vinarsky V, Mou H, Zhao R, et al. Identification of Distinct Layers Within the Stratified Squamous Epithelium of the Adult Human True Vocal Fold. The Laryngoscope. 2015 Sep;125(9):E313–9.
29. Carmichael RJB. Basal cells in the epithelium of the human cervical canal. J Pathol Bacteriol. 1939;(49):63–9.
30. Mansbridge JN, Knapp AM. Changes in keratinocyte maturation during wound healing. J Invest Dermatol. 1987 Sep;89(3):253–63.
31. McGowan K, Coulombe PA. The wound repair-associated keratins 6, 16, and 17. Insights into the role of intermediate filaments in specifying keratinocyte cytoarchitecture. Subcell Biochem. 1998;31:173–204.
32. McGowan KM, Coulombe PA. Onset of Keratin 17 Expression Coincides with the Definition of Major Epithelial Lineages during Skin Development. J Cell Biol. 1998 Oct 19;143(2):469–86.

4 Generation and characterisation of Organoid Cultures of the Murine Cervix

4.1 Introduction

Many *in vitro* models, including immortalised keratinocytes cell lines and have been established for the study of the cervix. Although these are important tools and have shed light on many aspects of the cervix, particularly the study of HPV proteins functions, they have numerous caveats as discussed in the introduction (chapter 1). They often lose epithelial phenotype and harbour chromosomal abnormalities. Primary cells cannot be cultured long-term, thus there is a lack of a physiologically relevant model system of the cervix. This has hindered progress in our understanding of the physiology of the normal cervix and the regulation of epithelial renewal and metaplasia.

Organoids are 3D cell culture system that closely resemble the *in vivo* tissue from which they are derived. This technology was first established in 2009 by Sato and Clevers, where they described a 3D culture system of the murine small intestine. This study has paved the way for the generation of organoids from many different organs in a systematic manner from both mouse and human (1). The organoid technology has several key advantages over conventional 2D cell lines, including genetic stability of the propagated primary cells, self-organisation into tissue-like structures, recapitulation of the molecular and functional characteristics of the original tissue, the ability to freeze/thaw thus allowing bio-banking, and the ability to be manipulated experimentally (2).

Organoids are cultured in Matrigel®-based systems enriched with signals that regulate the differentiation and propagation of progenitor cells of the organ/epithelium of interest. These signals are supplied by the extracellular factors and cytokines added to the medium which mimic the microenvironmental niche of the target cell population (3). Thus, in this way, primary cells can be grown indefinitely. At the start of this thesis, cervical organoid models have yet been reported. The establishment of cervical organoids not only provides an essential model to study the normal cervix, but it will also be a tool to investigate the responses to HPV infection and progression through pre-neoplasia to carcinoma and understanding the specific characteristics that render it vulnerable to these HR-HPV-associated cancers**.** The aim of the experiments described in this chapter is to establish an organoid model of both regions of the murine cervix: the endocervix and ectocervix.

4.2 Results

4.2.1 Optimisation of murine cervical organoids culture conditions

The key challenge in the establishment of any *in vitro* system, is to identify the optimal conditions that allow the growth of the primary cells whilst maintaining key in vivo characteristics. Furthermore, they must also permit differentiation so that the cells are able to acquire their full functional properties. To identify the culture conditions for the generation and expansion of murine cervical organoids, I first collated a list of potential growth factors to test based on: (i) existing organoid systems and (ii) reports on the signalling pathways involved in cervix development (table 4.1). Although tissue-derived organoid models established from different tissues each require specific culture conditions, there are some signalling pathways in common. The essential factors for maintenance of stem cells are EGF, Noggin and R-spondin (ENR) (1,2). The use of EGF enhances proliferation signals of intestinal progenitors when binding to their receptors (EGFR). Inhibition of BMP signalling by Noggin is used to induce expansion of crypt numbers, and R-spondin, a Wnt agonists to increase crypt proliferation (1). Other organoid models (4-8) have used ENR media successfully suggesting that these pathways are used across the epithelial populations from different tissues. Therefore, I decided to use ENR as my basal culture medium on which to test additional factors.

Organoids have been derived from other regions of the female reproductive tract: the fallopian tubes and endometrium (6,7,9). Although these are not stratified epithelia, there may be commonalities in the way the tissues are regulated and furthermore, these may be directly relevant for modelling the endocervix, which is continuous with the endometrium. The models have similar culture conditions including the use of ENR as a basal media, inhibition of TGFβ signalling and the addition of FGF10 (6,7,9). The use of R-spondin increased the size of organoids in the fallopian tube organoid culture (6) and helped expand endometrium organoids (7,9). The addition of EGF increased the number of formed organoids in both fallopian and endometrium organoids (6,7). Noggin allowed long-term expansion of endometrium organoids (7).

In the cervix, Wnt expression has been reported to play a role in the normal cervical epithelium. Stromal expression of Wnt4, Wnt5a and Wnt-7a has been reported throughout the Müllerian duct epithelium in mice. This expression gradually disappears from the vaginal epithelium after birth. This change in Wnts may play a role in the differentiation and development of the female reproductive tract (10). In humans, Wnt3a has been reported to be expressed in basal/parabasal

layers of normal cervix (11). Additionally, Wnt5a knockout mice lack normal cervical development (12).

Additionally, TGF-β signalling has been reported in normal cervical epithelium (including immature and mature metaplasia) (13). TGF-β1, TGF-β2, TGF-β3, TGF-βRI and TGF-βRII were detected by Immunostaining in normal endo-cervix (14). Epidermal growth factor receptor (EGFR) has been reported to be expressed in the lower layers of normal squamous epithelium of the cervix, but over-expressed reaching upper epithelial layers in dysplasia (15). Furthermore, the activation of MAPK signalling pathway through Fibroblast growth factor (FGF10) is important for epithelial progenitor expansion during organogenesis (16) and a key player in uterine/vaginal lineage determination in young mice (17).

To understand the ideal conditions to grow cervix organoids and to optimise the tissue from which to isolate cells for culture, I decided to use mouse cervixes (Figure 4.1) between the ages of 8-14 weeks as the starting point. This is because the full formation of SCJ and clear distinction between the two cervical lineages is seen from week 8 onwards (Figure 3.7).

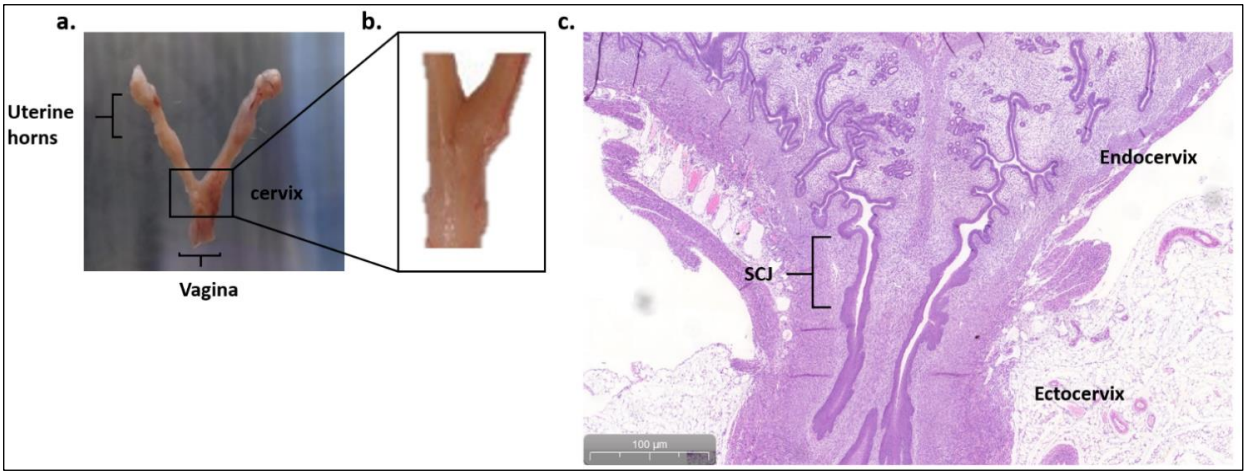

Figure 4.1: Dissection of mouse SCJ for the derivation of organoids. (a) Gross view of the murine female genital tract post dissection and harvest. (b) Gross view of the SCJ after removal of the uterine and vaginal ends. (c) A representative H&E section, showing the selected region used to derive murine cervical organoids, scale bar= 100µm.

The derivation procedure consists in culturing cells isolated by dispase (for 24 hours) followed by a trypsin enzymatic dissociation of the cervical tissue (see methods section 2.1.5). Dispase separates the epidermis from the dermis and trypsin is then needed for further cell dissociation. This protocol allowed the isolation of all epithelial populations from the cervix, that I then embed into the Matrigel® droplet. Finding the optimal digest protocol is important for my experimental approach as the identity and location of the stem cells of the cervix are unknown.

Thus, my starting digest must be enriched in all epithelial populations to ensure that if the correct culture conditions are used, it will expand the stem cells and allow the establishment of culture. In order to verify that this protocol allows the isolation of all epithelial cells, I first performed a cytospin smear of the cervical tissue digest and stained for pan-keratin and vimentin markers to determine the epithelial vs stromal cells ratio. The digest contained mostly epithelial cell, shown by pan keratin IF staining (Figure 4.2). Next, to ensure that both cervical lineages are present, I assessed the cytospin smear for both KRT17 squamous/reserve cell marker and KRT8 columnar marker via IF. The digest was a mix of both (Figure 4.2). Thus, the sequential digest protocol using dispase and trypsin allows the isolation of the two major epithelial lineages from cervical tissues. Subsequently, I pelleted the digest by centrifugation and resuspended in ice-cold Matrigel® at a ratio of 1:20 in a 20µL drops into 48-well plate (detailed in methods section 2.1.6).

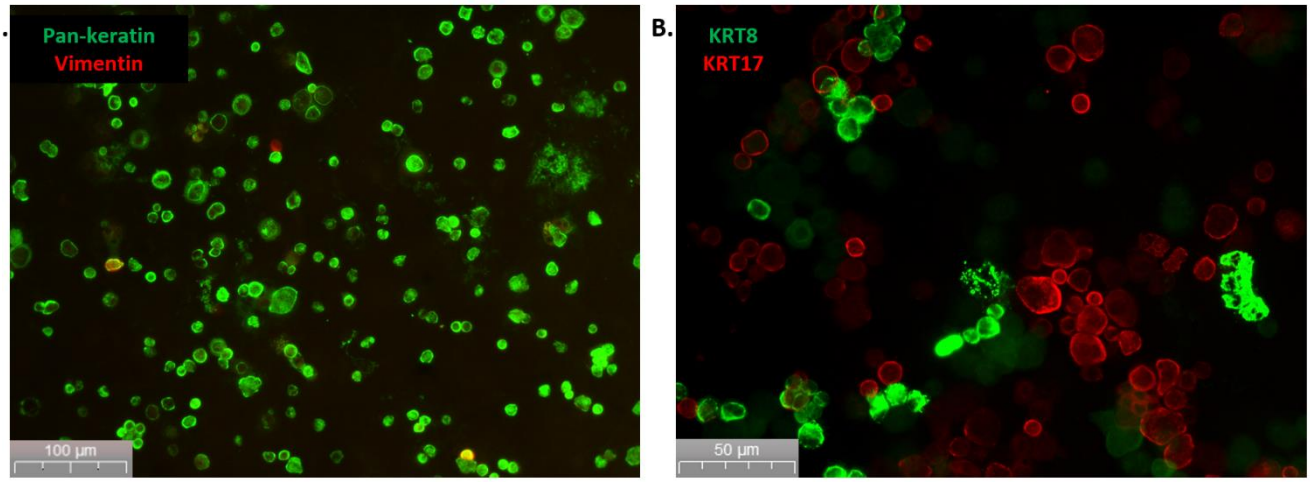

Figure 4.2: Cytospin of the mice cervixes harvest post digestion, stained with pan-keratin antibody as an epithelial marker and vimentin as mesenchymal marker. (A) Representative cervical digest stained with pan-kertain (green) and vimentin (red). The staining shows the digest indeed contained mainly of cells of epithelial origin, scale bar= 100µm. (B) Assessment for both KRT17 (red) squamous/reserve cell marker and KRT8 (green) columnar marker via IF of cytospin of the mice cervixes harvest post digestion, the digest showed mixed population of KRT17/KRT8, scale bar= 50µm.

Based on what has been reported on signalling in the cervix, and what has been essential to derive other female genital tract organoids, I have selected a number of factors to add to ENR medium (Table 4.1). Among the list of potential factors, I started with A83-01 and FGF10. These were added to ENR and their effect on organoid formation and number was observed over 10 days (Figure 4.3).

After 10 days, there were too many cells attaching to the bottom of the well and the Matrigel® became unstable, therefore I decided to passage and re-plate the cultures. Passaging was done by vigorous pipetting (~300 times), a procedure commonly used for other organoids, to break up the Matrigel® before resuspending the cells in a fresh drop (see section 2.1.6 for details). After the first passage, no significant cell growth was seen in the ENR-only medium (Figure 4.3a). The cultures grown in the presence of A83-01 (ENR+A) had few small spheroids with a lumen (Figure 4.3b). The addition of FGF10 (ENR+F) also resulted in a few spheroids growing but these were dense clusters that had no lumen (Figure 4.3c). The combination of A83-01 and FGF10 (ENR+AF) resulted in the highest number of organoids that were also larger in size compared to ENR+A (Figure 4.3d). Morphologically, the formed structures seemed complex with budding areas and appeared dense with varying sizes.

Table 4.1: Factors tested for the purpose of murine cervical derivation based on previous reports of organoid models from other organs.

Factor	stock	Final concentration	Manufacturer	Catalogue number
A83-01 (TGFβi)	1 mM	500 nM	Tocris Bioscience	2939
FGF-10	100 µg/mL	100 ng/mL	PeproTech	100-26
Prostaglandin E2 (PGE2)	25 mM	25 nM	Tocris Bioscience	2296
MAPK p38 inhibitor (p38i)	10 mM	10 µM	Tocris Bioscience	1264
Nicotinamide	1 M	10 mM	Sigma-Aldrich	N0636
CHIR99021 (GSK-3i)	1 mM	1 µM	Tocris Bioscience	4423

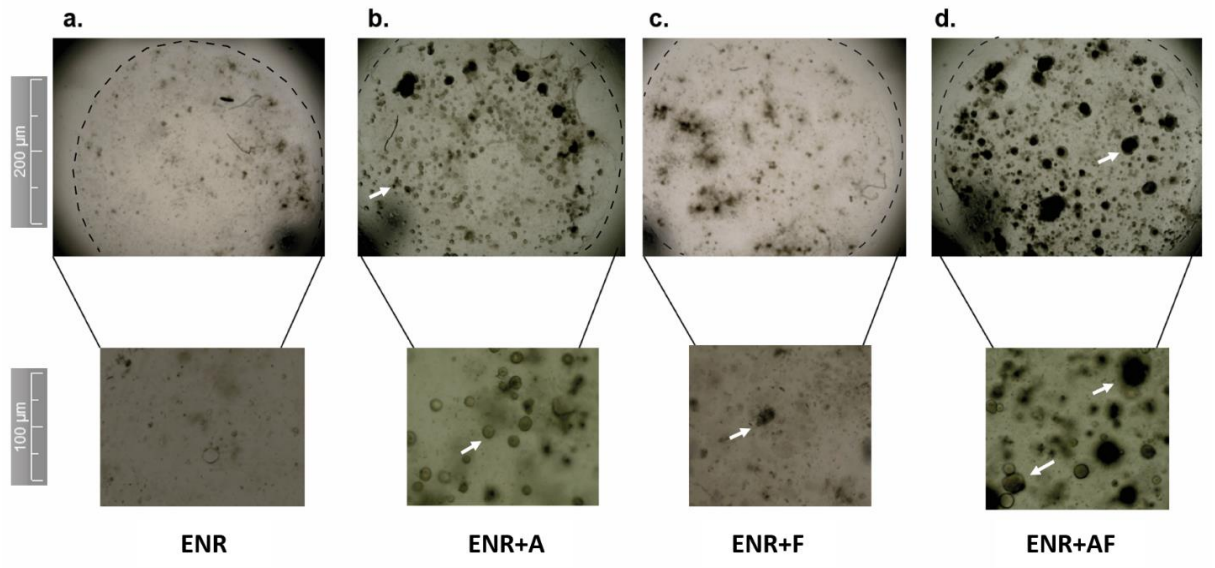

Figure 4.3: The effect of A83-01 and FGF10 addition to ENR. Representative bright field images showing that adding A83-01 (TGFβi) (b) and FGF-10 (c) to ENR media passage 0 day 7, a higher number and size of organoids was seen. Combining A83-01 and FGF-10 (d) showed the greatest effect. Top scale bar= 200µm and bottom scale bar= 100µm.

After the second passage of the cultures on day 9, the differences between the culture conditions and their ability to sustain growth became more apparent. In general, all cultures were cleaner as the stromal cells, which do not survive in Matrigel, are lost with passaging. ENR+AF contained many cellular structures that had spheroidal or complex morphologies (Figure 4.4).

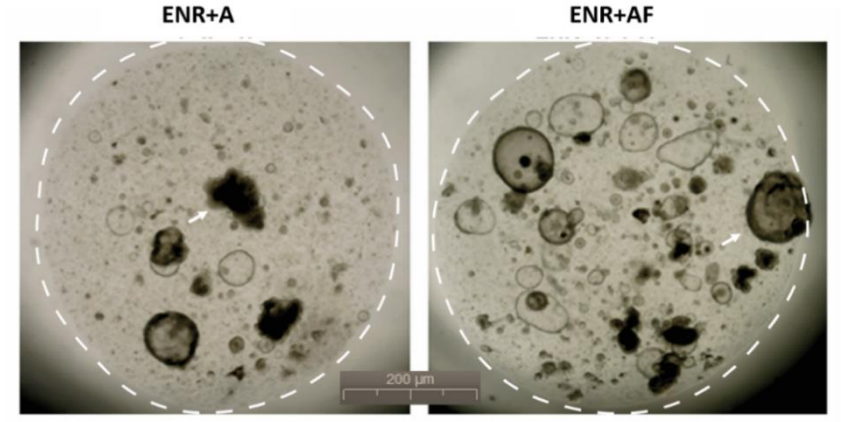

Figure 4.4: Following the effect of A83-01 and FGF10 addition to ENR. Representative brightfield images showing the addition of A83-01 (TGFβi) and FGF-10 to ENR media. At passage 2 day 9 the growth was greater when combining A83-01 and FGF-10 (left), scale bar= 200µm.

The culturing of murine cervical cell digest in the basal medium ENR supplemented with A83-01 and FGF10 (ENR-AF) allowed the generation and propagation of complex structures. However, these were hard to passage due to difficulties in breaking them up and therefore expand. Hence, I added an additional step of TrypLE® after manual pipetting to gently dissociate the cells (detailed in section 2.1.6).

My aim was to culture the two distinct cervical epithelial types: the secretory columnar lineage and the stratified squamous lineage. Since ENR-AF appears to favour the growth of a budding complex organoids (resembling the squamous lineage), I tested additional factors that have been reported to enhance long-term growth of ductal/secretory organoid cultures, to be able to grow the endocervical lineage. An example is Nicotinamide, a NAD+ precursor, that has been reported to enhance oxidative metabolism (18) and is vital for the culture of liver (19), pancreatic (20) and endometrial organoid (7). MAPK p38 inhibition (p38i) was also reported to be indispensable for the long-term culture of human small intestine and colon tissues (4). Prostaglandin E2 (PGE2) and CHIR99021 a GSK-3β inhibitor (GSK-3βi) are both implicated in the activation of the WNT pathway and have been reported to promote growth and proliferation of Lgr5+ colonic stem cells (21), prostate organoids (22), colon organoids (4) and trophoblast organoids (8).

Unlike the previous factors, evaluation of Nicotinamide, p38i and PGE2 was performed on single cells from and early passage of an established cultures (passage 4) and not directly from mouse cervical digest. This is because I assumed the presence of progenitor cells which sustained the growth in culture for a month. The results showed a beneficial effect of PGE2 within 4 days of its addition to ENR, with larger and more numerous spheroids (Figure 4.5). Spheroids in ENR-P2 condition are easy to break up for passaging, allowing better growth and propagation. The spheroids growing in ENR-P2 were passaged every 7-8 days, with vigorous pipetting (~300 times) to break the Matrigel® together with the spheroids before resuspending the spheroid fragments in a fresh droplet (see section 2.1.6 for details).

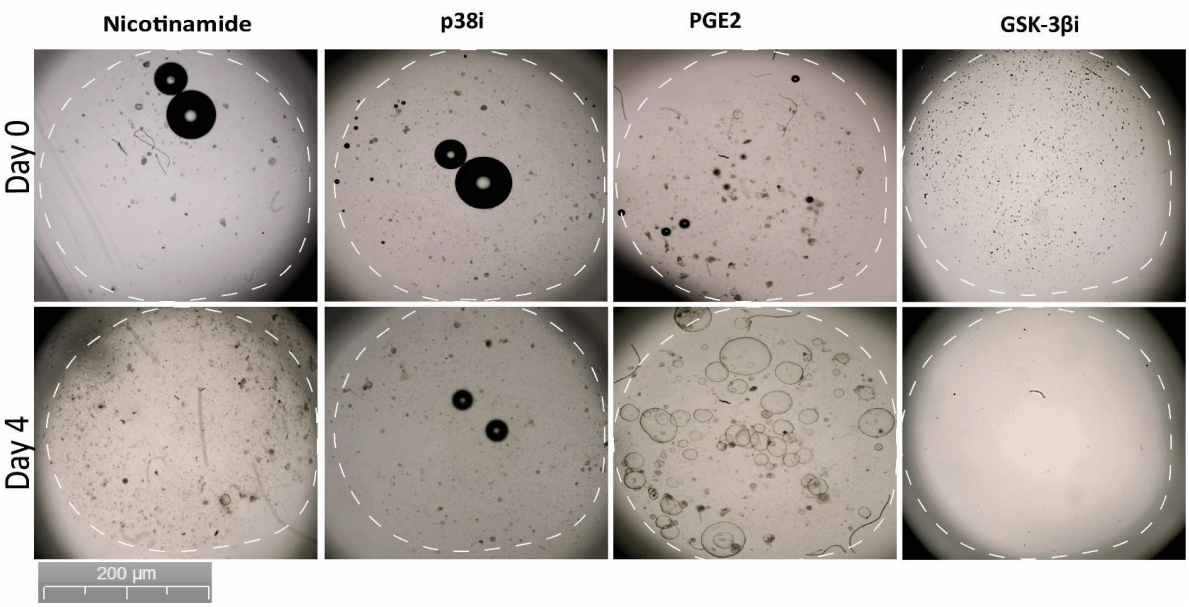

Figure 4.5: Factors tested to enhance cell growth. Representative brightfield images of 4-day-old cervix organoids under the effect of nicotinamide, p38 inhibitor, GSK-3β inhibitor and PGE2. At day 4 the addition of PGE2 showed substantial growth, scale bar= 200µm.

4.2.2 Characterisation of murine cervical organoids

After the identification of the culture composition to grown ectocervical and endocervical-like 3D structures, I next investigated the organisation, and the cell types present within these cultures grown in ENR-AF and ENR-P2. For this, I fixed the organoids in 10% Neutral buffered formalin (NBF) and processed them for paraffin blocks with the help of the department histologist Ms. Helen Skelton. I selected a panel of markers: KRT8 for endocervical columnar epithelia (23); KRT17 for cervical reserve cells (24); and a squamous marker of the ectocervix in mice (my observations, Chapter 3, Figure 3.10) (Table 4.2). Additionally, I also stained for TP63, a homologue of the tumour suppressor P53, that is active in embryonic stages of development (25) and a marker of both squamous basal cell (26) and reserve cells (24) that I showed earlier in Chapter 3 (Figure 3.12). Cell cycle activity marker MCM7 allows to assess proliferation within the organoids (27).

Table 4.2: Antibody panel used for characterisation of murine cervical organoids.

Antibody	Dilution used	Host	Amplification	Manufacturer	Catalogue number
Cytokeratin 17	1:250	Rabbit	-	abcam	Ab51056
Cytokeratin 8	1:50	Mouse	-	Santa Cruz	Ac-374275
Total P63	1:100	Mouse	Yes	abcam	Ab735
MCM7	1:100	Rabbit	Yes	abcam	Ab52489
Mucin 1	1:50	Rabbit	-	abcam	Ab109185
Mucin 5AC	1:500	Rabbit	Yes	Altlas	HPA040615

The staining of ENR-AF organoids revealed that it is indeed composed of a stratified squamous epithelium. KRT17 is present at the basal and parabasal layers together with TP63 (Figure 4.6). These markers decreased gradually, with no expression in the most differentiated innermost layers towards the lumen. This is consistent with the apical/basal orientation observed in other organoid systems, with the apical surface facing the lumen (Figure 4.6). KRT8+ cells are present in the superficial layers closest the lumen. Whilst MCM7+ cells are primarily in the basal layers of the organoid (Figure 4.6). The pattern of expression remarkably resembles what is seen *in vivo*, with KRT17+TP63+ cells found in the basal/parabasal layers of the ectocervical epithelium with gradual decline associated with differentiated layers, and KRT8 cells found on top of KRT17+ cells in the SCJ region in murine cervix. Similarly, the MCM7 pattern in organoids mimics MCM7 *in vivo* with proliferative cells in the basal layers (see chapter 3, section 3.2.3).

As suggested by their morphology, the spheroids grown under ENR-P2 conditions are composed of a single-layered epithelial structure. In contrast to ENR-AF, they are TP63-, KRT17- and uniformly KRT8+ as is the endocervix. Consistent with the observations of their high growth rates in culture, MCM7 expression was high and expressed in almost every cell (Figure 4.6). Although ENR-P2 were mostly negative but occasionally I see positive KRT17 cells (Figure 4.7).

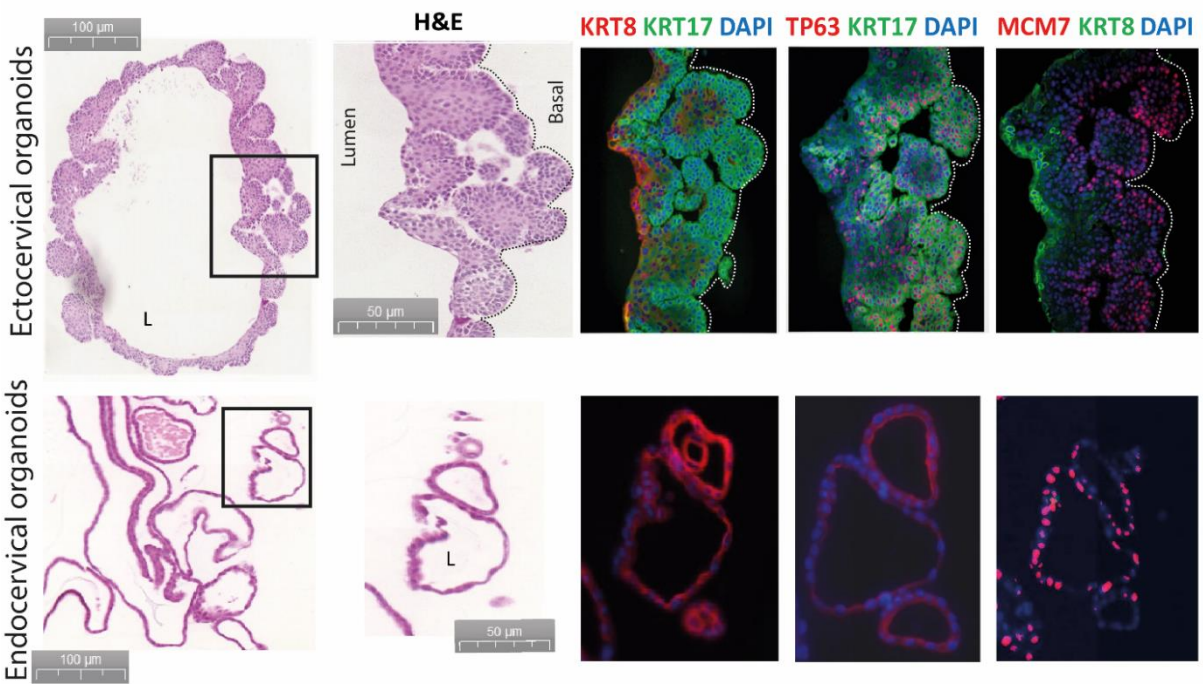

Figure 4.6: Characterisation of murine cervical organoids by IF. Representative H&E and fluorescence projections of murine cervix organoids, top row displays squamous ectocervical organoids, stratified organoids had a single layer of KRT8 cells in the superficial layer (close to the inner lumen), and KRT17/TP63 cells in basal, parabasal and intermediate layers with highest proliferation rate (shown by MCM7) is in KRT17 parabasal layers. Bottom row displays the columnar endocervical organoids, from left to right, H&E staining, IF for KRT8/KRT17 showing no KRT17 cells, TP63 progenitor marker colocalises with KRT17 and MCM7 proliferation marker. scale bar= 100µm and 50µm respectively. Blue colour indicates DAPI nuclear staining and L=lumen.

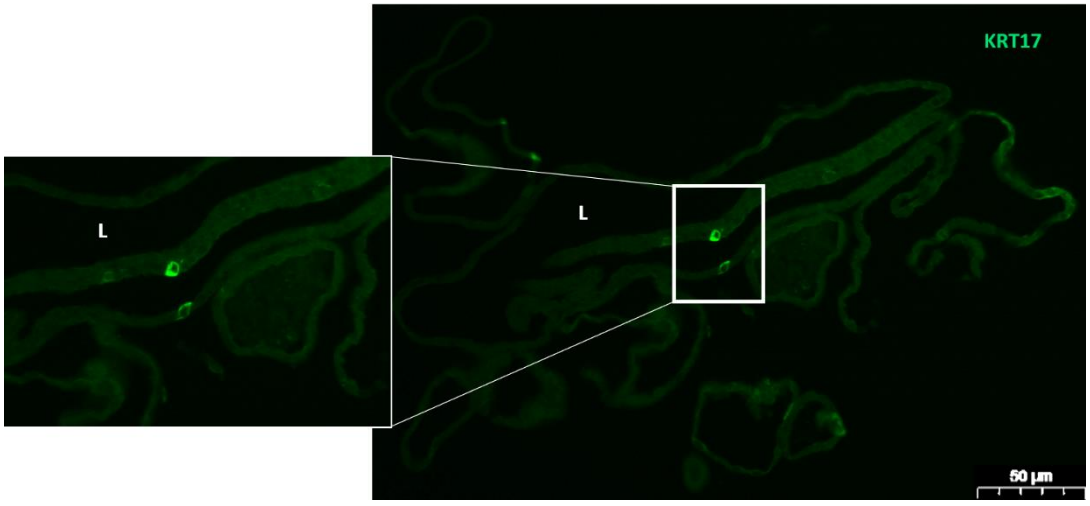

Figure 4.7: KRT17 staining in ENR-P2 spheroids. Representative IF projection showing an occasional KRT17+ cells (green) observed in ENR-P2 spheroids. Scale bar= 50µm, L=lumen.

So far, the expression patterns of cervical markers of the cultures grown in ENR-AF and in ENR-P2 suggests that the two different organoid systems recapitulate the endo and ectocervical regions. In order to further characterise these distinct phenotypes, I looked for additional markers that are differentially expressed between the two regions of the cervix. MUC1, a glycosylated transmembrane mucin protein, is found on the surface of most glandular epithelial cells and expressed throughout the entire female genital tract (28), although at lower levels in non-columnar cells *in vivo*. The apical surface of cells within ENR-P2 spheroids strongly stain for MUC1. The lumen becomes full of mucin with extended culture (more days in culture per a single passage). This is reminiscent of what was observed also in the endometrial organoids, which are also columnar epithelium (7). MUC1 is not present in the stratified organoids grown in ENR-AF (Figure 4.8). As MUC1 is widely expressed in other regions of the female reproductive tract, I also stained for MUC5AC (28) which is produced only by columnar epithelium of the endocervix *in vivo* (Figure 4.9). The pattern was similar with strong MUC5AC staining in the ENR-P2 cultures but absent in the stratified ENR-AF (Figure 4.8).

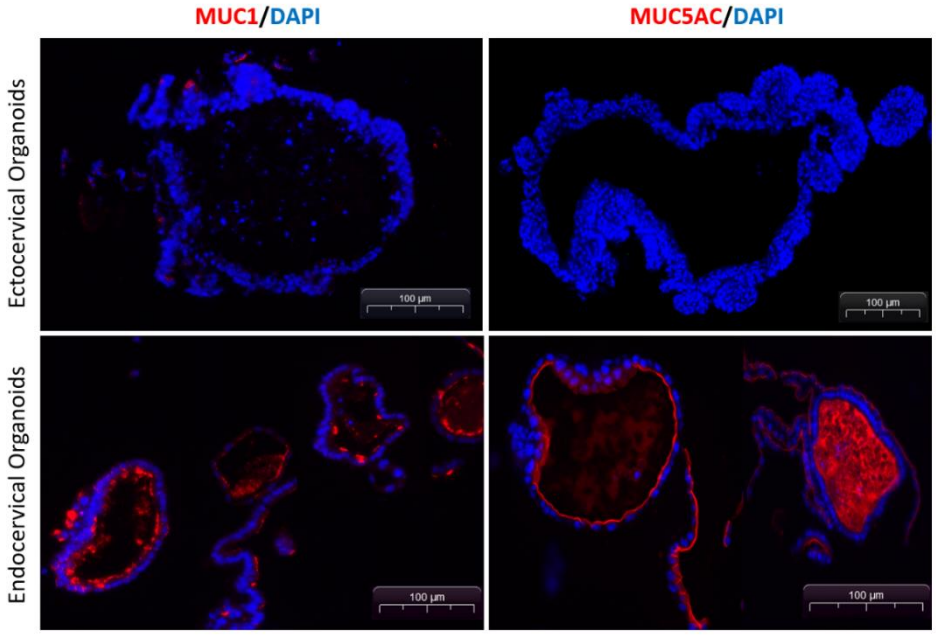

Figure 4.8: Staining cervical organoids with secretory markers MUC1 and MUC5AC. Representative fluorescence projections of murine cervix organoids (a) Cell surface mucin MUC1 (red) show strong positivity inside the lumen of endocervical ENR-P2 culture. (b) MUC1 shows faint pattern on ENR-AF squamous cultures. (c) MUC5AC (red) appear strong positivity in the lumen of endocervical ENR-P2 culture. (d) MUC5AC is negative on ENR-AF squamous cultures. Blue colour indicates DAPI nuclear staining and the scale bar= 100µm.

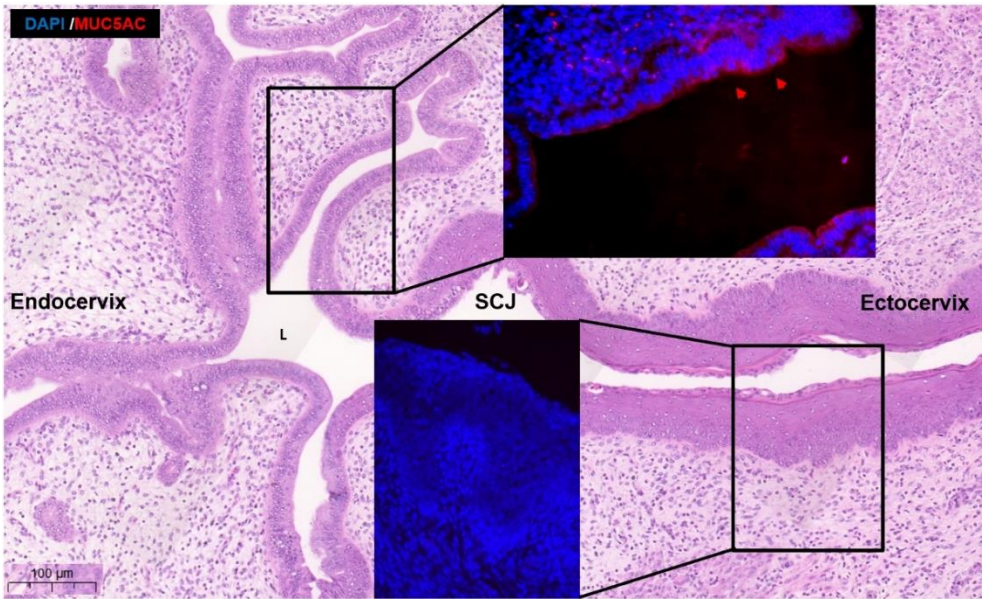

Figure 4.9: MUC5AC pattern in the mouse cervix. Representative H&E and fluorescence images showing MUC5AC positivity (red) in the endocervical columnar epithelium but not in the squamous epithelium of the ectocervix. Blue colour indicates DAPI nuclear staining, scale bar= 100µm and L=lumen.

It is clear that the medium components that are used for the derivation are essential for the establishment of organoid cultures of the cervix. Using the established murine cervical organoid cultures, both endo- and ecto-, I sought to establish the importance of each culture medium component for the propagation of the cultures once they are established. In order to do this, 5,000 single cells from established organoids generated by an enzymatic digest of ENR-P2 and ENR-AF were plated in the absence of each factor. The number of organoids present after one week was counted. The absence of PGE2 had a substantial effect on the growth of ENR-P2 cultures with less organoids growing (Figure 4.10). Therefore, PGE2 is essential for the maintenance and propagation of ENR-P2 cultures but also the presence of the basal media components EGF, Noggin and Rspondin-1 are necessary, confirming that this medium composition is optimal for endocervical organoids. For the ectocervical organoids, the withdrawal of A83-01 had the strongest effect on stratification in ENR-AF culture with less stratified complex structures (Figure 4.11).

In summary, under the two different conditions, organoids with distinct phenotypes can be established from murine cervical tissue. The presence of FGF10 together with inhibition of TGFβ allows extensive stratification (differentiation) and formation of complex cellular structures whilst PGE2 promotes the formation of spheroidal structures with a single-layered epithelium. Organoids cultured in ENR-AF are positive for KRT17+, TP63+ but are KRT8- and MUC5AC-. In ENR supplemented with PGE2, the organoids are a columnar epithelium

and are characterised by KRT8+ MUC5AC+ staining but are TP63- and mostly KRT17-. Overall, the cellular organisation and marker expression of the organoids are similar to what is seen in both the murine endocervix and murine ectocervical/SCJ. As the cervical cultures contain multiple cell types, I will henceforth refer to the stratified organoids grown in ENR-AF as ectocervical organoids and single epithelial layered organoids cultured in ENR-P2 as endocervical organoids.

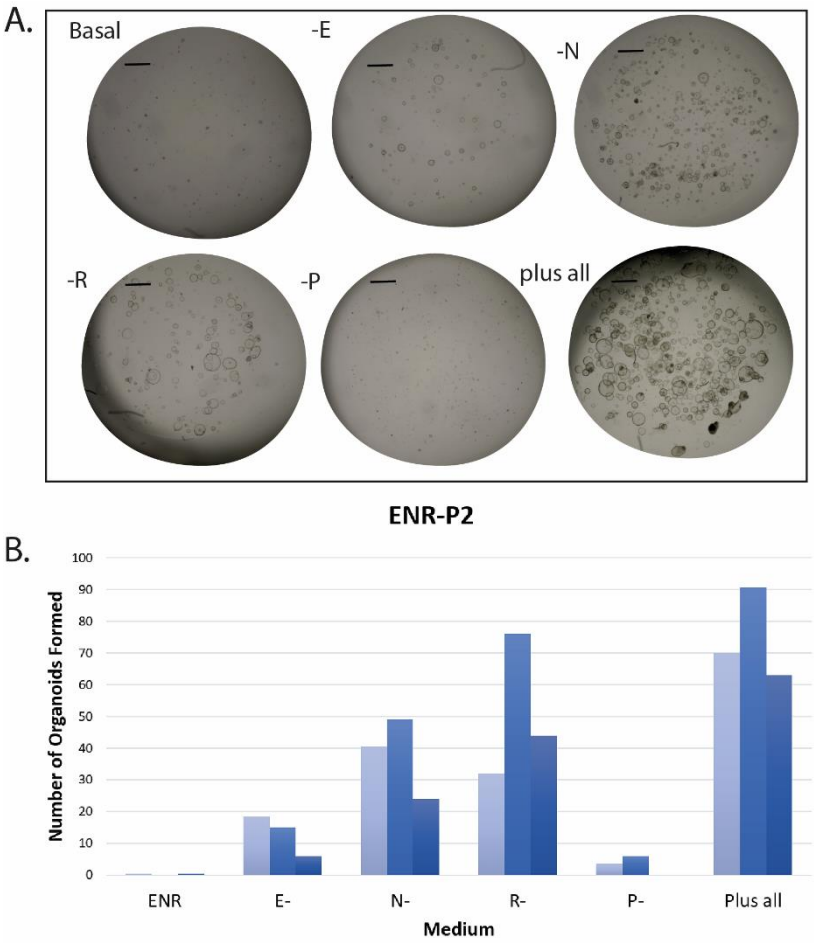

Figure 4.10: Effect of withdrawal of growth factors from ENR-P2. (A) Representative bright field images of organoid cultures in the absence of: EGF (-E), Noggin (-N), Rspondin-1(-R) or PGE2 (-P). The plus all refers to control conditions with complete medium, scale bar=200µm. (B) Quantification of the culture conditions tested. The number of organoids formed in the plus all condition was highest whilst the absence of PGE2 had the lowest rate of growth, *n=3* per all tested conditions.

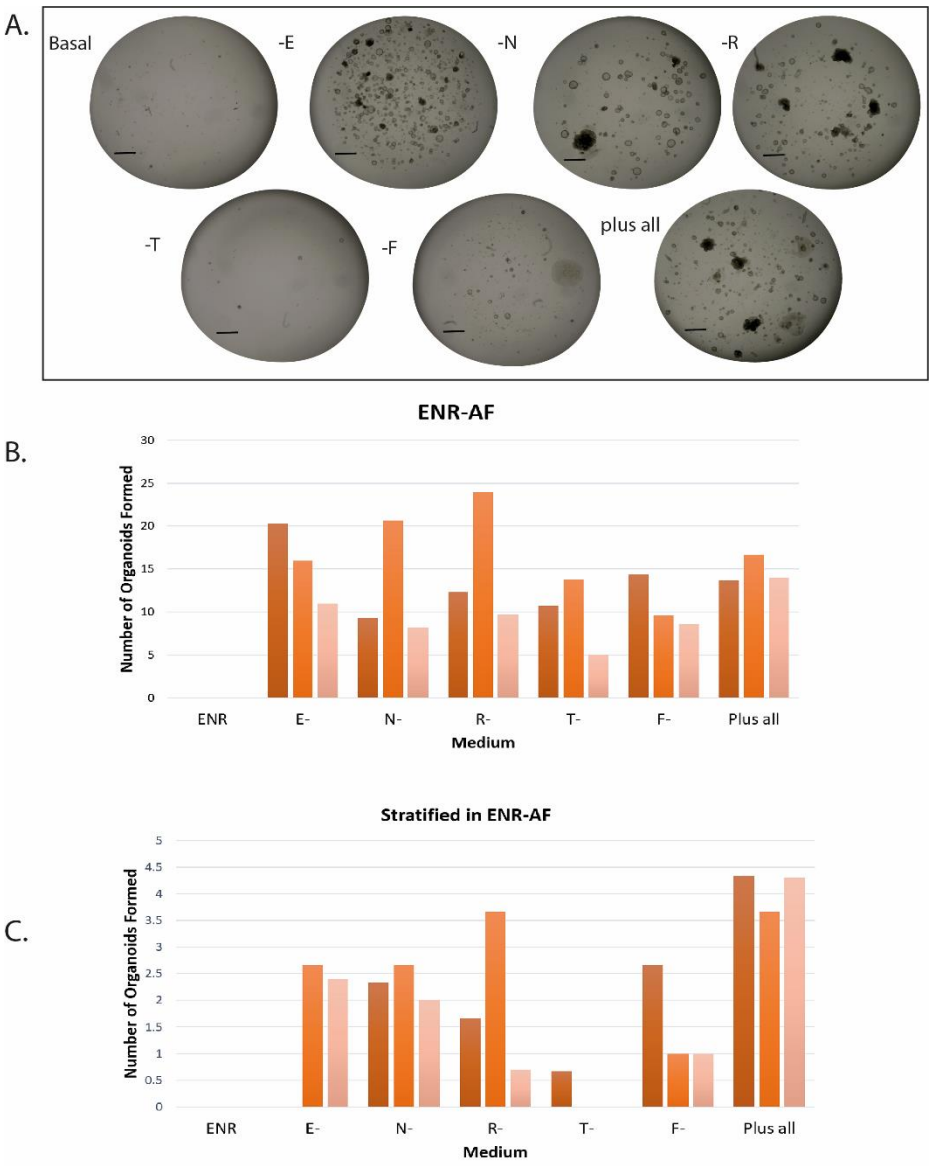

Figure 4.11: Effect of withdrawal of growth factors from ENR-AF. (A) Representative bright field images of organoid cultures in the absence of: EGF (-E), Noggin (-N), Rspondin-1(-R), A83-01 (-T) or FGF10 (-F). The plus all refers to control conditions with complete medium, scale bar=200µm. (B) Quantification of the culture conditions tested. The number of organoids formed in formed in the plus all condition had the highest growth, whilst the absence of A83-01 TGFβ inhibitor had the lowest number of organoids, n=3 per all tested conditions.

4.2.2.1 Investigating the signalling pathways directing proliferation and differentiation of the cervix in vivo using cervical organoids

Defining how stratification in the cervix is controlled and the microenvironment that influences cell fate in the junctional zone of the cervix where columnar cells and squamous cells meet are essential to increase our understanding of the etiology and progression of cervical carcinoma. However, our knowledge of this process is limited. The ectocervical and endocervical organoids that I established, present an opportunity to directly study the signalling pathways that may be implicated in the regulation of epithelial cell fate *in vivo*.

During the optimisation of the organoid culture conditions, I found that the presence of the TGFβ inhibitor A83-01, correlates with squamous stratification and differentiation of the cells within the organoids. On the other hand, the addition of PGE2 promoted secretory columnar phenotype of the organoids. Therefore, I sought to investigate the roles of TGFβ and PGE2 signalling in driving cervical organoids cultures towards either the squamous or columnar lineages.

In order to investigate the importance of TGFβ signalling in the cervix organoids, I used Activin, a TGF-β ligand that acts via Smad2 and Smad3 (29), to mimic the opposite effect of TGF- β inhibition by directly activating the pathway. Starting from murine cervical digests, I evaluated the growth and phenotype of the organoids under five different culture conditions (Table 4.3): **(1)** ENR-FAA (ENR media+F10+Activin A), in which TGFβ signalling is both endogenous and from Activin A induction; **(2)** ENR-F (ENR media+F10) depending on endogenous TGFβ signalling, **(3)** ENR-FP2 (ENR media+F10+P2) TGFβ is endogenous and cAMP is activated via PGE2, **(4)** ENR-AF (ENR media+A83-01+F10) where TGFβ was inhibited with A83-01, this media cocktail is what I use to derive ectocervical organoids, and **(5)** ENR-AFP2 (ENR media+A83-01+F10+P2) where TGFβ was inhibited with A83-01 and cAMP activated via PGE2.

Under these conditions, two levels of TGFβ activation (endogenous and via Activin A) were used to compare the effect along with the inhibition of the pathway via A83-01. FGF10 was added in all conditions to observe the limited effect (not to change many factors from what I default use as a stratification media) on TGFβ *in vitro* manipulation. TGFβ activation was tested with or without PGE2 (which had the greatest effect in deriving columnar spheroids).

Between passages 0 to 3, cultures in medium with active TGFβ signalling both endogenous (ENR-F, ENR-FP2) and via Activin A (ENR-FAA) showed greater growth compared to cultures where TGFβ signalling was inhibited (ENR-AF, ENR-AFP2). However, after the

second passage, cell survival was compromised when in ENR-FAA (Figure 4.12). PGE2 did not significantly alter growth rate during early passages (0-3), but a clear effect was observed at passage 5, where more spheroids were seen in the presence of PGE2 (Figure 4.14 for IF no data shown for bright field). FGF10 had clean spheroids at passage 3 (Figure 4.12) but could not be sustained long-term without PGE2 (later passage not shown).

Table 4.3: Five conditions chosen to investigate the roles of TGFβ and PGE2 pathways.

Factor	ENR-F	ENR-FP2	ENR-FAA	ENR-AF	ENR-AFP2
A83-01 (TGFβi)	-	-	-	+	+
PGE2	-	+	-	-	+
FGF10	+	+	+	+	+
Activin A	-	-	+	-	-

+ = added to media, - = absence.

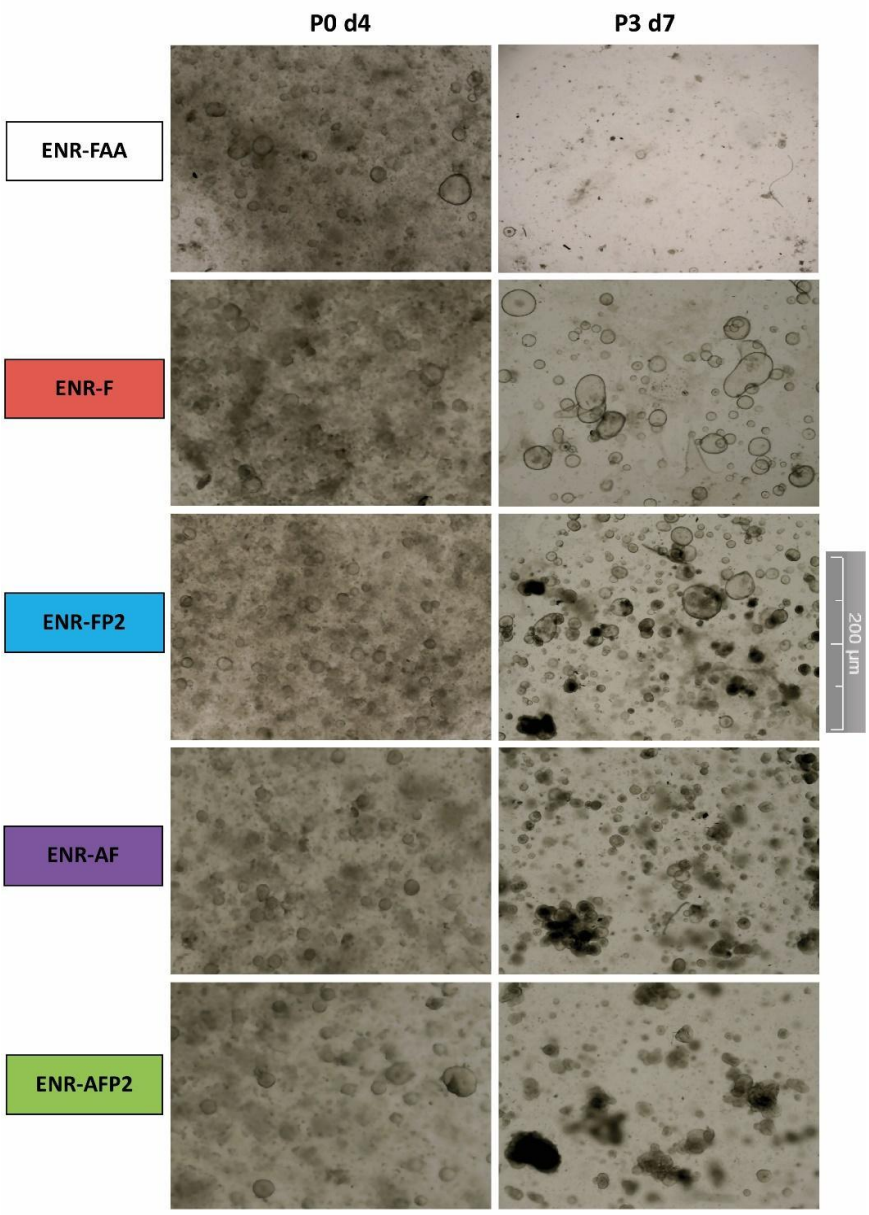

Figure 4.12: Bright field images comparing the five different conditions used for the study of TGFβ and PGE2 roles in the growth and differentiation of cervical organoids. Top row displays 4 days after initial plating, while the bottom one shows the phenotype at day 7 passage 3, scale bar=200µm.

For a quantitative assessment and comparison of the expression of the various markers of the different lineages between the culture conditions, I extracted RNA from the four conditions in which cultures could be maintained (passage number 5): ENR-F, ENR-FP2, ENR-AF and ENR-AFP2 for gene expression analysis by qRT-PCR. I selected the following markers: for the columnar lineage (*Krt8* and *Epcam*), for the squamous lineage (*Krt17*) and receptor for Rspondin-1, *Lgr5* were used. *Lgr5* is a marker of intestinal stem cells that is highly expressed in also cervical cancer (30). *Lgr5* is a target gene of Wnt signalling that is dependent on TGFβ signalling (31).

Under the different experimental conditions, the cultures showed high levels of the columnar markers *Krt8* and *Epcam*. *Krt17* was however higher in conditions were TGFβ was inhibited (ENR-AF and ENR-AFP2) (Figure 4.13). Generally, *Lgr5* was relatively low except for slightly higher expression levels in ENR-F.

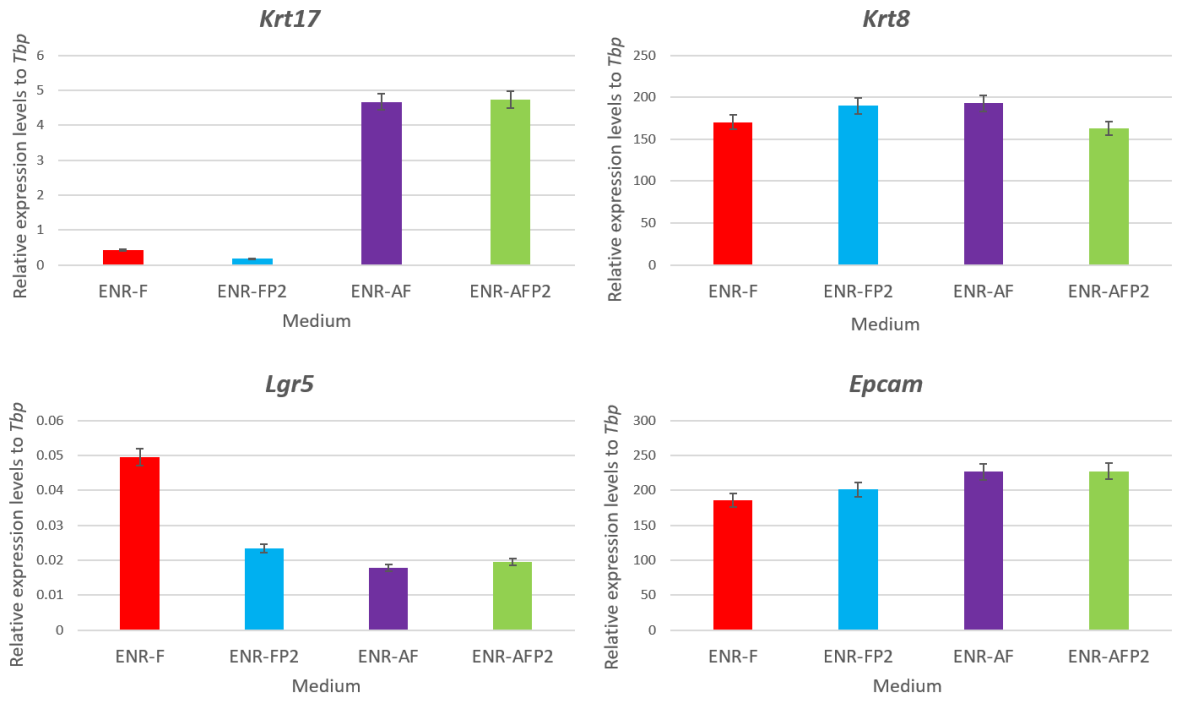

Figure 4.13: Comparison of lineage markers by qRT-PCR in culture conditions used for the study of TGFβ and PGE2 roles in the growth and differentiation of cervical organoids. Relative expression levels of target genes: *Krt17*, *Krt8*, *EpCAM* and *Lgr5*, against TATA-binding protein (TBP) housekeeping gene in conditions: ENR-AF, ENR-AFP2, ENR-F and ENR-FP2, at passage 5, this was done with 3 sets of biological replicates.

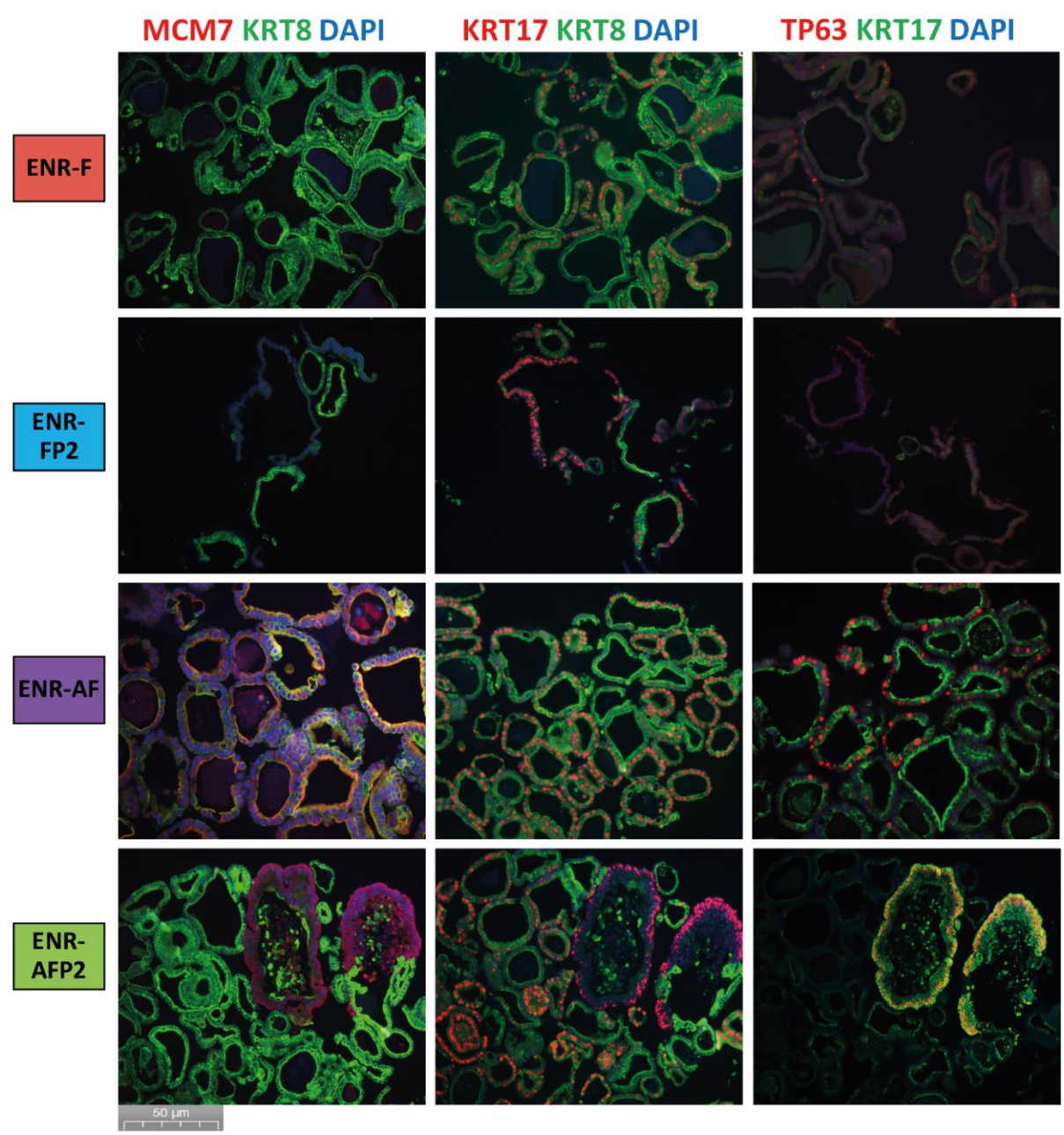

Figure 4.14: IF markers in the study of TGFβ and PGE2 roles in the growth and differentiation of cervical organoids. Fluorescence projections comparing TGFβ activation (ENR-F) with/without PGE2 and TGFβ inhibition (ENR-AF) with/without PGE2 at passage 5. Conditions with no TGFβ activity had a higher expression of KRT17/TP63. Blue colour indicates DAPI nuclear staining and the scale bar=50µm.

To validate the differences in lineage marker expression seen by qPCR, I collected the organoids for paraffin embedding and stained them with a selected panel of antibodies (Table 4.2). As predicted by the RNA analysis, KRT17 was mainly seen under conditions where TGFβ signalling was inhibited (i.e. ENR-AF and ENR-AFP2). ENR-AF produced spheroids with co-localisation of KRT8+ and KRT17+ with nuclear TP63. ENR-AFP2 gave rise to stratified organoids that resembled those seen ENR-AF (4≥ passage). These organoids were highly positive for KRT17, TP63 and highly proliferative at the basal layers (Figure 4.14). In contrast, spheroids in conditions with activated TGFβ signalling show almost no sign of squamous differentiation. They are KRT17-, TP63- expression and KRT8+. The differentiation seen in ENR-AFP2 was unexpected since the previous experiment showed no sign of stratification in the presence of PGE2.

To better understand the effects of PGE2 in conditions where TGFβ was inhibited and whether the expression of the markers changes over time (prior to initiation of stratification), I stained organoids at an earlier passage (passage 3) of ENR-AFP2 and compared the phenotype with a later passage (passage 5) when the organoids are established. This comparison showed that at an earlier passage, ENR-AFP2 conditions contains spheroids that have a pattern of expression that is indistinguishable from the spheroids seen in ENR-AF. They both have co-localisation of squamous (KRT17 and TP63) and columnar (KRT8) markers (Figure 4.15). This suggests that PGE2 had an acceleration effect in the squamous differentiation process. However, additional experiments need to be done to verify this finding.

In summary, culture conditions that permit active TGFβ signalling (ENR-F; ENR-FP2) show no sign of stratification verified by low expression levels of squamous markers. Furthermore, addition of TGFβ agonist (Activin A) did not support the long-term growth of spheroids. Organoids grown in conditions in which TGFβ was inhibited (ENR-AF; ENR-AFP2) have clear signs of differentiation demonstrated by IF (KRT17+TP63+ markers) and by qPCR for *Krt17*. These results shed insight into the possible role of TGFβ signalling *in vivo*.

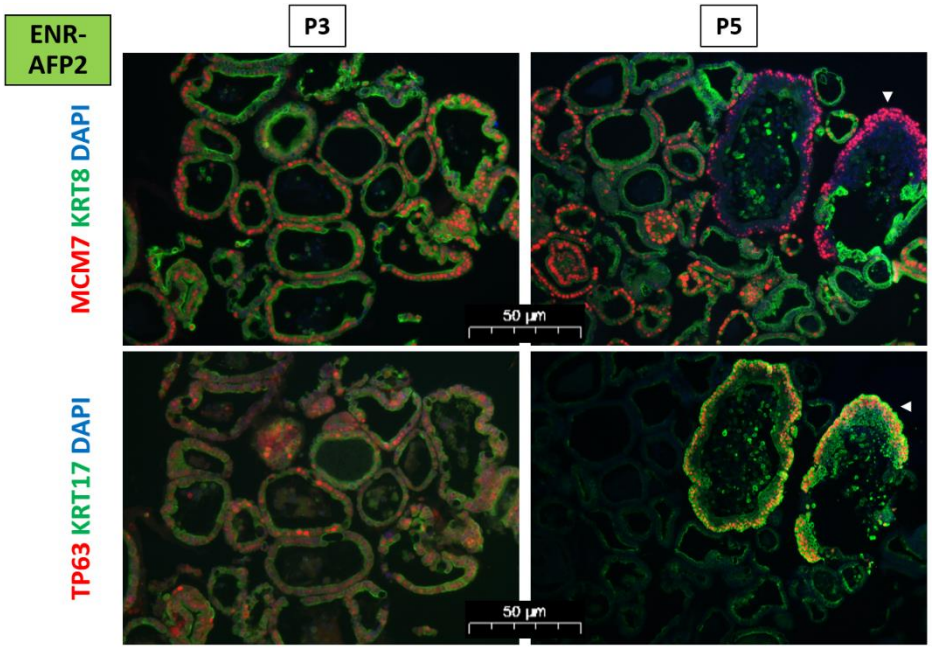

Figure 4.15: Comparison of lineage marker expression in ENR-AFP2 organoids at different passages. Representative fluorescence projections at an earlier time-point (passage 3) of condition ENR-AFP2 against passage 5, showing that stratification started with a KRT17+KRT8+ spheroids. Blue colour indicates DAPI nuclear staining and the scale bar=50µm.

4.2.3 Genome-wide transcriptomic analysis of the murine cervix *in vivo* and *in vitro*

My characterisation of the established cervical organoids suggest that they recapitulate key markers of the different regions of the mouse cervix. However, I have based myself on known markers so to further verify my findings, I sought to take an unbiased approach by analysing the general transcriptomic profiles of the organoids by microarray analysis. Therefore, the aims of the experiments described in this section are to: (i) compare the ecto- and endocervical organoids to the *in vivo* tissue to ensure their faithful representation and (ii) analyse the transcriptional signatures between the two different regions of the cervix (endocervix and ectocervix).

I initially explored the best way to obtain *in vivo* tissue samples for transcriptomic analysis. Cervical tissue in mice is small and difficult to dissect, therefore using an instrument that allows to dissect out specific regions of the tissues such as Laser-capture microdissection (LCM) technique (32), is ideal. I started by harvesting 3 adult, 11-week-old mice cervixes. I fixed the cervixes in Optimal cutting temperature compound (OCT) before using a cryostat to cut 8µm thick sections to mount them onto Polyethylene naphthalate (PEN) membrane frame slides (Life Technologies, Carlsbad, CA, USA) (method in details found in section 2.3). Before the

laser cut, I used Cresyl Violet stain to visualise the structure of the epithelium and to identify the areas of interest by morphology.

Four different tissue sites were collected: basal/parabasal cells from the squamous epithelium of the ectocervix and its underlying stroma and the columnar cells of the endocervix and its underlying stroma. The stroma plays an important role in the regulation of epithelial behaviour through paracrine signalling and thus, my approach would also permit the study of the tissue microenvironment underlying the two regions of the cervix. Approximately a total area of 50,000 μm was collected from each site within a period of 30 minutes from the beginning to end of the procedure to ensure RNA integrity.

The next step was to perform a quality control of the samples I collected. RNA Integrity Number (RIN) is rated 1 to 10, with 1 being the most degraded and 10 being the most intact. For development of the RIN, an algorithm which allows the determination of the electropherogram regions that indicates RNA quality is used. These include pre-region, 5S region, fast region, 18S fragment, inter region, 28S fragment, precursor region and post region markers, and is generated by the Bioanalyzer software. Epithelial compartments (basal/parabasal squamous and columnar cells) yielded better RIN than the stromal ones. I attempted several more collections focussing on the stroma to improve the yield and quality by collecting stromal regions from consecutive slides. However, this did not improve the RIN values. Although the collected epithelial compartments yielded higher RIN scores than the stroma, they were also below the required level to run a transcriptomic analysis (Figure 4.16).

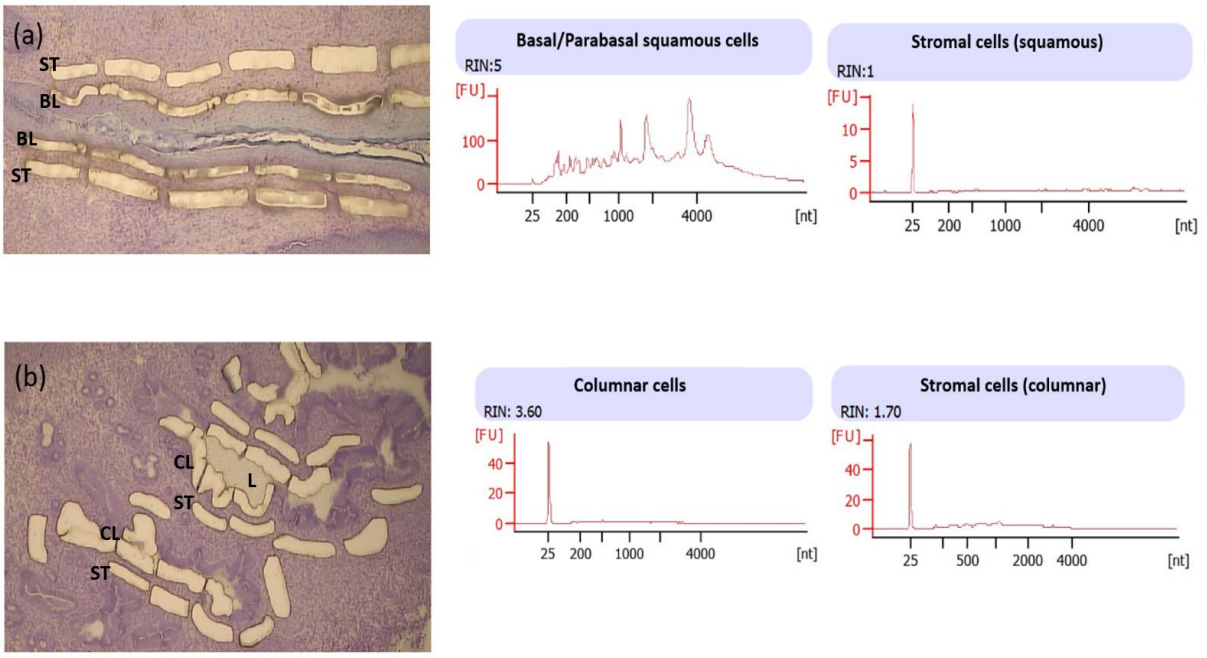

Figure 4.16: Collection of the different regions of the cervix by laser capture microdissection (LCM) technique and the quality of the RNA. (a) Top row left to right shows; LCM cuts of basal and parabasal layers of squamous epithelium and their underlying stroma visualised by Cresyl Violet stain, RNA Integrity Number (RIN) electropherogram of basal/parabasal squamous cells showing partially degraded RNA with integrity of 5 and the second RIN electropherogram showing totally degraded RNA with integrity of 1 from stromal cells collected from the ectocervix. (b) Bottom row left to right shows; LCM cuts of columnar cells of the endocervix and their underlying stroma visualised by Cresyl Violet stain, RIN electropherogram of columnar cells showing degraded RNA with integrity of 3.60 and the second RIN electropherogram showing degraded RNA with integrity of 1.70 from the complementing stroma. RIN value as calculated by The Agilent 2100 Bioanalyzer software is rated 1 to 10, with 1 being the most degraded and 10 being the most intact using the 28S:18S fragments ratio, 28S is approximately 5 kb and 18S is approximately 2 kb with the benchmark being 2:1. Nucleotide size (nt), Height Threshold [FU], BL=Basal Layer, CL=Columnar cells, ST=Stroma, L=Lumen.

Due to the challenges I experienced with LCM, I decided to extract RNA from bulk biopsies of endocervical and ectocervical regions from carefully dissected 11-week-old mice. As mentioned previously, dissection of the two regions in murine cervix is challenging. To ensure that I am able to accurately distinguish the two regions, I assessed the precision of the dissection using previously collected formalin blocks time-course of the formation of the SCJ in mice (discussed in chapter 3, Figure 3.7) and estimating where the uterine horns join the cervix in adult mice. Thus, I was able to collect tissue from the endocervical end (away from the junction) and ectocervical tissues from the SCJ from four mice.

Next, I generated endocervical and ectocervical organoid lines (n = 6 for each type) and collected them for RNA extraction at passage 6-7 when they are fully established and homogenous with clear phenotype (spheroids for endocervical and stratified organoids for ectocervical). I also included primary stromal cultures at an early passage (passage 1) from the

same mice from which organoids were generated as non-epithelial control samples. The assessed RIN of all organoids and stromal samples ranged from 10 (intact) to 6.9 (quality threshold) (Figure 4.17) and thus are of sufficient quality to be used for analysis.

Genome-wide transcriptomic analysis was carried out in collaboration with Cambridge Genomic Services (CGS) in our department. We used the Affymetrix Clariom S mouse HT array platform, which allows analysis of >20,000 annotated genes. Although the quality of RNA for all samples were adequate, some of the tissue samples had low concentrations of RNA and so we decided to amplify them with WT PLUS (see section 2.7 of methods for details). This method is widely used for the generation and amplification of biotinylated ss-cDNA for further hybridization.

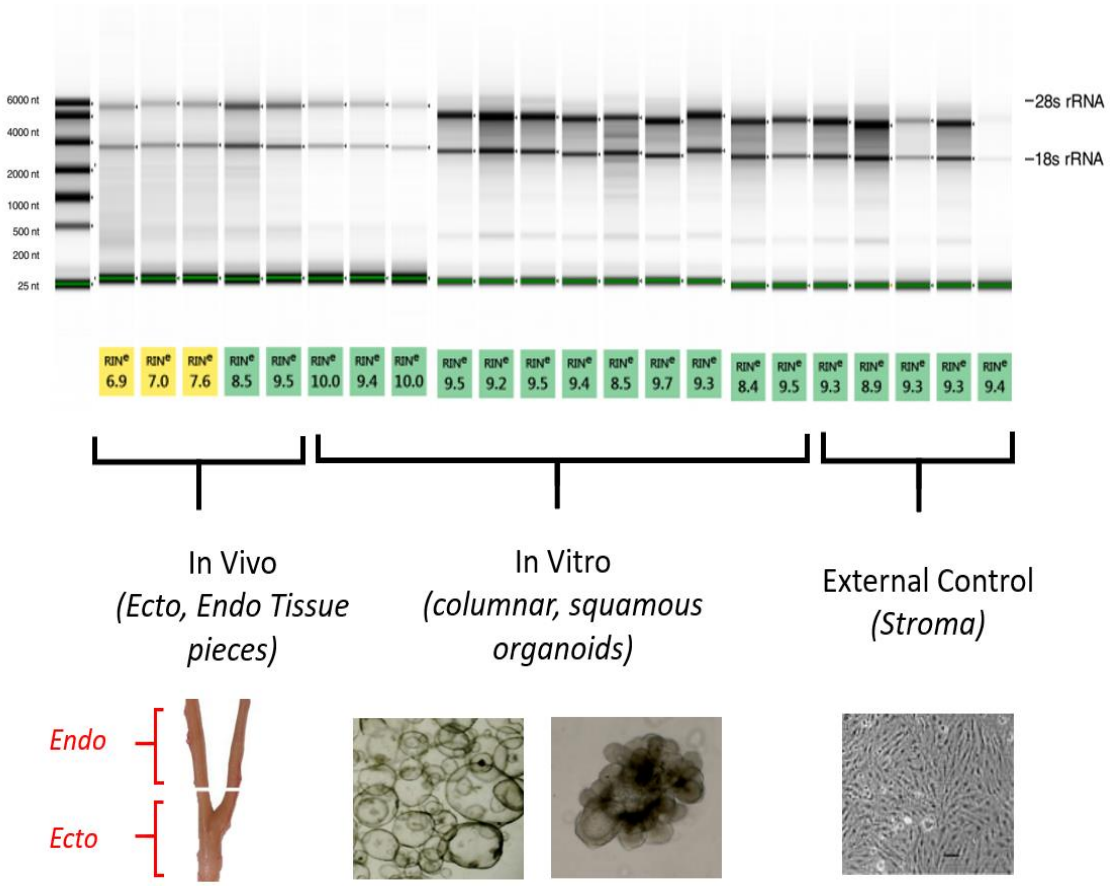

Figure 4.17: Smear gel analysis of the 22 samples used for the genome-wide transcriptomic analysis. List the number of samples for each group here. A ladder is shown for size calculation showing the 18S, 28S fragment bands. RIN=RNA Integrity Number.

I worked together with Ms. Stephanie Wenlock, a bioinformatician from CGS, to guide the analysis of the microarray data. The initial part of the analysis consisted of extracting and quality checking the raw data before normalisation, to reduce the non-biological variation across samples, as we are comparing *in vivo* and *in vitro* samples. In the comparison between *in vivo* samples (endo vs ecto), one sample (no. 4) showed a non-biological batch effect in the data. *In vivo* sample number 4 was causing batch variation due to differences in sample preparation (time of collection and freezing period), thus was excluded. In addition, when comparing the *in vitro* groups, squamous organoids (O_Sq) vs columnar organoids (O_Col), the data showed that 2 samples needed to be excluded due to the fact that both organoid lines (5 and 6) did not show stratification when H&E was examined, hence, causing bias in data analysis.

After exclusion of the aforementioned samples and normalisation of the dataset, we proceeded with hierarchical clustering of the samples in order to assess the similarities in the transcriptomic profiles between the different sample types (how the samples relate to their group and how the groups relate to each other). This was achieved using ~20K probes (s.d./mean > 0.1) and plotting the Euclidean distance between samples, calculations were based on their expression values. Two large branches were formed, one contained the samples with epithelial signatures (both *in vivo* and *in vitro*), and one with samples that lack epithelial markers (stroma). Indeed, this analysis confirmed that the organoid cultures cluster more closely to *in vivo* tissue than to stroma, most likely due to the epithelial component (Figure 4.18).

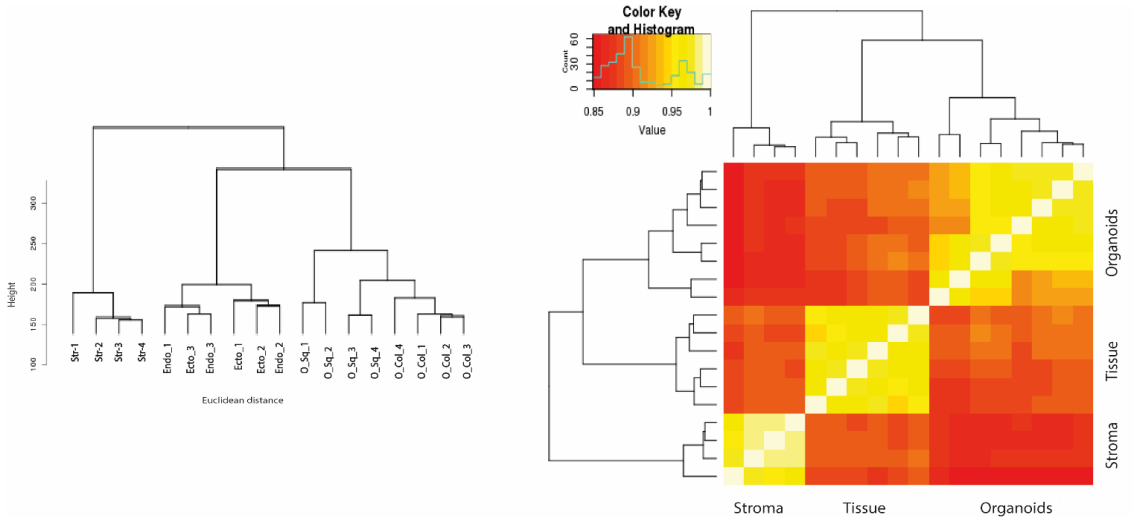

Figure 4.18: Genome-wide transcriptomic analysis of murine cervix in vivo and in vitro. On the left, hierarchical clustering analysis of global gene expression profiles by microarray, on the right clustered heatmap showing the three main groups compared in the array: in vivo (tissue), in vitro (organoids) and the stroma. Organoid cultures cluster more closely to in vivo tissue than to stroma. The R values are shown in the key above the heatmap plot.

4.2.3.1 Analysis of endocervix and ectocervix epithelial signatures in vivo

Despite the extensive studies on cervical pathologies, not much is known about the transcriptional regulation of the normal cervix. Thus, one of the aims of this experiment is to define endo/ectocervical transcriptomic profiles to explore potential molecular signatures that control cell fate of the two different epithelial lineages. This would provide a much-needed understanding of the molecular pathways that direct epithelial homeostasis at each site, therefore a comprehension of the consequences of HR-HPV viral gene expression and regulation that renders the site susceptibility and vulnerability to HR-HPV derived neoplasia.

The bulk tissue biopsies contain a mixture of epithelial and stromal populations. Therefore, in order to obtain information on the differences between the epithelia, the stromal samples were used as comparison against bulk cervical tissue to 'filter out' the stromal signature. To do this, we first compared *in vivo* bulk tissue samples of both endo and ectocervical regions to stroma ($P<0.05$). 5208 genes are commonly expressed between the stroma and the tissue samples, suggesting that part of these genes may describe the contribution of the stromal signature in the tissue samples (Figure 4.19). 1908 genes out of the 5208 are highly expressed in the epithelium, whilst 1112 are found in the stroma.

I first examined the gene lists obtained from these comparisons for generic epithelial markers. I reasoned that if these comparisons indeed allowed the filtering of the stromal signature to allow the comparison of epithelial signatures, I should see epithelial markers in the non-overlapping gene lists. Indeed, epithelial markers (E-cadherin (*Cdh1*), *Epcam* and *Esrp1*) and mucosal secretory cells (*Muc4* and *Pax8*) are among the highly expressed genes, validating our bioinformatic approach that has allowed to refine our gene list to epithelial genes (Supplementary table 3).

Next, I examined the list for known markers of endo and ectocervix to further validate these comparisons. Using fold change >2 and P-value <0.05, squamous markers (*Trp63*, *Krts10* and *Krt14*) are indeed more highly expressed in the ectocervical samples whilst markers of ciliated epithelial cells (*Foxj1*), *is* specifically expressed in the endocervical samples. Whilst potential lineage specific (endo or ectocervical) markers include transcription factor (*Pax2*) and *Plet1* surface protein in the ectocervix and *Cd44* in the endocervix (Table 4.4). Additionally, I found that different claudin proteins (CLDN) were expressed in the different parts of the cervix, *Cldn12* was only detected in the endocervix, whilst *Cldns: 1, 4, 8* and *10* were seen in the ectocervix (Table 4.4). Major urinary proteins (MUPs) also showed differential expression in

the different cervical lineages with *Mups 1,2,7,12* and *19* being commonly expressed in both endo and ecto-cervical epithelium, whereas *Mups 8* and *13* only in the ectocervix.

Table 4.4: Table showing the key epithelial signature that resulted from the in vivo overlap of endocervix, ectocervix and stroma, the first column shows genes in common in both lineages, the second column shows the key genes in the endocervix, whilst the last one shows the ectocervical genes.

	Common	**Endocervix**	**Ectocervix**
Epithelial markers	Pax8 Cdh1 Cldns: 3 and 7 Epcam Esrp1 Ehf Tcf7	Foxj1 Cldn12	Pax2 Trp63 Prep Krt14 Krt10 Tcf4 Cldn1, 4, 8 and 10
Signalling	TGF-β: Tgfbi WNT: Wnt2b and Wnt7a SHH: Gli1 MAPK: Ptger3 NOTCH: Dll4 FGFs: Fgf1 and Fgfr2 TNF: Tnfsf10 and 13	TGF-β: Inhba, Smad2 and Fst. WNT: Fzd7 and Ddk3 BMPs: Bmp1, Bmper SHH: Gli3 MAPK: Bdnf, Ptgr1 NOTCH: Notch3 FGFs: Fgf7 EGF: Egfr TNF: Tnfsf13b	TGF-β: Itgb6 WNT: Rspo1, Axin2 AKT: Wfdc2 Anti-viral: Apobec3
Stemness	Krt19	Cd44	Lgr4
Receptors and surface proteins	Mups 1,2,7,12 and 19 Esr1 Muc4 Tnfrsf21	Tnfrsfs: 1a, 12a and 23	Mups 8 and 13 Muc1 Cxcr4 Plet1 Tnfrsfs: 14 and 19

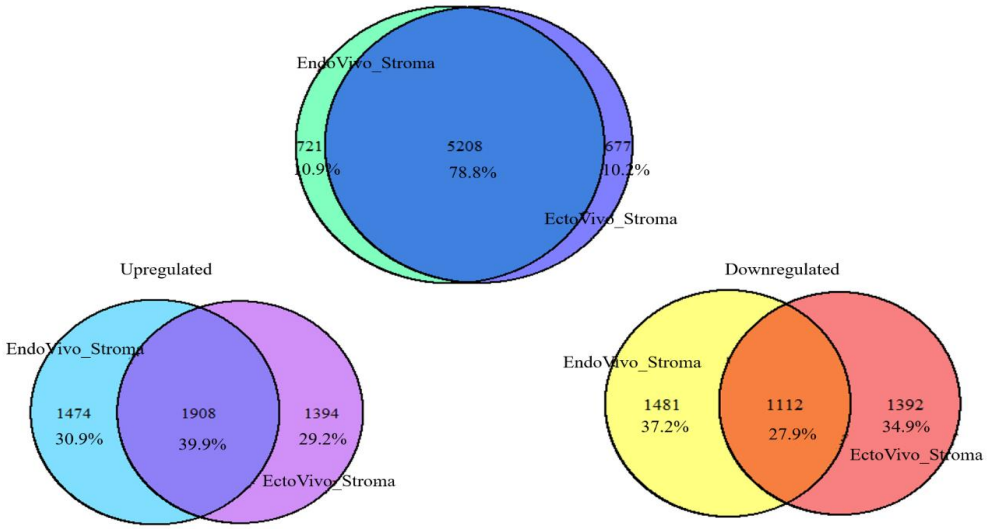

Figure 4.19: Using stroma to find key epithelial signatures in vivo. Venn overlaps showing FDR adjusted P<0.05 of in vivo comparison. 1908 genes out of the 5208 are highly expressed in the epithelium, whilst 1112 are found in the stroma.

4.2.3.2 Analysis of endocervix and ectocervix epithelial signatures in vitro

As my main goal in this chapter is to generate a physiologically relevant model of the mouse cervix, I wanted to ensure that the established *in vitro* organoid system is truly representative of their tissue of origin. To do so, I need to identify markers that are specific for endo or ectocervical lineage. Therefore, I examined the paired comparison of *in vitro* endocervical and ectocervical organoids. Using fold change >2 and P-value <0.05, comparative transcriptional analysis of organoids showed that ectocervical organoids indeed express squamous markers *Krt14, Krt17* and *Trp63*. However, for endocervical organoids, I did not observe any of the known columnar markers of the endocervix. A possible reason is that the number of samples was not enough to detect statistical significance. Additionally, I found that several cytokeratins were highly expressed in the ectocervical organoids including: *Krts 5, 13*, and *15*, Moreover nerve growth factor receptor (*Ngfr*) was one of the highly expressed genes in the ectocervical organoids (Figure 4.20).

In the endocervical organoids, although I did not detect any of the known epithelial columnar markers, several genes encoding proteins involved in secretory epithelial were highly expressed. These include: cystic fibrosis transmembrane conductance regulator (*Cftr*), transient receptor potential vanilloid 4 (*Trpv4*), peptidase D (*Pepd*) and colony stimulating factor-1 (*Csf-1*) (Figure 4.20) (Supplementary table 1).

In the stroma, *Lgr6* and surface integrin (*Itga5),* potentially interesting markers to further investigate, were highly expressed. *Lgr5 and Lgr6 are* stem cell markers in various organs including mouse skin (33), liver (5) and intestine (31) (Table 4.4). Whereas Itga5 plays a role in epithelial-mesenchymal transition in the oral squamous epithelium (34) and in wound healing (35). These have not been reported in the cervix yet.

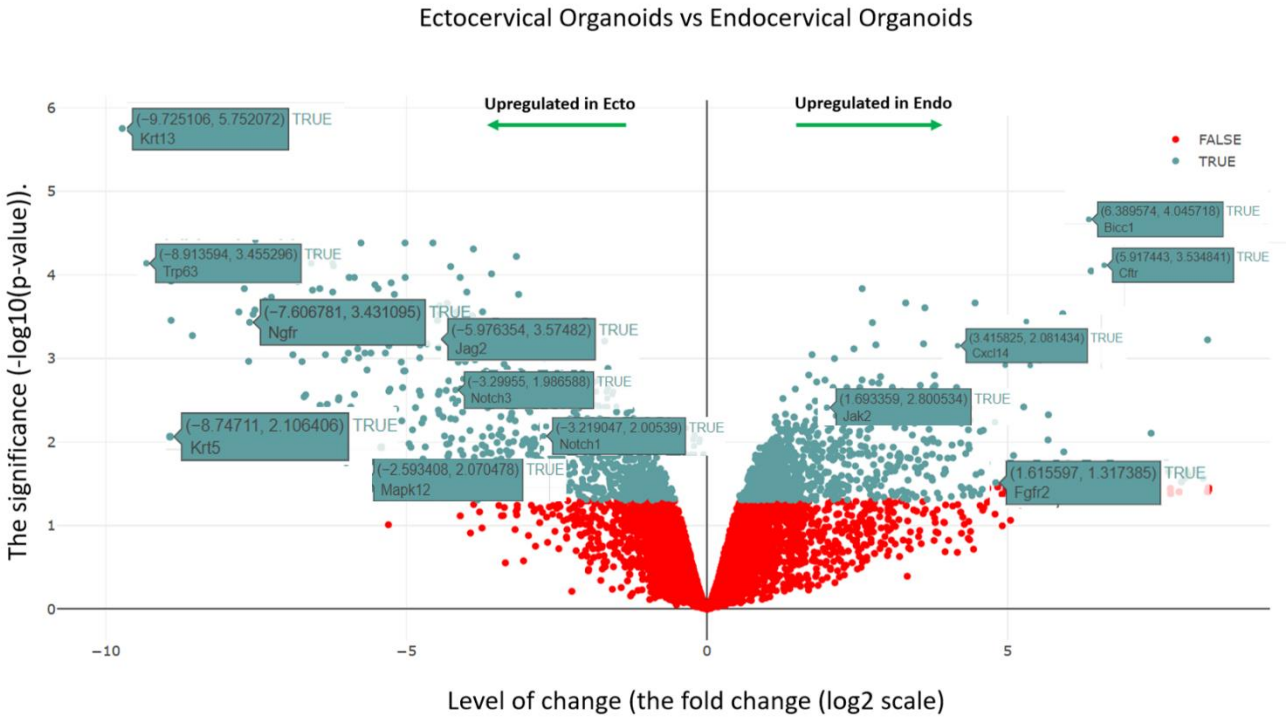

Figure 4.20: The volcano plot for ectocervical and endocervical organoids. Overview comparison of the level of change and the level of significance. The x axis shows the level of change (the fold change (log2 scale)), while the y axis represents the significance (-log10(adjusted p-value)).

One of the genes that was shown to be statistically significant in the ectocervical organoids is cytokeratin 5 (KRT5), an intermediate filament that forms the cytoskeleton of the basal epithelium of a number of epithelial tissues (36). To validate the RNA data, I stained mouse cervix and cervical organoids for KRT5 to detect the expression at the protein level. In the mouse cervix, KRT5 stained the ectocervical stratified squamous epithelium in a similar pattern to KRT17, with young mice (week 4) showing a pattern of reserve-cell-like KRT5+ cells underneath the KRT8 columnar cells of the endocervix (Figure 4.22). In cervix organoids, like what was observed with KRT17, KRT5 was staining the squamous layers of ectocervical (ENR-AF) organoids and not endocervical (ENR-P2) organoids (Figure 4.21). Additionally, I compared the staining to human cervix KRT5 in human cervix stained both squamous epithelium basal cells (not shown) and reserve cells (Figure 4.23).

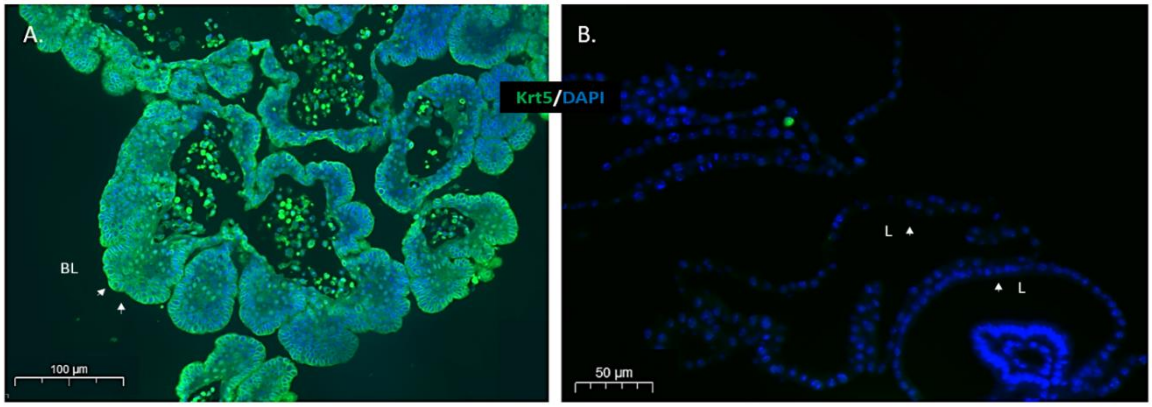

Figure 4.21: IF staining of KRT5 marker in mouse cervical organoids. (A) Ectocervical organoids showing positive KRT5 staining similar to *in vivo* pattern, scale bar=100µm. (B) Endocervical organoids negative for KRT5. Blue colour indicates DAPI nuclear staining, scale bar=50µm, BL= basal layer and L=lumen.

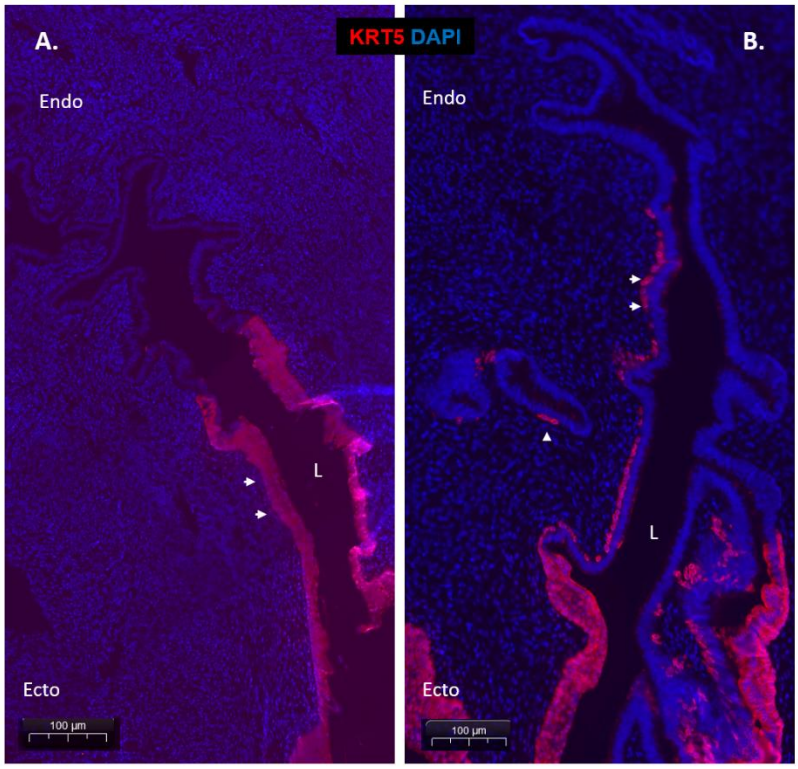

Figure 4.22: IF staining of KRT5 marker in mouse cervix. (A) Adult mouse cervix showing clear distinction between the area where KRT5 is positive (ectocervix) and where KRT5 in negative (endocervix). (B) Juvenile week 4 mouse cervix showing KRT5 under the columnar epithelium of the developing endocervix. Blue colour indicates DAPI nuclear staining, scale bar=100µm and L=lumen.

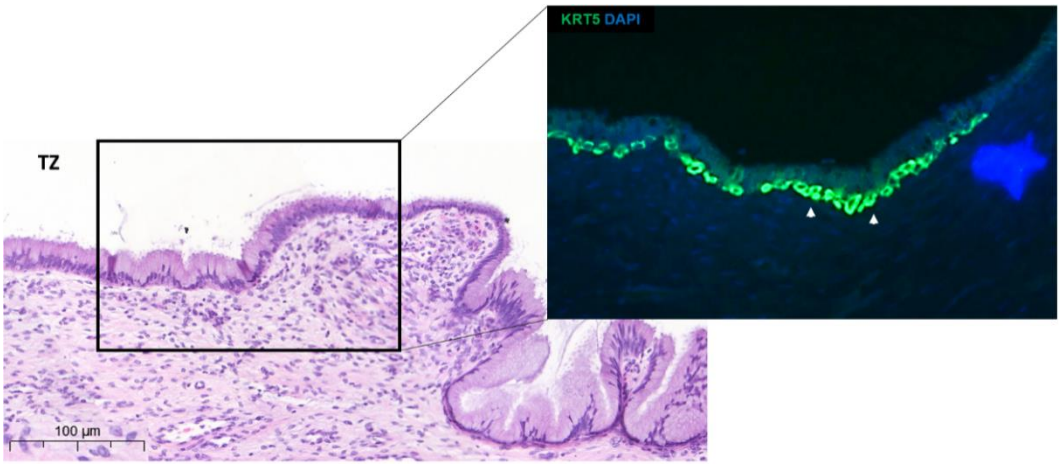

Figure 4.23: Human cervical transformation zone stained with KRT5. Representative IF images showing positive population of KRT5 cells (green) could be seen under the columnar epithelium in a similar pattern to what is seen in reserve cells. Blue colour indicates DAPI nuclear staining and the scale bar=100µm.

In addition to KRT5, KRTs 13 and 15 were highly expressed in the ectocervical organoids in the transcriptional comparison between the *in vitro* systems. Thus, I have stained for KRT13 and KRT15 and compared the pattern to the tissue of origin (Figure 4.24 and Figure 4.25). The RNA expression revealed by the array in vitro system comparison matched the protein expression seen by IF and was also faithfully representing the *in vivo* tissue with both keratins being expressive in ecto and not in endo parts of the cervical epithelium.

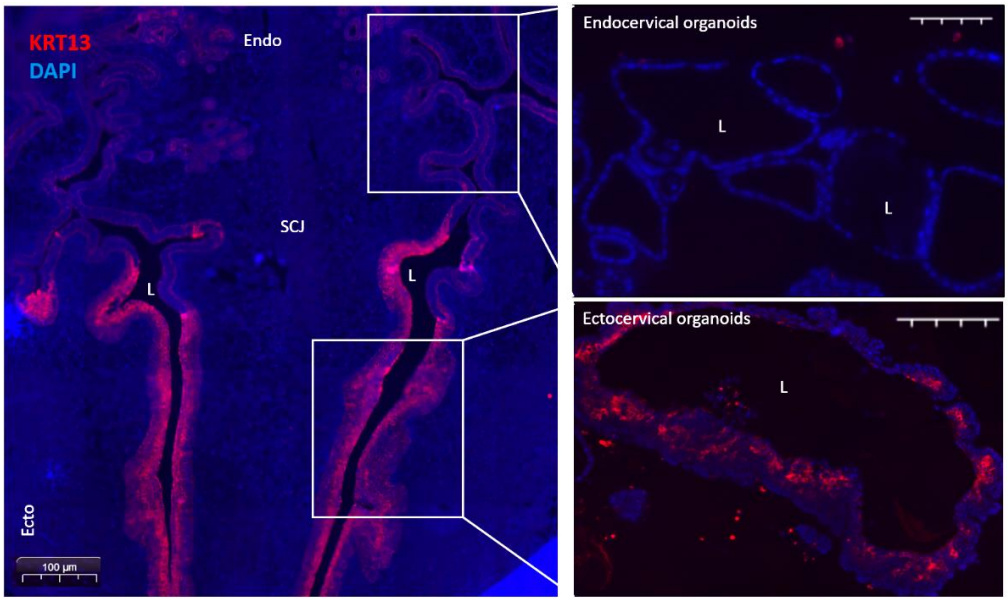

Figure 4.24: KRT13 IF staining of adult mouse cervix and cervix organoids. On the left positive KRT13 pattern is shown in the intermediate layers of the ectocervix. On the right pattern of KRT13 in mouse cervical organoids with similar pattern to what is seen *in vivo* with positivity in the intermediate squamous cells of the ectocervical organoids, *in vivo* scale bar=100µm, *in vitro* scale bar=50µm, blue colour indicates DAPI nuclear staining and L=lumen.

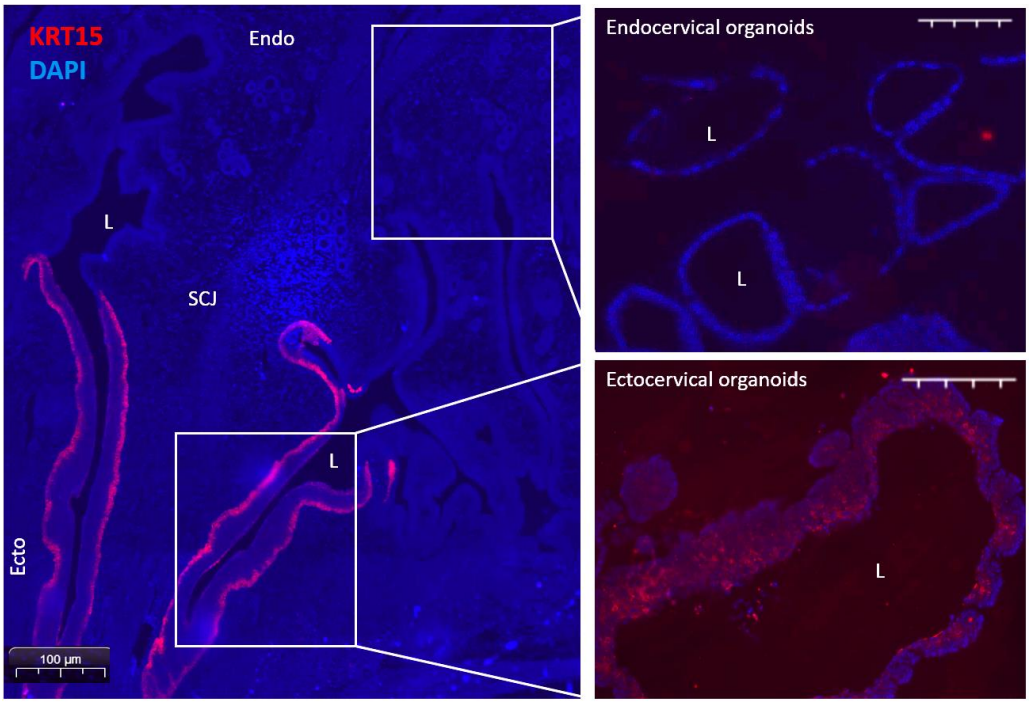

Figure 4.25: KRT15 IF staining of adult mouse cervix and cervix organoids. On the left positive KRT15 pattern is shown in the ectocervix but not in the endocervix. On the right pattern of KRT15 in mouse cervical organoids with similar pattern to what is seen *in vivo* with positivity in the squamous cells of the ectocervical organoids and not in the endocervical ones, *in vivo* scale bar=100µm, *in vitro* scale bar=50µm, blue colour indicates DAPI nuclear staining and L=lumen.

4.2.3.3 Nerve growth factor receptor (Ngfr)

The transcriptional profiling of ectocervix organoids identified a cell-surface marker NGFR (P75 neurotrophin receptor), a P75 glycoprotein that interacts with the neurotrophic factor NGF (37). NGF has a well-established role as a neurotrophic factor for nerve cells (37) but recently it has also been found to be involved in the regulation of wound healing and of the differentiation of keratinocytes (38,39). In skin, P75 is expressed in basal keratinocytes but not in terminally differentiated cells and was found to play a role in the autocrine epidermal cell proliferation (40). P75 was also reported to interact with Notch signalling pathway via NF-κB activation (41). NGFR has not been reported yet in the cervix.

To validate the transcriptional data and understand the role of NGF signalling in cervical epithelium regulation, I stained human cervix, mouse cervix and cervical organoids for P75 receptor. In mouse SCJ, P75 receptor was positive in basal layer of squamous epithelium but not in the endocervix with high expression in the stroma (Figure 4.26). In cervical organoids, P75 marked the basal cells of the ectocervical organoids but not the endocervical derived ones (Figure 4.27). P75 receptor expression suggests that neurotrophins play a role in the regulation

of the squamous lineage in the cervical epithelium. In human cervical sections, P75 positivity in the basal layer of squamous epithelium and in reserve cells (Figure 4.28).

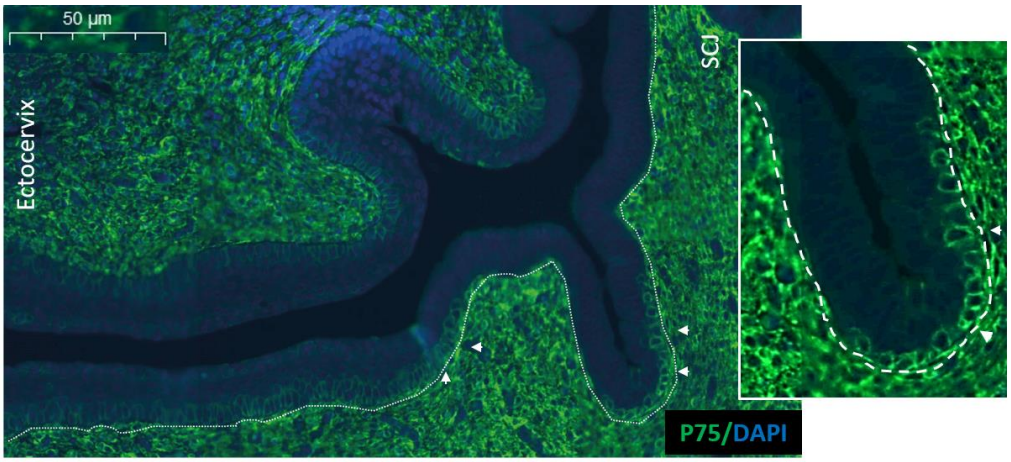

Figure 4.26: Mouse cervix with P75 IF staining. Representative IF images showing a discrete population of P75+ cells (green) in the basal layer of the squamous epithelium in the SCJ and ectocervix is seen, blue colour indicates DAPI nuclear staining and the scale bar=50µm.

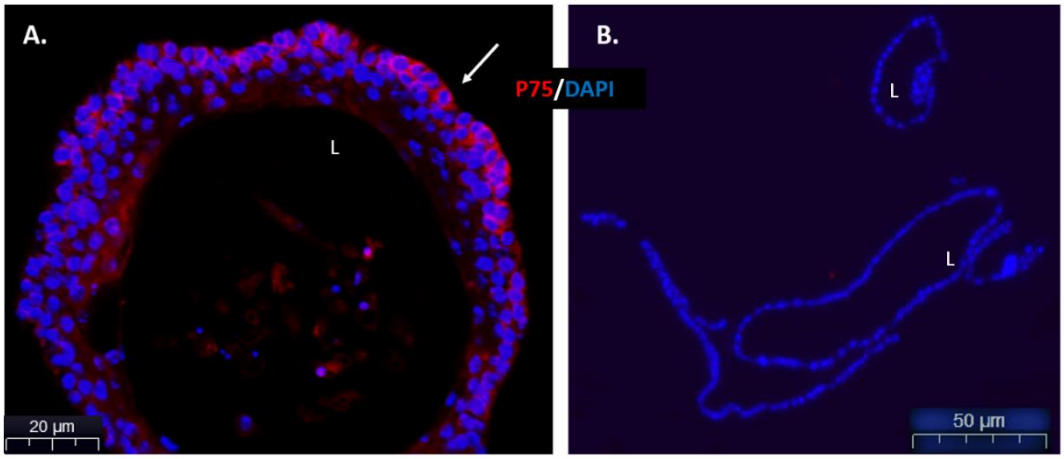

Figure 4.27: Murine cervical organoids with IF P75 staining. Representative IF images showing (A) Ectocervical organoids with positive P75 expression in the basal layers, scale bar=20µm. (B) Endocervical organoids negative for P75. Blue colour indicates DAPI nuclear staining, scale bar=50µm and L=lumen.

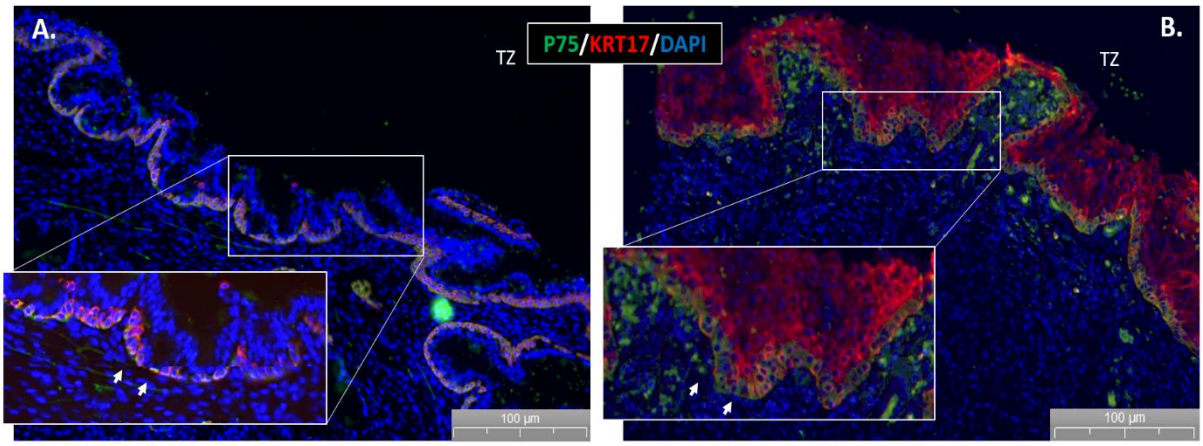

Figure 4.28: Human cervix with IF P75 and KRT17 staining. Representative IF images showing human sections of cervical transformation zone (TZ) with two different stages of metaplasia with P75 receptor staining localising with KRT17 reserve cells. Blue colour indicates DAPI nuclear staining and scale bar=100µm.

4.2.4 Investigation of signalling pathways from the transcriptional analysis of the endocervix and the ectocervix in both *in vivo* and *in vitro*

In addition to using the transcriptional analysis data to find endocervix and ectocervix epithelial signatures, I focussed on genes encoding components for the signalling pathways to identify potential specific signalling for each lineage (endo or ectocervical). When *in vivo* bulk tissue samples of both endo/ectocervical regions were compared to the stroma (fold change >2, P<0.05), both lineages expressed components of signalling pathways including TGF-β (*Tgfbi*), Wnt (*Wnt2b, Wnt7a*), Notch (*Dll4*) and Fgf (*Fgf1*) (Table 4.4). Components of Activin-A signalling pathway (*Inhba, Smad2)*, *Wnt* regulator Frizzled-7 (*Fzd7*) and *Fgf7* showed high expression in the endocervix *in vivo* comparison (Table 4.4). Whereas Wnt *antagonist (Axin2)*, TGF-beta-1 activator (*Itgb6*) were more highly expressed in the ectocervix (Table 4.4). The stromal signature is also informative to understand the signalling environment within the cervix. I found that stroma expresses high levels of Wnt antagonist Dickkopf (*Dkk2*), fibroblast growth factor 2 (*Fgf2*), neurotrophins including nerve growth factor (*Ngf*) and brain-derived neurotrophic factor (*Bdnf*) (Supplementary table 2).

Moreover, when comparing *in vitro* samples of both endo/ectocervical organoids (fold change >2, P<0.05), several signalling components were differentially expressed in the ectocervical organoids, including: dickkopf Wnt signalling pathway inhibitor 3 (*Dkk3*), fibroblast growth factor receptor 3 (*Fgfr3*), epidermal growth factor receptor (*Egfr*) and Notch pathway regulators (*Notch1*, *Notch3* and *Jag2*). Further investigation of these pathways might shed a light on the signalling that defines fate decision in the cervix. Whereas in the endocervical

organoids: fibroblast growth factor receptor 2 (*Fgfr2*) and phosphodiesterase 7B (*Pde7b*) cAMP regulator are highly expressed (Figure 4.20) (Supplementary table 1).

4.2.4.1 Activation of P63 via RUNX1/MAPK pathways to derive stratification in endocervical organoids

Transcriptomic analysis of the *in vivo* murine cervix showed expression of *Fgfr2* in the stroma (Table 4.4), in addition *Fgfr2* was found highly expressed in the endocervical organoids (section 4.2.4). *Fgfr2* is essential for vaginal epithelial squamous cell fate decision (13). Moreover, *Smad2* a transcription factor downstream of TGF-b/Activin signalling (40) is expressed by the endocervical epithelium of the murine cervix (Table 4.4). Activin A (ActA) and BMP4 were identified as factors produced by vaginal mesenchyme and play a key role in ΔNp63 (protein P63 isoform delta) induction and squamous differentiation (41). Therefore, I have tested the ability of deriving stratification of ENR-P2 endocervical organoids by activation of runt-related transcription factor 1 (RUNX1). ActA was added for induction of RUNX1 through SMAD-independent pathway, BMP4 via direct binding to SMAD 1/4/5/9 and FGF-10 for FGFR2IIIb-MAPK pathway activation. 100 ng/µl of BMP4, ActA and FGF-10 were added to ENR-P2 with and without Noggin (BMP inhibitor), this is to allow me to test different levels of BMP induction. The factors were added on single cells from established organoid cell lines (P5) and the effect followed for a week. After 7 days both cultures tested ER-P2 +BMP4+ActA+F10 (+ or – Noggin) struggled to survive with low number of spheroids forming compared to control (Figure 4.29), the (–Noggin) showed butter survival compared with the addition of Noggin, but did not survive a second passage, this was tested twice (Figure 4.29).

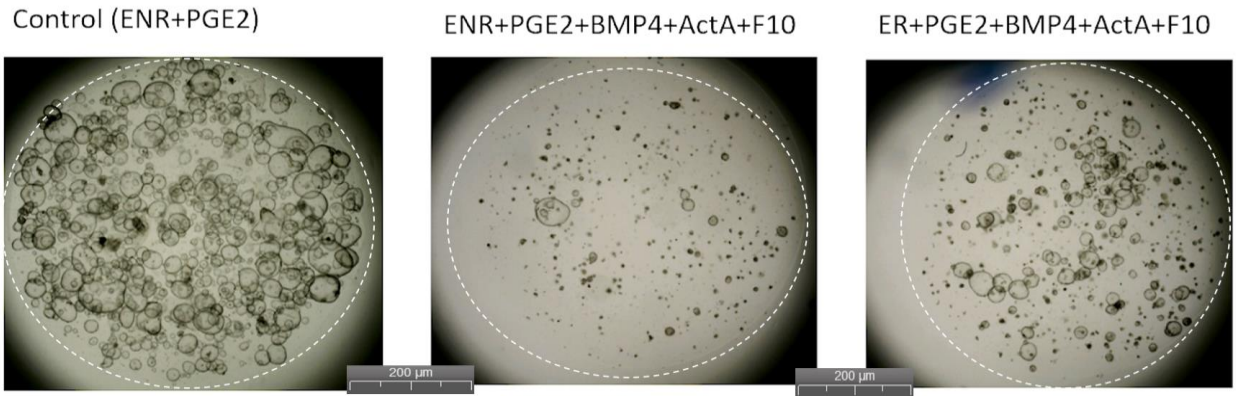

Figure 4.29: Derivation of stratification in endocervix organoids by activation of RUNX1. 100 ng/µl of BMP4, ActA and FGF-10 were added to ENR-P2 endocervical organoids media with and without Noggin (BMP inhibitor), this is to allow the testing of different levels of BMP induction. The factors were added on single cells from established organoid cell lines (P5). This resulted in compromising the survival of the endocervical organoids, with no signs of stratification. The absence of Noggin had relatively better survival rate. Scale bar= 200µm.

4.2.4.2 Murine cervical organoids response to indirect inhibition of Notch

In vivo transcriptomic analysis of the murine cervix showed expression on *Dll4* one of Notch ligands (36). Additionally, *in vitro* transcriptomic analysis of mouse cervix organoids revealed *Notch 1* and *Notch3* Notch receptors and *Jag2* Notch ligand (38). Notch signalling has been shown to regulate squamous epithelium homeostasis (42,43). Thus, to assess the effect of Notch inhibition in the stratified squamous ectocervical organoids (ENR-AF), DAPT (γ-secretase inhibitor) was added to single cells from established ectocervical organoids lines (P6) and chased for 48 and 96 hours before collection. After 48 hours the stratification of ENR-AF was limited to 3 layers compared to more in the control line (Figure 4.30), after 96 hours of γ-secretase inhibition ENR-AF showed no signs of stratification with only one layer of cells forming (Figure 4.30). To examine what kind of markers the spheroids from (ENR-AF+ DAPT) displayed, I stained for KRT8 and KRT17, both markers were positive with KRT17 being predominant (Figure 4.31).

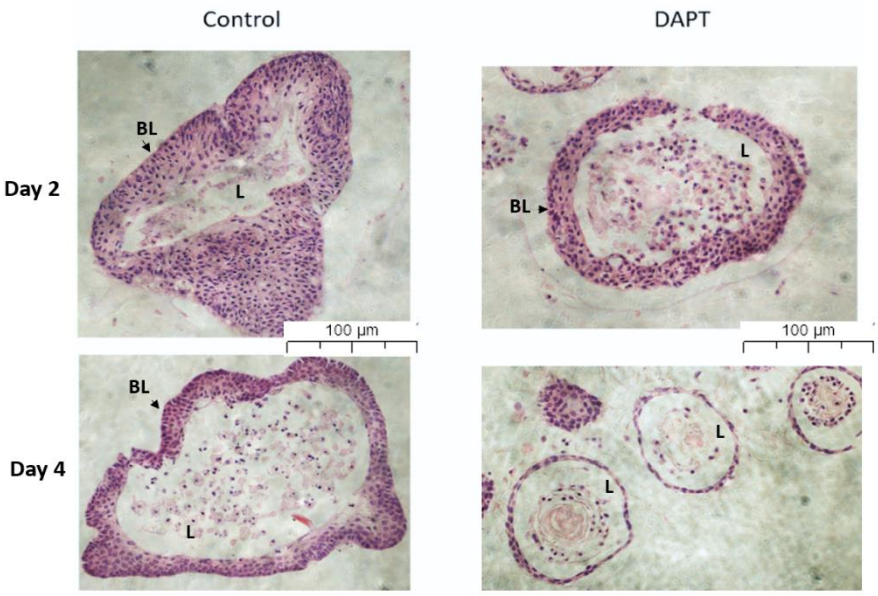

Figure 4.30: Indirect inhibition of Notch via DAPT (γ-secretase inhibitor) in organoids. Representative H&E of murine ectocervical organoids, top row shows the effect of Notch inhibition after 48 hours compared to the control culture. The stratification was restricted to 3 layers. Bottom row shows the effect of inhibiting Notch after 96 hours. No stratification was seen in day 4. Scale bar= 100µm, BL=basal layer, L=lumen.

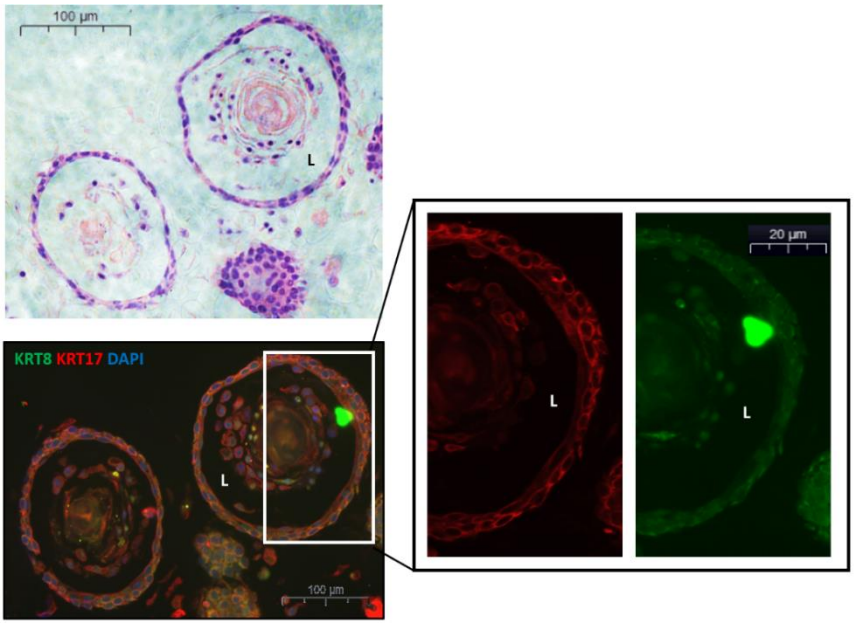

Figure 4.31: IF staining of ectocervical organoids under the effect of DAPT Notch inhibitor. Representative IF images showing both KRT8 (green) and KRT17 (red) were seen with KRT17 positivity dominating. Scale bar=100µm for images on the left hand-side, and 20µm for the right hand-side. Blue colour indicates DAPI nuclear staining and L=lumen.

4.3 Discussion

My aim was to generate an *in vitro* model of the two regions, the ecto and endocervix, of the normal murine cervix using the 3D organoid culture system. To do so, I first identified the culture conditions that would allow the establishment and propagation of organoids of the different regions of the cervix (endo and ectocervix). I then performed a thorough characterisation by qPCR and IF to validate the models. Cells from mouse cervixes were successfully treated by trypsin and cultured in 3D using the EGF, Noggin, Rspondin based culture method previously described by Sato and Clevers (1). Sphere-like structures (spheroids) were initially established, followed by the development of more complex structures (organoids) in ENR-AF (ENR basal medium with the addition of TGFβi and FGF10). These organoids had the same keratin expression pattern seen at the mouse SCJ, with KRT8; a marker of simple columnar epithelium being found above the KRT17+ cells, that are seen in the mouse stratified squamous epithelium. I was also able to distinguish the two populations according to their positivity for TP63; a marker of squamous epithelial progenitor (25), that was found only in the nucleus of the KRT17+ cells, and also by MUC5AC which was specific to endocervical. In order to develop an expansion medium that allow the propagation of endocervical organoids, several growth factors and cytokines were tested, and PGE2, a cAMP pathway agonist, was

added to the ENR medium, ENR-P2 (ENR basal medium with the addition of PGE2) medium and enabled the long-term growth of endocervical organoids easily and efficiently. Thus, I was able to define two media composition that resulted in the generation of the two distinct cervical epithelial lineages; ENR-AF, gave rise to stratified squamous epithelium, and ENR-P2, that generated secretory columnar epithelium (Figure 4.6).

TGFβ inhibition via A83-01 was essential for squamous differentiation in culture, whilst TGF-β signalling was active in endocervical organoids. This was confirmed with the transcriptional comparison of *in vivo bulk* tissue samples of both endo/ectocervical regions, the analysis showed that TGFβ ligands *Inhba, Smad2, Bmp1* and *Bmper* were highly expressed in the endocervix but not in the ectocervix.

R-spondin1 was supplied in murine cervix organoids to achieve a high activity of Wnt signaling. The importance of Wnt regulation in the cervix was previously described in the context of pathologies (44). Here the transcriptional comparison between the two cervical lineages showed high expression of *Fzd7* a Wnt regulator in the endocervix, whilst Wnt antagonist *Axin2* was seen in the ectocervix. This is in agreement with recent reports on the importance of Wnt to drive the formation of the columnar lineage of the endocervix but not in the ectocervix (45). Additionally, the contribution of cervical stroma signalling was revealed from the microarray analysis showing high levels of *Ngf, Bdnf* and *Dkk2* Wnt antagonist. The established *in vitro* ectocervical organoids had also confirmed this with *Dkk3* Wnt Signalling Pathway Inhibitor being highly expressed.

Ectocervical murine organoids were supplemented with FGF10 as it was shown to increase the number of formed organoids (section 4.2.1). FGF10 binds to FGFR2-IIIb, which was identified as a crucial factor in ΔNp63 activation leading to squamous cell fate in the mouse vagina along with BMP4 and Activin-A (17,46). As *Fgf2* was shown to be highly expressed in the cervical stroma, and *Fgfr2* was detected in the endocervical organoids (sections 4.2.3.1 and 4.2.3.2), I tested the potential of deriving stratification by the activation of RUNX1/ FGFR2IIIb-MAPK squamous pathways in ENR-P2 endocervical organoids. ActA was added to induce RUNX1 through SMAD-independent pathway, BMP4 was added for SMAD-dependent activation and FGF10 for FGFR2IIIb-MAPK pathway induction. No stratification was detected over the growth period from single cells to a full organoid (Figure 4.29). Moreover, the cell survival rate dropped significantly, indicating that the microenvironment supplied in culture medium did not support neither endocervical nor potential squamous transdifferentiation.

Numbl Notch signalling inhibitor was one of the highly expressed genes in the cervical stroma (section 4.2.4), and Notch pathway ligands *Notch1, Notch3* and *Jag2* were highly expressed in the ectocervical organoids. E6 protein of high-risk HPV types inactivate Notch pathway through interacting with NOTCH1 (47). Moreover, Notch signalling has been found to be crucial for squamous cell stratification in the cervix (45). To assess the effect of Notch pathway disruption in the ENR-AF stratified squamous ectocervical organoids, γ-secretase inhibitor (DAPT) was added, and the affect chased. Day 2 post Notch inhibition, the stratification was restricted to no more than 3 layers. In day 4 post γ-secretase inhibitor addition, no sign of stratification was detected (single layered organoids were formed) and showed markers of squamous epithelium with KRT17 positivity in addition to columnar marker KRT8 (Figures 4.30 and 4.31). This confirmed that the nature of the formed organoids was indeed squamous, and that the obstruction of Notch pathway supressed the ability of ectocervical organoids to build a multi-layered epithelium.

In addition to focusing on signalling pathways that regulates the cervical epithelium, I also investigated potential epithelial signatures (both known for confirmation or novel). When examining the epithelial signatures of *in vivo* bulk endo and ectocervical samples, there were common epithelial markers including *Cdh1, Epcam* and *Esrp1,* mucosal secretory cells markers *Muc4 and Pax8.* whilst others were more specific including *Foxj1* a reported marker of ciliogenesis in other sites (48-50) which was exclusive to the endocervix. Expectedly, upregulation of squamous keratins *10 and 14* (47) and nuclear basal marker of squamous epithelium *Tp63* (24) was seen in the ectocervix. In ENR-AF ectocervical organoids high expression of several cytokeratins was observed, including: *Krts 5, 6a, 13, 14, 15* and *17* in addition to *Tp63.* Detecting known markers of squamous and columnar origins confirmed the robustness of my dissection method and finding *Tp63* and the overlap in keratin expression (*Krt10* and *Krt14*) between the *in vitro* ectocervical organoids and the *in vivo* bulk ectocervix, confirmed their squamous nature.

The high expression of *Krt5* in the ectocervix organoids together with reports of KRT5 as a marker of stemness in the cervix (45) raised questions about the pattern of KRT5 expression in the cervix of mouse and human specifically in relation to reserve cells. In mouse cervix, KRT5 stained the ectocervical stratified squamous epithelium in a similar pattern to KRT17, in both week 4 (with reserve cells-like pattern) and in adult mice, with KRT5 under the KRT8 columnar cells of SCJ (Figure 4.21). Equally, the mouse ectocervical organoids showed positive KRT5 staining similar to the *in vivo* pattern, whilst endocervical organoids were

negative for KRT5. When examining the human cervix (Figure 4.22) KRT5 was positive in the squamous epithelium basal cells of the ectocervix (not shown) and in the reserve cells at the transformation zone (TZ) (Figure 4.23), unlike KRT17 which was reserve cell specific in the human cervix. These findings open a dispute of whether the presence of KRT5 in both basal cell of squamous epithelium and in reserve cell proves the argument of the nature of reserve cell being of displaced basal cell in the ‘’wrong’’ microenvironment (i.e. TZ) (45, 51).

Furthermore, the transcriptional analysis of ectocervix organoids showed high expression of cell-surface marker *Ngfr* (or P75), P75 responds to *Ngf*, which appears as one of the factors expressed by the cervical stroma (section 4.2.3.4). Using IF, P75 marked the basal layer of squamous epithelium of the ectocervix/TZ and in reserve cells in both humans and mice, with a similar pattern in ectocervical (ENR-AF) organoids. P75 has not been reported in the cervix, making this a potential new marker for detection and cell sorting (as it is a receptor protein) of reserve cells in the cervix.

Transcription factors *Pax8* and *Pax2* are reported to be expressed in the nuclei of the müllerian glandular epithelial cells (52), whilst *Pax8* was detected in both endo and ectocervical lineages, *Pax2* was specific to the ectocervix (Table 4.4), this agrees with reports of *Pax2* being detected in cervical high-grade squamous intraepithelial lesions but not in adenocarcinoma (53). In addition, *Plet1*, a marker of trophoblast stem cells in mice (54), was highly expressed in the ectocervix, hence the potential of *Pax2* and *Plet1* in deriving squamous lineage, however, further investigation of their protein level is required.

There was a differential expression of *CLDN* and *Mup* proteins in the mouse cervix with *Cldn12*, which was highly expressed in the endocervix, *Cldns*: *1, 4, 8* and *10* were highly expressed in the ectocervix. *CLDNs* play a role in the formation of tight junctions in epithelial and maintenance of cell polarity (55). *Mup* proteins *8* and *13* were highly expressed in the ectocervix, both *CLDN* and *MUP* proteins are cell surface proteins making them a potentially useful as markers.

In summary, this chapter describes a method for a reliable, chemically-defined, long-term culture of murine cervix organoids both endo and ectocervix. The generated organoids recapitulate the characteristics of their cells of origin and can be frozen-down and thawed without the loss of their proliferative ability.

Graphical summary for chapter 4

Establishing a physiological model to study the cervical transformation zone, human tissue is sparse so I use the mouse to optimise a 3D organoid system.

1. Establishemnt and characteristation of murine cervix organoids

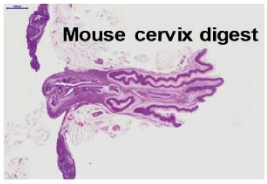

Endocervix organoids culture medium KRT8+

Ectocervix organoids culture medium KRT8+/ KRT17+

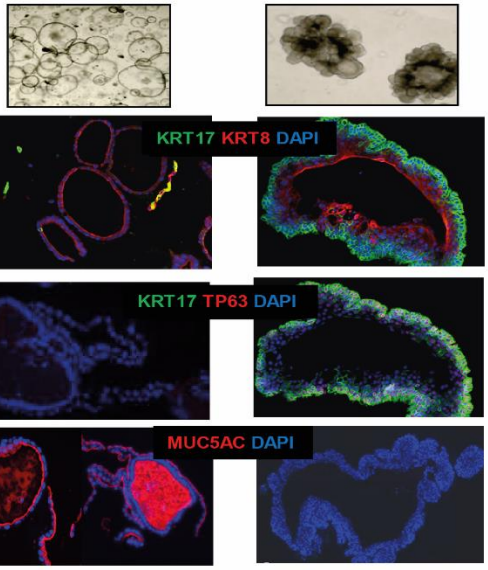

2. Investigation of signalling using mouse cervix organoids

2.1. TGFb inhibition was essential for squamous phenotype, while PGE2 helped propagate secretory phenotype.

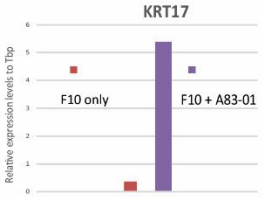

F10 only F10 + A83-01

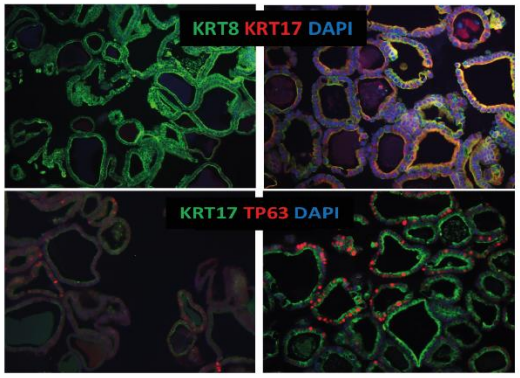

2.2. Ectocervical organoids had high expression of Dkk3, Notch1, Notch3 and Jag2

- Stroma was had high expression of Ngf, Bdnf, Fgf2, Numbl and Dkk2.
- In vivo endocervix was enriched in TGF-β and BMP signalling genes Inhba, Smad2, Bmp1 and Bmper.

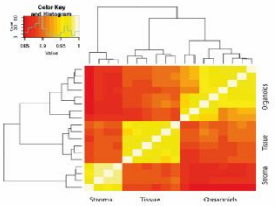

3. P75 as a novel marker for reserve cells

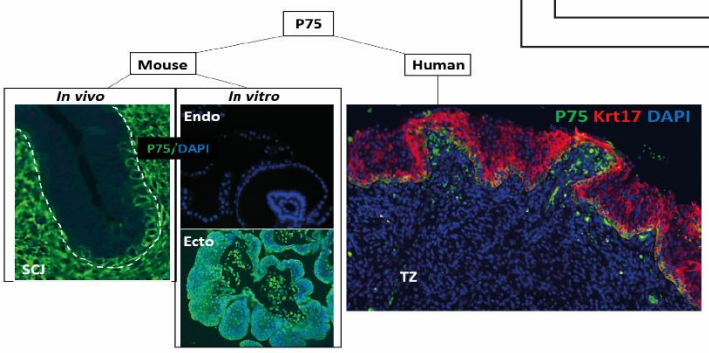

- Nerve Growth Factor P75 Receptor was found highly expressed in ectocervix organoids.
- P75 was also found in SCJ of mouse and in human TZ.
- P75 provides the potential for soring for reserve cells.

Chapter 4 references

1. Sato T, Vries RG, Snippert HJ, van de Wetering M, Barker N, Stange DE, et al. Single Lgr5 stem cells build crypt-villus structures in vitro without a mesenchymal niche. Nature. 2009 May 14;459(7244):262–5.
2. Lancaster MA, Huch M. Disease modelling in human organoids. Dis Model Mech. 2019;12(7).
3. Clevers H. Modeling Development and Disease with Organoids. Cell. 2016 Jun 16;165(7):1586–97.
4. Sato T, Stange DE, Ferrante M, Vries RGJ, Van Es JH, Van den Brink S, et al. Long-term expansion of epithelial organoids from human colon, adenoma, adenocarcinoma, and Barrett's epithelium. Gastroenterology. 2011 Nov;141(5):1762–72.
5. Huch M, Dorrell C, Boj SF, van Es JH, Li VSW, van de Wetering M, et al. In vitro expansion of single Lgr5+ liver stem cells induced by Wnt-driven regeneration. Nature. 2013 Feb 14;494(7436):247–50.
6. Kessler M, Hoffmann K, Brinkmann V, Thieck O, Jackisch S, Toelle B, et al. The Notch and Wnt pathways regulate stemness and differentiation in human fallopian tube organoids. Nat Commun. 2015 Dec 8;6(1):1–11.
7. Turco MY, Gardner L, Hughes J, Cindrova-Davies T, Gomez MJ, Farrell L, et al. Long-term, hormone-responsive organoid cultures of human endometrium in a chemically defined medium. Nat Cell Biol. 2017 Apr 10;19:568.
8. Turco MY, Gardner L, Kay RG, Hamilton RS, Prater M, Hollinshead MS, et al. Trophoblast organoids as a model for maternal–fetal interactions during human placentation. Nature. 2018 Dec;564(7735):263–7.
9. Boretto M, Cox B, Noben M, Hendriks N, Fassbender A, Roose H, et al. Development of organoids from mouse and human endometrium showing endometrial epithelium physiology and long-term expandability. Dev Camb Engl. 2017 15;144(10):1775–86.
10. Miller C, Degenhardt K, Sassoon DA. Fetal exposure to DES results in de-regulation of Wnt7a during uterine morphogenesis. Nat Genet. 1998 Nov;20(3):228–30.
11. Chakraborty C, Samadder S, Roychowdhury A, Roy A, Das P, Mandal RK, et al. Activation of Wnt-β-catenin pathway in basal–parabasal layers of normal cervical epithelium comparable during development of uterine cervical carcinoma. Mol Cell Biochem. 2018 Jun 1;443(1):121–30.
12. Mericskay M, Kitajewski J, Sassoon D. Wnt5a is required for proper epithelial-mesenchymal interactions in the uterus. Development. 2004 May 1;131(9):2061–72.
13. El-Sherif AM, Seth R, Tighe PJ, Jenkins D. Decreased synthesis and expression of TGF-β1, β2, and β3 in epithelium of HPV 16-positive cervical precancer: a study by microdissection, quantitative RT-PCR, and immunocytochemistry. J Pathol. 2000;192(4):494–501.
14. Farley J, Gray K, Nycum L, Prentice M, Birrer MJ, Jakowlew SB. Endocervical Cancer Is Associated with an Increase in the Ligands and Receptors for Transforming Growth Factor-β and a Contrasting Decrease in p27Kip1. Gynecol Oncol. 2000 Aug 1;78(2):113–22.
15. Dellas A, Schultheiss E, Almendral AC, Torhorst J, Gudat F. Assessment of EGFR and TGF-alpha expression in relationship to HPV status and Ki-67 distribution in cervical intraepithelial neoplasms. Int J Cancer. 1996 Jun 21;69(3):165–9.
16. Lombaert IMA, Abrams SR, Li L, Eswarakumar VP, Sethi AJ, Witt RL, et al. Combined KIT and FGFR2b signaling regulates epithelial progenitor expansion during organogenesis. Stem Cell Rep. 2013;1(6):604–19.
17. Terakawa J, Rocchi A, Serna VA, Bottinger EP, Graff JM, Kurita T. FGFR2IIIb-MAPK Activity Is Required for Epithelial Cell Fate Decision in the Lower Müllerian Duct. Mol Endocrinol Baltim Md. 2016 Jul;30(7):783–95.

18. Crowley CL, Payne CM, Bernstein H, Bernstein C, Roe D. The NAD + precursors, nicotinic acid and nicotinamide protect cells against apoptosis induced by a multiple stress inducer, deoxycholate. Cell Death Differ. 2000 Mar;7(3):314–26.
19. Huch M, Gehart H, van Boxtel R, Hamer K, Blokzijl F, Verstegen MMA, et al. Long-term culture of genome-stable bipotent stem cells from adult human liver. Cell. 2015 Jan 15;160(1–2):299–312.
20. Huch M, Bonfanti P, Boj SF, Sato T, Loomans CJM, van de Wetering M, et al. Unlimited in vitro expansion of adult bi-potent pancreas progenitors through the Lgr5/R-spondin axis. EMBO J. 2013 Oct 16;32(20):2708–21.
21. Fan Y-Y, Davidson LA, Callaway ES, Goldsby JS, Chapkin RS. Differential effects of 2- and 3-series E-prostaglandins on in vitro expansion of Lgr5 + colonic stem cells. Carcinogenesis. 2014 Mar 1;35(3):606–12.
22. Karthaus WR, Iaquinta PJ, Drost J, Gracanin A, van Boxtel R, Wongvipat J, et al. Identification of multipotent luminal progenitor cells in human prostate organoid cultures. Cell. 2014 Sep 25;159(1):163–75.
23. Moll R, Levy R, Czernobilsky B, Hohlweg-Majert P, Dallenbach-Hellweg G, Franke WW. Cytokeratins of normal epithelia and some neoplasms of the female genital tract. Lab Investig J Tech Methods Pathol. 1983 Nov;49(5):599–610.
24. Martens JE, Arends J. Cytokeratin 17 and p63 are Markers of the HPV Target Cell, the Cervical Stem Cell. ANTICANCER Res. 2004;6.
25. Yang A, Kaghad M, Wang Y, Gillett E, Fleming MD, Dötsch V, et al. p63, a p53 homolog at 3q27-29, encodes multiple products with transactivating, death-inducing, and dominant-negative activities. Mol Cell. 1998 Sep;2(3):305–16.
26. Nekulova M, Holcakova J, Nenutil R, Stratmann R, Bouchalova P, Müller P, et al. Characterization of specific p63 and p63-N-terminal isoform antibodies and their application for immunohistochemistry. Virchows Arch Int J Pathol. 2013 Sep;463(3):415–25.
27. Freeman A, Morris LS, Mills AD, Stoeber K, Laskey RA, Williams GH, et al. Minichromosome maintenance proteins as biological markers of dysplasia and malignancy. Clin Cancer Res Off J Am Assoc Cancer Res. 1999 Aug;5(8):2121–32.
28. Gipson IK, Ho SB, Spurr-Michaud SJ, Tisdale AS, Zhan Q, Torlakovic E, et al. Mucin genes expressed by human female reproductive tract epithelia. Biol Reprod. 1997 Apr;56(4):999–1011.
29. Namwanje M, Brown CW. Activins and Inhibins: Roles in Development, Physiology, and Disease. Cold Spring Harb Perspect Biol. 2016;8(7).
30. Sun B, Ye X, Li Y, Zhang W. Lgr5 is a potential prognostic marker in patients with cervical carcinoma. Int J Clin Exp Pathol. 2015 Feb 1;8(2):1783–9.
31. Barker N, van Es JH, Kuipers J, Kujala P, van den Born M, Cozijnsen M, et al. Identification of stem cells in small intestine and colon by marker gene Lgr5. Nature. 2007 Oct 25;449(7165):1003–7.
32. Emmert-Buck MR, Bonner RF, Smith PD, Chuaqui RF, Zhuang Z, Goldstein SR, et al. Laser capture microdissection. Science. 1996 Nov 8;274(5289):998–1001.
33. Huang PY, Kandyba E, Jabouille A, Sjolund J, Kumar A, Halliwill K, et al. Lgr6 is a stem cell marker in mouse skin squamous cell carcinoma. Nat Genet. 2017 Nov;49(11):1624–32.
34. Deng Y, Wan Q, Yan W. Integrin α5/ITGA5 Promotes The Proliferation, Migration, Invasion And Progression Of Oral Squamous Carcinoma By Epithelial–Mesenchymal Transition. Cancer Manag Res. 2019 Nov 13;11:9609–20.
35. Schnittert J, Bansal R, Storm G, Prakash J. Integrins in wound healing, fibrosis and tumor stroma: High potential targets for therapeutics and drug delivery. Adv Drug Deliv Rev. 2018;129:37–53.
36. Alam H, Sehgal L, Kundu ST, Dalal SN, Vaidya MM. Novel function of keratins 5 and 14 in proliferation and differentiation of stratified epithelial cells. Mol Biol Cell. 2011 Nov 1;22(21):4068–78.

37. Huang EJ, Reichardt LF. Trk receptors: roles in neuronal signal transduction. Annu Rev Biochem. 2003;72:609–42.
38. Di Marco E, Marchisio PC, Bondanza S, Franzi AT, Cancedda R, De Luca M. Growth-regulated synthesis and secretion of biologically active nerve growth factor by human keratinocytes. J Biol Chem. 1991 Nov 15;266(32):21718–22.
39. Li AK, Koroly MJ, Schattenkerk ME, Malt RA, Young M. Nerve growth factor: acceleration of the rate of wound healing in mice. Proc Natl Acad Sci U S A. 1980 Jul;77(7):4379–81.
40. Di Marco E, Mathor M, Bondanza S, Cutuli N, Marchisio PC, Cancedda R, et al. Nerve growth factor binds to normal human keratinocytes through high and low affinity receptors and stimulates their growth by a novel autocrine loop. J Biol Chem. 1993 Oct 25;268(30):22838–46.
41. Salama-Cohen P, Arévalo M-Á, Meier J, Grantyn R, Rodríguez-Tébar A. NGF Controls Dendrite Development in Hippocampal Neurons by Binding to p75NTR and Modulating the Cellular Targets of Notch. Mol Biol Cell. 2005 Jan;16(1):339–47.
42. Edenborough FP. Women with cystic fibrosis and their potential for reproduction. Thorax. 2001 Aug 1;56(8):649–55.
43. Yu JSL, Ramasamy TS, Murphy N, Holt MK, Czapiewski R, Wei S-K, et al. PI3K/mTORC2 regulates TGF-β/Activin signalling by modulating Smad2/3 activity via linker phosphorylation. Nat Commun. 2015;6.
44. Yang M, Wang M, Li X, Xie Y, Xia X, Tian J, et al. Wnt signaling in cervical cancer? J Cancer. 2018 Mar 20;9(7):1277–86.
45. Chumduri C, Gurumurthy RK, Berger H, Koster S, Brinkmann V, Klemm U, et al. Transition of Wnt signaling microenvironment delineates the squamo-columnar junction and emergence of squamous metaplasia of the cervix. bioRxiv. 2018 Oct 16;443770.
46. Laronda MM, Unno K, Ishi K, Serna VA, Butler LM, Mills AA, et al. Diethylstilbestrol induces vaginal adenosis by disrupting SMAD/RUNX1-mediated cell fate decision in the Müllerian duct epithelium. Dev Biol. 2013 Sep 1;381(1):5–16.
47. Kranjec C, Holleywood C, Libert D, Griffin H, Mahmood R, Isaacson E, et al. Modulation of basal cell fate during productive and transforming HPV-16 infection is mediated by progressive E6-driven depletion of Notch. J Pathol. 2017 Aug;242(4):448–62.
48. Stauber M, Weidemann M, Dittrich-Breiholz O, Lobschat K, Alten L, Mai M, et al. Identification of FOXJ1 effectors during ciliogenesis in the foetal respiratory epithelium and embryonic left-right organiser of the mouse. Dev Biol. 2017 Mar 15;423(2):170–88.
49. Ohm LA, Shirendeb U, Keator CS, Mah K, Rothlein SR, Slayden OD. Estrogen stimulates expression of FOXJ1 in the rhesus macaque fallopian tube. Fertil Steril. 2009 Sep 1;92(3):S116.
50. Caron A, Xu X, Lin X. Wnt/β-catenin signaling directly regulates Foxj1 expression and ciliogenesis in zebrafish Kupffer's vesicle. Dev Camb Engl. 2012 Feb;139(3):514–24.
51. Doorbar J, Griffin H. Refining our understanding of cervical neoplasia and its cellular origins. Papillomavirus Res. 2019 Apr 8;7:176–9.
52. Atsuta Y, Takahashi Y. Early formation of the Müllerian duct is regulated by sequential actions of BMP/Pax2 and FGF/Lim1 signaling. Development. 2016 Oct 1;143(19):3549–59.
53. Shukla A, Thomas D, Roh MH. PAX8 and PAX2 Expression in Endocervical Adenocarcinoma In Situ and High-Grade Squamous Dysplasia. Int J Gynecol Pathol. 2013 Jan;32(1):116–121.
54. Murray A, Sienerth AR, Hemberger M. Plet1 is an epigenetically regulated cell surface protein that provides essential cues to direct trophoblast stem cell differentiation. Sci Rep. 2016 Apr 28;6(1):1–14.
55. Krause G, Winkler L, Mueller SL, Haseloff RF, Piontek J, Blasig IE. Structure and function of claudins. Biochim Biophys Acta BBA - Biomembr. 2008 Mar 1;1778(3):631–45.

5 Establishment of organoids from the human cervix

5.1 Introduction

As discussed in the previous chapter, due to challenges in accessing sufficient tissue samples of the human cervix, I first optimised the organoid system using cervixes from the mouse. However, as previously reported, productive HPV infection with low grade squamous intraepithelial lesion (LSIL) was detected when HPV infects the ectocervix, whereas in the TZ and endocervix deregulation of HPV genes leads to high grade squamous intraepithelial lesion (HSIL) (1). To be able to understand the correlation between the site of infection and the diversity of HPV infection consequences, the development of human cervical organoids is necessary because Human Papilloma Virus (HPV) is species-specific (2).

For many tissues, organoid systems from both mouse and human have been established, including organoids of the small intestine (3), colon (4), liver (5), pancreas (6) and endometrium (7). An interesting finding is that for many of these, the culture conditions that were suitable for the mouse were not able to sustain long-term growth of human counterparts. Therefore, it was necessary to identify additional factors specific for human tissues. For example, for the colon, the addition of nicotinamide, TGFβ and p38 MAPK inhibitors were essential to sustain the proliferation of the human organoids (4). For some tissues such as the liver, adapting the murine organoid conditions remains a challenge as fully differentiated lineages cannot yet be obtained, even with the supplementation of additional factors (8).

At the start of my PhD, cervical organoids have not yet been established from mice or humans. The first organoids from the female reproductive tract, the fallopian tube organoids, was just published (9). The field has rapidly expanded in recent years and now several organoid systems of the female reproductive tract as well as from pathologies have been described (10). In this chapter I will describe the steps I have taken to identify the culture conditions to grow human cervical organoids based on my mouse cervix organoid systems.

5.2 Results

As discussed for the mouse cervixes in the previous chapter, also in humans, there is no knowledge about the identity and location of stem cells and progenitors of the cervix. Therefore, I took the same approach as for the establishment of the murine organoids by performing an enzymatic digest of the tissue on which to test the different culture conditions. The advantage of the human cervix is that due to its size and anatomical organisation, I was

able to dissect out the different cervical regions (endo, SCJ and ecto) which was not possible with murine tissues (Table 5.1). I collected human cervical samples from benign hysterectomies. These samples are rare, and I was only able to obtain 12 samples for this part of my project over 1.5 years. Hysterectomies for the surgical treatment of cervical carcinomas are more common, however, as the aim of this project is to establish organoids of the normal cervix, I excluded these samples for this study.

The starting tissue material is key for having a successful culture, thus the validation of the digestion method is critical. Initially, I used the digestion method, with sequential dispase followed by trypsin, that I set up for the establishment of mouse cervix organoids (explained in methods section 2.1.5) for the human cervix. However, this enzymatic protocol was not efficient for the isolation of cells from human tissue and I could not obtain enough material for culture. The human cervical tissue is densely packed and fibrous, therefore I reasoned that a collagenase V step (Sigma, C-9263) after the trypsin treatment may help improve the digest (explained in methods section 2.1.4). Indeed, I found that the combination of trypsin and collagenase treatments yielded more cellular material (Figure 5.1).

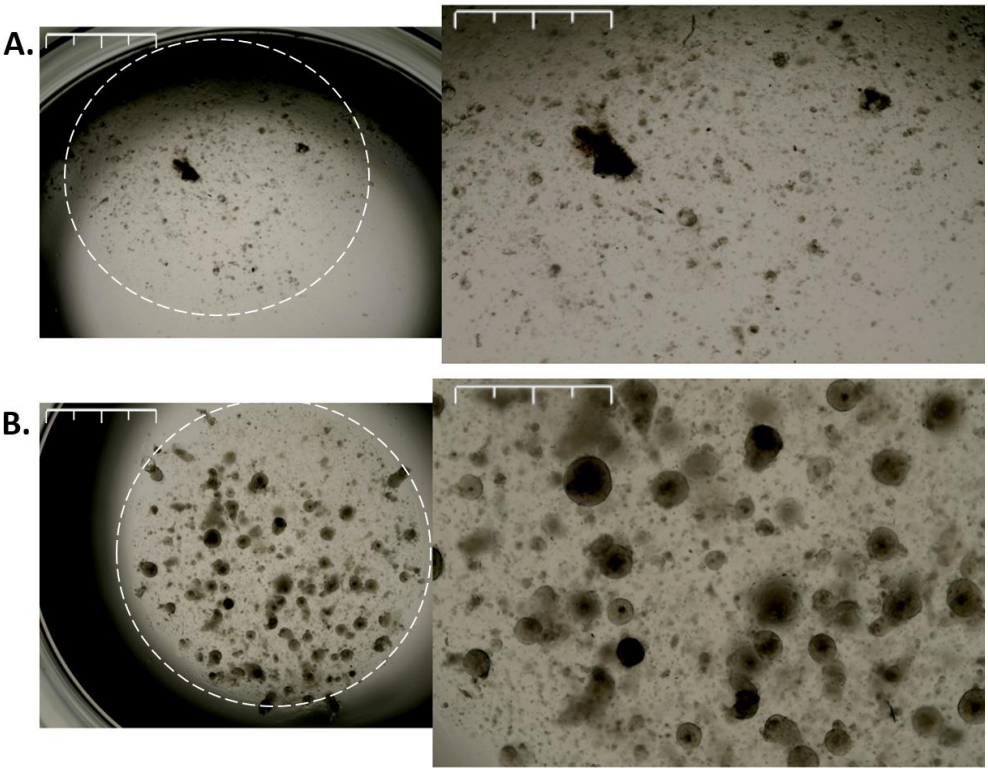

Figure 5.1: **Adjusting human cervix organoids digestion protocol.** (A) Bright field images of human cervical digest plated in matrigel®, the mouse cervix digestion protocol was applied (Trypsin), however the addition of Collagenase V enhanced the cellular digest (B). Images shown of cultures in passage 1 day 7, scale bar=200µm for left hand images and 100µm for right hand ones.

Next, I tested the effectiveness of the murine cervical protocol on human samples (from SCJ), in both ENR-AF (ectocervix organoids) and ENR-P2 (endocervix organoids). To begin with I was able to see growth in both (up to passage 2), however, at passage 3, I was not able to detect any cellular material (Figure 5.2).

The correct derivation site is crucial for growing an organoid culture, since I previously based my derivation from SCJ (both in mouse and in the first two human derivation trails), I wanted to examine the outcome from other sites (endo and ectocervix) and compare it to the SCJ. Thus, I performed the next cell extraction from three separate pieces of tissue, the endocervix, SCJ and from the ectocervix. I observed cellular structures growing from cells derived from endocervix and SCJ but not from the ectocervix, when plating cells from ectocervix, I saw a lot of cell debris (Figure 5.3).

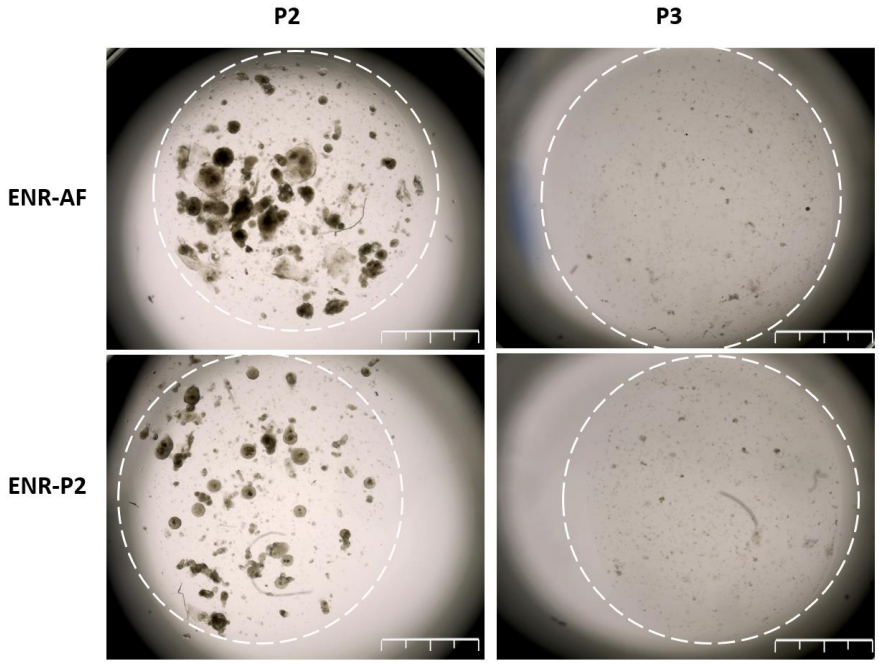

Figure 5.2: Derivation of human cervix organoids. Representative bright field images showing human cervix organoids that were derived using murine cervix protocol, at passage 2 there was an organisation of structures, however these structures did not survive the next passage, scale bar=200µm.

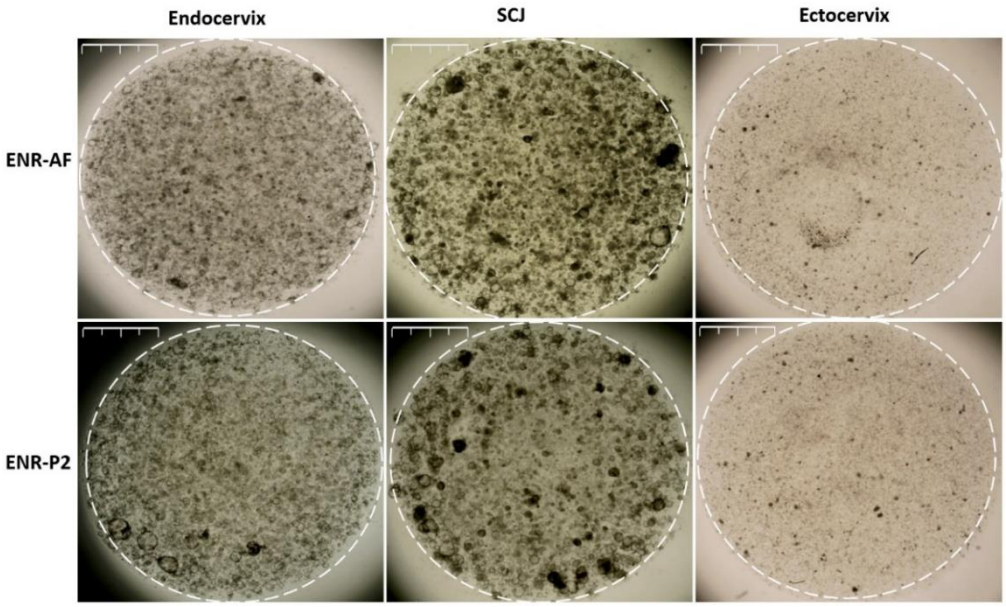

Figure 5.3: **The outcome of derivation of human cervix organoids from the different sites; endo, SCJ and ectocervix.** Representative bright field images shown at passage 1 day 5, cells plated from digested cellular material derived from endocervix, SCJ and ectocervix, in ENR-AF and ENR-P2. The ectocervix showed the poorest outcome, scale bar=200µm.

Subsequently, I tested several growth factors based on what has been used in literature to improve the derivation of organoids from human tissues (Table 5.1). The addition of SB202190 p38 inhibitor (p38i) was important in making the switch to human organoids in the small intestine (4). Nicotinamide (Nic) was also essential for human derived small intestine organoids (4). Moreover, Y27632; Rho Kinase inhibitor (Rocki), has been reported to be important for the long-term survival and proliferation of keratinocyte (11) and has been used in salivary gland organoids (12) and trophoblast organoids (13).

A satisfactory organoid criterion includes the formation of a self-organised 3D structure containing cells that retain the characteristics of the organ of which they were derived from. Initial evaluation includes the formation of spheroids and/or budding structures (depending on the site being modelled). I also assessed the ability of formed spheroids to expand in number when I break them up (passaged). Furthermore, I observe the growth sustainability of these formed spheroids for at least two months, their ability to expand and sustain growth shows their capability to reform and the presence of an epithelial stem cell in culture. Last, when all previous criteria have been met, I examine the presence of multiple cell types, and test possible aspects of the specialised function as in the organ of origin.

Based on what has been reported, I have tested the effect of the addition of Rocki, Nicotinamide and p38i on both ENR-AF (murine ectocervical organoids media) and ENR-P2 (murine

endocervical organoids media). When optimising a new culture condition, I passage the cells when the cultures became too dense, cells attach to the bottom of the well or when the Matrigel® became unstable. Passaging was done by vigorous pipetting (~ 300 times) and was every 7-10 days (detailed protocol in section 2.1.6). At passage 1, all additional factors that I tested did not show any further improvement to ENR-AF and ENR-P2 (Figure 5.4). At passage 3, cell survival was low under all conditions with almost no spheroids except for a few in the conditions that contained nicotinamide (Figure 5.5).

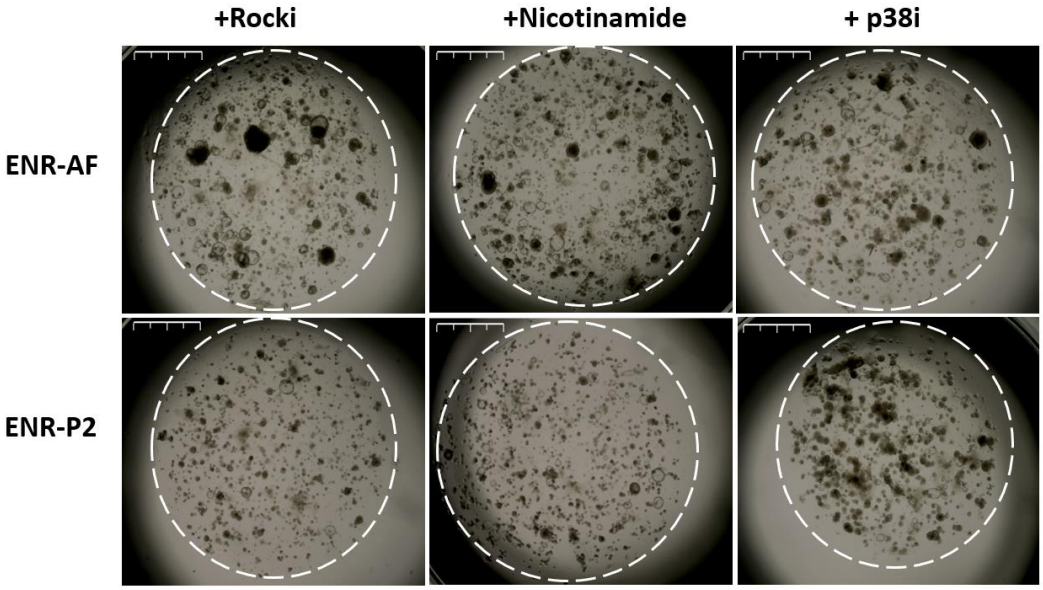

Figure 5.4: Testing factors Rocki, Nic and P38i on human cervix digest. Representative bright field images shown at passage 1 day 8, scale bar=200µm.

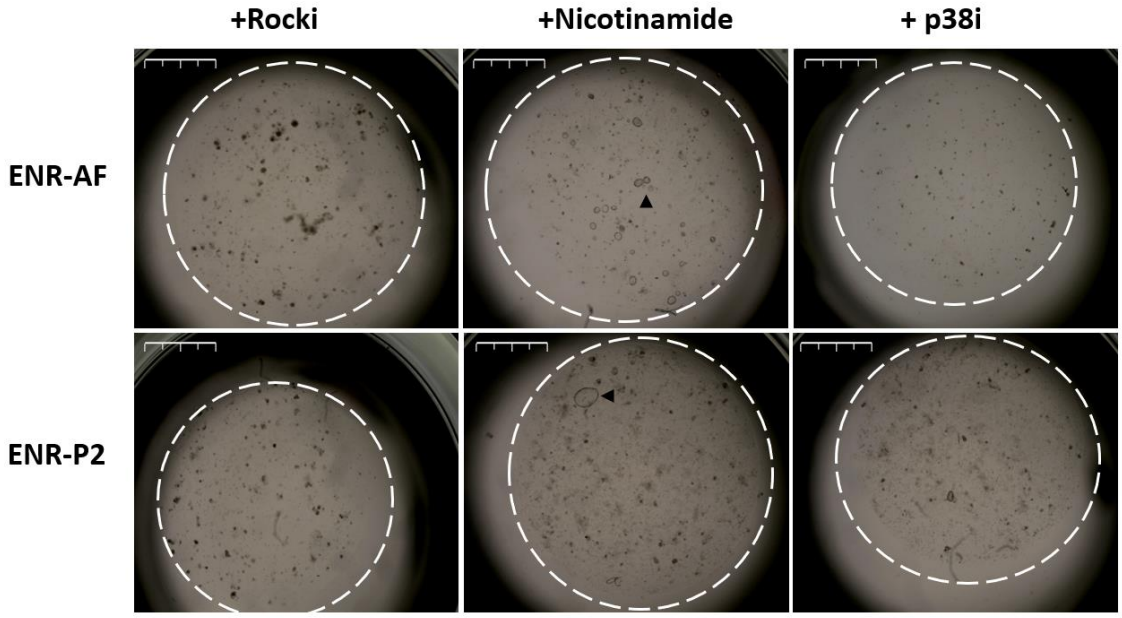

Figure 5.5: Follow up on testing factors Rocki, Nic and P38i on human cervix digest. Representative bright field images shown at passage 3 day 7. Nicotinamide showed few spheroids growing in both ENR-AF and ENR-P2, scale bar=200µm.

Table 5.1: Factors used for human cervix derivation and optimisation.

Factor	stock	Final concentration	Manufacturer	Catalogue number
A83-01 (TGFβi)	1 mM	500 nM	Tocris Bioscience	2939
FGF-10	100 µg/mL	100 ng/mL	PeproTech	100-26
Prostaglandin E2 (PGE2)	25 mM	25 nM	Tocris Bioscience	2296
MAPK p38 inhibitor (p38i)	10 mM	10 µM	Tocris Bioscience	1264
Nicotinamide	1 M	10 mM	Sigma-Aldrich	N0636
CHIR99021 (GSKi)	1 mM	1 µM	Tocris Bioscience	4423
Activin A	X500	20 ng/mL	R&D systems	338-AC-010
HGF	50 µg/mL	50 ng/mL	Peprotech	100-39H
FGF-2	50 µg/mL	50 ng/mL	Peprotech	100-18B
BMP7	100 µg/mL	100 ng/ml	Peprotech	120-03

Due to a lack of a clear improvement on the derivation of organoids with the factors, I decided to test the effect of hepatocyte growth factor (HGF) on human cervix digest. HGF is vital for the derivation of liver organoids (8), endometrium organoids (14) and trophoblast organoids (13). From my previous attempts, I saw that nicotinamide has enhanced the growth in both ENR-AF and ENR-P2 (Figure 5.5), therefore, I wanted to test HGF on a culture media that contains the combined effect of PGE2 (P2), Nicotinamide (Nic) and A83-01. Thus, I examined the outcome of: (i) ENR-AF+ P2+Nic, (ii) ENR-AF+HGF, and (iii) ENR-AF+ HGF+P2+Nic (Figure 5.6). The combination of PGE2, Nicotinamide and HGF yielded the highest growth (Figures 5.6, and Figure 5.7).

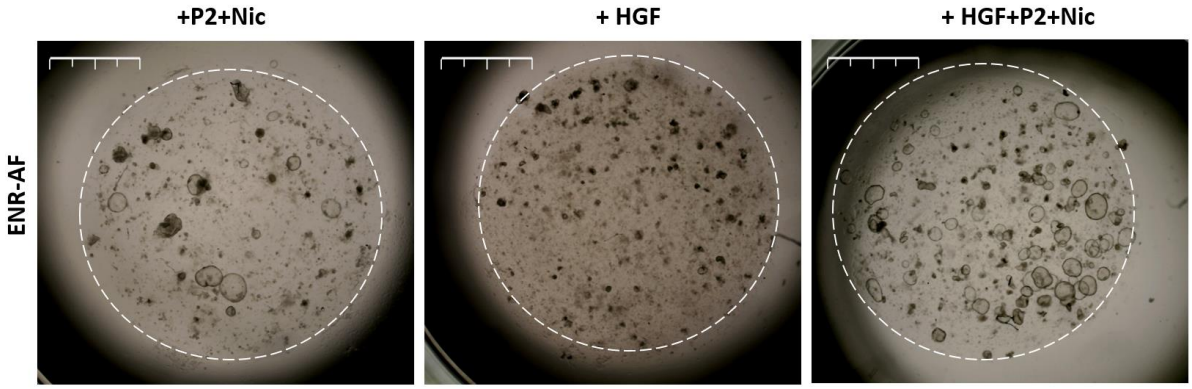

Figure 5.6: Testing factors PGE2, Nic and HGF on human cervix organoids. Representative bright field images shown at passage 2 day 6, an enhancement of the growth is shown in condition where PGE2, Nic and HGF are combined, scale bar=200µm.

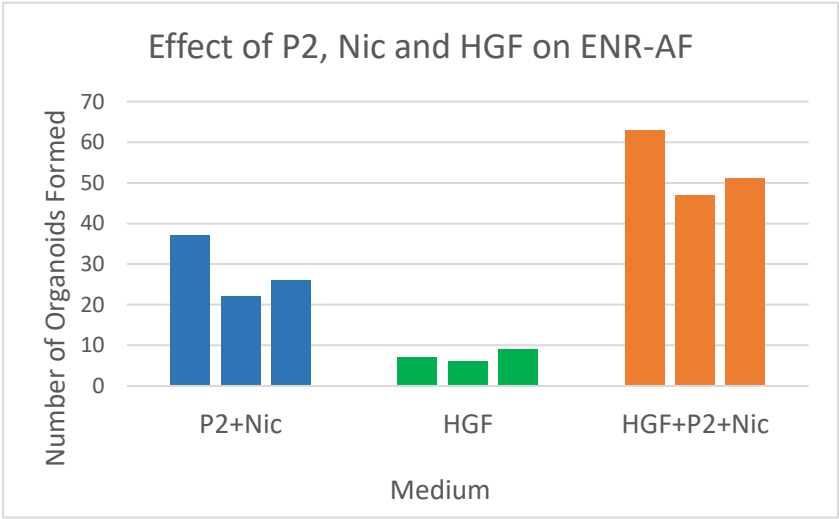

Figure 5.7: Testing the effect of factors PGE2, Nic and HGF on ENR-AF media. The factors were tested on three wells at passage 2 day 6. The highest growth was detected in condition where PGE2, Nic and HGF were combined, organoids with clear lumen were counted.

Culture medium ENR-AF with the addition of PGE2, Nicotinamide and HGF (ENR-AFP2NH) resulted in the highest growth and sustained longest growth, in this condition, cells were passaged every 7-8 days for 5 passages, over passages the spheroids started to collapse (not showing sphere-like structure with clear lumen) (Figure 5.8), and at passage 6 there was minimal growth detected.

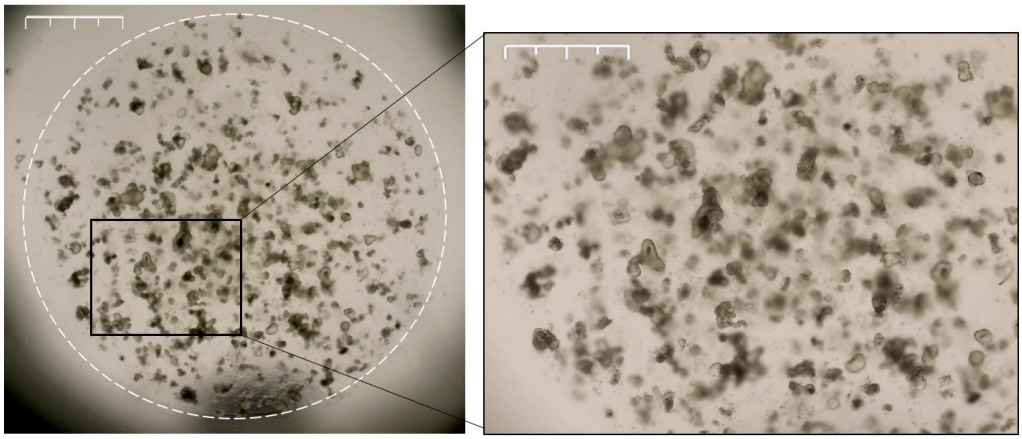

Figure 5.8: **Condition ENR-AF+(HGF+P2+Nic) at passage 5 post plating.** Representative bright field images showing the formed spheroids collapsed (not forming a clear lumen), before the growth was no longer sustained at passage 6, scale bar=200µm for the image on the left and 100µm for the right hand-side image.

This was nevertheless an encouraging improvement after many attempts. To increase the long-term growth of the organoids, I next tested additional factors using this medium composition as base (ENR-AFP2NH). CHIR99021 is a GSK-3β inhibitor (GSKi) that has been reported to be essential in the derivation of colon organoids (4), endometrium organoids (14) and trophoblast organoids (13). In addition, fibroblast growth factor 2 (F2) was reported to enhance the clonogenic capacity and efficiency of human intestinal organoids (4) and was used to increase viability of trophoblast organoids (13). Therefore, For the next optimisation cocktail, I tested the following conditions: **C1:** ENR-AFP2NH, **C2**: ENR-AFP2NH+p38i, **C3**: ENR-AFP2NH+GSKi, **C4**: ENR-AFP2NH+F2, **C5**: ENR-AFP2NH+p38i+GSKi, **C6**: ENR-AFP2NH+p38i+F2, and **C7**: ENR-AFP2NH+p38i+GSKi+F2.

In conditions where GSKi was added (C3, C5 and C7) there was a negative effect on the cells, with very few spheroids appearing (Figure 5.9) at passage 1 and almost none survived at passage 2 (not shown). Conditions ENR-AFP2NH and ENR-AFP2NH+F2 (ENR-AFP2NHF2) (C1 and C4) had the highest number of spheroids growing and sustained the longest growth (up to passage 5), whilst the addition of p38i had a detrimental effect (Figure 5.10).

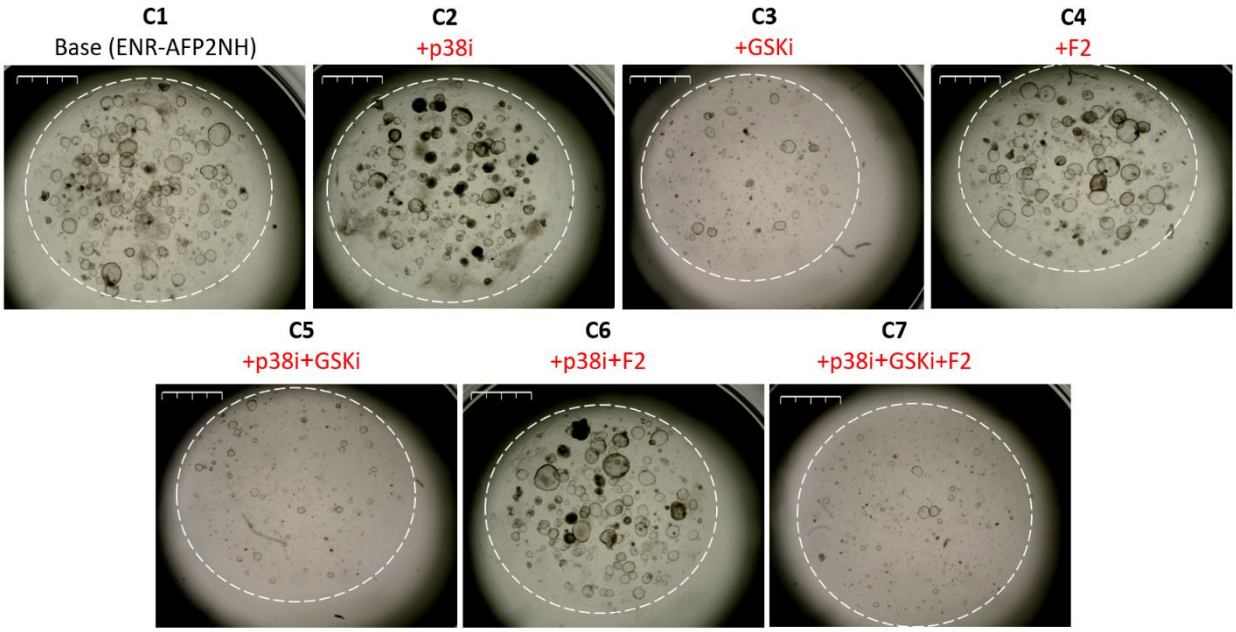

Figure 5.10: Testing the effect of factors p38i, GSKi and F2. Representative bright field images shown at passage 1 day 8, of the following conditions: **C1:** ENR-AFP2NH, **C2**: ENR-AFP2NH+p38i, **C3**: ENR-AFP2NH+GSKi, **C4**: ENR-AFP2NH+F2, **C5**: ENR-AFP2NH+p38i+GSKi, **C6**: ENR-AFP2NH+p38i+F2, and **C7**: ENR-AFP2NH+p38i+GSKi+F2. Scale bar= 200µm.

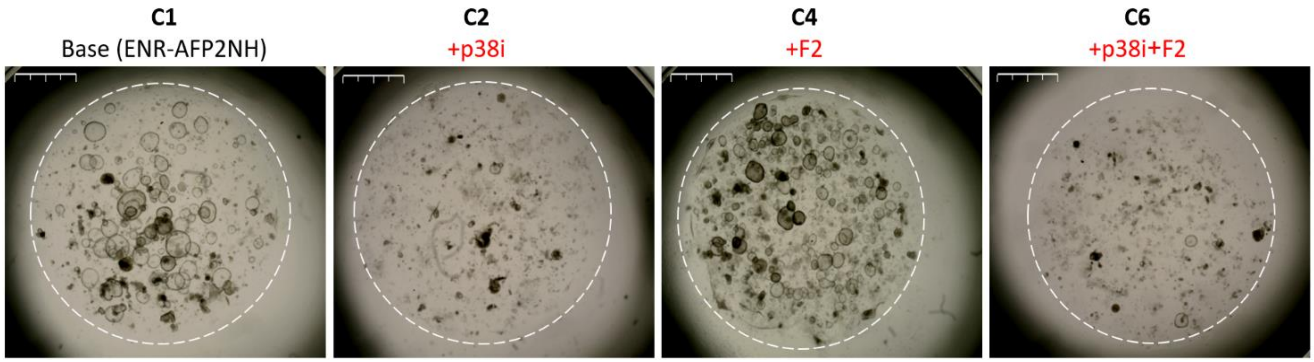

Figure 5.9: Following up on testing the effect of factors p38i, GSKi and F2. Representative bright field images shown at passage 2 day 6, with the loss of spheroids in conditions where GSKi was added. **C1:** ENR-AFP2NH, **C2**: ENR-AFP2NH+p38i, **C4**: ENR-AFP2NH+F2, **C6**: ENR-AFP2NH+p38i+F2, scale bar= 200µm.

So far, no condition sustained a long-term culture of human cervix. Therefore, I have decided to test an additional factor. Bone morphogenetic protein 7 (BMP7) signalling in female genital tract has been reported (15), moreover, BMP7 was crucial in deriving liver organoids (8), therefore, I have tested the effect of BMP7 on the conditions that proven to have the longest surviving culture (ENR-AFP2NHF2). Since Noggin is a BMP antagonist, I examined the effect of BMP7 with or without Noggin. The conditions tested were as following; **C1**: ENR-AFP2NHF2, **C2**: ENR-AFP2NHF2+BMP7, **C3**: ER-AFP2NHF2+BMP7. The addition of BMP7 (with or without Noggin) did not enhance the culture conditions, neither in number nor growth sustainability (Figure 5.11).

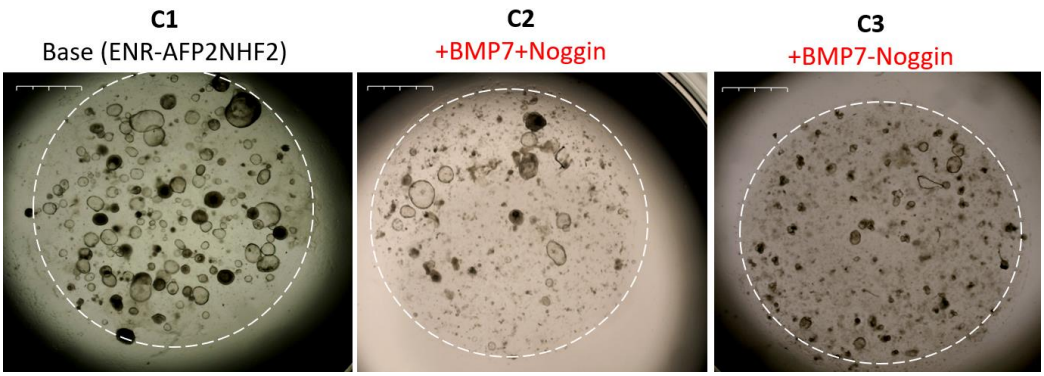

Figure 5.11: Testing the effect of BMP7 on ENR-AFP2NHF2 with or without Noggin. Representative bright field images of cultures at passage 3 day 7, the conditions were as following**;** **C1**: ENR-AFP2NHF2, **C2**: ENR-AFP2NHF2+ BMP7, **C3**: ER-AFP2NHF2+ BMP7, scale bar= 200µm

After testing the effect of different factors gradually (summarised in table 5.2), the combination that showed the best results and lasted for 6-7 passages was ENR-AF + HGF, PGE2, Nic and F2 (ENR-AFP2NHF2), however, I did not detect any sign of stratification in this condition (Figure 5.12). When I stained the formed organoids with columnar marker KRT8 and RC marker KRT17, both were positive (Figure 5.12).

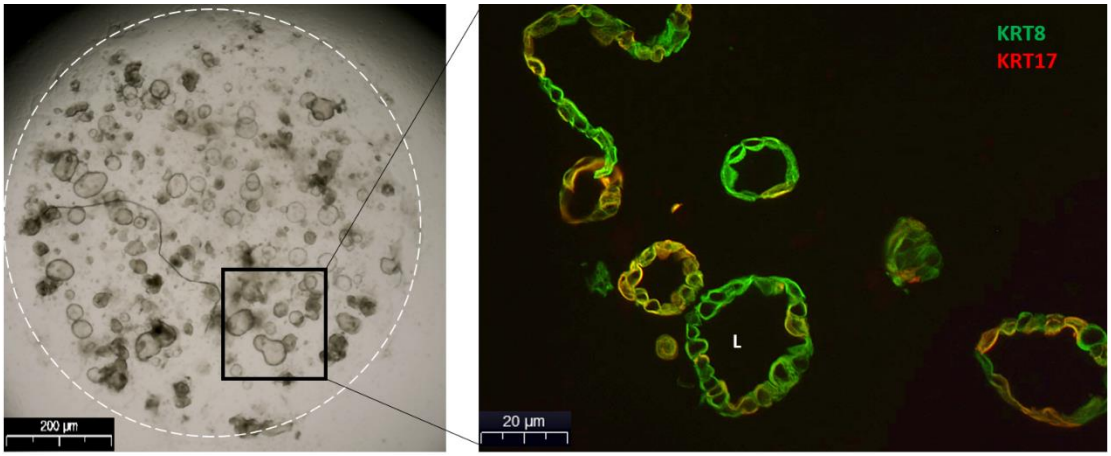

Figure 5.12: Human cervical organoids that were generated from AFP2NHF2. Left: shows representative bright field image of organoids in (ENR-AF)+HGF, PGE2, Nic and F2 passage 6. Right: shows representative IF staining of columnar marker KRT8 (green) and reserve cell marker KRT17 (red), both were positive, scale bar=200µm for the bright field image on the left and 20µm for the right hand-side IF image.

During this part of my project, a protocol for human cervical organoids (both endocervical and ectocervical) was reported (16). In this paper, the growth of endocervical organoids required Wnt activation, whilst inhibition of Wnt and activation of Notch was critical for derivation of squamous organoids (16). In the study of Chumduri et al, human cervical organoids were derived from two separate sites (endo and ectocervix) and not from SCJ which I have focused

on in my previous optimisation experiments. In their protocol, the samples were minced with surgical scissors before incubated in 0.5 mg/ml collagenase type II followed by trypsin (TrypLE) treatment. This digestion protocol is different from mine since I have treated the cells with trypsin prior to collagenase type V. Similar to my human cervix media that sustained the longest growth (ENR-AFP2NHF2), Chumduri et al. conditions include EGF and Noggin. It also contains FGF10, Nicotinamide and TGFβi (SB431542) which is also similar to ENR-AFP2NHF2, except I use A83-01 for TGFβ inhibition. Contrary to my observations, they use Y-27632 (Rocki) which has shown to be detrimental for my derived cultures (Figure 5.4). Moreover, in Chumduri et al. protocol, Wnt is enhanced in endocervical organoids culture with the addition of conditioned media enriched with Wnt3A and Rspondin-1, whilst I only depend on Rspondin-1 for Wnt in my cultures. Forskolin and Hydrocortisone were added to sustain ectocervical organoids in Chumduri et al. culture medium.

With my next tissue samples, I followed the derivation protocol and media conditions described in Chumduri et al., I also followed their passaging method which focusses on enzymatic digestion with TrypLE rather than the manual vigorous pipetting technique I use. I found that endocervical organoids showed enhanced growth however, this could not be sustained for more than 9 passages (Figure 5.13). Ectocervical organoids on the other hand, struggled at early passages and were difficult to break and expand with the squamous structures getting denser with minimum lumen (Figure 5.13). For my next sample I also tried plating SCJ cells in Chumduri et al, neither conditions were sustained for long-term.

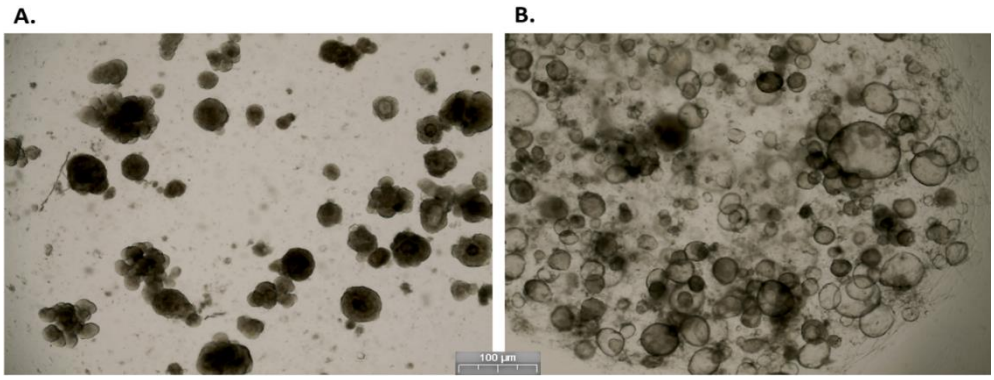

Figure 5.13: Following the protocol by Chumduri et al. to grow cervix organoids. representative bright field image when trying Chumduri's protocol, ectocervical media generated rigid complex structures that were difficult to break and expand (A). In endocervical media (B), growth was sustained but not for long-term, scale bar=100µm.

Table 5.2: Optimisation of human cervical organoids, replicates were not listed to avoid repetition.

Site	Digestion	Culture medium
1.5x2.5 cm piece from SCJ	Followed the mouse cervix digestion protocol (methods 2.1.5)	• ENR-AF • ENR-P2
1.5x2.5 cm piece from SCJ	Manual scraping of the stroma followed by Trypsin + collagenase	• ENR-AF • ENR-P2
1.5x2 cm pieces from endo, SCJ and ecto	Manual scraping of the stroma followed by Trypsin + collagenase	• ENR-AF • ENR-P2
2x2.5 cm piece from SCJ	Manual scraping of the stroma followed by Trypsin + collagenase	• ENR-AF+ Nic • ENR-AF+ p38i • ENR-AF+ Rocki • ENR-P2+ Nic • ENR-P2+ p38i • ENR-P2+ Rocki
1.5x2.5 cm piece from SCJ	Manual scraping of the stroma followed by Trypsin + collagenase	• ENR-AF + HGF • ENR-AF + PGE2 + Nic • ENR-AF+ HGF +PGE2 + Nic
1.5x2.5 cm piece from SCJ	Manual scraping of the stroma followed by Trypsin + collagenase	• ENR-AF+HGF+PGE2+Nic • ENR-AF+HGF+PGE2+Nic+ p38i • ENR-AF+HGF+PGE2+Nic+ GSKi • ENR-AF+HGF+PGE2+Nic+ F2 • ENR-AF+HGF+PGE2+Nic+ p38i+GSKi • ENR-AF+HGF+PGE2+Nic+ p38i+F2 • ENR-AF+HGF+PGE2+Nic+ p38i+GSKi+F2
1.5x2 cm piece from endo, SCJ and ecto	Manual scraping of the stroma followed by Trypsin + collagenase	• ENR-AF+HGF+PGE2+Nic+F2 • ENR-AF+HGF+PGE2+Nic+F2+ BMP7 • ER+AF+HGF+PGE2+Nic+F2+ BMP7 • ENR+AF+HGF+PGE2+Nic+F2+ Activin A • ENR-F+HGF+PGE2+Nic+F2+ Activin A
2x2.5 cm piece from endo and ecto	Followed protocol from Chumduri (16)	Chumduri (16)
1.5x2.5 cm piece from SCJ		

5.3 Discussion

The generation of human organoids is essential for HPV infection experiments as the virus is species specific. Therefore, I carried out optimisation steps to extend the murine cervical organoid system for the establishment of human cervical organoids. This was a major challenge as I had limited tissue samples on which to perform my experiments and several steps in the protocol had to be optimised starting from the digest method, culture conditions and passaging. With the help of Dr. Mercedes Jimenez-Linan, a gynaecological pathologist at the human tissue bank at Addenbrooke's Hospital, Cambridge, I was able to obtain different regions of the cervix (endo, SCJ and ectocervix) to test the cultures conditions. Deriving organoids from both endocervix and SCJ was feasible, but not from the ectocervix. This could be due to several reasons, including the fact that the ectocervical tissue consists of terminally differentiated cells and the isolation procedure does not allow enrichment for the proliferative population. Furthermore, the size of the tissue pieces was minimal and sufficient number of cells were difficult to obtain. After many trials I found that the best human cervical cell extraction method was manual scraping of the stroma, after using scissors to cut the epithelium from the stroma, followed by the addition of trypsin and collagenase treatments (detailed method described in section 2.1.4).

Once the tissue digest method was optimised, I tested the effect of the murine organoid media conditions on the human cervical cell isolates. However, this did not allow the growth of organoids and therefore I tested a series of different factors to improve the derivation. I found that TGF-β inhibition was important to get the human cervix organoids growing, Nicotinamide increased the number of spheroids, whilst FGF2 helped spheroids longevity. WNT signalling, which is important for the growth of many organoid systems, surprisingly had the opposite effect for the cervical cells. In the presence of CHIR99021, which inhibits GSK-3β and thus sustaining WNT signalling, the cells struggled to survive and could not be passaged. Moreover, BMP signalling via BMP7 did not enhance the culture condition and had a detrimental effect. Overall, after gradual optimisation steps of culture media (summarised in table 5.2), the combination that showed the best cell survival (6-7 passages) was ENR-AF with the addition of HGF, PGE2, Nicotinamide and FGF2. The generated organoids were single layered and spheroidal and did not show signs of stratification. The organoids had both columnar (KRT8) and squamous/reserve cell markers (KRT17), suggesting the presence of my target cell population in culture (Figure 5.12), which did confirm that the site of derivation and the

digestion method were correct. Additionally, the co-expression of KRT8 and KRT17 in the preliminary human cervix organoids was similar to my observations of the first passage of endocervical and ectocervical mouse organoids (forthcoming in chapter 6, section 6.2.1) in which KRT8 and KRT17 were also co-expressed. This changes after the organoids develop (passage 4 onwards) where it seems there is a lineage commitment with either KRT8 secretory sphere-like organoids, or a majority of KRT17 cells (with superficial KRT8 on top) stratified squamous epithelium. As I saw similarities between the human and mouse SCJ (section 3.6.3, Figure 3.10), I hypothesise a similar organoid developing pattern. Hence, it appears as my culture condition so far is sufficient to derive human cervix organoids but does not sustain long-term propagation of the cells of interest. I expect more factors are needed to support expansion and longevity.

Recently, a study describing the derivation of human cervical organoids was published (16). In this report the growth of endocervical organoids required Wnt activation, whilst squamous organoids required Notch signalling. Culture media for endocervical organoids included: Wnt3A, Rspondin-1, Noggin, Nicotinamide, EGF, FGF10, SB431542 and Y-27632. Whilst for ectocervical organoids: Noggin, Nicotinamide, EGF, FGF10, SB431542, Y-27632, Forskolin and Hydrocortisone. In the Chumduri et al. study, high concentrations (10μM) of Y-27632 Rho kinase inhibitor was added to both endo and ectocervix human organoids. In our lab and as others reported (17,18), the use of Y-27632 enhances the recovery rate of cells after freezing and post sorting. However, from my observations of adding Y-27632 to ectocervix mouse organoids (not shown), I found that the long exposure of cells to Y-27632 leads to a deformation in the stratification process, with clumping of cells and impaired budding of the squamous organoids (squamous organoids take a round shape). When following this protocol (Chumduri et al.), I also saw similar features (increased clumping and round eccentric complex structures). I was not able to assess the organoids under these conditions due to limited expansion of cultures and thus I did not have enough material to make paraffin blocks. However, based on what I observed in mouse ectocervix derivation experiments and on the organoid morphology, I suspect that Y-27632 causes hyperkeratinisation of the squamous cells. These were also very difficult to break-down and thus passage. In Chumduri ’s protocol, passaging is done by mechanical fragmentation using a fire-polished glass Pasteur pipette, which we did not have the set-up for in our lab, hence this could explain my inability to expand using their method. Endocervical organoids however, sustained growth but not for more than 9 passages. Overall, organoids were difficult to grow and neither conditions were continuous

for long-term. Thus, optimal conditions for the long-term growth of human cervical organoids is still ongoing work.

To summarise, in this chapter I was able to identify several factors to derive human cervix organoids: EGF, Noggin, Rspondin-1, A83-01, FGF10, HGF, PGE2, Nicotinamide and FGF2. Although this cocktail did not sustain growth for more than 6 passages, and the expansion was limited, it was encouraging to see the expression of my cells of interest (KRT8 and KRT17) in the formed spheres (Figure 5.12). A new study has reported the generation of human cervix organoids (both endo and ectocervix), however, by following their protocol I experienced difficulties in expanding and sustaining long-term survival of culture. I should emphasise that the number of benign human samples was limited, thus I did not have enough material to make blocks and stain the generated organoids from Chumduri et al.

Graphical summary for chapter 5

To be able to understand the correlation between the site of infection and the diversity of HPV infection consequences, the development of human cervical organoids is necessary because HPV is species-specific. Here i show the key steps taken to etablish human cervix organoids.

1- The mouse cervix organoids media was not sufficient to sustain growth of human cervix organoids, the addition of Nicotinamide increased the number of spheroids, FGF2 helped achieving longer growth, and the combining effect of PGE2, Nicotinamide and HGF increased the number of spheroids substantially. However, the condition was not enough to have a long-term culture.

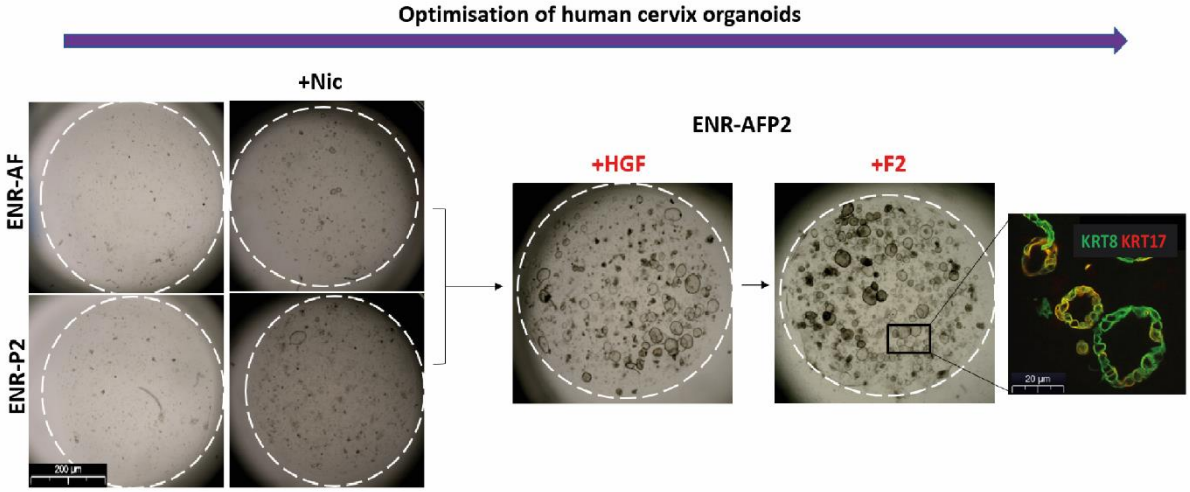

2- During my trials a report on human cervix organoids was released. In it Wnt was used to derive endocervix organoids but not ectocervix organoids. The report supports the presence of two seperate stem cells for the columnar and squamous lineages. It should be pointed that Chumduri and and colleagues did not show KRT markers of their derived organoids, however, TP63 was used to show squamous lineage.

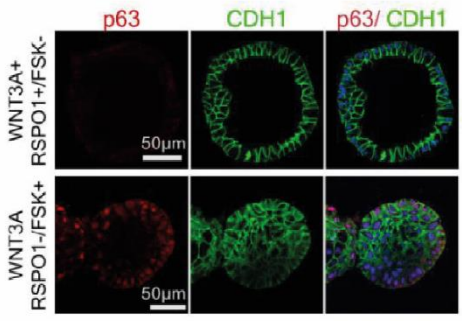

adapted from Chumduri et al., 2018.

• When I followed their protocol the ectocervix did not have any lumen and was difficult to break and passage. The endocervix was easier to grow and lasted longer, however, both did not sustain long-term culture.

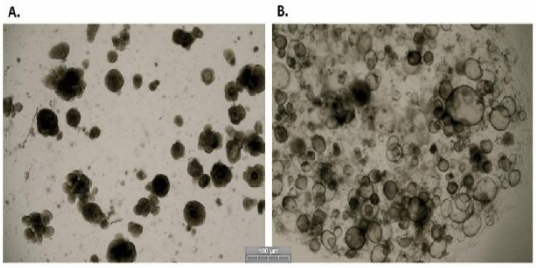

Chapter 5 References

1. Egawa N, Egawa K, Griffin H, Doorbar J. Human Papillomaviruses; Epithelial Tropisms, and the Development of Neoplasia. Viruses. 2015 Jul 16;7(7):3863–90.
2. Shadan FF, Villarreal LP. Coevolution of persistently infecting small DNA viruses and their hosts linked to host-interactive regulatory domains. Proc Natl Acad Sci U S A. 1993 May 1;90(9):4117–21.
3. Sato T, Vries RG, Snippert HJ, van de Wetering M, Barker N, Stange DE, et al. Single Lgr5 stem cells build crypt-villus structures in vitro without a mesenchymal niche. Nature. 2009 May 14;459(7244):262–5.
4. Sato T, Stange DE, Ferrante M, Vries RGJ, Van Es JH, Van den Brink S, et al. Long-term expansion of epithelial organoids from human colon, adenoma, adenocarcinoma, and Barrett's epithelium. Gastroenterology. 2011 Nov;141(5):1762–72.
5. Hu H, Gehart H, Artegiani B, LÖpez-Iglesias C, Dekkers F, Basak O, et al. Long-Term Expansion of Functional Mouse and Human Hepatocytes as 3D Organoids. Cell. 2018 29;175(6):1591-1606.e19.
6. Boj SF, Hwang C-I, Baker LA, Chio IIC, Engle DD, Corbo V, et al. Organoid models of human and mouse ductal pancreatic cancer. Cell. 2015 Jan 15;160(1–2):324–38.
7. Boretto M, Cox B, Noben M, Hendriks N, Fassbender A, Roose H, et al. Development of organoids from mouse and human endometrium showing endometrial epithelium physiology and long-term expandability. Dev Camb Engl. 2017 15;144(10):1775–86.
8. Huch M, Gehart H, van Boxtel R, Hamer K, Blokzijl F, Verstegen MMA, et al. Long-term culture of genome-stable bipotent stem cells from adult human liver. Cell. 2015 Jan 15;160(1–2):299–312.
9. Kessler M, Hoffmann K, Brinkmann V, Thieck O, Jackisch S, Toelle B, et al. The Notch and Wnt pathways regulate stemness and differentiation in human fallopian tube organoids. Nat Commun. 2015 Dec 8;6(1):1–11.
10. Alzamil L, Nikolakopoulou K, Turco MY. Organoid systems to study the human female reproductive tract and pregnancy. Cell Death Differ. 2020 Jun 3;1–17.
11. Chapman S, McDermott DH, Shen K, Jang MK, McBride AA. The effect of Rho kinase inhibition on long-term keratinocyte proliferation is rapid and conditional. Stem Cell Res Ther. 2014 Apr 28;5(2):60.
12. Koslow M, O'Keefe KJ, Hosseini ZF, Nelson DA, Larsen M. ROCK inhibitor increases proacinar cells in adult salivary gland organoids. Stem Cell Res. 2019 Dec 1;41:101608.
13. Turco MY, Gardner L, Kay RG, Hamilton RS, Prater M, Hollinshead MS, et al. Trophoblast organoids as a model for maternal–fetal interactions during human placentation. Nature. 2018 Dec;564(7735):263–7.
14. Turco MY, Gardner L, Hughes J, Cindrova-Davies T, Gomez MJ, Farrell L, et al. Long-term, hormone-responsive organoid cultures of human endometrium in a chemically defined medium. Nat Cell Biol. 2017 Apr 10;19:568.
15. Atsuta Y, Takahashi Y. Early formation of the Müllerian duct is regulated by sequential actions of BMP/Pax2 and FGF/Lim1 signaling. Development. 2016 Oct 1;143(19):3549–59.
16. Chumduri C, Gurumurthy RK, Berger H, Koster S, Brinkmann V, Klemm U, et al. Transition of Wnt signaling microenvironment delineates the squamo-columnar junction and emergence of squamous metaplasia of the cervix. bioRxiv. 2018 Oct 16;443770.
17. Xu X, Cowley S, Flaim CJ, James W, Seymour LW, Cui Z. Enhancement of cell recovery for dissociated human embryonic stem cells after cryopreservation. Biotechnol Prog. 2010 Jun;26(3):781–8.
18. Claassen DA, Desler MM, Rizzino A. ROCK Inhibition Enhances the Recovery and Growth of Cryopreserved Human Embryonic Stem Cells and Human Induced Pluripotent Stem Cells. Mol Reprod Dev. 2009 Aug;76(8):722–32.

6 Investigating the mechanisms regulating the formation of the transformation zone in the cervix using *in vitro* and *in vivo* models

6.1 Introduction

In humans, transformation zones (TZs) are well-defined histological junctions where two distinct types of epithelia meet. There are number of epithelial TZs in the body including; between the anal canal and the rectum, the oesophagus and the stomach, the cornea and the conjunctiva and in the junction between the endocervix and ectocervix. An interesting observation about the TZs is the increased cancer prevalence in these areas (1).

Cervical carcinoma has two histologically distinct types; adenocarcinomas and squamous cell carcinomas, and both predominantly arise at the TZ (2,3). Although High-risk human papilloma virus (HR-HPV) infects many other epithelial sites (4), the cervix has the highest cancer association with nearly 100% of cervical cancers having HR-HPV genome detected in them (5). The reasons behind why the cervical TZ is vulnerable for developing of carcinomas and what is the target cell of HPV infections remain elusive.

My previous results have shown that the TZ has a concentration of sub-glandular KRT17+ reserve cells (chapter 3, section 3.6.2) and this has also been reported by others (6). Reserve cells have been suggested as a possible cervical stem cell (7), however, its origin and bi-potential ability to give rise to both columnar and squamous lineages is yet to be proven, mainly because of the lack of suitable models.

As the TZ has two distinct epithelia, I hypothesise the existence of a delicate balance which is regulated by a unique signalling and a potential stem cell niche (1). The presence of TZ in other species enables animal models to be used, and my investigation of mouse cervix (chapter 3, section 3.6.3) shows enough similarities to the human cervix including KRT17+ expression pattern, justifying the use of mice to model the human TZ. Lineage tracing using transgenic mice will enable specific cell populations to be marked and for that mark to be transmitted to their cell progenies (8). Lineage tracing methods have been used to identify the stem cell populations of many different organs, one example is the identification of Lgr5+ intestinal stem cells using an *Lgr5-EGFP-ires-Cre*^{ERT2}*/Rosa26*^{lacZ} mouse model (22). Thus, I expect that this approach will allow the understanding of how a specific cell population behaves in maintaining homeostasis of cervical epithelium.

In this chapter, I use the murine cervix organoids that I have established to examine dual fate ability of KRT17 reserve cells. Additionally, I explore and make a preliminary evaluation of the lineage tracing techniques using transgenic mouse models to follow the fate of KRT17+ cells within the cervix to understand their contribution in building a TZ.

6.2 Results

6.2.1 Investigating the dual fate ability of the established murine cervical organoids

During the establishment of the murine cervix organoid cultures (in Chapter 4), I observed an occasional KRT17+ cell in the endocervical (ENR-P2) organoids (Figure 4.7). This observation was interesting because it suggests a common origin of endo- and ectocervix organoids. Furthermore, when I supplemented A83-01, FGF10 and PGE2 to ENR (ENR-AFP2) to a mouse cervical digest and followed a time-course of organoids growth (Figure 4.15), there was a mixture of columnar and squamous organoids in culture (section 4.2.2.1), this was also suggestive of a common progenitor.

Together with these observations, there are several lines of evidence that suggest the stemness of KRT17+ cells. Firstly, the role of KRT17+ cells in the squamous differentiation and maintenance in the touch dome (9) and hair follicle (10). Secondly, the pattern of sub-glandular KRT17+ reserve cells in both the human and mouse SCJ that I observed (chapter 3, sections 3.6.2 and 3.6.3). Thus, I raised the question of whether KRT17+ reserve cells are the stem cells of the cervix and whether they have dual cell fate capability.

In order to address this question, I took two different experimental approaches, by using my murine cervical organoid system and transgenic mouse models. One of the functional characteristics of a stem cell is their ability to generate different cell lineages from a single cell. Organoids have been used to demonstrate clonogenic ability. For example, in endometrial organoids, single cells were grown into clonal organoid lines and stimulated with hormones to show that both ciliated and secretory lineages can be generated starting from a single cell (11). I took a similar approach to test the clonogenic ability and the bipotential capability of KRT17+ and KRT8+ cervical cells. I implemented the limiting dilution assay using established endocervical or ectocervical organoids to assess their clonal capacity (21). This technique consists in preparing a cell suspension at a concentration so that 0.5 cells per Matrigel droplet, thus ensuring that a droplet will either contain 0 or 1 cell. I then plated this cell suspension into 96-well plates and followed their growth over 7-14 days. No organoids or spheroids formed from either the endocervical or ectocervical cultures, even after 14 days (this was repeated

three times). The limiting dilution assay is a very selective assay as only cells that are able to grow in isolation will be able to form an organoid. Therefore, I decided to perform a serial dilution assay by plating 10, 100 and 1000 cells (each into 10 wells of a 48 well plate) and follow their growth over 7-14 days. Doing a serial dilution assay would provide me with an estimation of the density required for the cells to generate organoids. Endocervical organoids grew well under all three dilutions. In contrast, ectocervical organoids were able to grow only at the dilution of 1000 cells per Matrigel droplet. The reason for the difficult recovery of squamous cells might be because of differences in cell-cell junction between columnar epithelium and squamous epithelium, with columnar cells linked by apical junctions and desmosomes, whilst squamous by adherens junctions and focal adhesion (integrin-extracellular matrix interactions) (12-15).

Since it was not feasible to assess the clonogenic potential of the cervical organoids due to their limited ability to grow under clonogenic conditions, I took an alternative approach to investigate the bipotential fate of KRT17+ cells. I carried out a time-course of the murine cervical organoids during their establishment by assessing their phenotype starting from passage 1 (not collected before) and passages 3 and 5. At the first passage, ectocervical organoids (ENR-AF) and endocervical organoids (ENR-P2) both displayed spheroid-like phenotype with co-expression of columnar lineage marker (KRT8) and squamous lineage marker (KRT17) (Figure 6.1). The size of the lumen varied between the two conditions, denser spheroids with smaller lumen was seen in ENR-AF (ectocervical organoids) and larger spheroids with wider lumen in ENR-P2 (columnar organoids), whilst ENR-AF-although single layered- appeared more thickened when compared to ENR-P2.

By passage 3, cells seem to commit to either columnar or squamous lineages depending on media conditions, as they are no longer express KRT8 and KRT17 simultaneously. Ectocervical organoids are TP63+, KRT17+, KRT8- (only few non proliferative near lumen) and MUC5AC-, whilst endocervical organoids are KRT8+, KRT17-, TP63- and MUC5AC+ as described in chapter 4 (Figure 4.6).

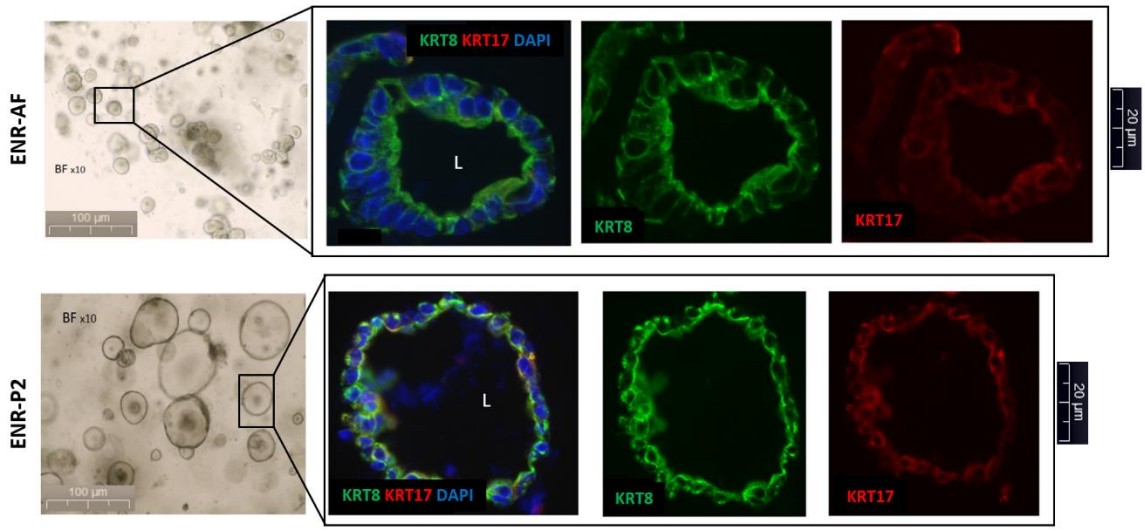

Figure 6.1: Mouse cervix organoids at an early timepoint in their derivation (passage 1). Representative IF staining Expression of columnar lineage marker (KRT8) and squamous lineage marker (KRT17) in both endocervical organoids (ENR-P2) and ectocervical organoids (ENR-AF) could be seen. Scale bar for bright-filed images=100µm and for IF images=20µm. Blue colour indicates DAPI nuclear staining and L= lumen.

As the co-expression of KRT8 and KRT17 markers was seen at passage one in both ENR-P2 and ENR-AF conditions, I questioned whether the established cultures (endo/ectocervix) still retained this plasticity to change cell fate if the signalling environment is exchanged. To test the plasticity potential of KRT17/KRT8 cells, I plated single cells from established cultures (passage 6) of both ectocervical and endocervical organoids and grew them in medium that promotes the opposing-lineage (ectocervical in ENR-P2 and endocervical in ENR-AF) for four passages (approximately 1 month in culture). When I cultured endocervical cells (KRT8+) in the medium that favours the growth of squamous cells (ENR-AF), the organoids maintained the single layered spheroid phenotype and no stratification was detected. Furthermore, growth rates decreased substantially with smaller and fewer spheroids forming (Figure 6.2). In contrast, when I plated ectocervical organoids (KRT17+) in the medium for columnar epithelium (ENR-P2), there was a gradual shift in phenotype. Whilst the starting population were 100% ectocervical generating complex stratified organoids, when I re-plated them as single cells in ENR-P2, stratification gradually decreased, with less than 10% of the generated organoids showing signs of stratification (Figure 6.3, Figure 6.4). At passage 2 post media exchange, all ectocervical organoids passaged in ENR-P2 medium lost their stratified phenotype and grew as spheroids with a clear lumen resembling the endocervix organoids (Figure 6.3 and Figure 6.4).

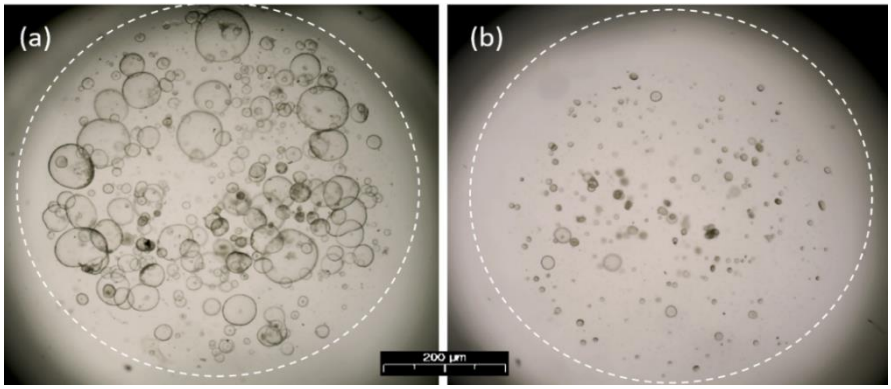

Figure 6.2: Examining the switch of media condition from ENR-P2 to ENR-AF ectocervical media on established endocervical organoids. Representative bright field images where (a) are control, i.e. endocervical organoids in their normal environment (ENR-P2). (b) endocervical organoids in ENR-AF ectocervical media, showing decrease in growth. Magnification x2, scale bar= 200µm.

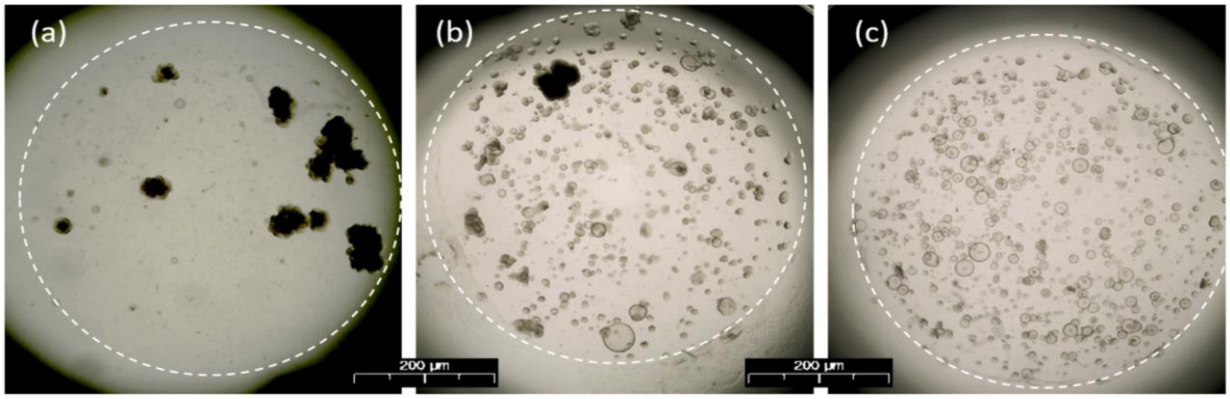

Figure 6.3: Examining the switch of media condition on ectocervical organoids. Representative bright field images where (a) are ectocervical organoids in ENR-P2 (control). (b) is passage 1 of ectocervical organoids in ENR-P2, showing spheroid-like organoids arising and only one complex-squamous-like structure growing. (c) at passage 2, no complex structures are growing, and the organoids showing a change in phenotype, scale bar= 200µm.

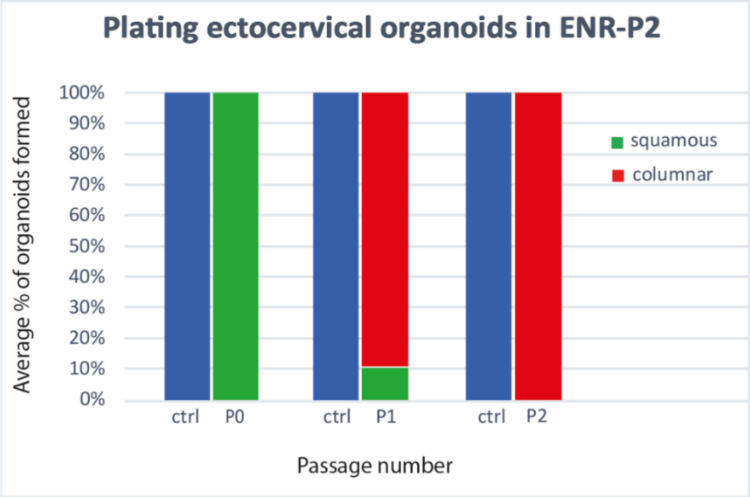

Figure 6.4: The ability of ectocervix KRT17+ cells to give rise to endocervix organoids. when supplied with endocervical media (ENR-P2). I plated with a starting population of a well-established ectocervix organoids (P6), in which 100% of the population were ectocervical. After passaging and plating single cells, at the 1st media change (P1) less than 10% of the generated organoids showed signs of stratification, and by the second passage (P2) 100% of generated organoids had sphere-like phenotype with clear lumen, similar to what I see with endocervix organoids. Control (ctrl) in the ectocervical organoids in their normal condition (ENR-AF).

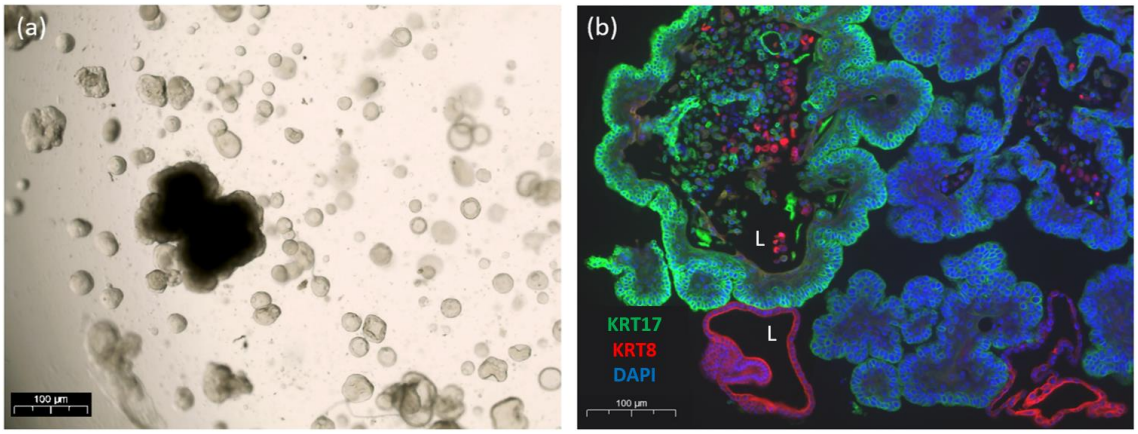

Figure 6.5: Intermediate stage of ectocervical organoids in ENR-P2. (a) bright field image of passage 2 of ectocervical organoids in ENR-P2 (intermediate stage of lineage switch) (b) IF staining of ectocervical organoids in ENR-P2 during fate transition, showing KRT8+KRT17- endocervical single layered spheroids, and KRT17+ stratified squamous epithelium in the same culture, scale bar= 100µm.

When I stained passage 1 post media exchange (intermediate stage of lineage switch) of the ectocervical organoids in columnar medium (ENR-P2), with KRT17, KRT8 and MUC5AC, the change in phenotype was confirmed with the presence of KRT8+ KRT17- (Figure 6.5) and MUC5AC (not shown) endocervical single layered spheroids. These spheroids were seen along with KRT17+ stratified squamous organoids in the same culture (Figure 6.5). Surprisingly, over time the endocervical single layered spheroids takes over and stratified squamous organoids disappear (Figure 6.3, IF not shown).

To summarise, during the establishment of organoids (early time-points), cultures grown in ENR-AF or ENR-P2 both express markers of the columnar (KRT8) and squamous (KRT17) lineages. This changes later, and commitment to either lineages occurs depending on the microenvironment provided from the supplied medium. The change in microenvironment after the lineages are established (passage three and above), did not result in a switch of phenotype in endocervical organoids, however, ectocervical (KRT17+) organoids were able to gradually switch fate based on observed markers (Figure 6.5) and mucin production (not shown).

6.2.2 Genetic lineage tracing using transgenic mice

My preliminary data show that the expression pattern of KRT17+ cells in younger mice (week 4) display an interesting profile of sub-columnar reserve cells under the KRT8 in the endocervix (Figure 3.9). This is similar to what I see in metaplastic cervical epithelium in humans. Furthermore, KRT17+ ectocervical organoids were able to give rise to KRT8 secretory columnar organoids when cultured in ENR supplemented with PGE2 (Figure 6.5). In my view, this suggests a plasticity of KRT17+ cells that I would like to further investigate. Since the organoids derived from wild-type mice do not allow the analysis of stem and progenitor cells progress. I chose to further explore the ability of KRT17+ cells to give rise to the different lineages with lineage tracing techniques using transgenic mice. The use of *in vivo* lineage tracing techniques allows labelling of cells and for cell clones to be followed over extended periods of time. Two mice strains were tested to understand the role of KRT17+ in the SCJ formation, *Krt17Cre*;*Rosa26-tdTomato* and *K17CreERT2; ROSA26-ZsGreen1*.

6.2.2.1 C57BL/6N-Krt17$^{tm1(cre,Cerulean)Murr}$/GrsrJ x B6.Cg-Gt(ROSA)26Sor$^{tm9(CAG-tdTomato)Hze}$/J

Little is known about how the cervical SCJ is maintained and the role of KRT17+ reserve cells in the process of cervical metaplasia. In order to investigate the contribution of KRT17+ cells in SCJ formation, I use the *Cre/lox* system in mice to label KRT17+ cells and to follow their

progenies. To this end, two strains were used: Krt17$^{cre/cerulean}$ mice (JAX, #018151) and ROSA26Sor$^{tm9(CAG-tdTomato)}$ (JAX, #007909). Krt17$^{cre/cerulean}$ mice contains *Cre* recombinase and the cerulean variant of green fluorescent protein (*GFP*) driven by the endogenous keratin 17 (*Krt17*) promoter. ROSA26Sor$^{tm9(CAG-tdTomato)}$ contains the *loxP* site-flanked STOP cassette in the Rosa26 locus and the red fluorescent protein variant tdTomato as a permanent genetic mark. The cross of these two strains will result in *Cre*-mediated deletion of the floxed STOP cassette in Krt17+ cells. Therefore KRT17+ cells will be cerulean+ (GFP+) and tdTomato+ (TdT+). Whilst its progeny that no longer express KRT17 will only be TdT+ (Figure 6.6). This would allow me to identify the differential pattern of gene expression in squamous, columnar and SCJ cells, and will clarify reserve cells function, and establish whether these cells originate from another cell type (e.g. endocervical).

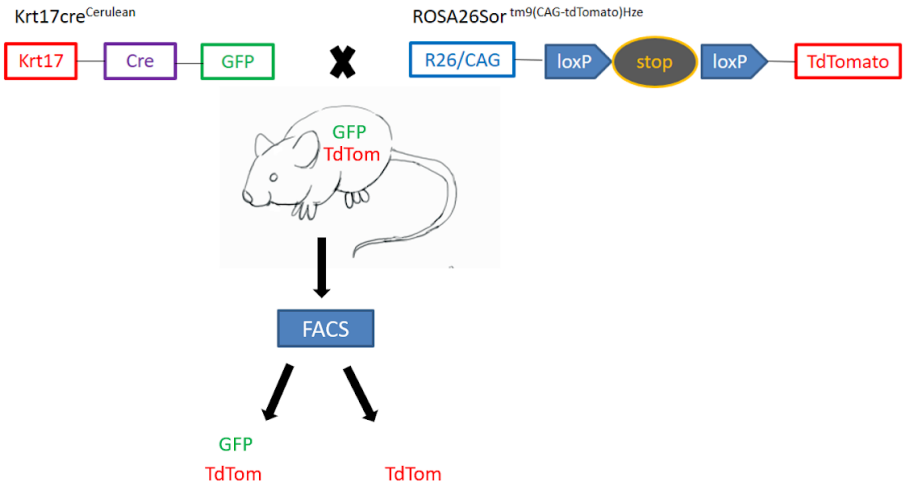

Figure 6.6: Krt17$^{cre/cerulean}$ mice crossed with Gt(ROSA)26Sor$^{tm9(CAG-tdTomato)}$. Cre recombinase and the cerulean variant of green fluorescent protein (GFP) driven by the endogenous keratin 17 (Krt17) promoter, crossed with Gt(ROSA)26Sor$^{tm9(CAG-tdTomato)}$ which contains loxP-flanked sequence, when deletion of the floxed sequences in the Cre-expressing cells of the offspring resulting in tdTomato fluorescence.

Krt17$^{cre/cerulean}$ stock were heterozygous for the *Krt17cre/cerulean* allele, thus after the first interspecies breeding, I detected both genomic *Krt17* (WT) and *Krt17$^{cre/cerulean}$* (mutant) (Figure 6.7). To get the desired experimental animals, I selected mice with 460 bp band (mutant) to be crossed in the next breeding round (more in methods section 2.2).

To establish a homozygous colony for mice carrying *Rosa-CAG-LSL-tdTomato-WPRE* conditional allele, I genotyped the first generation of bred animals of both wild type (Gt(ROSA)26Sor locus) and mutant alleles (Rosa-CAG-LSL-tdTomato-WPRE) (Figure 6.7). Later, I crossed animals with homozygous mutant alleles for both *Krt17cre/cerulean* and *Rosa-CAG-LSL-tdTomato-WPRE*. The progeny of the crossing would carry both alleles allowing the discrimination between the clonal progeny (TdT+) of neighbouring progenitor cells within the same niche (GFP+) (Figure 6.6).

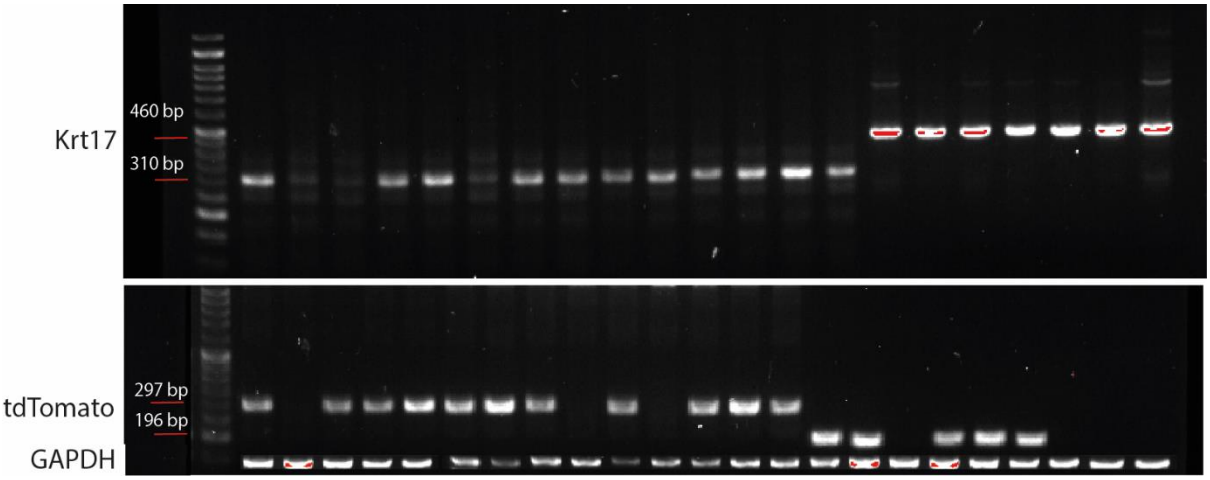

Figure 6.7: Genotyping using ear notch of Krt17cre;Rosa26-tdTomato mice, of both genomic Krt17 (WT) and Krt17$^{cre/cerulean}$ (mutant). Animals 460 bp band (mutant) were selected for breeding. Genotyping of Rosa-CAG-LSL-tdTomato-WPRE conditional allele, of both wild type (297 bp) and mutant (196 bp) alleles was done, and animals with mutant allele were selected to be bred with mutant Krt17$^{cre/cerulean}$.

According to The Jackson Laboratory website, the tdTomato line may express low levels of red fluorescence in the absence of *Cre* recombinase and that leakiness might be found in a small subset of the animals. From my trials, I have found that the animals were very leaky (Figure 6.8), leading to the whole body becoming pink (e.g. the skin of the limbs), this was also recently reported by others (16).

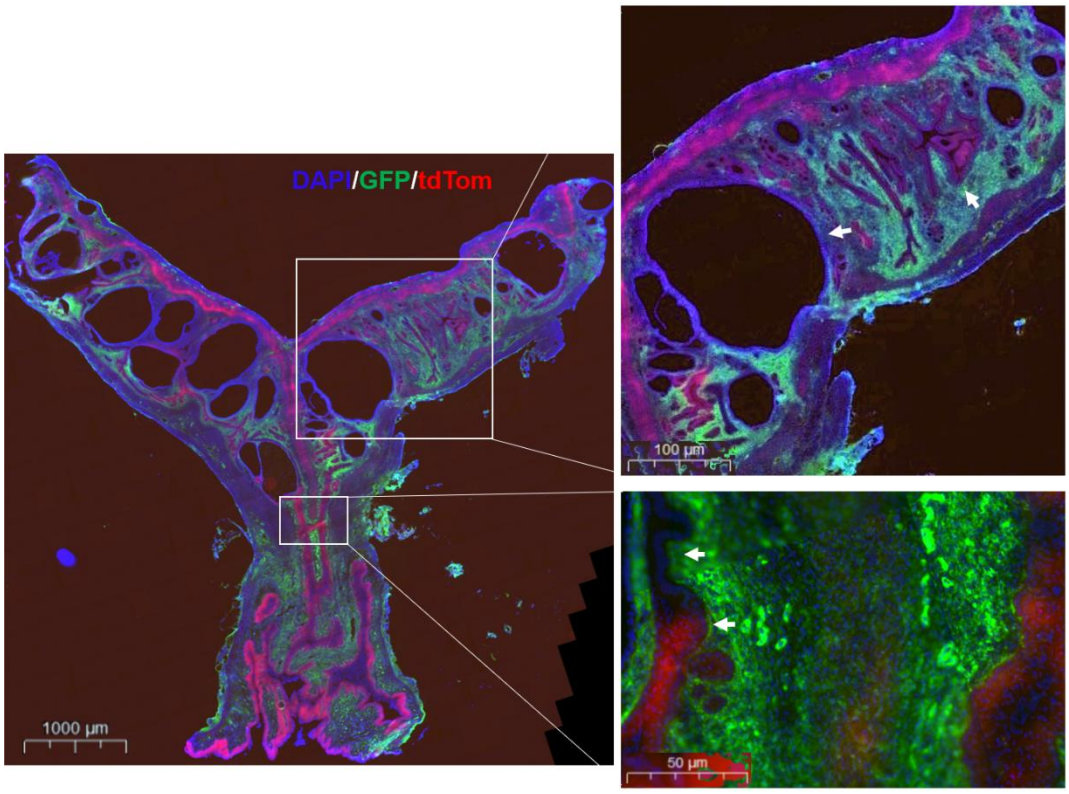

Figure 6.8: **Krt17cre;Rosa26-tdTomato mice showing GFP which is under the endogenous promotor of Krt17, and tdTomato (TdT) which a fluorescent protein marking KRT17 progeny cells.** GFP was seen in the stroma and not contained in the epithelium, whilst TdT was seen in the vagina, cervix and some of the endocervical glands, scale bar=1000µm for image on left hand-side, 100µm for top-right and 50µm for bottom right hand-side image.

To understand the contribution of KRT17-expressing cells (green), and their progeny (red) in the morphogenesis of the murine cervical SCJ, I harvested the cervix of double positive mice with both *GFP* from endogenous *Krt17* promoter and TdT and validated the expression using frozen sections. TdT expression was strong and can be seen without the use of an antibody, however GFP signal was weak hence I used anti-GFP antibody to detect the expression pattern (Figure 6.8). The green fluorescence was extensive in the stroma, and faintly in some of the basal epithelial layers of the squamous epithelium. The red (TdT+) was in both the squamous epithelium, and a large subset of the columnar (some glands were negative).

To investigate the phenotype seen *in vivo*, I harvested two 8-week-old mice cervixes and carried out the digestion according to the previously described protocol (explained in methods section 2.1.5). Next, I carried out Fluorescence-activated cell sorting (FACS) for green (GFP+) and red (TdT+), this was done with the help of Dr. Nigel Miller from the flow cytometry facility at our department. The cell populations with highest green and red fluorescence peaks (Double

positive for GFP and TdT) were collected in one tube, and cell populations with highest red fluorescence (TdT) only were collected in another (Figure 6.9). Subsequently, I plated murine cervical organoids of both lineages in ENR-AF (ectocervical media) and ENR-P2 (endocervical media).

After cell sorting, I used the two populations (double positives and single positives) to derive murine cervical organoids. Cell viability post sorting was low, thus I added Rock inhibitor (Rocki) to increase cell survival as seen by our lab and others (17). Rocki was supplied to the medium for the first three days post plating and organoids started to form at passage 2 (approximately 2 weeks).

The growth in both ENR-AF (ectocervical medium) and ENR-P2 (endocervical medium) had a squamous phenotype. However, it did not resemble the squamous organoids derived from wild-type mouse cervix. One of the main differences was complete absence of KRT8 cells, the lack of lumen, and the formation of keratin pearl (squamous cells form concentric layers) this was seen from both double positive coloured population (GFP+/TdT+) and single positive population (TdT+) (Figure 6.10 and Figure 6.11).

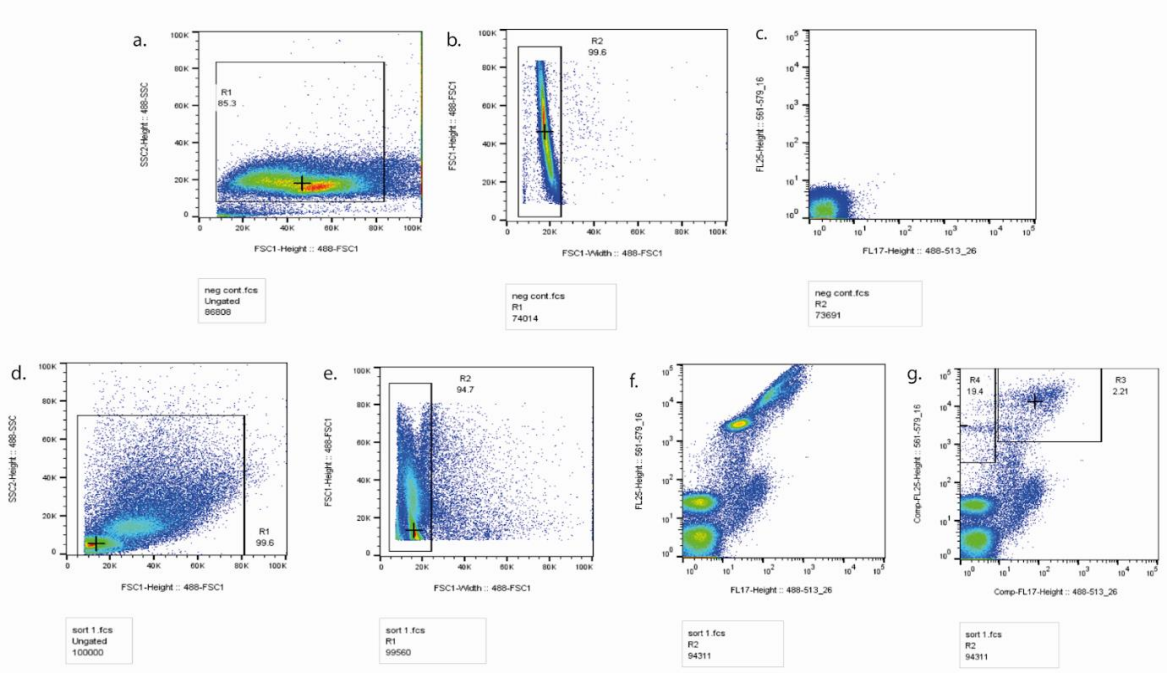

Figure 6.9: Sorting GFP and tdTomato from Krt17^{cre};Rosa26^{tdTomato} cervical digest. Top row is showing a negative control sample **(a)** 488-SSC-H;488-FSC1-H to get rid of debris **(b)** 488-FSC1-H;488-FSC1-W to get singlets **(c)** 561-579/16-H-log;488-513/26-H-log to get the highest intensity. Bottom row contain a digest from Krt17cre;Rosa26-tdTomato **(d)** 488-SSC-H;488-FSC1-H to get rid of debris **(e)** 488-FSC1-H;488-FSC1-W to get singlets **(f)** 561-579/16-H-log;488-513/26-H-log to get the highest intensity **(g)** 561-579/16-H-comp;488-513/26-H-comp where the highest green and red signals were gated and sorted (n=3).

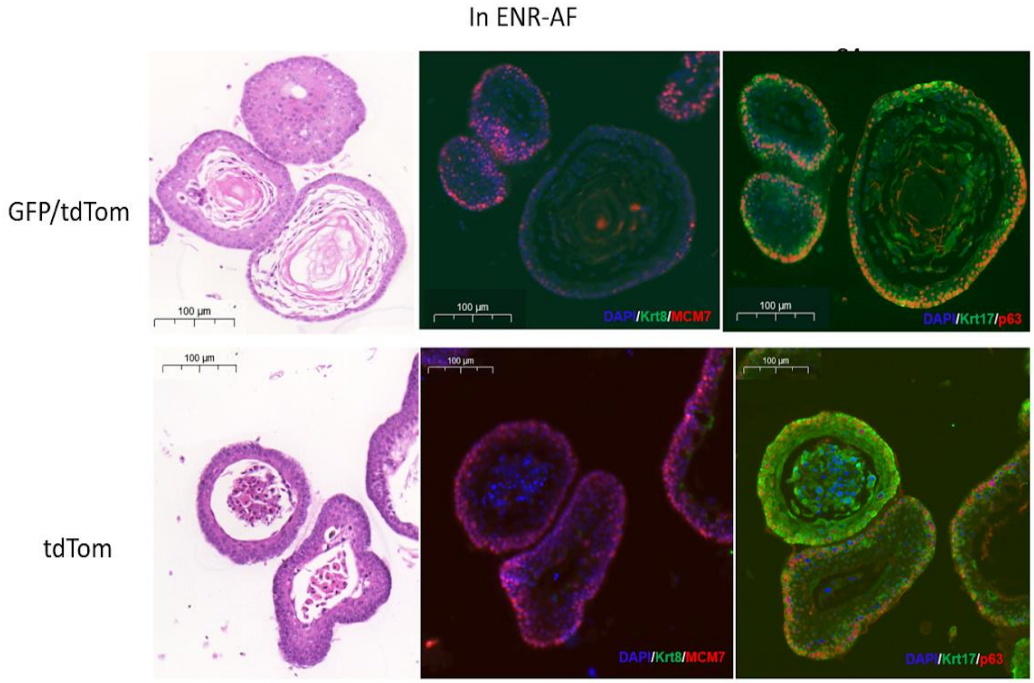

Figure 6.10: Generation of ectocervical organoids from Krt17^{cre};Rosa26^{tdTomato}. Ectocervix organoids (ENR-AF) from Krt17^{cre};Rosa26^{tdTomato} double positive population (GFP/tdTomato) and single positive population (tdTomato). IF of columnar marker KRT8, squamous markers KRT17 and TP63 and proliferation marker MCM7. Both populations showed elements of squamous differentiation, with the addition of keratin pearl formation in GFP/tdTomato, scale bar=100µm.

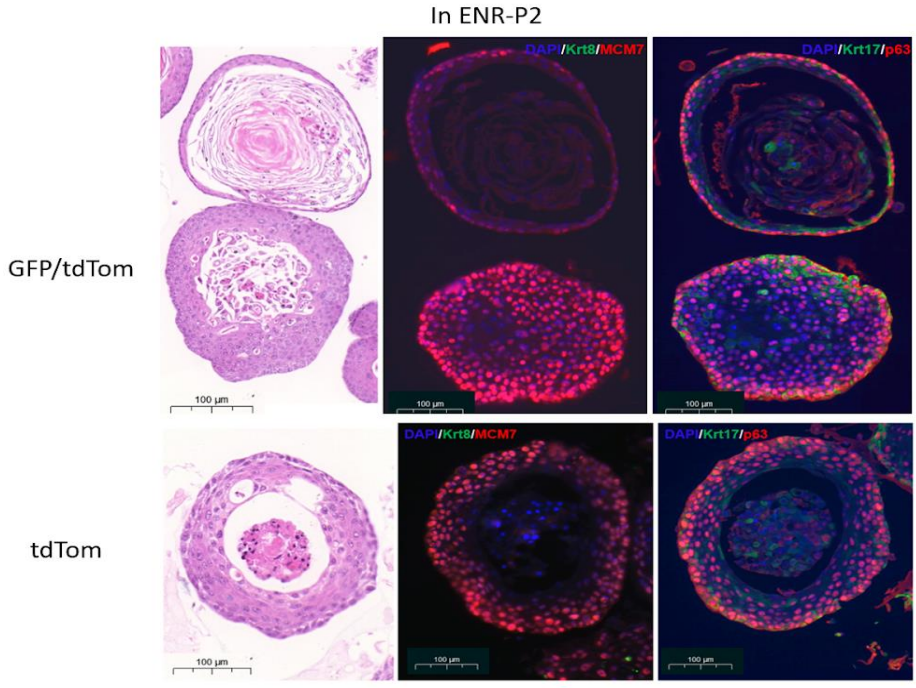

Figure 6.11: Generation of endocervical organoids from Krt17^{cre};Rosa26^{tdTomato}. Endocervix organoids (ENR-P2) from Krt17^{cre};Rosa26^{tdTomato} double positive population (GFP/tdTomato) and single positive population (tdTomato). IF of columnar marker KRT8, squamous markers KRT17 and TP63 and proliferation marker MCM7. Both populations showed elements of squamous differentiation, with the addition of keratin pearl formation in GFP/tdTomato, scale bar=100µm.

6.2.2.2 Krt17^{CreERT2} X B6.Cg-Gt(ROSA)26Sor$^{tm6(CAG-ZsGreen1)Hze}$/J

Since the *Krt17cre X* Rosa-*tdTomato* did not show a clear distinctive pattern to answer my question, I decided to move into a more tightly regulated transgenic model where Cre-mediated recombination can be controlled not only via Cre/loxp but also through tamoxifen administration. Using K17CreER^{T2} mice (9), where the tamoxifen inducible *Cre* recombinase (*CreERT2*) is expressed under the control of the mouse endogenous *Krt17* promoter. When crossed with a fluorescent reporter mice, pulse and chase experiments can be performed under the control of tamoxifen administration.

Here I used homozygous K17CreER^{T2} mice (obtained from Dr David Owens lab), to be bred with male hemizygous transgenic Ai6 (ROSA26-ZsGreen1) (*JAX*, # 007906) reporter mice (gifted from Dr Stacey Efstathiou's Lab), thus generating an inducible green reporter strain (*K17CreERT2;ROSA26RZsGreen*) (Figure 6.12). This inducible system is useful to study *Cre* subcellular localisation, perform lineage tracing analysis and track the fate of single KRT17-expressing cells.

After crossing, I confirmed the presence of both *ZsGreen* mutant and the *Cre* via PCR on ear biopsies (detailed in methods section 2.2.1.1.2) (Figure 6.13) and animals with the desired genotype were then used to carry the tamoxifen induction experiment.

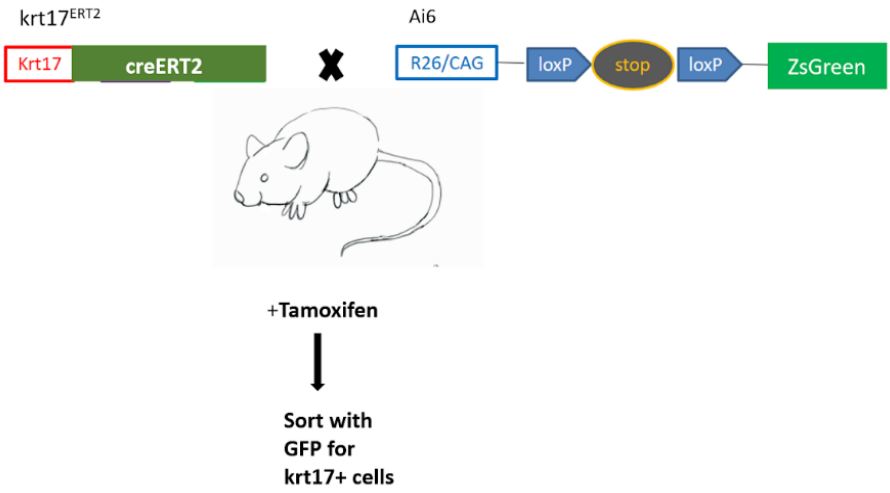

Figure 6.12: K17CreER^{T2} mice crossed with ROSA26-ZsGreen1. K17CreERT2 has tamoxifen inducible cre recombinase under the control of endogenous Krt17 promoter, crossed with a fluorescent reporter mice Ai6(ROSA26-ZsGreen1) with green fluorescent protein ZsGreen1.

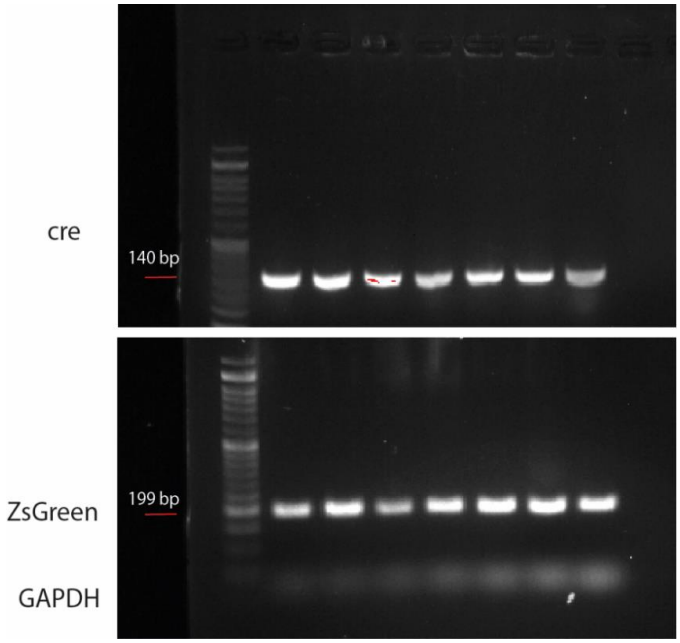

Figure 6.13: Genotyping using ear notch of K17Cre^{ERT2};ROSA26^{RzsGreen} mice. Confirmation of both ZsGreen mutant (199bp) and Cre (140 bp) was carried out on ear biopsies of K17CreERT2;ROSA26RzsGreen mice.

According to the Jackson lab website, some ZsGreen1 expression may be present prior to *Cre* recombinase, but the ZsGreen1 expression levels after *Cre* recombination are significantly greater than those of baseline levels. To induce ZsGreen1 expression in *K17CreERT2; Ai6(RCL-ZsGreen),* I carried out mice intraperitoneal injections of 2 mg of tamoxifen (TAM) (*Sigma*) or sunflower oil alone (vehicle) for control. Initially one or two doses of TAM were given to mice (2 injections of tamoxifen with 24h in between) and collected after one or two weeks. Subsequently, I used frozen sections to observe the number of green cells (ZsGreen1) (see methods 2.5.2.2). The expression of ZsGreen1 was strong and I was able to see it using immunofluorescent microscope without the use of an antibody. The green cells in control (vehicle only) were constricted in the squamous epithelium of the vagina and I did not detect any in the cervix or the uterine horns (Figure 6.14). In mice injected with TAM, expression level was not better when using 2 consecutive doses (data not shown). The green fluorescence from 2 weeks post induction was more extensive than in the 1-week chase, and I was able to detect ZsGreen1 in the ectocervix, SCJ and few cells in the endocervix. In the 2-week chase the endocervical glands appeared expanded, which could be a secondary effect of tamoxifen. ZsGreen1 expression was strong in the squamous epithelium whilst columnar cells were mostly negative (Figure 6.14).

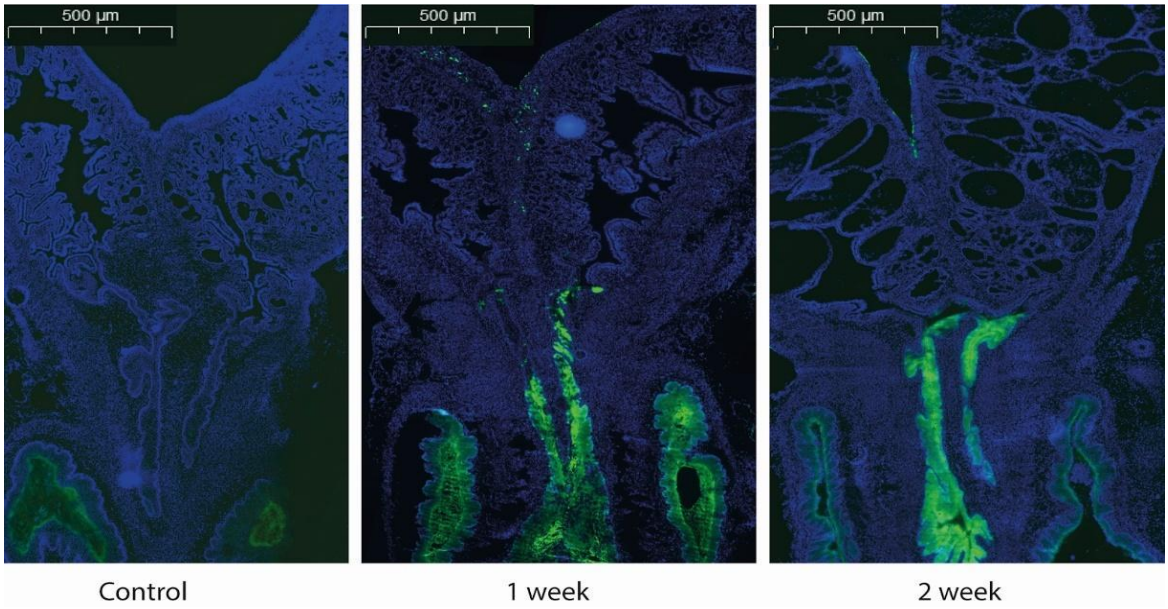

Figure 6.14: ZsGreen1 expression in 2-weeks post tamoxifen induction. ZsGreen1 expression was more extensive than in the 1-week chase when examining KRT17+ cells in the cervix of K17CreERT2; Ai6(RCL-ZsGreen) mice. The endocervical glands looked expanded in week 2, scale bar=500µm.

6.3 Discussion

A question that is of importance to be addressed is whether KRT8+/TP63- endocervical organoids have the same progenitor cell as the KRT17+/TP63+ ectocervical/SCJ organoids. Although it was challenging to carry a clonal assay due to the squamous cells survival rate when carrying a limiting dilution, I investigated the organoids expression at an early time point (passage 1). During a premature state of murine cervical organoid development (passage 1) both ectocervical organoids (ENR-AF) and endocervical organoids (ENR-P2) displayed co-expression of columnar lineage marker (KRT8) and squamous lineage marker (KRT17), before committing to one lineage at an advance passage number (~P3-4), which propose plasticity potential.

To test the plasticity potential of KRT17 and KRT8 cells, I plated single cells from established cultures of both ectocervical and endocervical organoids and I switched the media between the two (i.e. endocervical in ENR-AF and ectocervical in ENR-P2) and followed the progress for four passages before collection and IF staining. The ectocervical cells (KRT17+) in media that favours the growth of columnar epithelium (ENR-P2) showed a shift in phenotype towards secretory KRT8+ single cell layered organoids, whilst endocervical cells from endocervical organoids (KRT8) in ectocervical media (ENR-AF) did not. This result favours the possibility

of the dual fate capability of KRT17+ cells but not KRT8+ cells, however, further investigation is needed to confirm the hypothesis.

To understand the role of KRT17+ cells in cervical regeneration and metaplastic process, *Krt17*$^{cre/cerulean}$ mice with *Cre* recombinase and *GFP* activated by endogenous *Krt17* promoter were crossed with *ROSA26Sor*$^{tm9(CAG\text{-}tdTomato)}$ which contains *loxP*-flanked sequence. Cre-mediated recombination will result in deletion of the floxed sequence resulting in the *cre*-expressing cells (here Krt17+) progenies to express tdTomato. When examining the cervix of *Krt17cre;Rosa26-tdTomato,* GFP was found broadly in the stroma, and faintly in the basal layers of the squamous epithelium, whilst tdTomato was in the squamous epithelium, subset of the columnar epithelium of the endocervix and extensively in the skin of the mouse.
After cell sorting for GFP and TdT was carried out, two cell populations were collected, GFP/TdT positive cells and TdT positive only cells. According to the reserve cell (KRT17+) hypothesis, the double positive population (GFP+/TdT+) represent the progenitor dual-fate population, whilst the single positive (TdT+) population is the progeny of the GFP/TdT cells, hence we do not expect this population to produce endocervical/ectocervical organoids. However, when I plated the two populations (double and single positives) in ENR-AF (ectocervical medium) and ENR-P2 (endocervical medium), squamous growth was overtaken even in ENR-P2, and the growth appeared abnormal when compared with organoids driven from wild-type mice with the formation of keratin pearls in both double positive coloured population (GFP/TdT) and single positive population (TdT).
This result indicates that neither of the starting populations (GFP/TdT and TdT) contained the progenitors needed to sustain healthy long-term murine cervical organoids, possible cause is that the FACS sorting was not accurate. Another is that the *Krt17cre;Rosa-tdTomato* line leakiness is compromising the precision of the experiment.

The usefulness of the Krt17CreERT2 line was explored after being crossed with a reported ROSA26RZsGreen mice. Since this experiment was performed at the end of this PhD, a long-term chase on this line was not done, thus I cannot fully evaluate the potential of the pulse/chase using *K17CreERT2* mice. Nevertheless, using *K17CreERT2;Ai6(RCL-ZsGreen)* mice I examined the cellular dynamics of KRT17+ cells in the SCJ. ZsGreen1 expression was present prior to *Cre* recombinase, but none in the cervical epithelium, after *Cre* recombination the ZsGreen1 expression was significantly greater than those of baseline levels. The green fluorescence of ZsGreen1 was chased for 1 week and 2 weeks post tamoxifen induction. In

week 2, the expression was more extensive and the ZsGreen1 was seen in the ectocervix, SCJ and few cells in the endocervix. Additionally, In the 2-week chase the endocervical glands looked expanded, which is a possible effect of tamoxifen. Overall, the transgenic strain with tamoxifen control (*K17CreERT2* mice) were promising and showed better control of KRT17 induction compared to the Cre/loxp only (Krt17cre/cerulean) strain.

To further probe the cellular dynamics of the SCJ niche, selective genetic ablation (here for KRT17 cell population) can be used if bred with a Cre-inducible *Diphtheria* toxin receptor (DTR) (18), upon toxin administration, this approach will allow defects in murine cervix development and homeostasis to be monitored in the absence of KRT17 cells. In addition, crossing *K17CreERT2* with *Brainbow2.1-confetti* mice (19), here the administration of tamoxifen would result in the 'Brainbow2.1' cassette being recombined exclusively in KRT17-expressing cells allowing their fate to be followed.

One limitation that should be addressed in tamoxifen-induced Cre-recombination, is that tamoxifen binds to estrogen receptor (ER), which can be challenging in a hormonally regulated epithelium like the cervix. Tamoxifen can be both an agonist and antagonist of ER signalling, depending on tissue type (20), thus understanding the effect of the dose on cervical epithelium requires cautious assessment.

Graphical summary for chapter 6

In this chapter, I use the established murine cervix organoids to examine dual fate ability of KRT17 reserve cells. Additionally, I evaluate the use of lineage tracing techniques using transgenic mouse models to follow the fate of KRT17+ cells within the cervix and understand their contribution in building a TZ.

1- Mouse cervix organoids of both lieage at passage 1, showed co-expression of columnar lineage marker (KRT8) and squamous lineage marker (KRT17) before committing to either fate in P4.

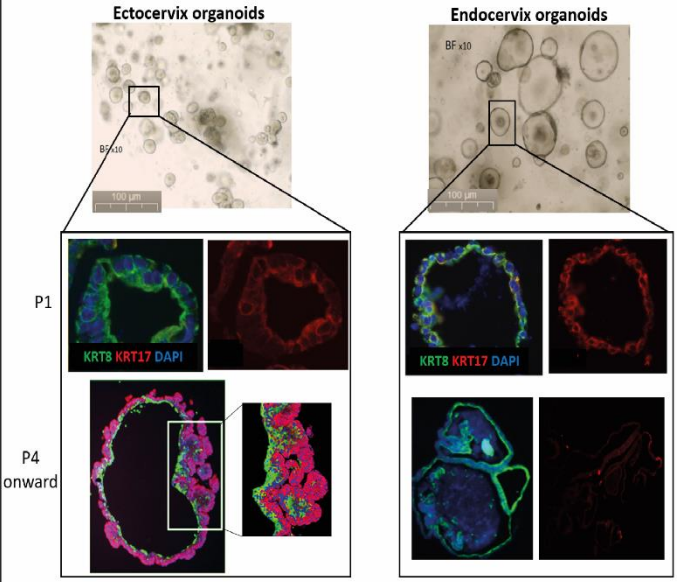

• Next, I examined the ability of established lineages to switch fate when supplied with the opposing lineage (i.e. squamous organoids in columnar media and vice versa). KRT17+ ectocervical organoids were able to give rise to secretory KRT8 organoids but endocervix organoids did not have the ability ot generate squamous organoids.

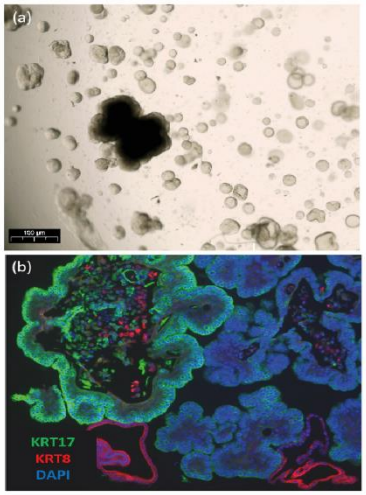

2- In Krt17Cre(GFP);Rosa26tdTomato a two colour system was assessed, where Krt17+ cells would carry GFP (under Krt17 promotor), whilst their KRT17-progony would express the red tdTomato. However, this mouse background showed leakiness in tdTomato expression, and KRT17 was seen extensively in the stroma.

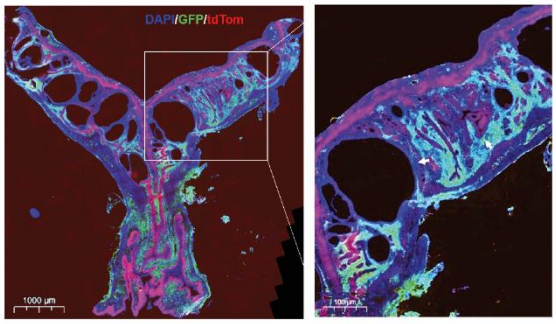

• K17CreERT2 mice showed confined clonal expansion of KRT17+ cells in the SCJ, detected by ZsGreen reporter strain, even with a short-period genetic pulse chase (2 weeks) and low level tamoxifen induction (one dose of 2 mg/ml).

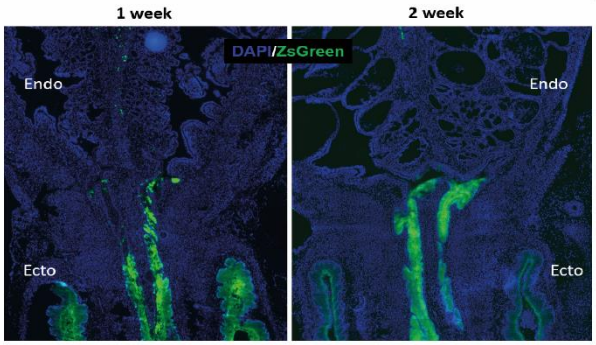

Chapter 6 references

1. Mcnairn AJ, Guasch G. Epithelial transition zones: merging microenvironments, niches, and cellular transformation. Eur J Dermatol EJD. 2011 May;21 Suppl 2:21–8.
2. Petignat P, Roy M. Diagnosis and management of cervical cancer. BMJ. 2007 Oct 13;335(7623):765–8.
3. Fluhmann CF. Carcinoma in situ and the transitional zone of the cervix uteri. Obstet Gynecol. 1960 Oct;16:424–37.
4. de Martel C, Georges D, Bray F, Ferlay J, Clifford GM. Global burden of cancer attributable to infections in 2018: a worldwide incidence analysis. Lancet Glob Health. 2020 Feb;8(2):e180–90.
5. Walboomers JM, Jacobs MV, Manos MM, Bosch FX, Kummer JA, Shah KV, et al. Human papillomavirus is a necessary cause of invasive cervical cancer worldwide. J Pathol. 1999 Sep;189(1):12–9.
6. Martens JE, Smedts FMM, Ploeger D, Helmerhorst TJM, Ramaekers FCS, Arends JW, et al. Distribution Pattern and Marker Profile Show Two Subpopulations of Reserve Cells in the Endocervical Canal. Int J Gynecol Pathol. 2009 Jul;28(4):381.
7. Martens JE, Arends J. Cytokeratin 17 and p63 are Markers of the HPV Target Cell, the Cervical Stem Cell. ANTICANCER Res. 2004;6.
8. Fan H, Liu X, Shen Y, Chen S, Huan Y, Shan J, et al. In Vivo Genetic Strategies for the Specific Lineage Tracing of Stem Cells. Curr Stem Cell Res Ther. 2019;14(3):230–8.
9. Doucet YS, Woo S-H, Ruiz ME, Owens DM. The touch dome defines an epidermal niche specialized for mechanosensory signaling. Cell Rep. 2013 Jun 27;3(6):1759–65.
10. Tong X, Coulombe PA. Keratin 17 modulates hair follicle cycling in a TNFα-dependent fashion. Genes Dev. 2006 May 15;20(10):1353–64.
11. Turco MY, Gardner L, Hughes J, Cindrova-Davies T, Gomez MJ, Farrell L, et al. Long-term, hormone-responsive organoid cultures of human endometrium in a chemically defined medium. Nat Cell Biol. 2017 Apr 10;19:568.
12. Iwamoto DV, Calderwood DA. Regulation of integrin-mediated adhesions. Curr Opin Cell Biol. 2015 Oct;36:41–7.
13. Farkas AE, Capaldo CT, Nusrat A. Regulation of epithelial proliferation by tight junction proteins. Ann N Y Acad Sci. 2012 Jul;1258:115–24.
14. Johnson JL, Najor NA, Green KJ. Desmosomes: regulators of cellular signaling and adhesion in epidermal health and disease. Cold Spring Harb Perspect Med. 2014 Nov 3;4(11):a015297.
15. Capaldo CT, Farkas AE, Nusrat A. Epithelial adhesive junctions. F1000prime Rep. 2014;6:1.
16. Zhao X-F, Alam MM, Liao Y, Huang T, Mathur R, Zhu X, et al. Targeting Microglia Using Cx3cr1-Cre Lines: Revisiting the Specificity. eNeuro. 2019 Jul 1;6(4).
17. Emre N, Vidal JG, Elia J, O'Connor ED, Paramban RI, Hefferan MP, et al. The ROCK Inhibitor Y-27632 Improves Recovery of Human Embryonic Stem Cells after Fluorescence-Activated Cell Sorting with Multiple Cell Surface Markers. PLOS ONE. 2010 Aug 13;5(8):e12148.
18. Buch T, Heppner FL, Tertilt C, Heinen TJAJ, Kremer M, Wunderlich FT, et al. A Cre-inducible diphtheria toxin receptor mediates cell lineage ablation after toxin administration. Nat Methods. 2005 Jun;2(6):419–26.
19. Roy E, Neufeld Z, Livet J, Khosrotehrani K. Concise review: understanding clonal dynamics in homeostasis and injury through multicolor lineage tracing. Stem Cells Dayt Ohio. 2014 Dec;32(12):3046–54.
20. Goodsell DS. The Molecular Perspective: Tamoxifen and the Estrogen Receptor. The Oncologist. 2002;7(2):163–4.

21. Sieburg HB, Cho RH, Müller-Sieburg CE. Limiting dilution analysis for estimating the frequency of hematopoietic stem cells: Uncertainty and significance. Exp Hematol. 2002 Dec 1;30(12):1436–43.
22. Barker N, Clevers H. Lineage tracing in the intestinal epithelium. Curr Protoc Stem Cell Biol. 2010 May;Chapter 5:Unit5A.4.

7 General discussion

High-risk Human Papillomavirus (HPV) causes cancer at a number of epithelial sites (1), but the cancer rate in these sites varies. Cervical cancer affects over 500,000 women per year worldwide and almost 100% of cervical cancer is caused by HPV (2). However, at the adjacent vulva and vagina, HPV-associated cancer causes only around 20,000 cases per year (3). This fact, combined with studies showing increased rate of neoplasia formation in different transformation zones (TZ) including anorectal, oropharyngeal, corneal limbus and between the endocervix and the ectocervix (4-7), raises the question of site-specific vulnerability for HPV-driven cancers.

The reason for TZ regions susceptibility to HPV-associated cancers is poorly understood. In order to understand how these infections can lead to cancer, there is a need to first understand the normal biology of how the TZ is regulated. Knowledge about epithelial stem cell regulation in TZ will not only help understand site homeostasis and repair, but also the progression of disease and our current understanding is limited due to a lack of tractable systems to study the human cervix.

The cervix is a complex epithelial structure, with two distinct epithelial lineages (columnar epithelium of the endocervix and stratified epithelium of the ectocervix) meeting at the squamo-columnar junction (SCJ). After puberty, the anatomical change creates a need to build a new protective squamous layer when the columnar cells of the endocervix get exposed to the low pH of the vagina, also in response to local irritation (8,9). The columnar epithelium of the endocervix is replaced by stratified squamous epithelium generating an area of transformation (i.e. TZ) by the process of metaplasia (10). Metaplasia is meditated by KRT17+ sub-columnar reserve cells (11). Reserve cells are a specialised type of cervical stem cells present under the columnar epithelium close to the cervical SCJ (11). These cells are termed ‘reserved’ as they have the ability to be induced during injury (12). The origin of reserve cells is still controversial. Some believe they may originate from a population of cuboidal cells found at the SCJ (13), whilst others have suggested that they might be derived from embryonic origins (14). More recently, the possibility of reserve cells arising from the basal cells of the ectocervix has been reported (15).

Evidence suggests that the consequences of HPV infection differ depending on the site of infection. This was based on observations that correlated different biomarkers at different stages of cervical neoplasia: HPV-encoded E4 protein (marks active virus production) and

p16^{INK4a} tumour suppressor protein (marks deregulated HPV). In high-grade lesions, E4 is absent (abortive infection) and p16^{INK4a} is extensive throughout the full thickness of the epithelium whilst in low-grade lesions, E4 expression was increased and p16^{INK4a} was lost (16,17). This pattern was also confirmed using organotypic raft cultures derived from primary human keratinocytes. These experiments showed that the infection of the basal epithelial layer of stratified ectocervix results in a productive HPV infection (high E4, low p16$^{INK4a)}$ in which the life-cycle of the virus is supported (18). On the other hand, infection of the columnar cells of the endocervix did not support the viral life-cycle, causing deregulation of viral gene expression and the development of cancer (19,20). Herfs and colleagues have also pointed out that the majority of high-risk HPV infections in the ectocervix do not progress to high-grade lesions (21).

There is a need to understand how these epithelial sites are regulated and viral gene expression may control genes in the specific sites where high-risk HPV types causes cancer. The aim of my research was to contribute to the understanding of the epithelial homeostasis in the cervix by exploring the utility of mouse models to study human cervical renewal dynamics and metaplasia. Moreover, I optimised and generated an *in vitro* organoid culture system of the murine cervix, which provides a tool to examine the local microenvironment that controls the formation of the endocervix, the SCJ, and the ectocervix. This approach also offers a system to explore the changes that drive metaplasia. Subsequently I use the knowledge from the mouse model to optimise a human cervical organoid system. Since HPV only infects human cells (22), human cervix organoids would provide a crucial HPV infection tool. Although conclusions about the requirements for the long-term propagation of human cervical organoids have not been drawn in this thesis, several steps that might pave the way have been described. Lastly, I explored the utility of lineage tracing via transgenic mice, which will potentially allow the understanding of the complex nature of the cervical transformation zone origin.

7.1 Cervical reserve cells - in human and mouse

Although the origin of reserve cells is still controversial, there have been several attempts to characterise these cells using immunohistochemistry. In addition to their physical location under the endocervical crypts, cervical reserve cells express KRT17, BCL-2 and TP63 (23). The importance of cervical reserve cells is due to the hypothesis that they might be a possible progenitor of both squamous and columnar epithelia lineages (23,24). Furthermore, reserve cells are hypothesized as the target cell of cervical cancer (23). There has not been a clear staging of the steps by which hyperplasia of reserve cells initiate the process of metaplasia. The

results presented in this thesis (chapter 3) confirms the presence of a discrete population of KRT17+ in the cervical TZ and shows the stages of reserve cell hyperplasia during cervical metaplasia. When the TZ is being generated in the human cervix, reserve cells that reside in a quiescent state (based on their low proliferative capacity) at the endocervix proliferates, forming rows of cells that continue to build a new layer of squamous epithelium in a stage termed immature metaplasia. Reserve cells continue to generate a fully mature stratified squamous epithelium (mature metaplasia) which becomes indistinguishable from the ectocervix and can only be recognised by the presence of endocervical crypts underneath.

A need for an *in vivo* model of cervical TZ is crucial to further understand the origin and potential of the reserve cells. Thus, the utility of the mouse was investigated and the expression pattern of KRT17+ cells in the mouse cervix was explored. Following the progress of KRT17+ cells in mouse cervix at two weeks post-birth, the cervix was underdeveloped and the SCJ was not well defined KRT17 cells were at the basal layer of the vagina and in small, localised colonies in the cervix (Figure 3.8). At week 4, a row of proliferative (marked by MCM7) KRT17+ cells were seen under the columnar epithelium of the developing uterine horns (Figure 3.9). And by week 8, columnar and squamous lineages are histologically distinct, with KRT8+ columnar cells occupying the endocervical end and KRT17+ cells covering the ectocervix. The two lineages meet in a junction where KRT17+ cells underlie columnar KRT8+ cells (Figure 3.10). The presence and pattern of KRT17+ reserve cells in the developing mouse cervical epithelium (week 4) resembles what is seen in human metaplasia. This suggests a fundamental similarity to the regulatory mechanisms that control the potential ability of the KRT17+ reserve cells to differentiate into either a single layered columnar epithelium, or a multi-layered epithelium of the squamous transformation zone.

Some anatomical and histological differences are apparent between the human and mouse cervical epithelium, including the anatomical organisation of the uterine body and the persistence of KRT17 expression in the ectocervix. KRT17 persistence across the stratified epithelium in the mouse ectocervix, is possibly explained by the hypothesis that short-lived rodents lack quiescent stem cells in their epithelia (25). The control of DNA damage, protein translation and epigenetics all take a part in the quiescent stem cell regulation, evolutionary adaptation for the long-lived animal (e.g. humans) vs short-lived ones (e.g. mice) might play a role in the differences observed between the two species in regards to reserve cells (25).

Based on the reserve cells staging and their characterisation using a series of lineage markers of human cervical sections, evidence presented in this thesis support the hypothesis of the reserve cells hyperplasia role in generating TZ. No specialised KRT7 cells were detected in the TZ (Figure 3.6) and thus, no proof was found to support the KRT7 cuboidal cells theory. In this theory described by Herfs and colleagues, a group of cuboidal cells marked by KRT7, are at the SCJ and have the ability to give rise to a 'reserve cell-like' population underneath them to initiate metaplasia (13). A possible reason for this discrepancy, is the small sample size analysed in their study.

7.2 Organoid tissue culture models of the murine cervix

In order to establish a physiologically relevant model of the cervix to propagate and investigate KRT17+ cells, I established murine cervical organoids. In chapter 4 I describe the culture conditions that I optimised which allow the establishment and propagation of the two distinct cervical epithelial lineages; endocervix and ectocervix starting from cells isolated from the adult murine cervix. ENR-AF (ENR basal medium with the addition of A83-01 (TGFβi) and FGF10), gave rise to stratified squamous epithelium, and ENR-P2 (ENR basal medium with the addition of PGE2), generated secretory columnar epithelium.

The two cervical organoids showed distinct phenotypes that recapitulated each region of the cervix. Endocervical organoids were secretory as they stained for mucins: MUC1 that is expressed along the female reproductive tract and an endocervix-specific mucin, MUC5AC. These endocervix organoids were positive for columnar marker KRT8 and negative for squamous markers, as the endocervix *in vivo.* In contrast, ectocervical organoids recapitulated the multi-layered epithelial phenotype *in vivo* and were positive for squamous markers KRT17 and TP63, whilst they were negative for secretory markers. The endocervical and ectocervical identity of the organoids was confirmed by a genome-wide transcriptional analysis by microarray to compare them to the *in vivo* tissue.

One of the key questions in the regulation of the different regions of the cervix is to define the signalling pathways involved in maintaining the columnar epithelium and those that instead drive stratification. The culture conditions I defined for the endocervix and ectocervix organoids provide insight into the nature of these signalling pathways. I found that TGFβ and cAMP signalling via PGE2 were important for the derivation and long-term maintenance of endocervix organoids. This is in agreement with transcriptional analysis of *in vivo* endocervix as I found that it was enriched in genes of the TGF-β as well as BMP signalling pathways:

Inhba, Smad2, Bmp1 and *Bmper*. Furthermore, the endocervical organoids express high levels of *Cftr*, a cAMP-activated protein and *Pde7b*, a cAMP regulator. I also found that *Fzd7* a receptor for Wnt was detected in the endocervical mouse epithelia from the transcriptional analysis (chapter 4, section 4.2.6.2). Although I do not add Wnt in the medium for endocervical organoids, Rspondin-1, a ligand for LGR receptors which amplifies Wnt signalling, is present. For the ectocervix organoids on the other hand, inhibition of TGFβ and activation of FGFR2IIIb pathway was crucial for their long-term propagation and maintenance. In the ectocervix, *Fgfr3* was detected in the *in vitro* transcriptional analysis of ectocervical organoids, whilst the stromal analysis showed *Fgf2*. Notch pathway ligands *Notch1, Notch 3* and *Jag2* were detected in the ectocervical organoids. This agrees with reports on the involvement of the Notch pathway in the human cervix, with cleaved Notch1 reported extensively in the parabasal layers of the ectocervix (18). Additionally, the transcriptomic analysis of the murine cervix showed expression on *Dll4,* one of Notch ligands. The effect of interfering with Notch pathway was investigated in the ectocervix organoids. γ-secretase inhibitor (DAPT) was added, and the effect was followed for 4 days. At day 2, the stratification was restricted to no more than 3 layers, and at day 4 post γ-secretase inhibitor addition, no sign of stratification was detected (Figures 4.30). The single layered sphere-like organoids were positive for both squamous epithelium marker KRT17 and columnar marker KRT8 (Figure 4.31). This verified the importance of Notch pathway in the ability of ectocervical organoids to build a multi-layered epithelium. A key follow-on experiment is to investigate whether the KRT8/KRT17 cells were an unstratified ectocervical cells or there was a change in cellular fate.

A key finding from the transcriptional analysis of mouse cervix organoids was the identification of a cell-surface marker *NGFR* (Nerve Growth Factor Receptor, or *P75*) in ectocervical organoids. In addition, when I examined the transcriptional analysis of cervical stroma (derived from *in vivo*), I found that *NGF* was highly expressed. P75 is the receptor for NGF and is a marker of progenitor cells in many epithelia, including: the basal cells of the normal oesophageal epithelium (26), laryngeal squamous epithelial cells (27), oral (28) and corneal keratinocytes (29). Furthermore, P75 is expressed in the human embryonic stem cell line derived from blastocysts (30). To my knowledge there have been no reports of P75 expression in the cervix, thus it was interesting to investigate the pattern in both mouse and human cervix. Using Immunofluorescence, P75 was seen at the basal layer of squamous epithelium of the ectocervix/TZ and in reserve cells in both humans and mice, with similar

pattern in ectocervical (ENR-AF) organoids (chapter 4, section 4.2.6.4.1). P75 might open the possibility to sort for basal squamous cells/reserve cells.

Krt5 was one of the markers highly expressed in the transcriptional analysis of *in vitro* ectocervix organoids (section 4.2.3). This was an interesting finding, since it is one of the markers reported for the progenitor cells in the transitional columnar epithelium of the oesophagus (31). Thus, I examined whether KRT5 and KRT17 are co-expressed. In mouse cervix, KRT5 stained the ectocervical stratified squamous epithelium in a similar pattern to KRT17, in both young (weeks 3-4) and in adult mice (week 8), with KRT5 under the KRT8 columnar cells of SCJ (Figure 4.21). The same expression pattern was found in mouse cervix organoids. The mouse ectocervical organoids showed positive KRT5 at the basal layer, whilst endocervical organoids were negative for KRT5. In the human cervix, KRT5 expression is different from KRT17 as KRT17 is mostly negative in the basal squamous layers of the ectocervix and is only induced physiologically upon a metaplastic event. KRT5 however, was found in the squamous basal cells of the ectocervix (not shown) and in the reserve cells at the transformation zone (TZ) (Figure 4.23), unlike KRT17 which was reserve cells specific in the human cervix.

Although mouse endocervix organoids were mostly negative for KRT17, there was an occasional KRT17+ cell in a number of the developing endocervix cultures. This raised the question about the commonality of origin of endocervix and ectocervix organoids and whether one lineage can undergo transdifferentiation. When examining early time points (passage 1) during the establishment of organoids in chapter 6, both mouse ectocervical organoids and mouse endocervical organoids co-expressed columnar lineage marker (KRT8) and squamous lineage marker (KRT17) (Figure 6.1), before one lineage dominates at a later stage (~P3-4), this was also seen in human cervix organoids (chapter 5). This was an interesting observation as it suggests a common progenitor. The co-expression of these markers has not been reported before.

My results on the co-expression of the columnar and squamous lineage markers suggests that the cells may have dual fate ability, thus I examined whether each mouse cervical organoid lineage (endocervix and ectocervix) is able to switch fate when changing the microenvironment. Endocervical organoids were cultured in ectocervix/stratifying medium ENR-AF, whilst ectocervical organoids were supplied with endocervix- medium ENR-P2. Cells from ectocervical organoids were capable of giving rise to KRT8+, TP63-, secretory organoids (MUC1 and MUC5AC). However, the endocervix did not thrive in the ectocervix

organoids medium and did not stratify. This supports the dual fate potential of KRT17 cells, however, further lineage tracing experiments must be carried out to confirm this finding.

7.3 Establishing the human cervix organoid model

HPV is able to replicate and complete its life cycle only in human cells. Thus, to be able to study HPV-associated neoplasia and cancer progression, the establishment of cervix organoids which are derived from humans is crucial. Generation of an *in vivo* infection model of columnar or stratified organoids, will allow a first insight into the pathways that simultaneously regulate cell fate and viral gene expression. I initially used the culture conditions for growing mouse cervix organoids to grow human cervical organoids. However, they were not able to sustain growth of cells isolated from the human cervical samples, so I have extensively optimised the derivation method by culturing cells isolated from different locations of the cervix (endo, SCJ and ectocervix). Derivation from both endocervix and SCJ has generated preliminary growth, but not the ectocervix. A possible explanation is that the majority of the layers in the ectocervix are terminally differentiated, thus multiple ectocervical pieces might be required to have an adequate basal/parabasal layers.

After gradually building knowledge of culture media growth factors using several optimisation steps (chapter 5), the combination that showed the best cell survival rate (6-7 passages) was ENR-AF (A83-01, FGF10) with the addition of HGF, PGE2, Nicotinamide and FGF2. TGF-β inhibition via A83-01 was key for culture survival, and the addition of Nicotinamide increased the number of spheroids. FGF2 helped achieving relatively long-term growth, and the combining effect of PGE2, Nicotinamide and HGF increased the number of spheroids substantially. The generated sphere-like organoids were single layered and had both columnar (KRT8) and reserve cell marker (KRT17).

Recently, a human cervical organoid protocol was reported (15). In this publication, the growth of endocervical organoids required Wnt activation, this agrees with the presence of Wnt in the endocervical transcriptional analysis data presented in chapter 4 (section 4.2.3). In the other hand, Chumduri et. al, reported that the derivation of squamous lineage required the activation of Notch signalling, in agreement to what I see in transcriptional analysis of ectocervical organoids with expression of Notch pathway ligands *Notch1, Notch 3* and *Jag2*.

Chumduri and colleagues, propagated endocervical organoids in a media that contained Wnt3A, Rspondin-1, Noggin, Nicotinamide, EGF, FGF10, SB431542 and Y-27632. Whilst ectocervical organoids required Noggin, Nicotinamide, EGF, FGF10, SB431542, Y-27632,

Forskolin and Hydrocortisone to be propagated. I have followed this protocol and endocervical organoids growth was substantially increased in this media condition, however, not for long-term (9 passages). Ectocervical organoids were more challenging to expand, one reason could be the high concentration of Rock inhibitor (Rocki) Y-27632 in the media, from personal observation, extending the exposure of cervical organoids to Rocki leads to the formation of squamous pearls (keratin pearl), which are difficult to passage and expand, resulting in cell death. In addition to finding the correct microenvironment and tailor the culture media, another reason for the challenge in maintaining the human cervical organoids for long-term is the fact that organoids are self-renewing, therefore, the presence of the tissue-resident stem/progenitor cells in the digest is crucial. Although Chumduri and colleagues did not investigate the expression of KRT17 in the cervix, they identify the basal squamous cell with KRT5. KRT5 was one of the highly expressed markers in the transcriptional analysis of *in vitro* ectocervix (section 4.2.3). Further work is yet needed to have a long-term cervical organoid culture.

7.4 Lineage tracing using transgenic mice

The cervical TZ is rich in KRT17+ reserve cells which have been speculated to be the stem cells of the cervix (23). Although the organoid model is useful in many aspects including the study of signalling and infectivity *in vitro*, it is limited when it comes to investigating the developmental aspects of cervical epithelial formation. As I have seen a hyperplasia-like pattern of KRT17+ cells in a mouse SCJ development time-course (Figure 3.9), in addition to KRT17+ ectocervical organoids having the ability to transdifferentiate giving rise to KRT8 secretory columnar organoids (Figure 6.5), further investigation was needed to confirm that KRT17+ reserve cells are indeed the stem cells of the cervix. Therefore, I have taken an additional approach by using *in vivo* lineage tracing mice.

Genetic labelling *in vivo* can shed light on cell fate determination during development, and dynamics of stem and progenitor during tissue homeostasis and repair. The utility of two strains were examined, $Krt17^{Cre(GFP)};Rosa26^{tdTomato}$ and $K17^{CreERT2};Ai6^{(RCL\text{-}ZsGreen)}$. Both strains had *Cre* under the endogenous *Krt17* promoter, however in $K17^{CreERT2}$ the Cre/loxp system is under the control of tamoxifen induction as well. Similar approach has been applied in studying Barrett's metaplasia in the oesophageal SCJ (31).

In $Krt17^{Cre(GFP)};Rosa26^{tdTomato}$ a two colour system was assessed, where KRT17+ cells would carry GFP (under Krt17 promotor), whilst their KRT17-progony would express the red tdTomato. However, this mouse background showed leakiness in tdTomato expression, and was dismissed after several organoid derivation experiments (chapter 6, section 6.2.2.1).

K17Cre^{ERT2};Ai6$^{(RCL-ZsGreen)}$ where *Cre*-mediated recombination is activated via tamoxifen administration. After one dose of tamoxifen and two-week chase only, the expression was seen extensively with ZsGreen1 seen in the ectocervix, SCJ and few cells in the endocervix. Although the full advantage of the mouse background was not fully evaluated due to the fact it was carried at the end of my PhD, the system showed potential with reliable and confined induction. This system if crossed with a mouse strain with 'Brainbow2.1' cassette, would present a great tool to follow KRT17+ fate (more in 7.5.2).

7.5 Future Perspectives

7.5.1 Future directions of cervical organoids technology

In this project, I was able to generate a robust organoid model from mice, both endocervix and ectocervix. These organoids were utilised to understand the signalling that derives the different lineages in the cervix and uncover novel markers in the site. There is still much to learn however about the cervical epithelial regeneration, maintenance, and differentiation. Combining organoid technology with CRISPR/Cas9 gene editing present a way to address many of these questions. Site-specific targeting with CRISPR/Cas9 can be used to modify a genetic locus of interest to further investigate a specific transcription factor.

Several additional observations from my work suggest the utility of the organoid system to explore other biological processes. For example, the transcriptional analysis of mouse endocervix showed *Foxj1 a* marker of ciliogenesis, which is directly regulated via Wnt signalling (20), thus these organoids might present a robust model for studying ciliogenesis *in vitro* which is still poorly understood. Additionally, *Esr1* estrogen receptor was detected in the transcriptional analysis of the cervix (chapter 4). Evidence suggests the involvement of estrogen signalling in HPV-derived carcinogenesis in the cervix (36). On the contrary, the role of progesterone in the pathogenesis of cervical disease lacks in knowledge. Thus, the reported cervix organoids could provide an *in vitro* tool to investigate the responsiveness of cervix organoids to hormones and their interaction with different signalling pathways (e.g. Wnt). Cervical organoids contain the epithelial compartments of the tissue only and therefore lack some of the cellular complexity. The immune system components play a key role in the homeostasis and function of the cervix. And the fate of HPV clearance or pathogenesis is determined by the immune response (37). Additionally, signalling between epithelia and the stroma guides the pathways that regulated the tissue homeostasis. Recently, an epithelial-mesenchymal co-culture model of the endometrium was developed with both cell types being

functionally responsive to hormones (38). The study of cellular interactions with multicellular organoid co-culture systems such as fibroblasts, epithelial cells, and immunes cells can offer depth of how the pathogens behave in their native host environment.

Although conclusions about the requirements for the long-term propagation of human cervical organoids have not been drawn in this thesis, the trials and the combinations described might open the way for the generation of human cervix organoids. The addition of organoid technology to the experimental models for the study of the human cervix would be a useful tool for the propagation and maintenance of primary cells that recapitulate the original tissue both healthy and pathological. Additionally, human cervix organoids would provide an *in vitro* infection, and with combination with single cell technology, it would offer a new method to identify the target cell of the HPV abortive infection (Figure 7.1).

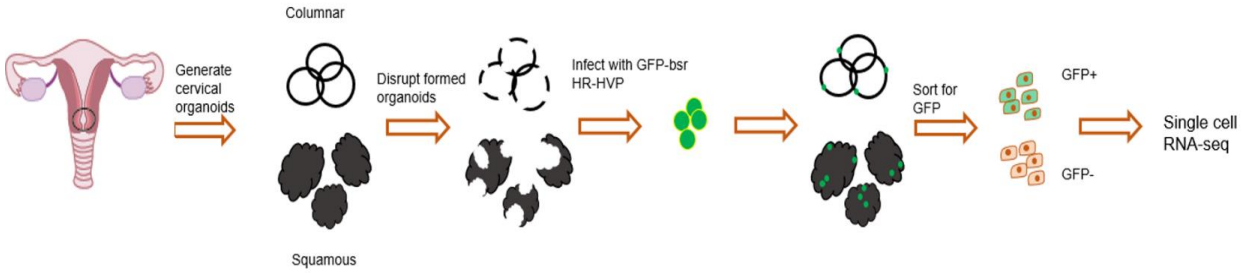

Figure 7.1: A potential method to understand the target cell of HPV abortive infection. Infection of Human cervical organoids derived from anatomically normal cervix using GFP-tagged HR-HPV genome.

7.5.2 Future directions of mouse lineage tracing

My initial evaluation of *K17Cre*^{ERT2} (32) mice were encouraging, even though I did a short-period genetic pulse chase trial (2 weeks), low level tamoxifen induction (one dose of 2 mg/ml) showed confined clonal expansion detected by ZsGreen reporter strain. This will provide the tools to explore the role of KRT17+ population in the cervical epithelial development in mice. Additionally, organoids generated from KRT17 labelled mice will enable FACS isolation of KRT17 cells, this will help us determine the cell origin of the phenotypes observed in my generated murine organoids. Furthermore, the possibility of crossing *Krt17Cre*^{ERT2} with *Gt(ROSA)26Sor*$^{tm1(CAG-Brainbow2.1)Cle}$ confetti mice (33) would be valuable in understanding cell-fate disputes in the cervix. Also, crossing *Krt17Cre*^{ERT2} and *Gt(ROSA)26Sor*$^{tm1(HBEGF)Awai}$ mice (34) will allow conditional expression of the diphtheria toxin receptor (DTR), to promote the selective ablation of the KRT17 cell population upon toxin administration (32,34). This

approach will permit defects in murine cervix development and homeostasis to be monitored in the absence of KRT17 cells.

Genetic fate-mapping studies using lineage-specific strains were applied in other systems including the mammary gland. *R26*^{Confetti}*;R26*^{CreERT2} mouse model was used to analyse clonal progeny of luminal (KRT8/18) or basal (KRT5/14) lineages reviled unipotent progenitors that give rise to ductal morphogenesis (35). Additionally, a similar approach was utilised by Jiang and colleagues with the use of *Krt7Cre*^{ERT2} in their oesophageal cancer studies. And given that KRT7 cervical cuboidal cells are reported as one of the possible origins of reserve cells, the use of these mice in addition to *Krt17Cre*^{ERT2} would allow real-time comparison of the two hypotheses.

7.6 Conclusion and final word

In this dissertation, I use a combination of *in vivo* and *in vitro* methods to address the role of reserve cells in normal cervical epithelium homeostasis and in HR-HPV infections. 3D murine cervical organoid model was generated with two distinct microenvironments to grow both endocervix and ectocervix organoids. This *in vitro* system was then utilised to investigate the signalling pathways responsible for the regulation of the two different cervical lineages i.e., endo- and ectocervix. Merging the *in vitro* and *in vivo* data allowed the uncovering of signalling pathways such as Wnt for the regulation of the endocervix, and Notch for maintaining the ectocervical epithelium. Additionally, the established organoids were combined with lineage tracing techniques to investigate how the cervical transformation zone in formed and maintained. At the end of this thesis, steps were taken to optimise human cervix organoids. Human cervix organoids would open doors to construct models for infectious diseases. Moreover, it would permit a future protocol that involves the use of co-culture techniques, allowing the study of how different cell types interact with the cervical epithelium.

Chapter 7 references

1. de Martel C, Georges D, Bray F, Ferlay J, Clifford GM. Global burden of cancer attributable to infections in 2018: a worldwide incidence analysis. Lancet Glob Health. 2020 Feb;8(2):e180–90.
2. Brianti P, De Flammineis E, Mercuri SR. Review of HPV-related diseases and cancers. New Microbiol. 2017 Apr;40(2):80–5.
3. Kreimer AR, Pierce Campbell CM, Lin H-Y, Fulp W, Papenfuss MR, Abrahamsen M, et al. Incidence and clearance of oral human papillomavirus infection in men: the HIM cohort study. Lancet. 2013 Sep 7;382(9895):877–87.
4. Assi R, Reddy V, Einarsdottir H, Longo WE. Anorectal Human Papillomavirus: Current Concepts. Yale J Biol Med. 2014 Dec 12;87(4):537–47.
5. You EL, Henry M, Zeitouni AG. Human papillomavirus–associated oropharyngeal cancer: review of current evidence and management. Curr Oncol. 2019 Apr;26(2):119–23.
6. Hanbazazh M, Gyure KA. Ocular Human Papillomavirus Infections. Arch Pathol Lab Med. 2018;142(6):706–10.
7. Mirkovic J, Howitt BE, Roncarati P, Demoulin S, Suarez-Carmona M, Hubert P, et al. Carcinogenic HPV infection in the cervical squamo-columnar junction. J Pathol. 2015 Jul;236(3):265–71.
8. Singer A, Jordan JA. The Functional Anatomy of the Cervix, the Cervical Epithelium and the Stroma. In: The Cervix. John Wiley & Sons, Ltd; 2009. p.13–37.
9. Vooijs GP. The problem of replacement and differentiation of the intestinal epithelium. Cancer Cytopathol. 1997;81(6):317–22.
10. Regauer S, Reich O. CK17 and p16 expression patterns distinguish (atypical) immature squamous metaplasia from high-grade cervical intraepithelial neoplasia (CIN III). Histopathology. 2007;50(5):629–35.
11. Martens JE, Smedts FMM, Ploeger D, Helmerhorst TJM, Ramaekers FCS, Arends JW, et al. Distribution Pattern and Marker Profile Show Two Subpopulations of Reserve Cells in the Endocervical Canal. Int J Gynecol Pathol. 2009 Jul;28(4):381.
12. Hellman LM, Rosenthal AH, Kistner RW, Gordon R. Some factors influencing the proliferation of the reserve cells in the human cervix. Am J Obstet Gynecol. 1954 Apr 1;67(4):899–915.
13. Herfs M, Vargas SO, Yamamoto Y, Howitt BE, Nucci MR, Hornick JL, et al. A novel blueprint for "top down" differentiation defines the cervical squamocolumnar junction during development, reproductive life, and neoplasia. J Pathol. 2013 Feb;229(3):460–8.
14. Martens JE, Smedts F, van Muyden RCPA, Schoots C, Helmerhorst TJM, Hopman A, et al. Reserve cells in human uterine cervical epithelium are derived from müllerian epithelium at midgestational age. Int J Gynecol Pathol Off J Int Soc Gynecol Pathol. 2007 Oct;26(4):463–8.
15. Chumduri C, Gurumurthy RK, Berger H, Koster S, Brinkmann V, Klemm U, et al. Transition of Wnt signaling microenvironment delineates the squamo-columnar junction and emergence of squamous metaplasia of the cervix. bioRxiv. 2018 Oct 16;443770.
16. Griffin H, Soneji Y, Van Baars R, Arora R, Jenkins D, van de Sandt M, et al. Stratification of HPV-Induced Cervical Pathology using the Virally-Encoded Molecular Marker E4 in Combination with p16 or MCM. Mod Pathol Off J U S Can Acad Pathol Inc. 2015 Jul;28(7):977–93.
17. Egawa N, Egawa K, Griffin H, Doorbar J. Human Papillomaviruses; Epithelial Tropisms, and the Development of Neoplasia. Viruses. 2015 Jul 16;7(7):3863–90.
18. Kranjec C, Holleywood C, Libert D, Griffin H, Mahmood R, Isaacson E, et al. Modulation of basal cell fate during productive and transforming HPV-16 infection is mediated by progressive E6-driven depletion of Notch. J Pathol. 2017 Aug;242(4):448–62.

19. Kranjec C, Doorbar J. Human papillomavirus infection and induction of neoplasia: a matter of fitness. Curr Opin Virol. 2016;20:129–36.
20. Doorbar J, Griffin H. Refining our understanding of cervical neoplasia and its cellular origins. Papillomavirus Res. 2019 Apr 8;7:176–9.
21. Yang EJ, Quick MC, Hanamornroongruang S, Lai K, Doyle L, McKeon FD, et al. Microanatomy of the cervical and anorectal squamocolumnar junctions: a proposed model for anatomical differences in HPV-related cancer risk. Mod Pathol Off J U S Can Acad Pathol Inc. 2015 Jul;28(7):994–1000.
22. Shadan FF, Villarreal LP. Coevolution of persistently infecting small DNA viruses and their hosts linked to host-interactive regulatory domains. Proc Natl Acad Sci U S A. 1993 May 1;90(9):4117–21.
23. Martens JE, Arends J. Cytokeratin 17 and p63 are Markers of the HPV Target Cell, the Cervical Stem Cell. ANTICANCER Res. 2004;6.
24. Weikel W, Wagner R, Moll R. Characterization of subcolumnar reserve cells and other epithelia of human uterine cervix. Demonstration of diverse cytokeratin polypeptides in reserve cells. Virchows Arch B Cell Pathol Incl Mol Pathol. 1987;54(2):98–110.
25. Dunaway S, Rothaus A, Zhang Y, Luisa Kadekaro A, Andl T, Andl CD. Divide and conquer: two stem cell populations in squamous epithelia, reserves and the active duty forces. Int J Oral Sci. 2019 Aug 27;11(3):1–13.
26. Okumura T, Tsunoda S, Mori Y, Ito T, Kikuchi K, Wang TC, et al. The Biological Role of the Low-Affinity p75 Neurotrophin Receptor in Esophageal Squamous Cell Carcinoma. Clin Cancer Res. 2006 Sep 1;12(17):5096–103.
27. Li X, Shen Y, Di B, Li J, Geng J, Lu X, et al. Biological and clinical significance of p75NTR expression in laryngeal squamous epithelia and laryngocarcinoma. Acta Otolaryngol (Stockh). 2012 Mar 1;132(3):314–24.
28. Nakamura T, Endo K, Kinoshita S. Identification of Human Oral Keratinocyte Stem/Progenitor Cells by Neurotrophin Receptor p75 and the Role of Neurotrophin/p75 Signaling. STEM CELLS. 2007;25(3):628–38.
29. Girolamo ND, Sarris M, Chui J, Cheema H, Coroneo MT, Wakefield D. Localization of the low-affinity nerve growth factor receptor p75 in human limbal epithelial cells. J Cell Mol Med. 2008;12(6b):2799–811.
30. Pyle AD, Lock LF, Donovan PJ. Neurotrophins mediate human embryonic stem cell survival. Nat Biotechnol. 2006 Mar;24(3):344–50.
31. Jiang M, Li H, Zhang Y, Yang Y, Lu R, Liu K, et al. Transitional basal cells at the squamous-columnar junction generate Barrett's oesophagus. Nature. 2017 Oct 26;550(7677):529–33.
32. Doucet YS, Woo S-H, Ruiz ME, Owens DM. The touch dome defines an epidermal niche specialized for mechanosensory signaling. Cell Rep. 2013 Jun 27;3(6):1759–65.
33. Lloyd-Lewis B, Harris OB, Watson CJ, Davis FM. Mammary Stem Cells: Premise, Properties, and Perspectives. Trends Cell Biol. 2017;27(8):556–67.
34. Šale S, Lafkas D, Artavanis-Tsakonas S. Notch2 genetic fate mapping reveals two previously unrecognized mammary epithelial lineages. Nat Cell Biol. 2013 May;15(5):451–60.
35. Davis FM, Lloyd-Lewis B, Harris OB, Kozar S, Winton DJ, Muresan L, et al. Single-cell lineage tracing in the mammary gland reveals stochastic clonal dispersion of stem/progenitor cell progeny. Nat Commun. 2016 Oct 25;7(1):13053.
36. Clarke R, Liu MC, Bouker KB, Gu Z, Lee RY, Zhu Y, et al. Antiestrogen resistance in breast cancer and the role of estrogen receptor signaling. Oncogene. 2003 Oct;22(47):7316–39.
37. Stanley MA. Epithelial Cell Responses to Infection with Human Papillomavirus. Clin Microbiol Rev. 2012 Apr 1;25(2):215–22.

38. Abbas Y, Brunel LG, Hollinshead MS, Fernando RC, Gardner L, Duncan I, et al. Generation of a three-dimensional collagen scaffold-based model of the human endometrium. Interface Focus. 2020 Apr 6;10(2):20190079.

Appendix

Supplementary table 1: The top 100 differentially expressed genes showing between the two in vitro systems (endo and ectocervix organoids). The average of the ectocervix organoids (Av.O.Sq) and the endocervix organoids (Av.O.Col). The adjusted p-value is the FDR corrected or Benjamini-Hochberg corrected p-value and the logFC is a log2FC.

Gene	*logFC*	*P.Value*	*adj.P.Val*	*Av.O.Sq*	*Av.O.Col*
Krt13	-9.72511	1.56E-10	1.77E-06	16.12626	6.401153
Olfml2a	-7.79605	1.67E-08	4.16E-05	12.67836	4.882305
Psca	-8.72827	1.74E-08	4.16E-05	13.46778	4.739502
Cysrt1	-7.08621	1.85E-08	4.16E-05	13.26015	6.173948
Trim29	-8.45371	2.51E-08	4.16E-05	14.11829	5.664581
Krt15	-8.98837	3.63E-08	4.16E-05	15.58407	6.595698
D030025P21Rik	-4.55957	3.88E-08	4.16E-05	9.247187	4.687617
Palld	-5.02271	3.95E-08	4.16E-05	12.84649	7.823778
Stk26	-6.88624	3.98E-08	4.16E-05	11.81469	4.928446
Zfp750	-5.75581	4.01E-08	4.16E-05	12.30725	6.551442
Gpr87	-8.66116	4.02E-08	4.16E-05	14.7939	6.132746
Tmigd1	-9.04901	5.32E-08	4.91E-05	13.69509	4.64608
Col17a1	-7.37139	5.72E-08	4.91E-05	12.80757	5.436177
Tslp	-6.96311	6.8E-08	4.91E-05	12.07574	5.112625
Grhl3	-6.62866	6.89E-08	4.91E-05	14.05512	7.426461
Sncg	-8.3132	7.38E-08	4.91E-05	13.87746	5.564258
Hmga1	-3.88658	7.64E-08	4.91E-05	14.49103	10.60445
Snai2	-6.89553	7.77E-08	4.91E-05	13.18871	6.293181
Tmprss11b	-7.28042	8.75E-08	5.23E-05	11.9732	4.692781
Hmga1-rs1	-3.17051	1.06E-07	6.03E-05	15.04579	11.87529
Serpinb2	-7.28741	1.11E-07	6.03E-05	12.99131	5.703903
Dapl1	-8.12427	1.31E-07	6.78E-05	13.94654	5.822274
Krt6a	-4.26414	1.61E-07	7.96E-05	16.00617	11.74203
Aqp3	-7.69133	1.85E-07	8.75E-05	14.18568	6.494349
Bicc1	6.389574	1.98E-07	9E-05	6.058188	12.44776
Ppp1r18	-3.58347	2.23E-07	9.74E-05	10.1862	6.602725
Chit1	-6.57351	2.53E-07	0.000107	12.5162	5.942691
Fscn1	-7.43218	2.73E-07	0.000108	11.51161	4.07943
Psapl1	-5.9523	2.86E-07	0.000108	13.03997	7.087669
Pkp1	-6.85758	2.9E-07	0.000108	14.21552	7.357945
Nccrp1	-8.27014	3E-07	0.000108	13.45362	5.18348
Dse	-5.86676	3.07E-07	0.000108	11.22331	5.356549
Tfap2c	-4.10532	3.15E-07	0.000108	8.693167	4.587844
Bcl11b	-5.02032	3.28E-07	0.000108	9.478504	4.458186
Dsc3	-8.0091	3.31E-07	0.000108	13.31415	5.305052
Gm3776	-5.25344	3.95E-07	0.000125	13.10872	7.855277
Lrmp	-5.52343	4.28E-07	0.000131	10.19681	4.673388
Krt17	-7.69618	4.96E-07	0.000146	14.3097	6.613525
Fat2	-6.4413	5.13E-07	0.000146	11.44792	5.006619

Fgfr3	-5.47273	5.19E-07	0.000146	13.71226	8.239531
Pepd	2.581172	5.28E-07	0.000146	10.38743	12.9686
Antxr1	-6.56149	5.64E-07	0.000153	11.55893	4.99744
Tpm2	-6.22641	6.08E-07	0.000161	12.89805	6.671638
Sprr1a	-3.99493	6.22E-07	0.000161	9.896606	5.901678
Ltbp2	-5.19981	6.9E-07	0.000171	10.99643	5.796622
Il33	-3.13399	6.94E-07	0.000171	10.74192	7.607932
Tgfbi	-7.24619	7.65E-07	0.000185	13.19664	5.950445
Ly6d	-7.34705	8.64E-07	0.000205	14.66125	7.3142
Pde7b	4.458631	9.43E-07	0.000217	5.724183	10.18281
Ggt1	3.306158	9.55E-07	0.000217	6.67234	9.978498
Rab7b	-4.32007	9.88E-07	0.00022	10.65386	6.333793
Artn	-4.44836	1.07E-06	0.000235	9.863556	5.415198
9130230L23Rik	3.624459	1.16E-06	0.000248	6.874243	10.4987
Arhgef9	-4.75899	1.22E-06	0.000258	9.893386	5.134399
Sox15	-6.49212	1.3E-06	0.000264	11.87407	5.381957
Clip4	-7.51897	1.3E-06	0.000264	12.61621	5.097236
Jag2	-5.97635	1.33E-06	0.000266	10.86257	4.886219
Dennd2c	-4.16749	1.42E-06	0.000278	10.56291	6.395425
Pvrl1	-6.75396	1.47E-06	0.000278	12.4383	5.684338
Mmp15	-4.87148	1.48E-06	0.000278	11.8476	6.97612
Prkca	-3.73293	1.49E-06	0.000278	11.4356	7.702674
Serpinb10	-7.78548	1.53E-06	0.000279	13.75774	5.97225
Mgat3	-5.76155	1.54E-06	0.000279	11.9834	6.22185
Chst15	-6.4795	1.6E-06	0.000283	11.10445	4.624954
Vsnl1	-4.44058	1.66E-06	0.00029	12.93812	8.497537
Bmp7	-5.70668	1.69E-06	0.000292	9.539555	3.832877
Cftr	5.917443	1.72E-06	0.000292	6.697869	12.61531
Mgp	-7.54906	1.78E-06	0.000297	13.65604	6.106975
Sfn	-3.90876	1.87E-06	0.000307	14.72422	10.81545
Tmprss11g	-6.23981	2.21E-06	0.000351	13.69793	7.458119
Trp63	-8.91359	2.23E-06	0.000351	15.52927	6.615681
Camk1d	-4.48264	2.24E-06	0.000351	10.3059	5.823265
S100a14	-6.95491	2.25E-06	0.000351	14.58335	7.628443
Sh3bp1	-5.78758	2.3E-06	0.000351	12.73145	6.943872
Calml3	-6.54627	2.32E-06	0.000351	14.64283	8.096563
Efs	-5.20541	2.36E-06	0.000353	9.637947	4.432539
Ngfr	-7.60678	2.51E-06	0.000371	13.54601	5.939232
Lynx1	-4.12984	2.57E-06	0.000374	12.16022	8.030381
Rundc3b	2.75129	2.6E-06	0.000374	5.391825	8.143114
Ifi202b	-6.22485	2.64E-06	0.000375	11.4243	5.199442
Six1	-6.00134	3E-06	0.000422	14.19172	8.190373
Art4	-7.1516	3.12E-06	0.000433	11.61357	4.461967
Id2	-3.29929	3.55E-06	0.000487	14.84742	11.54813
Prss27	-4.94596	3.78E-06	0.000511	11.00385	6.05789
Lypd2	-8.55941	4.01E-06	0.000533	14.01632	5.45691
Rgs12	-4.15357	4.03E-06	0.000533	10.55595	6.402384
Etnppl	8.327505	4.59E-06	0.0006	5.552892	13.8804

Gsta2	-5.22872	4.7E-06	0.000607	13.76483	8.536103
Adgrf4	-6.74212	4.81E-06	0.000614	11.84894	5.106818
Duox1	-3.45448	5.15E-06	0.000647	7.846993	4.392511
Evpl	-2.88047	5.18E-06	0.000647	11.41037	8.529895
Apobec1	-4.65699	5.43E-06	0.00067	11.40029	6.743301
Gpd1l	3.601412	5.48E-06	0.00067	7.467776	11.06919
Cdc42ep3	-3.18962	5.58E-06	0.000675	13.1555	9.965883
Sardh	2.809624	5.76E-06	0.000689	6.070017	8.879641
Tshr	4.155837	5.9E-06	0.000694	6.501197	10.65703
Pard6g	-4.77009	5.92E-06	0.000694	14.0943	9.324212
Clic3	-5.29139	6.08E-06	0.000706	10.6193	5.327914
Wnt10a	-3.79195	6.42E-06	0.000737	8.814681	5.022731

Supplementary table 2: The top 100 differentially expressed genes between the two in vivo regions. Average ectocervical expression (Av.ecto) and average endocervical expression (Av.endo). The adjusted p-value is the FDR corrected or Benjamini-Hochberg corrected p-value and the logFC is a log2FC.

Gene	*logFC*	*P.Value*	*adj.P.Val*	*Av. ecto*	*Av. endo*
Krt5	-10.1548	2.13E-08	0.000247	14.70786	4.553088
Krt13	-9.38236	4.64E-07	0.002614	15.53054	6.148184
Krt14	-10.5064	6.78E-07	0.002614	16.17942	5.673054
Ppbp	-8.21937	9.67E-07	0.002638	14.3468	6.127424
Ly6d	-7.99611	1.14E-06	0.002638	14.66008	6.663975
Krt15	-7.60867	1.85E-06	0.003563	13.10096	5.492286
Clip4	-3.56217	3.93E-06	0.006498	11.24683	7.684657
Dsc3	-5.67445	8.89E-06	0.012843	10.4156	4.741148
Krt6a	-7.40072	1.15E-05	0.01476	14.90483	7.504108
Dapl1	-5.9915	1.45E-05	0.016813	10.81022	4.818718
Trp63	-4.92366	2.02E-05	0.019584	11.57292	6.649263
Gpr87	-5.23031	2.03E-05	0.019584	11.46851	6.238204
Sptssb	-6.13241	2.34E-05	0.020824	10.88416	4.751749
Il1f9	-5.98739	3.47E-05	0.026452	12.59842	6.611024
Dsg3	-5.51401	3.56E-05	0.026452	11.51402	6.000005
Mxd1	-2.67184	3.72E-05	0.026452	11.27851	8.606666
Apod	-3.83298	3.89E-05	0.026452	12.96873	9.135742
Zfp750	-2.8718	5.21E-05	0.033471	8.411354	5.539553
Vsnl1	-2.63065	6.31E-05	0.038403	8.006004	5.375358
Serpinb10	-4.03111	6.98E-05	0.040367	9.261128	5.230022
Olfm4	-7.92327	7.36E-05	0.040492	12.02243	4.099159
Prss27	-5.56456	8.06E-05	0.042353	10.77013	5.205576
Muc13	-4.22376	8.51E-05	0.04277	8.881944	4.658182
Tmprss11b	-5.78993	9.39E-05	0.045249	10.22853	4.438601
Aqp4	-3.34975	0.000118	0.053372	8.553492	5.20374
Calml3	-5.61057	0.00012	0.053372	12.56711	6.956535
Il1rn	-3.84963	0.000126	0.053814	10.33088	6.481252

Ly6k	-2.71316	0.000133	0.054748	7.971848	5.25869
Anxa8	-4.27345	0.000144	0.054748	13.67095	9.397499
Epyc	-3.051	0.000144	0.054748	8.013888	4.962888
S100a8	-5.18555	0.000147	0.054748	10.73942	5.553869
Cxcl5	-4.34079	0.000161	0.05805	8.567906	4.227113
Ucp1	-9.18904	0.000176	0.061791	14.05424	4.865204
Six1	-3.0173	0.000199	0.067594	11.35892	8.341623
Tuba8	-3.3737	0.00021	0.067594	10.10439	6.730694
Mmp12	-3.51016	0.000215	0.067594	10.25199	6.741827
S100a9	-3.93709	0.000216	0.067594	11.41585	7.478761
Hcar2	-2.30555	0.000238	0.0724	8.476224	6.170674
Crabp2	-2.3863	0.000355	0.105126	13.82293	11.43663
Srd5a1	-3.56807	0.000367	0.106085	12.96868	9.400612
Cidea	-4.99742	0.000382	0.10764	9.421613	4.424194
Duoxa1	-3.09784	0.000445	0.122457	9.712521	6.61468
Cox8b	-4.03477	0.000503	0.13411	14.41718	10.38241
Akr1c18	-4.76678	0.00051	0.13411	10.75121	5.984439
S100a14	-5.9918	0.000564	0.144795	10.69662	4.704822
Wnt2b	1.705011	0.000606	0.149315	8.08135	9.786361
Csf3r	-3.9129	0.000607	0.149315	10.75963	6.846722
Lypd2	-5.11401	0.000632	0.152238	10.22556	5.111552
Tgm1	-4.55427	0.000662	0.156181	12.01738	7.463115
Csta1	-4.97024	0.000683	0.157653	9.564552	4.594317
Tmem255a	2.171386	0.000695	0.157653	9.179322	11.35071
1810032O08Rik	-1.20777	0.000714	0.158646	9.3536	8.145827
Cd300lf	-2.16714	0.000765	0.166941	8.709232	6.542092
Aldh3b2	-3.37261	0.000844	0.17855	9.98216	6.609551
Arg1	-6.65237	0.000849	0.17855	13.40518	6.752809
Spink5	-5.86371	0.000967	0.19647	11.46029	5.596578
Tmprss11g	-6.10314	0.000969	0.19647	12.8779	6.774763
Serpinb11	-6.62704	0.001081	0.211142	13.02857	6.401531
Trim29	-4.81628	0.001095	0.211142	9.778037	4.961759
Perp	-3.20458	0.001102	0.211142	14.33805	11.13346
Ppp1r3b	-1.99419	0.001114	0.211142	9.825757	7.83157
Aqp3	-3.56443	0.00114	0.212581	10.03636	6.471936
Krt10	-5.29972	0.001184	0.217348	12.18759	6.887869
Scel	-4.56663	0.001406	0.253944	11.48704	6.920416
Ecm1	-1.58516	0.00146	0.259632	11.39136	9.806201
Myrf	1.455257	0.001505	0.260297	9.84342	11.29868
Cox7a1	-4.0812	0.001509	0.260297	12.85075	8.769555
Il1r2	-3.98452	0.001532	0.260482	9.425019	5.440499
Slc5a9	-2.11994	0.001627	0.272548	8.163463	6.043522
Gna15	-1.56511	0.001687	0.27868	7.483093	5.917979
Sprr1a	-3.31242	0.001844	0.300232	8.576912	5.264494
Pkp1	-4.65705	0.001874	0.300856	10.58041	5.923366
Aqp7	-2.10572	0.00195	0.308813	11.35139	9.245667
Dnah7b	0.987278	0.002004	0.310127	7.104595	8.091873
Fam25c	-6.65884	0.002032	0.310127	11.50433	4.845491

Serpinb5	-3.30859	0.002039	0.310127	11.66419	8.355596
Paqr9	-1.00165	0.002099	0.315223	7.674808	6.673155
Aqp9	-2.43575	0.00223	0.330574	8.654248	6.218496
Fgf1	2.165795	0.002263	0.331214	9.16346	11.32925
Krt4	-4.0252	0.00242	0.349715	8.79558	4.770384
Cds1	-1.50279	0.002467	0.349827	8.764495	7.261707
Atp1a3	-1.03312	0.002488	0.349827	7.690108	6.656984
Adgrf4	-1.63362	0.002513	0.349827	7.921143	6.287522
Scnn1b	-1.12824	0.002542	0.349827	7.772854	6.644614
Abat	1.050038	0.002581	0.35106	10.46907	11.51911
Cspg4	-1.20234	0.002635	0.354259	8.325654	7.12331
Cyp2f2	-4.18009	0.002813	0.373823	10.7988	6.618702
Zfp462	1.130907	0.003031	0.398143	6.592448	7.723356
Clca3b	-4.89234	0.003149	0.407657	12.05609	7.163749
Kng2	1.199484	0.003174	0.407657	7.409484	8.608968
Plk3	-1.12971	0.003231	0.41053	7.864749	6.735044
Ift80	1.103939	0.003477	0.433959	7.864574	8.968513
Lypd3	-4.51728	0.003491	0.433959	9.118521	4.601243
Slc4a8	1.626077	0.003753	0.461538	7.204305	8.830381
Flrt1	1.7679	0.00391	0.47587	8.008332	9.776232
Grhl3	-2.98989	0.003987	0.47634	10.15014	7.160245
Rab44	-1.57302	0.003997	0.47634	7.960775	6.38775
Dusp4	-1.10754	0.004038	0.47634	9.481561	8.374024
Dmkn	-5.47088	0.004168	0.482518	12.93538	7.4645

Supplementary table 3: Venn comparison of in vivo samples using the stroma to filter out signature markers. The venn diagrams were generated by taking the results file (for each comparison respectively) and only looking at the genes with an adjusted p-value of <0.05. Then the genes were categorised as either upregulated or downregulated based on their logFC.

Epithelial signature	*vivo 1 (ecto) specific*	*vivo 2 (endo) specific*	*stromal signature*
MUP12	MUP8	INHBA	CDKN2A
GM2083	CCL21B	SERPINE1	FBLN2
RETN	MUP13	ANKRD1	CH25H
MUP1	GM1987	VGLL3	TNFSF15
MUP2	SMIM22	SERPINB9B	LRRC32
THRSP	HBB-BT	BRINP1	COL11A1
PDZK1IP1	CES1D	ASB5	NOV
MUP7	CHDH	APLP1	VCAM1
FERMT1	MYO3B	H60B	NGF
HBB-BS	RAB25	HS6ST2	PCDH19
MUP19	GRB7	SLC1A6	CPT1C
GM13304	HPGD	CCK	FSTL3
CCL21C	GRHL2	FAM198B	PTPRN
GM10591	CCL21A	BDNF	SESN2

CDH1	DLX6	BMPER	RENBP
ORM1	RGS2	HTR2A	LTBP2
CLDN7	NTRK2	KIRREL	COL5A2
CD74	ST14	GPR176	LHFP
PCP4	TMEM45B	BASP1	CCL2
EPCAM	PAX2	FOLH1	EFEMP2
HBA-A2	ADIG	COL4A1	BC022687
4833423E24RIK	CD300LH	CAR6	CYP1B1
ADGRG7	MACC1	9030617O03RIK	ELFN1
HBA-A1	EPB41L4B	MRC2	TRNP1
CORO2A	RETNLA	FGF7	FAM214B
CLEC3B	ABCD2	HTR1B	DDIT3
SERPINA1E	ANPEP	AEN	LOXL3
ESRP1	CXCL17	FOXF1	AVPR1A
EHF	SLC35F2	IL6	TIMP1
CFD	SALL1	P4HA1	SYNPO
FXYD3	MOB3B	FSCN1	AGA
LGALS12	ADH1	DBN1	GATSL3
ADIPOQ	ITGB6	BMP1	FLYWCH1
CRB3	MUC1	PSRC1	FADS3
DGAT2	H2-EB1	WISP1	CD80
ALOX15	AMY1	ADORA2B	FGF2
CAPSL	PLIN1	GPC4	AKAP2
RBP4	MYO5B	FSD1	MXRA7
KCNK1	AW112010	DDIT3	P4HA2
FAM84A	RXFP1	P3H1	MFGE8
CBR2	TMEM54	COL4A2	SERPINE2
CLDN23	ENPP3	FBLN7	NPY1R
KCTD12	CELSR1	THBS1	ADRA1D
PDLIM3	CBLC	OLR1	CTSK
PLBD1	WFDC2	ANO3	SSC5D
CAR3	ACP5	AZIN2	LRRC27
GPD1	PPL	CHPF2	CSF1
LAMA3	NAIP5	LAYN	HOMER3
PTPRC	FCGR2B	SPG7	LOX
MAL2	SPINT1	ST3GAL2	NR2F1
GPR160	TSPAN1	MARK4	UCHL1
BC048679	NET1	GRIA3	DDAH1
SLC1A1	APOBEC3	LOXL2	ANGPT4
DLX5	MAL	CPXM1	PAPPA
SLC39A4	GYLTL1B	MAP3K7CL	TMEM150A
PPARGC1A	PLCH1	ADAM19	PLEKHF1
PTGER3	ADGRG1	EPB41L3	SLC6A8
SPRR2F	CD209F	MDM2	HHAT
WFDC15B	KRTCAP3	PDZRN3	GLIPR2
DENND2D	AIM1	E2F1	CCND2
IFITM1	TACSTD2	CRLF1	MPP1
CASP1	AOX3	CHST12	CNN2

FOLR2	A530016L24RIK	PLOD3	WBSCR17
MRC1	SORL1	ADAMTS14	FIBIN
ACSL1	LRRC17	HTATIP2	RND1
CYP2E1	TRF	PARP3	CDH2
ST6GALNAC2	PLEKHH1	PCOLCE	KCND1
CHPT1	LYZ1	CCL7	NCS1
LIPE	SLA	CDKN2B	RCN2
SLC23A1	PLET1	ADAMTS5	SRXN1
KRT19	SCD1	PDPN	PLPPR2
ESR1	TJP3	NEK6	PDIA5
PAX8	SLC16A6	PHLDB2	MLLT11
TMPRSS2	CCDC141	UGCG	FEZ2
SLC44A4	CYBB	FN1	PPP1R18
ASPA	AP1M2	VAX2	ASAP3
AIF1	AQP1	FKBP10	PDRG1
H2-AB1	CDO1	SLIT3	TCAF2
GMFG	FGL2	COIL	CREB3
GM11710	EPB41L4A	TRIB3	ASB6
AKR1C19	ALDH1A7	MCFD2	GREM1
CLDN3	CD36	PALM2	PTRH1
IRF6	ATP1A2	FLOT1	FAS
BCL2L15	BARX2	THBS2	FHL3
CIDEC	FMO1	FHL2	TMEM19
CYBRD1	PSD	FST	NQO1
SMOC1	GCNT3	PPEF1	DOK5
BSPRY	CCR2	ZYX	CYB5R1
PLEKHS1	F13A1	PRMT2	TULP3
FXYD4	NCF4	ARSA	SNTA1
EPSTI1	KIF5C	PLPPR2	ADAM15
EGFL6	BLNK	GRB14	AGBL2
ACVR1C	CAR5B	INF2	MGMT
TNFSF10	VNN3	GDF6	CRYAB
LTF	LCN2	HSPG2	ITGA5
TUSC5	PDIK1L	FBN1	TMEM181C-PS
COX8B	AU021092	B3GALT1	TCEA3
COL6A4	CD86	FZD7	JPH1
MUP3	SH3BGRL2	ATP6V0D1	DKK2